THE UNIVERSITY
of EDINBURGH

A system for *in vivo* ablation of MeCP2-deficient neurons in the Rett Syndrome mouse model

Katie Paton

Thesis presented for the degree of Doctor of Philosophy

The University of Edinburgh

2021

Declaration

I declare that this thesis was composed by me, and the research presented is my own unless stated otherwise. This work has not been submitted for any other degree or personal qualification.

Katie Paton

October 2021

Abstract

Rett syndrome (RTT) is an X-linked neurological disorder caused by loss-of-function mutations in the *MECP2* gene. Heterozygous RTT females express a phenotype due to mosaic expression of their wild type (WT) copy of *MECP2* caused by random X-chromosome inactivation. Furthermore, neurons expressing WT *MECP2*, which have the capacity to function normally, are interspersed with neurons expressing the mutant allele, which function inappropriately and compromise the whole neuronal network. Re-expression of MeCP2 in *Mecp2*-mutant adult mice reverses the neurological phenotype. Thus, therapeutic avenues explored so far to treat RTT, focus on repairing MeCP2 expression in MeCP2-deficient neurons. One of the most challenging aspects of this approach is maintaining MeCP2 levels within physiological limits, as both too much and too little MeCP2 expression lead to neurological disease. An alternative approach based on silencing or removal of the functionally mutant neurons from the mosaic neuronal network has not yet been explored but could in theory be curative. I seek to selectively ablate MeCP2-deficient neurons at different stages in development in the heterozygous mouse model of RTT to determine whether the removal of 50% of neurons in the developing brain is compatible with viability at various developmental stages. The ultimate goal is to ask: does the removal of the MeCP2-deficient neurons ameliorate the RTT-like phenotype?

This thesis describes the development of an inducible *in vivo* cell ablation system for selective removal of *Mecp2* knock-out neurons in the heterozygous RTT mouse model. The novel *Mecp2*$^{FLExDTR(OFF)}$ genetically engineered mouse line was generated which facilitates Cre-dependent expression of the Diphtheria Toxin Receptor (DTR) from the *Mecp2* locus in place of the *Mecp2* gene. Mice are resistant to Diphtheria toxin (DT), so expression of the DTR in a cell-type of interest, allows ablation of those cells upon DT administration. Importantly, un-recombined *Mecp2*$^{FLExDTR(OFF)}$ (*cre*-negative) mice were shown to be resistant to high doses of DT and therefore comparable to WT littermates. DTR expression was activated only in the presence of Cre recombinase. The combination of the *Mecp2*$^{FLExDTR(OFF)}$ allele with a transgenic Cre driver allows targeting of DTR expression to MeCP2-deficient cells in the tissue of interest. A preliminary neuronal *in vivo* ablation experiment was performed where DT was

administered to heterozygous *Mecp2*$^{FLExDTR(OFF)/+}$*,SNAP25-IRES2-cre* neonatal mice. At 5 weeks following a single subcutaneous injection of DT at postnatal day 0-2, *Mecp2*$^{FLExDTR(OFF)/+}$*,cre+* mice showed no signs of overt neurological phenotypes and had no substantial skewing towards MeCP2+ neurons in the brain. It was unclear whether any ablation of MeCP2– neurons had occurred. Further experiments are required to optimise the *in vivo* ablation protocol to achieve efficient removal of MeCP2– neurons. This thesis discusses the associated challenges and future applications of this inducible *in vivo* cell ablation mouse model.

Lay Summary

Rett Syndrome is a disease of the nervous system which effects 1 in 10-15,000 girls. Girls with Rett Syndrome develop relatively normally for the first 6-18 months of their life until symptoms of Rett syndrome appear. They lose skills such as speech and language, purposeful hand use, and their ability to crawl or walk. The girls develop repetitive hand movements such as clapping and rubbing and commonly suffer from breathing difficulties and epileptic fits. These disabilities are caused by DNA mutations or mistakes in the gene called *MECP2*. This means that the *MECP2* gene does not function properly and no longer makes the MeCP2 protein which is required for brain cells (neurons) to work properly.

Females have two copies of the *MECP2* gene and only one copy has the mutation in it, the other one works normally. Only one copy of the *MECP2* gene is active at a time in each neuron. This means that roughly half of the neurons in the brain have the normal *MECP2* gene active and function properly, and the other half of neurons have the mutated gene active and are dysfunctional. As neurons form a complex network with one another, the interspersed dysfunctional neurons damage the entire network causing the symptoms of Rett Syndrome.

Treatments that have been explored so far focus on trying to restore function in the neurons which have the mutated *MECP2* gene active. An alternative approach would be to remove these dysfunctional neurons from the network of brain cells to allow the normal neurons (which have the normal *MECP2* gene active) to function properly. This would require the brain to re-wire itself considerably and compensate for the loss of these neurons.

This project explores this idea during brain development in mouse models of Rett Syndrome. A modified mouse model was produced which allows the selective elimination of the dysfunctional neurons. These neurons were tagged with the Diphtheria Toxin Receptor. When Diphtheria Toxin is injected into mice, the tagged cells are selectively killed. This thesis describes the production and characterisation of this mouse model, preliminary experiments and the future applications of the system.

Acknowledgements

Thank you to the many people, friends and family who have supported me and enabled this PhD to happen.

Firstly, I'd like to thank Adrian Bird for offering me the PhD position and for his excellent supervision and mentorship throughout. Thanks to him I have gained a considerable variety of valuable research experiences, contacts and skills that prepare me well for a future career in research. Thank you to the UK Centre for Mammalian Synthetic Biology BBSRC, MRC and EPSRC for funding the PhD. Thank you to my second supervisor Susan Rosser and my thesis committee Andrew Smith and Jamie Davies for their continued support and advice during my yearly progress meetings.

A huge part of what I have learnt in the last 4 years has come from Jacky Guy. Jacky's infinite wisdom about genetically engineering mouse embryonic stem cells and caring for them as 'needy pets' ensured that they would produce mice as required. This lead to many weekend visits to the lab to "feed and nurture my cells" which always made my family and friends giggle. Most of the protocols I used throughout my PhD came from Jacky.

Jim Selfridge managed all the mice lines, set up the breeding pairs and helped me to design the mouse experiments. Jim performed the blastocyst injections to generate the *Mecp2*^{StopDTR} line. He also performed and assisted me to perform some of the IP injections. Jim made the *Mecp2*^{mCherryStop} mouse line which I used for my Cre characterisation experiments. Thank you to Dina De Sousa, Justyna Cholewa-Waclaw and Verdiana Steccanella for genotyping all of the mice used in these experiments.

John Connelly provided me with information on how to write the risk assessments for working with Diphtheria Toxin. Thank you to Prof. Neil Mabbott and Rachel Young for supplying us with aliquots of Diphtheria Toxin for some of the mouse experiments.

Many thanks to the Bioresearch and Veterinary Sciences (BVS) animal facility staff for overseeing the day-to-day breeding, maintenance and welfare of the mice and for their help and advice throughout. In particular thank you to Christopher Flockhart and Gordon Melville for devoting their time and remarkable patience whilst training me to

handle mice and perform IP injections. The BVS Central Transgenic Core facility performed the blastocyst injections which made the second *Mecp2*$^{FLExDTR(OFF)}$ mouse line.

Martin Waterfall assisted me with flow cytometry and David Kelly helped me with microscopy.

A big thank you to the whole of the Bird lab team, those present and past members who have made the last 4 years such a lovely experience. Every lab member has shared reagents, protocols, given me helpful tips and advice at some point or another. I have made some friends for life! Thank you to Bea and Laura for being so fantastic, all of your support has meant the world to me. Laura has been my PhD student 'sister' in the lab. Thank you for helping me remember to achieve the various PhD milestones on time, for being there to share the stress of big presentations and of organising the Institute Christmas Party 3 years in a row. I am very proud of you for persevering and smashing your PhD.

Thank you to my family for their support. Especially Mum who has always been my inspiration to further my academic career! Last but not least, a huge thank you to my partner Jack for being the best support I could have dreamt of. We both did PhDs alongside each other. To add an extra test to the relationship, our thesis writing coincided with pandemic lockdown in our one-bedroom flat. In May 2020 Hamish our beloved border terrier puppy joined the family. Hamish was the best tonic to the long days of writing providing excuses for work-breaks and making everything more enjoyable.

Contents

List of Figures

List of Tables

Chapter 1 Introduction

1.1 Rett Syndrome

1.1.1 Discovery of Rett Syndrome as a distinct neurological disorder

Rett Syndrome (RTT) was first described in 1966 by Andreas Rett, a neurodevelopmental paediatrician in Vienna (Rett, 1966). He described a disease exclusively in girls, characterised by a period of normal development followed by the regression of acquired skills including spoken language and purposeful hand movements, together with the development of stereotypic hand movements and gait abnormalities. Around the same time the Swedish neurologist, Bengt Hagberg described girls with similar features. Hagberg and colleagues published an article in English in the Annals of Neurology in 1983 detailing the clinical features of a group of European patients and attributed the name Rett Syndrome (RTT) to the condition (Hagberg et al, 1983). This paper spurred a worldwide search for undiagnosed females with similar phenotypes and led to an explosion in literature on RTT. Other detailed case series followed providing crucial information for the medical community about the clinical features of the disorder (Naidu et al, 1986; Kerr & Stephenson, 1985). The prevalence of RTT was soon to be estimated at 1 in 10-15,000 live female births (Hagberg, 1985).

Hagberg and colleagues continued to make important contributions to the clinical field including outlining the initial clinical diagnostic criteria (Hagberg et al, 1985), developing a staging system for RTT (Hagberg et al, 1986) and identifying variant forms of RTT (Hagberg & Skjeldal, 1994). The accumulation of clinical and molecular data has led to multiple iterations of the diagnostic criteria. The most recent revision includes separate criteria for typical and atypical RTT classification (also referred to as classic or variant forms) as summarised in Table 1.1.3. (The Rett Syndrome Diagnostic Criteria Work Group, 1988; Hagberg *et al*, 2002; Neul *et al*, 2010).

Although a genetic basis for RTT was hypothesised as early as 1983, it wasn't until 1999 when the Methyl-CpG binding protein 2 (*MECP2*) gene was found to be causative for the disease (Amir et al, 1999). Following this, the first mouse model was

developed which recapitulated key phenotypes of RTT (Guy et al, 2001; Chen et al, 2001). Mouse models have been instrumental in tackling the underlying neurobiology and disease-causing molecular mechanism. Natural history studies and international databases of patient clinical and genetic data complemented by mouse models have informed our understanding of genotype-phenotype relationships. A revolutionising study in 2007 found that Rett Syndrome-like phenotypes in the mouse were reversible which provided the stimulus for finding a cure (Guy *et al*, 2007). In the last decade there have been huge advances towards this goal. Through coordinated efforts of scientists, clinicians, family organisations and the biomedical industry, there are exciting therapeutic prospects ahead.

1.1.2 Identification of the genetic cause of Rett Syndrome

The almost exclusive occurrence of RTT in females suggested a genetic cause and lead to the early hypothesis that it was an X-linked dominant disorder (Hagberg *et al*, 1983). This was reinforced by twin data that showed dis-concordance in dizygotic twins and concordance in monozygotic twins with RTT, as well as, rare familial cases (0.5 – 1% of cases) containing multiple affected females (reviewed by: Zoghbi, 1988; Naidu *et al*, 1988). Studying these families identified nonpenetrant carrier mothers who had skewed X-chromosome inactivation (XCI) towards the normal X-chromosome. This protected them from the disease, allowing them to transmit the mutated allele to their affected daughters who had random XCI. Exclusion mapping in rare familial cases mapped the causal locus to Xq28 (Schanen & Francke, 1998; Sirianni *et al*, 1998). This information lead to the identification of loss-of-function mutations in the gene encoding Methyl CpG-Binding Protein 2 (*MECP2*) in both common sporadic cases and rare familial cases of RTT (Amir *et al*, 1999). The MeCP2 protein had been previously identified in the epigenetics research field through its ability to bind to methylated DNA (Lewis *et al*, 1992). The identification of the relationship between *MECP2* and RTT resulted in a convergence of clinical, neuroscience and epigenetics researchers to collectively begin to decipher the underlying disease-causing mechanism.

The burgeoning availability of genetic testing in multiple countries now allows many patients who are suspected to have the clinical RTT diagnosis to have their *MECP2* gene sequenced. A dependence on clinical data alone remains in some parts of the world where genetic testing is inaccessible and emphasises the need for clear unambiguous diagnostic criteria. Following advances in sequencing technologies the recognition rate of *MECP2* mutations has been estimated at approximately 96% of the individuals who are suspected to have the clinical diagnosis for typical RTT (Cuddapah *et al*, 2014). Genetic information of RTT patients is submitted to RettBASE (Christodoulou *et al*, 2003), the MECP2 Variation Database, which has a unique role in cataloguing the range of different genetic variants, both pathogenic and non-pathogenic. This supplies researchers with fundamental information needed to decipher the molecular mechanism of MeCP2 and how different mutations cause RTT.

1.1.3 Clinical features of Rett Syndrome and MECP2-Related disorders

1.1.3.1 Clinical progression of typical Rett Syndrome

The clinical progression of Rett Syndrome has been shown to go through four stages (Hagberg *et al*, 1986). Children with RTT are born after an apparently normal gestation and delivery (Leonard & Bower, 1998). Early diagnostic criteria included an initial period of ~6 months of normal psychomotor development (Hagberg *et al*, 1985; The Rett Syndrome Diagnostic Criteria Work Group, 1988), although, subtle irregularities have been identified in RTT babies, such as: placidity, hypotonia, difficulty weightbearing and feeding difficulties (Leonard & Bower, 1998). Revised diagnostic guidelines outlined that "grossly abnormal" psychomotor development in the first 6 months of life was an exclusion criteria for a diagnosis of typical RTT (Table 1.1.3)(Neul *et al*, 2010).

Between 6 - 18 months of age affected children enter a stage of developmental stagnation (Stage 1) (Hagberg *et al*, 1986). The onset of decelerated head growth is commonly one of the first features to be identified and it can alert the clinician to the potential diagnosis (Neul *et al*, 2010; Hagberg *et al*, 2000). An estimated 80% of typical RTT patients present with abnormal deceleration of head growth (Percy *et al*, 2010b).

Rett Syndrome Diagnostic Criteria 2010

Consider diagnosis when postnatal deceleration of head growth is observed.

Required for typical or classic RTT

1. A period of regression followed by recovery or stabilisation
2. All main criteria and all exclusion criteria
3. Supportive criteria are not required, although often present in typical RTT

Required for atypical or variant RTT

1. A period of regression followed by recovery or stabilization
2. At east 2 out of 4 main criteria
3. 5 out of 11 supportive criteria

Main criteria

1. Partial or complete loss of acquired purposeful hand skills
2. Partial or complete loss of acquired spoken language
3. Gait abnormalities: Impaired (dyspraxic) or absence of ability
4. Stereotypic hand movements such as hand wringing/squeezing, clapping/tapping, mouthing and washing/rubbing automatisms

Exclusion Criteria for typical RTT

1. Brain injury secondary to trauma (peri- or postnatally), neurometabolic disease, or severe infection that causes neurological problems
2. Grossly abnormal psychomotor development in first 6 months of life

Supportive Criteria for atypical RTT

1. Breathing disturbances when awake
2. Bruxism when awake
3. Impaired sleep pattern
4. Abnormal muscle tone
5. Peripheral vasomotor disturbances
6. Scoliosis/kyphosis
7. Growth retardation
8. Small cold hands and feet
9. Inappropriate laughing/screaming spells
10. Diminished response to pain
11. Intense eye communication – “eye pointing”

Table 1.1.3. Rett Syndrome Diagnostic criteria, revised in 2010. Table taken from: Neul JL, et al., (2010) Rett syndrome: Revised diagnostic criteria and nomenclature. *Ann. Neurol.* **68:** 944–950 (Neul *et al*., 2010). See reference for further details.

The second stage in the progression of RTT is a period of active regression, with onset between 1 and 4 years of age (Hagberg *et al*, 1986). Affected children experience a complete loss or deterioration in their acquired developmental skills particularly their

practical hand use, and learned spoken language (Hagberg *et al*, 1983). The regression of communicative behaviour and the manifestation of autistic features such as social withdrawal, diminished eye contact and impaired ability to respond to stimuli are commonly observed (The Rett Syndrome Diagnostic Criteria Work Group, 1988; Neul, 2012). The diagnosis of autism may be entertained at this stage - a significant proportion of RTT patients have a previous diagnosis of autism (Young *et al*, 2008). The regression period is an important hallmark of RTT and an individual MUST experience a period of regression in order to be diagnosed with typical or atypical RTT (Table 1.1.3)(Neul *et al*, 2010).

The regression period is followed with the pseudo-stationary period (Stage 3), where deterioration stabilises (Hagberg *et al*, 1986). A period of stabilisation distinguishes cases of RTT from relentless neurodegenerative conditions. Communication skills may partially recover including improved eye gaze and increased interest in social interactions (Neul, 2012). Spoken language and purposeful hand movements remain significantly impaired throughout life.

The distinctive repetitive stereotypic hand movements clinically described as hand "washing or wringing" is a main diagnostic criteria of RTT (Table 1.1.3)(Neul *et al*, 2010) and may coincide, precede or follow the noticeable period of regression (Lee *et al*, 2013). Another major feature of RTT to become apparent at this time if not already present, is the deterioration of balance and development of gait ataxia (Neul, 2012). Truncal rocking, tremor and bruxism (teeth grinding) are other commonly observed movement abnormalities (Neul, 2012). Additional comorbidities to develop at variable stages throughout the progression of RTT include: breathing abnormalities such as hyperventilation, breath-holding and abdominal bloating (Julu *et al*, 2001; Weese-Mayer *et al*, 2006). Around 60% of RTT individuals are diagnosed with epilepsy (Glaze *et al*, 2010; Nissenkorn *et al*, 2015; Bao *et al*, 2013). The average onset of seizures is around 3-5 years of age with increased frequency with age through to puberty. Growth deceleration including weight, height, hand and foot growth in addition to head circumference is observed (Schultz *et al*, 1998). Enteral support to assist the management of feeding difficulties and poor weight gain is a common practice (Downs *et al*, 2014). Progressive scoliosis is a relentless symptom affecting

75% of RTT girls by the age of 15 (Downs *et al*, 2016). Sleep problems such as poor night time sleeps and frequent day time naps, night laughing and screaming often are a considerable burden on the affected individual and their family (Ellaway *et al*, 2001; Young *et al*, 2007; Wong *et al*, 2015).

The final stage (Stage 4) of RTT is late motor deterioration (Hagberg *et al*, 1986). The onset of this is beyond 10 years and the progression is slower than preceding stages. Late motor deterioration is characterised by: progressive scoliosis, muscle wasting and rigidity and decreased mobility (The Rett Syndrome Diagnostic Criteria Work Group, 1988; Neul, 2012). The degree of motor dysfunction varies but RTT patients frequently become wheelchair bound. Despite the appearance of severe symptoms in early childhood and later motor deterioration, RTT women typically live long into adulthood. A longitudinal study in the USA estimated that more than 70% survive to 50 years of age (Tarquinio *et al*, 2015). The most common causes of mortality are cardiorespiratory issues such as pneumonia or aspiration. Other mortality risks include infection, seizures, gastrointestinal issues and scoliosis. Quality of life and survival may be improved by physiotherapy, medication or medical interventions to alleviate symptoms, and nutritional plans (Tarquinio *et al*, 2015; Neul, 2012).

1.1.3.2 Atypical Rett Syndrome, RTT-related disorders and *MECP2*-related disorders

There is a considerable amount of clinical variability and heterogeneity amongst girls with RTT which creates diagnostic difficulties. Atypical RTT deviates from the characteristic RTT pattern in age of onset, clinical progression, and presence or severity of expected symptoms and is recognised as a separate entity to typical RTT. The diagnostic criteria provides guidelines to distinguish the different forms of RTT (Table 1.1.3.)(Neul *et al*, 2010). For the main criteria invariably observed in typical RTT patients: abnormal gait and hand stereotypies are commonly observed in patients with atypical RTT (~95% of individuals), whereas, loss of hand use and spoken language are less commonly observed (~55%)(Percy *et al*, 2010b). The revised clinical diagnostic criteria post-genomic era aimed to reflect the variability likely to be encompassed by the same biological disorder, however, only approximately 76% of patients clinically diagnosed with atypical RTT have an identified *MECP2* mutation

(Cuddapah *et al*, 2014). Likewise, a proportion of typical RTT patients, albeit small (~5%), do not have an identified *MECP2* mutation. This illustrates that an *MECP2* mutation is not synonymous with RTT and consequently RTT remains a clinical diagnosis. In those individuals diagnosed with RTT which do not have an identified *MECP2* mutation, their phenotypes might be caused by unidentified variants in non-coding regions of *MECP2* which have an effect on expression. Alternatively, they may carry variants in other genes with overlapping molecular functions with MeCP2. Determining the underlying genetic variant in patients with RTT is invaluable for the research field attempting to underpin the molecular function of MeCP2 and therapeutically targetable pathways.

Early descriptions of the range of clinical manifestations of RTT describe specific variant forms: the preserved speech variant (Zappella, 1992), the congenital variant (Rolando, 1985) and the early seizure variant (Hanefeld, 1985). The preserved speech variant is a milder form of RTT and the majority of cases are caused by mutations in *MECP2* (Renieri *et al*, 2009). Affected girls show the same stages of RTT but retain more motor function, they can walk unassisted, may be able to draw and, as the name suggests, retain some level of speech. Autistic features are more common in girls with the preserved speech variant RTT (Zappella *et al*, 2003). Mutations in different loci have been identified to be associated with the congenital variant and early seizure variant forms: FOXG1 and CDKL5 genes respectively (Fehr *et al*, 2013; Ariani *et al*, 2008). Individuals with mutations in these genes often present with features distinct from RTT including the absence of clear regression – an essential criteria for both typical and atypical RTT (Neul *et al*, 2010). One of the hallmark features of CDKL5 disorder is early-onset epilepsy at around 3 months of age which is uncommon in typical RTT (Fehr *et al*, 2013). Patients with FOXG1 mutations present with severe microcephaly and mental retardation from birth as well as characteristic structural brain abnormalities such corpus callosum hypogenesis (Kortüm *et al*, 2011). These genetic disorders can masquerade as RTT and are considered as differential diagnoses for certain patients without an *MECP2* mutation. Research into the function of these two proteins is required to uncover why variants in these genes can cause overlapping phenotypes.

Mutations in *MECP2* have been identified in individuals with neurological disorders that are clinically distinct from RTT, referred to as *MECP2*-related disorders (Neul *et al*, 2010). *MECP2* mutations have been identified in girls with disorders with overlapping phenotypes such as Angelman-like syndrome (Watson *et al*, 2001). Non-RTT causing mutations have also been identified in females with mild intellectual disability and autism (Carney *et al*, 2003; Lam *et al*, 2000). In many of the latter cases the mutations found to be responsible would be predicted to retain more MeCP2 protein function. Causes of the phenotypic variability associated *MECP2* mutations is discussed further in section 1.4.

1.1.3.3 *MECP2* mutations in males

Clinically defined RTT is rarely seen in males. One reason is that almost all *de novo* *MECP2* mutations arise on the paternal X chromosome during spermatogenesis and so are transmitted exclusively to female offspring who inherit one X chromosome from both parents (Trappe *et al*, 2001). Males inherit their single copy of the *MECP2* gene from their mothers. The second major factor is that boys who are hemizygous for *MECP2* are comparatively more severely affected than heterozygous females with mosaic expression of WT and mutant *MECP2*. Mutations known to cause RTT in heterozygous girls commonly present as early progressive encephalopathy and premature lethality in boys within the first 3 years of life (Kankirawatana *et al*, 2006). Distinguishing neurological features in these boys include: neonatal-onset progressive deceleration of head growth, respiratory insufficiency with irregular breathing, severe hypotonia, feeding problems, limb rigidity and movement disorders including myoclonus, tremors and dystonia, and lack of motor and cognitive development (Kankirawatana *et al*, 2006; Schüle *et al*, 2008). There is an absence of RTT features such as stereotypic hand movements. Rare cases of males with clinically defined RTT have been described. However, in many of these cases additional genetic features are present which lead to the dilution of mutant cells among normally expressing cells such as Kleinfelter syndrome (XXY) (Schwartzman *et al*, 2001; Leonard *et al*, 2001; Hoffbuhr *et al*, 2001; Vorsanova *et al*, 2001) and somatic mosaicism (Armstrong *et al*, 2001; Clayton-Smith *et al*, 2000; Topçu *et al*, 2002). Other cases of typical RTT in boys with a normal karyotype and no somatic mosaicism have been reported for males

with mutations which cause milder cases of RTT in females (Masuyama *et al*, 2005; Budden *et al*, 2005; Dayer *et al*, 2007). The diagnostic criteria for RTT was extended to include the rare cases of male variant RTT in 1998 (The Rett Syndrome Diagnostic Criteria Work Group, 1988). Non-RTT causing *MECP2* mutations have been identified in males with mild to severe mental retardation in association with diverse neurological symptoms and occasionally psychiatric illness (Villard, 2007; Cohen *et al*, 2002; Klauck *et al*, 2002). Overall, phenotypes associated with *MECP2* mutations in males, as in females, cover a huge spectrum of neurological disorders from severe early encephalophagy to mild mental retardation with complex cases of RTT-like syndrome with or without mosaicism of some form. Much of this variation is caused by the type of mutation (discussed further in section 1.4.1).

1.1.3.4 *MECP2* duplication syndrome

MECP2 overexpression as opposed to loss-of-function causes a discrete *MECP2*-related disorder predominantly in males called *MECP2*-duplication syndrome (Meins *et al*, 2005; Van Esch *et al*, 2005). *MECP2* overexpression is caused by the duplication of the Xp28 region surrounding *MECP2* and results in symptoms overlapping with RTT including: early infantile hypotonia, delayed psychomotor development, absent to very limited speech, abnormal gait, gastrointestinal motility problems, epilepsy, and spasticity (Van Esch, 2011). The majority of patients suffer from recurrent infections especially respiratory tract infections which are responsible for early death (before 25 years of age). The duplication of the interleukin receptor-associated kinase 1 (*IRAK1)* gene closely linked to *MECP2* has been postulated as the causal factor for recurrent infections but the mechanism remains unclear (Van Esch, 2011). Unlike RTT, the majority of cases of *MECP2* duplication syndrome are familial where the duplicated X chromosome is inherited from asymptomatic or mildly affected carrier mothers who have extreme XCI skewing (Van Esch *et al*, 2005). The presence of syndromes caused by both overexpression and loss-of-function of *MECP2* demonstrates that humans are highly sensitive to *MECP2* gene dosage: too much and too little MeCP2 can have deleterious neurological consequences.

1.1.4 Mouse models of RTT and MECP2-related disorders

Much of the work into determining the disease-causing mechanism of RTT has relied on patient derived cells and genetically modified mice. Some of the key overt neurological phenotypes of mutations in *MECP2* in humans are recapitulated in the mouse. In contrast it is challenging to detect significant disease phenotypes in cell culture systems. Consequently, mice are invaluable when studying RTT and *MECP2*-related disorders. This is reflected in the vast number of different *Mecp2* mutant mouse models that have been produced to date including: knock-out (KO) and conditional KO models (Guy *et al*, 2001; Chen *et al*, 2001), the *Mecp2* re-expression model where *Mecp2* is silenced and can be re-activated by Cre-mediated recombination (Guy *et al*, 2007), *Mecp2* overexpression and hypomorph mice (Guy *et al*, 2001; Collins *et al*, 2004), mice with *Mecp2* truncations (Tillotson *et al*, 2017), and mice expressing RTT patient specific mutant forms of *Mecp2* (Goffin *et al*, 2012; Brown *et al*, 2016; Guy *et al*, 2018; Lawson-yuen *et al*, 2007; Pitcher *et al*, 2015; Baker *et al*, 2013; Lyst *et al*, 2013; Lamonica *et al*, 2017; Johnson *et al*, 2017; Gandaglia *et al*, 2019; Heckman *et al*, 2014; Merritt *et al*, 2020). Histological and biochemical analysis on mouse tissues at different stages of development and in different *Mecp2* mutant models has enabled detailed characterisation of the molecular role of MeCP2 *in vivo*. The RTT causing missense mutation spectrum has been particularly useful in highlighting important functional domains of MeCP2. The conditional KO models and re-expression models have been extensively used to determine the requirement of MeCP2 in different tissues and developmental stages. Studying large cohorts of inbred RTT mutant knock-in mice with very little genetic diversity allows strong genotype-phenotype correlations to be drawn. A phenotypic severity scoring system developed in the Bird lab (Guy 2007), has been routinely used in the field to study genotype-phenotype relationships, and to determine the level of phenotypic rescue following therapeutic interventions.

The first mouse models of RTT were *Mecp2* KO mice simultaneously generated by the Bird and Jaenisch labs in 2001 (Guy *et al*, 2001; Chen *et al*, 2001). Both labs used *Cre-loxP* technology to produce *Mecp2* conditional KO alleles by flanking crucial exons with *loxP* sites. Ubiquitous deletion of *Mecp2* exons was achieved using constitutive expression of Cre recombinase during early embryogenesis (Guy *et al*,

2001) or Cre-expression in the germline (Chen *et al*, 2001). Both approaches produced efficient functional KO alleles upon recombination. As heterozygous loss-of-function mutations in *MECP2* cause *RTT*, the more accurate genetic representation of RTT patients are heterozygous female mice. The female heterozygous KO mice develop neurological symptoms including inertia, gait ataxia, hind limb clasping and breathing abnormalities after a period of 3-12 months of apparently normal development (Guy *et al*, 2001; Chen *et al*, 2001). Heterozygous KO mice do not experience rapid deterioration and the phenotype remains relatively stable as in RTT. Unexpectedly, the onset of neurological phenotypes is at a much later developmental time point compared to humans. Bizarrely, the absolute timing of symptom onset overlaps in heterozygous humans and mice. As expected, *Mecp2-null* male or female mice display more overt neurological phenotypes than heterozygotes with an earlier onset of 3-8 weeks (Guy *et al*, 2001; Chen *et al*, 2001). *Mecp2-null* mice develop a stiff uncoordinated gait, reduced spontaneous movements, hind-limb clasping, irregular breathing and a tremor. Other common phenotypes include uneven wearing of the teeth and misalignment of the jaws. *Mecp2-null* mice rapidly deteriorate following symptom onset resulting in premature death between 6 and 12 weeks following a marked period of weight loss. This is consistent with early lethality in humans with *MECP2* loss-of-function mutations (Kankirawatana *et al*, 2006). In humans, *MECP2* loss-of-function mutations usually cause premature lethality before the age of 2 years, whereas *Mecp2-null* mice survive until early adulthood. As in heterozygous females, the phenotype associated with MeCP2 deficiency is less severe in mice compared to humans.

Male hemizygous *Mecp2-null* (*Mecp2* knock-out) mice or *Mecp2*-mutant knock-in mice carrying RTT-causing mutations are mainly used to study RTT and the molecular role of MeCP2 instead of female heterozygotes. Strictly speaking the male *Mecp2* mutant mouse is actually a model of neonatal encephalopathy as opposed to RTT. However, hemizygous *Mecp2* mutant mice do recapitulate many of the key RTT phenotypes including motor defects, gait impairments, breathing abnormalities and tremors. The increased severity, earlier onset, and reduced variability of phenotype compared to the heterozygote enable clear genotype-phenotype relationships to be drawn. Premature lethality is a particularly useful phenotype to determine phenotypic rescue or improvement. The late onset of disease phenotype does allow female mice

to be used for breeding purposes to transmit modified *Mecp2* alleles. The phenotypic severity scoring system was developed based on the main phenotypes observed in the *Mecp2-null* mouse model: activity, gait, hind-limb clasping, breathing, tremor and general condition (Guy *et al*, 2007). In addition to overt neurological phenotypes, behavioural phenotypes such as significantly reduced activity, impaired motor function, increased anxiety, learning and memory defects, and impaired social interaction can be robustly detected in *Mecp2* mutant models. Histological examination of brain tissue and electrophysiology in the mice at different stages of development and in different mutant models has recapitulated the findings in patients. RTT models have enabled researchers to interrogate the neuropathology of RTT further without the restriction of non-invasive methods or analysis of post-mortem tissue.

1.2 Neurobiology of MeCP2

1.2.1 Neuropathology in the RTT brain and mouse model

The profound neurological phenotype of RTT implies that the predominant role of MeCP2 is in the central nervous system where the major morphological abnormality is reduced brain size. Autopsies revealed that the brain weight of RTT patients is 12-34% reduced compared to age matched unaffected individuals (Jellinger *et al*, 1988). Although there is an overall growth reduction in RTT (Schultz *et al*, 1993), compared to other organs the brain weighs significantly less than expected for a patients' height, suggesting that the brain is preferentially affected (Armstrong *et al*, 1999). RTT girls are born with a normal head circumference and deceleration (largely driven by growth of brain tissue) begins around 3 months of age (Schultz *et al*, 1993). Although head growth impairments are even more extreme in hemizygous males with *MECP2* loss-of-function mutations who present with neonatal-onset progressive encephalopathy, prenatal development of these boys remains normal, head circumference is within the normal range for gestational age (Schüle *et al*, 2008). The decelerated brain weight phenotype is recapitulated in *Mecp2-null* mice (Chen *et al*, 2001). Brain weight becomes progressively reduced compared to WT during postnatal development.

In general postnatal attenuation of brain growth arises due to disruptions in later-stage neurodevelopmental processes (neuronal arborization, synaptogenesis, gliogenesis, pruning and myelination), whereas, prenatal brain growth impairments are more likely to reflect disruptions in neurogenesis which is largely complete at birth in humans (van Dyck & Morrow, 2017). Postnatal microcephaly may raise concern about juvenile onset neurodegeneration. However, growth stabilizes in RTT following the period of deceleration and no progressive decline in brain weight is observed throughout the lifetime of a patient, suggesting that neurodegeneration is not the mechanism (Armstrong *et al*, 1995, 1999). This is consistent with there being no evidence of progressive loss of cognition or the appearance of dementia in RTT girls following the stabilization of regression (Kerr *et al*, 1987).

In an attempt to determine why the RTT brain is reduced in size, no obvious signs of degeneration, change in neuron number, migration defects, alteration in myelin, or changes in glia have been detected (Armstrong, 2005; Jellinger *et al*, 1988). To rule out subtle impairments in neurogenesis, neural progenitor cells have been isolated from embryonic or mature (6 week old) *Mecp2-null* mice and differentiated in culture (Kishi & Macklis, 2004; Smrt *et al*, 2007). *Mecp2-null* precursors were found to be indistinguishable to WT cells in their ability to proliferate and differentiate into neurons and glia. What is apparent in RTT patient and *Mecp2-null* mice brains is a reduction in neuronal size and increased cell packing density (Bauman *et al*, 1995; Chen *et al*, 2001). Analysis of neuron morphology has reproducibly identified reduced dendritic length and branching patterns as well as reduced dendritic spine density and altered spine morphology (Armstrong *et al*, 1995; Belichenko *et al*, 1994; Chapleau *et al*, 2009; Belichenko *et al*, 2009b; Kishi & Macklis, 2004; Smrt *et al*, 2007; Fukuda *et al*, 2005). In male patients with neonatal encephalopathy, the reduced dendritic complexity is more severe compared to the RTT brain (Schüle *et al*, 2008). Reduced number of dendritic spines (postsynaptic neuronal protrusions that receive input from axons at the synapse), suggests a reduction in synaptic input which could contribute to the neurological dysfunction in RTT. Furthermore, the remaining spines have altered morphology: decreased spine head size and increased spine neck length (Belichenko *et al*, 2009b), which further suggests alterations in synaptic contacts. Presynaptically, a reduction in the number of excitatory glutamatergic synapses has been identified in

primary neuronal cultures from *Mecp2-null* mice and *in vivo* in the hippocampus during early postnatal development but less apparent later in development (Chao *et al*, 2007). Abnormalities in axonal targeting of *Mecp2* mutant mouse models have also been reported (Belichenko *et al*, 2009b; Matarazzo *et al*, 2004; Degano *et al*, 2009).

1.2.2 Neurophysiological abnormalities in the RTT brain and mouse model

In support of synaptic dysfunction and hypoconnectivity, neurochemical studies have revealed reduced levels of neurotransmitters, their receptors, neuromodulators, and transporters across multiple systems in the *Mecp2*-deficient brain (reviewed in: Gadalla *et al*, 2011; Pozzo-Miller *et al*, 2015). Findings in RTT patient samples are inconsistent and depend on the age of the patient and severity of symptoms (Armstrong, 2001, 2005).

Neurophysiological studies of RTT patients show evidence of dysfunction of the central and autonomic nervous systems. Symptomatic RTT patients invariably have an abnormal electroencephalogram (EEG)(reviewed in Glaze, 2005). There are no diagnostic EEG patterns, but certain characteristic EEG patterns have been described to commonly occur in RTT patients including: generalized background slowing, loss of occipital rhythm during wakefulness and diminished sleep characteristics. Epileptiform abnormalities occur frequently and are most prominent during the latter part of clinical stage 2 (regression) and early stage 3 (stabilisation). This coincides with when seizures are frequently reported. Autonomic nervous system dysfunction is evident from increased incidence of long Q-T intervals during electrocardiographic recordings and diminished heart rate variability (Glaze, 2005). Seizure incidence is low in RTT mouse models, however, these mice display spontaneous irregular EEG discharges similar to RTT patients (D'Cruz *et al*, 2010; Goffin *et al*, 2012). Similarly, abnormal EEG hyperexcitability is observed in mice with *Mecp2* deleted in inhibitory neurons (Chao *et al*, 2010).

At the microcircuit level, loss of MeCP2 results in complex alterations in the excitation to inhibition (E/I) synaptic balance. Consistently, MeCP2 loss has been shown to lead to cortical hypoexcitability resulting from decreased excitatory neurotransmission

and/or increased inhibitory neurotransmission (Dani *et al*, 2005; Wood & Shepherd, 2010; Nelson *et al*, 2006; Durand *et al*, 2012; Sceniak *et al*, 2016). In contrast, subcortical areas of the hippocampus and hindbrain display a shift in E/I balance towards hyperexcitability (Calfa *et al*, 2015; Zhang *et al*, 2008; Medrihan *et al*, 2008; Taneja *et al*, 2009; Kline *et al*, 2010; Abdala *et al*, 2010; Kron *et al*, 2012). Maintaining the excitatory/inhibition (E/I) balance is essential for neuronal network function. The regional patterns of destabilization accord well with the clinical features of RTT (Katz *et al*, 2016).

Several laboratories have detected impairments in long-term potentiation (LTP) and long-term depression (LTD), cellular mechanisms of prolonged synaptic plasticity central to learning and memory, in MeCP2 deficient brain slices (Asaka *et al*, 2006; Guy *et al*, 2007; Weng *et al*, 2011; Goffin *et al*, 2012). In pre-symptomatic mice, synaptic plasticity appears normal but shows progressive impairment in older symptomatic mice (Guy *et al*, 2007; Weng *et al*, 2011). It is clear from morphological and neurophysiological findings that RTT can be considered a synaptopathy (disease of the synapse). The exact mechanism by which absence of functional MeCP2 produces a synaptic defect remains to be determined.

1.2.3 Upregulation of MeCP2 during neuronal maturation

The spatial and temporal expression of *MECP2* endorses the hypothesis that RTT is a disease of the nervous system, furthermore, a disease of neuronal maturation and maintenance. The expression of MeCP2 is dynamic during brain development where it increases through embryonic and postnatal development and plateaus at around 10 years in humans (Shahbazian *et al*, 2002a), and 5 weeks in mice (Skene *et al*, 2010). The upregulation of the expression of MeCP2 coincides with the maturation of post-migratory neurons as opposed to differentiating neural progenitors (Kishi & Macklis, 2004; Shahbazian *et al*, 2002a; Akbarian *et al*, 2001; Mullaney *et al*, 2004; Jung *et al*, 2003). Cortical development proceeds in an "inside-out" formation: neurogenesis occurs in the ventricular zone (VZ) and post-mitotic neurons migrate away from the proliferative regions (Stiles & Jernigan, 2010). Neurons occupying deep cortical layers migrate first and later-born neurons move past these older neurons to form the more

superficial cortical layers. MeCP2 is progressively upregulated in the deep cortical layers followed by the later migrating superficial layers (Kishi & Macklis, 2004; Shahbazian *et al*, 2002a). MeCP2 expression has also been shown to track maturation gradients in other brain regions including: olfactory neurons and the cerebellum (Cohen *et al*, 2003; Mullaney *et al*, 2004). The increase in MeCP2 levels during differentiation can be recapitulated during *in vitro* differentiation of neuronal precursors derived from mouse embryos (Kishi & Macklis, 2004). Neuronal precursors were differentiated into neurons and glia and MeCP2 levels increased progressively in neurons during differentiation but not in glia. The high abundance and upregulation of MeCP2 levels during neuronal maturation and the sustained high levels of MeCP2 in the developed brain (Skene *et al*, 2010), is consistent with a hypothesis that MeCP2 plays an important role in both the establishment and maintenance of mature neurons.

1.2.4 Does MeCP2 have a role in neuronal maturation and or maintenance?

As neurons mature, dendritic arborization increases. Reduced dendritic complexity of RTT neurons does point towards a defect in neuronal maturation. Tracking the morphological changes in the *Mecp2-null* mouse brain found that cortical thickness and neuronal density of 4, 6 and 8 week old mice did not differ from 2 week old WT mice consistent with a maturation arrest (Fukuda *et al*, 2005). Studies in the olfactory system, an area that undergoes continuous neurogenesis, of *Mecp2-null* mice have reported a transient delay in terminal differentiation characterised by more neurons expressing immature developmental stage-specific markers, impaired synaptic connectivity and disorganised axonal targeting (Matarazzo *et al*, 2004; Degano *et al*, 2009; Palmer *et al*, 2008). Other studies in the hippocampus have suggested that an immature neuronal state persists into adulthood consistent with the notion of maturation arrest (Smrt *et al*, 2007). Overall, there is a body of evidence to suggest that neuronal maturation is impaired in RTT.

Does the loss of MeCP2 during development cause irrevocable damage to neurons? Is MeCP2 needed for the maintenance of neuronal function of mature neurons? To

explore these outstanding questions further, Guy and colleagues (2007) carried out a powerful genetic study where the *Mecp2* gene was silenced by a *floxed* transcriptional *Stop* cassette (*Mecp2*^{Stop}) and then reactivated in the adult symptomatic brain using ligand-regulated site-specific recombination (Logie & Stewart, 1995). The *Mecp2*^{Stop} allele was combined with an ubiquitously expressed transgene encoding a fusion protein where Cre recombinase is fused to a mutant estrogen receptor (Cre-ER^{TM}) (Hayashi & McMahon, 2002). The Cre-ER^{TM} protein remains sequestered in the cytoplasm until exposed to the estrogen analog tamoxifen, which binds to the Cre-ER^{TM} and causes its nuclear translocation where Cre can then interact with the *Mecp2*^{Stop} allele. Excitingly, reactivation of *Mecp2* in mice with advanced symptoms leads to the reversal of the majority of the neurological phenotypes including premature lethality in hemizygous males. A follow up study assessed the reversal of breathing phenotypes and motor impairments of hemizygous *Mecp2*$^{Stop/y}$ mice following reactivation in more detail as well as the reversibility of RTT-like morphological abnormalities (Robinson *et al*, 2012). Near-complete reversal of dysrhythmias and reduced frequency of abnormal sigh-like breaths was achieved upon reactivation of *Mecp2*. Motor coordination and balance was significantly improved (assessed by a wide range of tasks) however, defects in gait persisted. Following reactivation, morphological abnormalities including neuronal soma size, dendritic length, complexity and spine density were significantly improved, approaching or reaching WT levels. Interestingly, despite reversal of morphological abnormalities, cortical thickness was not significantly reversed, suggesting that the structural plasticity at the cellular level was not relayed to the tissue and surrounding skull. Rapid reactivation of *Mecp2* over days instead of weeks was lethal (Guy *et al*, 2007), a possible explanation being that the brain cannot cope with rapid remodelling of MeCP2 deficient neurons. Overall, this pivotal experiment showed that according to the behavioural and physiological evaluation done so far following reactivation of *Mecp2* in the mature brain, there is no irrevocable neurological damage from the lack of MeCP2 during development.

An interpretation of the reversibility of RTT-like neurological phenotypes when *Mecp2* is reactivated in the adult mouse brain could be that the introduction of MeCP2 reinvigorates stalled neurodevelopmental process. The molecular preconditions for

MeCP2 function, and indeed "normal" neurological function are not lost. What was not determined was whether MeCP2 is required to maintain proper neuronal function in mature neurons throughout life. The high expression level of MeCP2 throughout adulthood in mice does suggest a continued importance of MeCP2 (Skene *et al*, 2010). To address this knowledge gap, mouse models of adult onset RTT were generated (McGraw *et al*, 2011; Cheval *et al*, 2012; Nguyen *et al*, 2012; Du *et al*, 2016). Male mice with intact *Mecp2* expression during development but later inactivated in the adult brain developed RTT-like symptoms similar in severity and progression to germline *Mecp2-null* mice. Remarkably, deletion of *Mecp2* in adult mice led to a significant shrinkage of the brain, compaction of neuronal cell bodies and reduction in dendritic complexity similar to the anatomical abnormalities in the *Mecp2-null* mice (Nguyen *et al*, 2012; Du *et al*, 2016). Tracking the effects of switching off the *Mecp2* gene over time, showed that MeCP2 depletion led to the retraction of already existing dendrites (Nguyen *et al*, 2012). These studies show that MeCP2 function during development is not sufficient to prevent disease in adult animals when MeCP2 is taken away. The temporal association of disease onset with postnatal development seems to be unrelated to a role of MeCP2 to set up an epigenetic program during a defined developmental stage. The discrepancy between the onset of neurological symptoms in developmental time in humans and in mice supports this. Instead, MeCP2 is required to maintain function of neurons throughout life.

1.2.5 Importance of MeCP2 in different brain regions or neuronal subtypes

RTT patients and MeCP2 deficient mice show a range of neurological symptoms that are not linked functionally to particular brain regions. Morphological and neurotransmission defects in the MeCP2 deficient brain do not appear to be regional. The relative reduction of brain volume has been suggested to be more in the cerebral hemispheres than the cerebellum (Armstrong, 2005). MeCP2 is expressed throughout the brain however expression is significantly lower in the cerebellum compared to the forebrain, midbrain and spinal cord (Ross *et al*, 2016), highlighting an interesting correlation between MeCP2 protein level and relative growth impairment. The brain functions via large networks of both neurons and glia, therefore, a defect in one cell

type could result in dysfunction of the entire network which might not be directly sensitive to the loss of MeCP2. The conditional *Mecp2* KO (cKO) mouse and *Mecp2*^{Stop} reactivation lines have been extensively used to determine the importance of MeCP2 in different cell types and brain regions, by crossing these modified lines to transgenic Cre driver lines which express Cre from different cell-type specific promoters.

Overall, the deletion of MeCP2 in different brain regions and neuronal cell types leads to phenotypes associated with compromised neuronal function in that region for example: *Mecp2* knockout in forebrain excitatory neurons (CamKII-Cre) leads to impaired motor coordination, increase anxiety and impaired social behaviour (Chen *et al*, 2001; Gemelli *et al*, 2006). MeCP2 loss in regions of the hypothalamus (Sim1-Cre) leads to an abnormal stress response, hyperphagia and increased aggression (Fyffe *et al*, 2008). Deletion in the brainstem and spinal cord leads to abnormal breathing in response to hypoxia challenge, decreased basal heart rate and early lethality (Ward *et al*, 2011). *Mecp2* deletion in all major cell types in the cerebellum caused a comparatively mild motor learning delay phenotype that was overcome with additional training (Achilly *et al*, 2021).

Mecp2 has been deleted in different neurotransmission systems to analyse their contribution to the RTT-like phenotype. Mice lacking MeCP2 in neurons expressing dopamine, adrenaline, or serotonin neurotransmitters, which have restricted roles and pathways in the CNS, have a small number of mild phenotypes and a normal life-span (Samaco *et al*, 2009). In contrast *Mecp2* deletion in GABAergic inhibitory neurons, the major inhibitory neurons ubiquitous throughout the brain, closely recapitulates the *Mecp2-null* phenotype with delayed symptom onset of ~5 weeks, progressive motor dysfunction, impaired cognition, repetitive behaviours, abnormal EEG hyperexcitability, respiratory dysfunction and premature lethality (~50% survival at 26 weeks) (Chao *et al*, 2010). An additional phenotype observed in these cKO mice not usually seen in *Mecp2-null* mice is overgrooming and self-mutilation. The severe phenotype likely reflects the dependence of all brain circuits on GABAergic inhibitory neurons. GABAergic neurons have been suggested to contribute to 80% of the workload of the brain (Goffin & Zhou, 2012). *Mecp2* deletion in the major excitatory

neurons in the brain, glutamatergic neurons, leads to anxiety and tremor phenotypes that are distinct from those revealed upon *Mecp2* deletion in inhibitory neurons along with ataxia, acoustic startle deficits and premature lethality (Meng *et al*, 2016). Restoring MeCP2 levels in GABAergic or glutamatergic neurons using the Mecp2^{Stop} conditional rescue mouse line, leads to rescue of the phenotypes seen in the cKOs (Meng *et al*, 2016; Ure *et al*, 2016). Survival was similarly improved but not fully rescued by restoring MeCP2 expression in either inhibitory or excitatory neurons showing that a normal lifespan is dependent upon both neuron types (Meng *et al*, 2016; Ure *et al*, 2016). Other phenotypes not rescued by restoration of MeCP2 in either excitatory or inhibitory neurons and therefore dependent upon both types of neuron included laboured breathing and ataxia. These studies suggest that loss of MeCP2 alters the overall excitation/inhibition balance in brain circuits with greater emphasis on GABAergic neurons.

The identification of an anatomically restricted region within the brain in which restoration of MeCP2 function would lead to dramatic phenotypic reversal has important implications for therapeutics. Regional deletion experiments suggest that localized disruption in different brain regions or systems results in a subset of the commonly observed RTT symptoms. The GABAergic neuronal subtype does seem to be particularly sensitive to MeCP2 loss. Caution must be taken when drawing conclusions from the cKO models as specificity of transgenic Cre line can be imperfect and further complicate the picture.

1.2.6 Cell-autonomous function of MeCP2

Mosaic expression of MeCP2 in the female heterozygous brain due to X chromosome inactivation causes a RTT phenotype. The primary cause of RTT could be cell autonomous, where the mosaic distribution of MeCP2-negative (MeCP2–) dysfunctional neurons amongst MeCP2-positive (MeCP2+) functional neurons compromises the entire neuronal network. Alternatively, MeCP2– neurons could impact the function of surrounding MeCP2+ neurons through non-cell-autonomous mechanisms. The dramatic difference in severity between hemizygous males with *MECP2* mutations compared to heterozygous females suggests that the functionality

of MeCP2+ neurons prevents premature lethality and improves neuronal function. Additionally, the phenotypic reversibility by reactivation of *Mecp2* in the heterozygous *Mecp2*$^{Stop/+}$ mice suggests that any non-cell autonomous action of MeCP2 is also reversable upon restoration of MeCP2 to MeCP2– cells.

Biochemical analysis in cKO models has highlighted the cell-autonomous action of MeCP2, illustrated by a reduction in neurotransmission, neurotransmitter content and expression of enzymes involved in neurotransmitter biosynthesis specifically in MeCP2– cells compared to controls and other regional cKO models (Chao *et al*, 2010; Samaco *et al*, 2009). In the GABAergic inhibitory neuron cKO, miniature inhibitory postsynaptic currents (mIPSCs) were reduced in amplitude and charge in cortical brain slices, whereas, miniature excitatory postsynaptic currents (mEPSCs) were similar to controls, suggesting that MeCP2 deficiency in GABAergic neurons does not have a non-cell autonomous impact on synaptic function of glutamatergic excitatory neurons (Chao *et al*, 2010). Other studies focussing on the morphology of MeCP2+ neurons versus MeCP2– neurons have accumulated evidence supporting both cell-autonomous and non-cell-autonomous effects. Neuronal transplantation experiments where either *Mecp2-null* or WT neuroblasts were transplanted into either *Mecp2-null* or WT recipients showed that the complexity of dendritic morphology and soma size were predominantly effected by cell-autonomous action of MeCP2 (Kishi & Macklis, 2010). Analysis of neuronal morphology in the heterozygous female brain compared to WT and *Mecp2-null* male brain suggests that MeCP2– neurons measurably impact the dendritic structure of MeCP2+ neurons (Belichenko *et al*, 2009a). Also, findings of subtle differences between MeCP2– neurons in the female and MeCP2– neurons in the hemizygous male suggest MeCP2+ neurons could slightly mitigate the effect of MeCP2 deficiency, although males and females were not age matched for this analysis so age-related effects could explain this difference. One study suggests that MeCP2– neurons could negatively impact the expression level of MeCP2 in the surrounding MeCP2+ neurons in the MeCP2+/– heterozygote (Braunschweig *et al*, 2004). Finally, there is evidence that MeCP2+ glia can have positive effects on MeCP2– neurons (Ballas *et al*, 2009)(see below). Collectively, although the major mechanism of neuronal dysfunction in RTT is likely cell-autonomous there is evidence of non-cell-

autonomous effects on surrounding MeCP2+ cells. This is perhaps unsurprising considering the brain is a complex network of cells communicating with one another.

1.2.7 MeCP2 in non-neuronal cells in the brain

Quantitative western blotting in NeuN (neuronal marker) positive nuclei from the adult mouse brain, estimated that the MeCP2 level in non-neuronal nuclei is ~6-8-fold lower than in non-neuronal nuclei (Skene *et al*, 2010). Glial cells in the central nervous system consist of astrocytes, oligodendrocytes and microglia which perform a vast array of essential roles to maintain and optimise CNS function and their dysfunction have been implicated in the pathology of neurological disease. Astrocytes promote neuronal maturation, synaptogenesis and neuronal survival during development, they regulate levels of ions and neurotransmitters, and provide metabolic and structural support at the synapse as well as contribute to the integrity of the blood-brain barrier (Wang & Bordey, 2008). Oligodendrocytes are the myelinating cells in the brain (Baumann & Pham-Dinh, 2001). Finally, microglia are the inflammatory cells of the brain with important roles in brain development and adult neuronal plasticity and function through continuously remodelling of neuronal circuits (Tremblay *et al*, 2011).

Hippocampal astrocytes of *Mecp2-null* mice like neurons show a reduced morphological complexity (Nguyen *et al*, 2012). Conditional deletion of *Mecp2* in astrocytes had minor phenotypic consequences, whereas, restoration of MeCP2 in astrocytes only, prolonged lifespan, normalized breathing defects, and partially rescued locomotion and anxiety compared to *Mecp2-null* mice (Lioy *et al*, 2011). This result together with the inability of restoration of MeCP2 in GABAergic or glutamatergic circuits to correct breathing phenotypes and survival discussed above suggests that breathing and normal lifespan could rely on the interplay between proper excitation, inhibition and astrocyte function (Meng *et al*, 2016; Ure *et al*, 2016). Restoration of MeCP2 in astrocytes identified a non-cell-autonomous positive effect on dendritic morphology of *Mecp2-null* neurons *in vivo* which had also been observed in primary co-culture experiments (Ballas *et al*, 2009). Inversely, co-culture of *Mecp2-null* astrocytes with WT neurons was shown to have a negative effect on

dendritic morphology: WT neurons had fewer and shorter processes than those cultured with WT astrocytes.

Mice lacking MeCP2 in oligodendrocytes, the myelinating cells in the brain, develop a severe hindlimb clasp indicative of general neurological disease (Nguyen *et al*, 2013). Restoration of MeCP2 expression exclusively in oligodendrocytes in otherwise *Mecp2-null* mice, mildly prolonged lifespan, normalised weight, and significantly improved hindlimb clasping and locomotor deficits.

Genetic restoration of MeCP2 expression in microglia on a *Mecp2-null* background was reported to lead to improvements in overall appearance and growth, substantially prolonged lifespan, and significantly reduced apnoea and breathing irregularities (Derecki *et al*, 2012). Derecki and colleagues (2012), performed bone marrow transplants (BMT) containing WT microglia into irradiated *Mecp2-null* mice and reported an amelioration of some of the RTT-like phenotypes and significantly prolonged lifespan. However, both of these findings were completely contradicted by a later study that could not reproduce these results (Wang *et al*, 2015). Despite successful microglial engraftment, BMTs from WT donors did not rescue the *Mecp2-null* phenotype. Furthermore, using a different Cre driver to activate *Mecp2* expression in microglia on *Mecp2-null* background did not achieve significant amelioration of RTT-like phenotypes in contrast to the previous findings. The discrepancy was shown to be due to off-target neuronal expression of the *LysM-Cre* transgene used by Derecki and colleagues (2012). These findings show that the role of microglia in RTT pathology is controversial and emphasises the importance of careful characterisation of Cre transgene expression.

Collectively, the minor phenotypes associated with MeCP2 deficient glia suggests that MeCP2 loss in neurons is the dominant driver of the RTT. Although, amelioration of breathing abnormalities when MeCP2 expression is restored in astrocytes, highlights, that astrocytes should not be overlooked in therapeutic design as breathing impairments are common debilitating symptoms of RTT.

1.2.8 Importance of MeCP2 in peripheral tissues

MeCP2 is ubiquitously expressed however is much less abundant in peripheral tissues compared to the brain. MeCP2 is approximately 10-fold as abundant in the brain compared to other tissues in the mouse including: heart, lung, liver, kidney, spleen and skeletal muscle (Ross *et al*, 2016). Deletion of *Mecp2* exclusively in the CNS phenocopies *Mecp2*-null mice illustrating that CNS dysfunction is the major contributor to RTT phenotypes (Guy *et al*, 2001; Chen *et al*, 2001). These studies assessed gross aspects of the RTT-like phenotypes such as survival, brain weight and body weight. Subsequent studies have identified phenotypes which reflect dysfunction of peripheral systems as a result of global MeCP2 deficiency such as cardiac abnormalities (Panighini *et al*, 2013; McCauley *et al*, 2011), lung lesions (De Felice *et al*, 2010), fatty liver and metabolic disease (Kyle *et al*, 2016; Buchovecky *et al*, 2013), adverse bone health (O'Connor *et al*, 2009; Kamal *et al*, 2015), and skeletal muscle defects (Conti *et al*, 2015). It is difficult to determine whether these symptoms arise as a consequence of impaired function of the nervous system or whether they have genuine peripheral origin.

It is possible that the premature lethality of the *Mecp2-null* model masks the peripheral phenotypes which might be subtle or delayed in onset. To address this problem mice were generated where *Mecp2* was silenced in peripheral tissues and reactivated prenatally in the nervous system (Ross *et al*, 2016). This was achieved using *Nes-cre* mediated activation of the $Mecp2^{Stop}$ allele predominantly in neuronal and glial precursors in the developing central nervous system. This study revealed that the key features of RTT, including breathing, balance and gait abnormalities, can be attributed to MeCP2 loss in the nervous system, however, less severe but clinically relevant symptoms such as pronounced exercise fatigue, and RTT-like bone defects result from lack of MeCP2 in peripheral tissues (Ross *et al*, 2016). In agreement with this: there is evidence of a cell-autonomous role of MeCP2 in the function of osteoblasts (Blue *et al*, 2015). No abnormalities in cardiac or respiratory measures, or skeletal muscle morphology and innervation were detected in the peripheral *Mecp2* KO (PKO) mice compared to WT mice (Ross *et al*, 2016). Accordingly, skeletal muscle phenotypes observed in the whole body *Mecp2* KO were not recapitulated in the conditional mouse

model selectively depleted of *Mecp2* in skeletal muscles (Conti *et al*, 2015). Elevated serum cholesterol levels reported in *Mecp2-null* mice and the liver specific *Mecp2* cKO mice (Buchovecky *et al*, 2013; Kyle *et al*, 2016), were not recapitulated in the PKO mouse (Ross *et al*, 2016). The dysregulation of cholesterol metabolism in the liver is not consistently observed in different strains of *Mecp2*-null mice (Buchovecky *et al*, 2013), questioning its relevance to RTT. Other phenotypes of metabolic dysfunction reported in the *Mecp2-null* mouse such as insulin resistance, glucose intolerance, and increased circulating fatty acids and glycerol did not arise from selective deletion of *Mecp2* in the liver (Kyle *et al*, 2016). Overall, loss of *Mecp2* from the brain is responsible for the majority of RTT-like behavioural, sensorimotor and autonomic phenotypes, therefore, the nervous system should be the main target for therapeutics. Less prominent aspects of the disorder such as stamina and bone abnormalities are at least partially caused by lack of MeCP2 in the periphery, and these phenotypes may therefore benefit from systemic interventions.

1.3 Molecular role of MeCP2

1.3.1 MeCP2 is a reader of the DNA methylome

The MeCP2 protein was initially identified through its ability to bind to methylated CG (mCG) dinucleotides by Southwestern assay (Lewis *et al*, 1992). The Methyl-CpG binding domain (MBD) was identified to be responsible for methylated DNA binding (Figure 1.3.1)(Nan *et al*, 1993). Evidence now suggests that MeCP2 does not exclusively recognise mCG dinucleotides but also binds to mCAC trinucleotides and to a lesser extent mCAT (Lagger *et al*, 2017). Non-CG methylation (mCH where H=A/C/T) is enriched in the brain where it approaches the level of mCG methylation (Lister *et al*, 2013). Motif analysis has identified a prominent preference of mCH for the mCAC trinucleotide in both mouse and human neurons (Guo *et al*, 2014; Varley *et al*, 2013). Unlike mCG which remains relatively stable during development, mCH accumulates during postnatal development coinciding with neuronal maturation and interestingly MeCP2 upregulation (Skene *et al*, 2010; Lister *et al*, 2013; Shahbazian *et al*, 2002a). mCH patterns are more variable between neuronal subtypes compared to mCG patterns suggesting it has a pronounced role in cell-type specific patterns of

gene expression (Mo *et al*, 2015; Renthal *et al*, 2018). As expected from the high abundance of MeCP2 in neurons (~16 x 10^6 molecules per neuronal nucleus) and the number of potential binding sites, MeCP2 binds globally throughout the genome and tracks methylation density according to Chromatin Immunoprecipitation (ChIP) and whole genome bisulfide (WGBS) experiments (Skene *et al*, 2010; Kinde *et al*, 2016; Lagger *et al*, 2017). MeCP2 has therefore been postulated to have a role in global gene repression in mature neurons in the brain by reading both mCG and mCAC methylation.

Disruption of binding of MeCP2 to methylated DNA is sufficient to cause RTT. There are many RTT-causing missense mutations which map to the MBD most of which have been determined to impair binding to methylated DNA and in addition many mutations reduce protein stability (reviewed in Tillotson & Bird, 2020). Both impaired DNA binding and instability contribute to the disease phenotype. Knock-in mouse models of MBD mutations; R106W, Y120D, T158M, T158A and R133C show that these mutations both disrupt methylated DNA binding and protein stability to variable degrees and cause a RTT-like phenotype (Gandaglia *et al*, 2019; Johnson *et al*, 2017; Brown *et al*, 2016; Lamonica *et al*, 2017; Goffin *et al*, 2012). Transgenic mice expressing $MeCP2^{R111G}$ at WT levels phenocopy *Mecp2-null* mice showing that loss of DNA binding alone is sufficient to cause RTT (Heckman *et al*, 2014). Accordingly, mice expressing reduced levels of WT MeCP2 protein have a milder phenotype than mice expressing similar levels of mutant proteins (Kerr *et al*, 2008; Samaco *et al*, 2008).

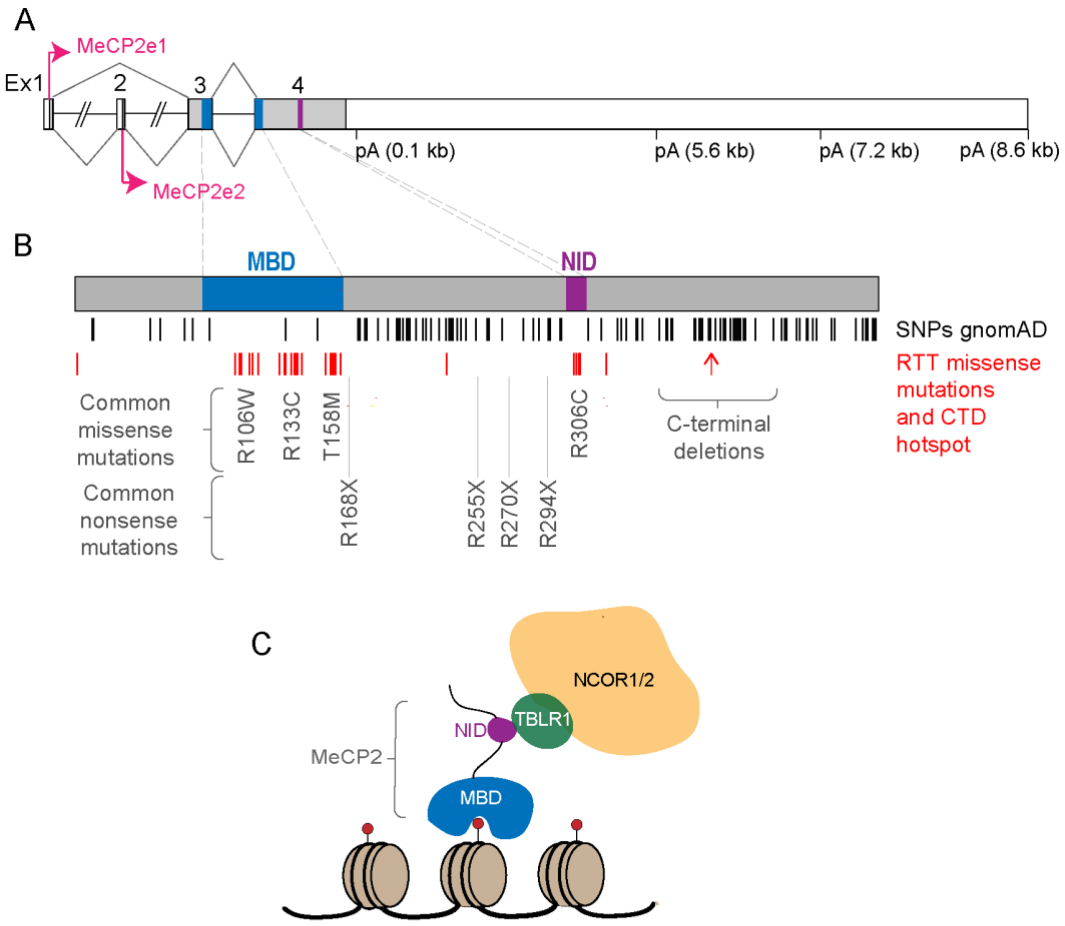

Figure 1.3.1. The *MECP2* gene structure, RTT-causing missense mutation spectrum and MeCP2 protein function. A) Schematic diagram of the *MECP2* gene comprising of four exons which are alternatively spliced to form the e1 and e2 isoforms. Isoform e1 mRNA is formed from splicing together exons 1, 3 and 4. The protein is translated from the AUG in exon 1. Isoform e2 mRNA is formed from splicing together all four exons and the protein is translated from the AUG in exon 2. Alternative polyadenylation termination sites (pA) in the 3'UTR are used by either isoform. Exon 3 and 4 contain the majority of the protein coding sequence including the two functional domains: the Methyl-CpG binding domain (MBD) and the NCOR1/2 interaction domain (NID). B) Schematic diagram of the coding region of *MECP2* aligned with the neutral variants found in healthy males in the gnomAD database (black lines), RTT-causing missense mutations (red lines) and the C-terminal deletion mutation hotspot (red arrow). The positions of common missense, nonsense and C-terminal deletions are annotated. The diagram is adapted from: Tillotson R & Bird A (2020). C) MeCP2 has been proposed to function as a bridge between methylated DNA and the NCOR1/2 co-repressor complex. MeCP2 binds to methylated cytosine (red circles) via the MBD and binds to TBLR1 a core component of the NCOR1/2 complex via the NID.

1.3.2 MeCP2 regulates DNA methylation-dependent gene expression

A large body of evidence supports the notion that the role of MeCP2 is to mediate DNA methylation-dependent gene expression. Transfection experiments using methylated reporter constructs have illustrated mCG or mCH methylation-dependent

repression by MeCP2 (Nan *et al*, 1997, 1998; Guy *et al*, 2001; Lyst *et al*, 2013; Guo *et al*, 2014). Gene expression analysis in the *Mecp2-null* brain revealed subtle gene expression changes at a large number of genes in both directions: genes become both upregulated and downregulated (Tudor *et al*, 2002; Chahrour *et al*, 2008). In mice overexpressing MeCP2, the opposite expression patterns were observed, genes that were upregulated in the *Mecp2-null* model were downregulated in the overexpression model (Chahrour *et al*, 2008). Integrating MeCP2 ChIP-seq data from WT brain samples and RNA-seq data in the *Mecp2-null* brain samples identified that the upregulated genes have a higher enrichment of MeCP2 binding and the downregulated genes have a lower enrichment, suggesting that the upregulation of genes is due to a loss of the direct repression of MeCP2 at these genes and the downregulation of genes is an indirect consequence of MeCP2 loss (Kinde *et al*, 2016; Lagger *et al*, 2017). The magnitude of upregulation of gene expression has been shown to correlate with the density of both mCG and mCA sites (Lagger *et al*, 2017; Cholewa-waclaw *et al*, 2019; Gabel *et al*, 2015). Other studies suggest that the total number of MeCP2 binding sites per gene best predicts the degree of gene up-regulation (Kinde *et al*, 2016). Analysis of gene expression differences between mutant and WT neurons within the same human mosaic Rett Syndrome brain identified that cell-type-specific DNA methylation patterns predict the degree of gene mis-regulation in *MECP2* mutant neurons (Renthal *et al*, 2018).

1.3.3 MeCP2 recruits the NCOR1/2-corepressor complexes to methylated DNA

Early attempts to determine the region of MeCP2 responsible for transcriptional repression using fragments of MeCP2 fused to the GAL4 DNA-binding domain identified the broad transcriptional repression domain (TRD) situated towards the C-terminus of the protein (Nan *et al*, 1997). Comparing the RTT causing missense mutation spectrum (RettBase: http://mecp2.chw.edu.au) with sites of neutral polymorphisms in the general population (gnomAD https://gnomad.broadinstitute.org/) highlights two crucial functional domains of the MeCP2 protein: the MBD and a second discrete site within the TRD (Figure 1.3.1). The C-terminal cluster of mutations was found to destroy the interaction between

MeCP2 and the NCOR1/2 co-repressor complexes (Lyst *et al*, 2013). The crystal structure of the NCOR1/2 interaction domain (NID) and the WD40 domain of TBLR1 a core component of the NCOR1/2 confirmed that those residues mutated in RTT make key contacts with TBLR1 (Kruusvee *et al*, 2017). Knock-in mice carrying the most common RTT causing NID mutation R306C (accounts for 5% of all RTT cases) have the same phenotypic signature as other RTT models (Brown *et al*, 2016; Lyst *et al*, 2013). The pattern of transcriptional dysregulation in *Mecp2*^{R306C} mice is the same as in *Mecp2-null* mice (Gabel *et al*, 2015). Characterization of knock-in mice has revealed that NID mutations and MBD mutations are both sufficient to cause RTT. Additionally, NCOR1/2 recruitment via the NID of MeCP2 is essential for the overexpression phenotype as well as the *null* phenotype. Inserting the R306C NID mutation into the extra copy/copies of *Mecp2* in overexpression mouse models leads to complete rescue of premature lethality and behavioural phenotypes (Heckman *et al*, 2014; Koerner *et al*, 2018).

The importance of the MBD and the NID in the pathology of RTT has led to the "bridge hypothesis" which predicts that MeCP2 acts as a bridge between methylated DNA and the NCOR1/2 corepressor complex to mediate methylation-dependent gene expression in the brain (Figure 1.3.1). There have been multiple lines of enquiry to test this hypothesis. Investigation into the disease mechanism of RTT causing mutations which lie outside of the MBD and NID including 3 point mutations A2V, P225R and P322L and a cluster of C-terminal deletions do not uncover novel functions of MeCP2 but suggest that these mutations cause RTT by greatly reducing MeCP2 abundance (Martínez de Paz *et al*, 2019; Guy *et al*, 2018). In addition, the proline missense mutations also impair TBLR1 recruitment to methylated DNA. Other domains in the MeCP2 protein which have been assigned a function such as AT hook 1 and the NLS have been disrupted in mice with mild to no phenotypic consequences (Lyst *et al*, 2018; Xu *et al*, 2018). Knock-in mice expressing truncated versions of MeCP2 which lack the N terminus or C terminus of MeCP2 are indistinguishable from WT mice and mice expressing a radically truncated version (ΔNIC) which lacks the N, C and intervening domain of MeCP2 between the MBD and the NID (retained 32% of full-length MeCP2 protein sequence), have mild neurological defects but normal survival

(Tillotson *et al*, 2017). The ΔNIC protein is expressed at 50% of WT level and so neurological defects could be partially attributed to protein level.

An interpretation of the "bridge hypothesis" is that there might be mutations in components of the NCOR1/2 complex which break the bridge and cause RTT-like phenotypes. This is complicated by the fact that NCOR1/2 corepressors have been implicated in wide-ranging roles in development and metabolism including for example mediating transcriptional repression of thyroid hormone nuclear receptors in the absence of ligands. Core components of the NCOR1/2 complexes are essential for embryonic development (Jepsen *et al*, 2000, 2007; Bhaskara *et al*, 2008; Guo *et al*, 2015; Dickinson *et al*, 2016). MeCP2 can bind to TBLR1 and its paralog TBL1 which form a central TBLR1/TBL1 tetramer within the core corepressor complex (Oberoi *et al*, 2011). The phenotypic effects of mutations in either TBLR1 or TBL1 might be masked by functional redundancy between both proteins. The *TBLR1* gene is autosomal and *TBL1X*, the gene encoding TBL1, is X-linked but escapes X-inactivation (Bassi *et al*, 1999). Heterozygous mutations in either gene would not be expressed mosaically, unlike MeCP2 mutations, and therefore the associated phenotypes might differ. Nonetheless, missense mutations in TBLR1 but not TBL1X have been associated with intellectual disability (DECIPHER https://decipher.sanger.ac.uk/). Intriguingly, the heterozygous mutation D370N was identified in a patient diagnosed with RTT who does not have any mutations in MeCP2 (Zaghlula *et al*, 2018), suggesting that some mutations in TBLR1 can cause RTT, potentially by disrupting binding to only MeCP2 exclusively and having a dominant negative effect on the TBLR1/TBL1 tetramer. Furthermore, TBLR1 is the more abundant paralog in the brain (Spruijt *et al*, 2013), suggesting that it might have a predominant role in neuronal maintenance. Although this accumulated evidence suggests a predominant importance of the MBD and the NID for MeCP2 function, regions outside of these domains are highly conserved and could be required for more subtle functional differences, such as cognition, which might not have been vigorously tested in these different models. Accordingly, mutations in MeCP2 have been identified in patients with intellectual disability, autism and schizophrenia.

The importance of intact binding of MeCP2 methylated DNA and recruitment of NCOR1/2 to prevent global gene dysregulation and RTT is clear. Given the subtle changes in gene expression due to MeCP2 loss and the broad distribution of MeCP2 binding to chromatin, it has been challenging to decipher the mechanism of how MeCP2 together with NCOR1/2 mediate gene repression. The NCOR1/2 co-repressor complexes contain the histone deacetylase (HDAC) HDAC3, suggesting that in the absence of MeCP2, the upregulation of highly methylated genes may be a result of decreased HDAC3 activity. Increased global histone H3 acetylation levels in *Mecp2-null* and mutant neurons has been detected (Shahbazian *et al*, 2002c; Skene *et al*, 2010). Elegant ChIP-seq experiments have shown small but significant increases in acetylation marks known to be removed by HDAC3 specifically over the transcription start site (TSS) and gene bodies of genes that are upregulated in *Mecp2*^{R306C} mice (Boxer *et al*, 2020). The preferential repression of genes with high levels of gene body MeCP2 binding has led to the hypothesis that MeCP2 might function to impede transcriptional elongation of RNA polymerase II (Cholewa-waclaw *et al*, 2019; Kinde *et al*, 2016). In contrast, using genome-wide experimental measurements of transcriptional elongation and initiation rates in the WT and *Mecp2*-mutant brain, a recent study has suggested a model whereby MeCP2 inhibits transcriptional initiation, without having an effect on elongation (Figure 1.3.3)(Boxer *et al*, 2020). This model involves gene body-TSS chromatin contacts which position MeCP2 and NCOR1/2 close to the promoter to repress transcriptional initiation.

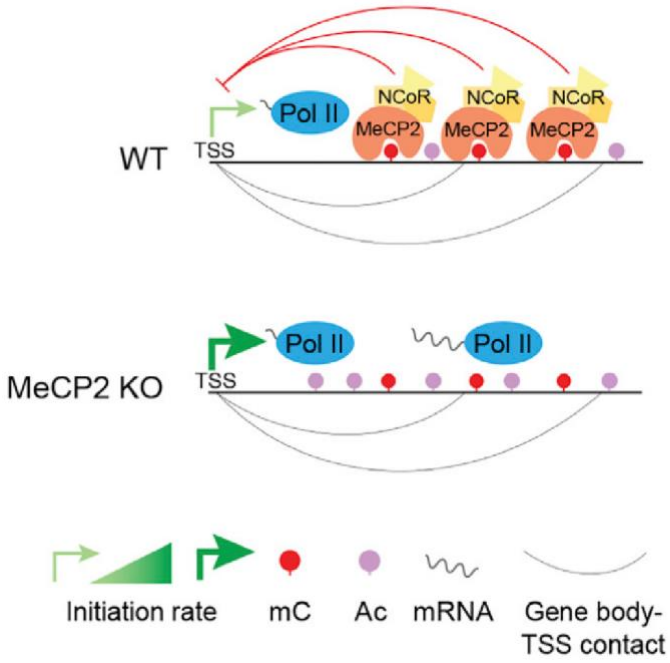

Figure 1.3.3. Model for MeCP2-dependent repression of transcription initiation of highly methylated genes. Schematic taken from Boxer LD et al., (2020) MeCP2 Represses the Rate of Transcriptional Initiation of Highly Methylated Long Genes. Mol. Cell 77: 294-309.e9

1.4 Causes of the phenotypic variability in Rett Syndrome

1.4.1 Genotype versus phenotype

Studies using genotypic and phenotypic information from large cohorts of RTT patients with known *MECP2* mutations have been instrumental in determining genotype-phenotype relationships. Phenotypic scoring systems including the Kerr (Kerr *et al*, 2001), Percy (Schanen *et al*, 2004) and Pineda (Monrós *et al*, 2001) scores have been established to define the clinical severity of RTT cases. Two seminal studies using data from InterRett (Bebbington *et al*, 2008) and from the US Natural History study (Neul *et al*, 2008) and later publications which further corroborated these findings (Bebbington *et al*, 2010, 2012; Cuddapah *et al*, 2014), identified that the *MECP2* mutations which are commonly associated with highest clinical severity are: large deletions and insertions, R106W, R270X, R255X, R168X as well as other early truncating mutations, whereas: R133C, R294X, R306C and C-terminal deletions produced less-severe phenotypes (Figure 1.4.1). When addressing RTT symptoms separately, individuals with mutations associated with more severe presentations were found to be less likely to reach early milestones and be diagnosed earlier (Fehr *et al*, 2011), have a more pronounced growth failure including decreased head

circumference (Tarquinio *et al*, 2012), have an earlier onset of scoliosis (Downs *et al*, 2016), and earlier onset and increased incidence and severity of seizures (Bao *et al*, 2013; Nissenkorn *et al*, 2015; Glaze *et al*, 2010). Relationships between breathing abnormalities and genotype remain largely unknown (Leonard *et al*, 2016). Individuals with mutations associated with milder presentations are more likely to use words before and after regression and regress later than those with severe mutations (Urbanowicz *et al*, 2015). The milder preserved speech variant form of RTT is most often associated with the R133C mutation or C-terminal deletions (Urbanowicz *et al*, 2015; De Bona *et al*, 2000). For very mild *MECP2* variants there is a fine line between classifying these individuals as individuals with or without RTT (Suter *et al*, 2014).

The development of inbred RTT mouse models has allowed in-depth molecular and phenotypic consequences of different *Mecp2* mutations to be investigated to determine how genotype-phenotype correlations can be explained by the degree of functionality of mutant MeCP2. Using the phenotypic severity score developed in the Bird lab (Guy *et al*, 2007), mouse models with different knock-in RTT patient mutations have been compared and the phenotypic severity spectrum recapitulates that observed in humans. Mice expressing the severe mutations R270X, R255X, R168X and R106W closely resemble *Mecp2-null* mice (Baker *et al*, 2013; Lawson-yuen *et al*, 2007; Pitcher *et al*, 2015; Johnson *et al*, 2017). On the other hand, mice with the milder mutations R133C, R294X, R306C and C-terminal deletions have a comparatively milder phenotype, shown clearly by increased survival and reduced phenotypic severity (Brown *et al*, 2016; Merritt *et al*, 2020; Guy *et al*, 2018).

As described in the previous section the functional consequence of each *Mecp2* mutation is determined by its effect on methylated DNA binding, NCOR1/2 recruitment and protein stability. Those mutations which cause a milder phenotype retain more MeCP2 function, for example the milder MeCP2^{R133C} has been shown to retain some ability to bind to DNA compared to the more severe MeCP2^{T158M} and is also more stable compared to MeCP2^{T158M} (R133C = 55% and T158M = 30% of WT protein level) (Brown *et al*, 2016). The R306C mutation described earlier disrupts NCOR1/2 binding and does not affect protein abundance, therefore, the milder phenotype compared to the *Mecp2-null* model is likely attributed to a slight retention

of NCOR1/2 recruitment. The disease causing mechanism of the two most common C-terminal truncation mutations (L386HfsX5 and P389X) which are commonly categorised as milder mutations were shown to be reduced protein and mRNA stability, their DNA binding and NCOR1/2 recruitment functions are intact (Guy *et al*, 2018) .

The severe RTT causing mutations which cause an *Mecp2-null*-like phenotype, tend to have little to no MeCP2 function and or very low abundance of the mutant protein. The early truncation mutations R168X and R255X dramatically reduce the protein abundance (Pitcher *et al*, 2015; Lawson-yuen *et al*, 2007). The R106W mutation was shown to both substantially reduce protein abundance (70-80% reduction) and also impair DNA binding. MeCP2^{R106W} had an even lower ability to bind to chromatin compared to MeCP2^{T158M} (Johnson *et al*, 2017). The R270X mutation truncates the MeCP2 protein before the NCOR1/2 interaction domain. In the *MECP2*^{R270X}-GFP transgenic mouse model, the MeCP2^{R270X}-GFP protein abundance and DNA binding was comparable to WT (Baker *et al*, 2013), but the MeCP2^{R270X}-GFP protein was shown to be defective in transcriptional repression. This shows that the *Mecp2-null*-like phenotype in this line is due to the inability of the truncated protein to recruit NCOR1/2. We are unable to determine the effect that the R270X mutation has on protein abundance from analysis in the transgenic model as the copy number of transgene integrations and effect of C-terminal GFP tag is unknown, however, the MeCP2^{R270X} protein is undetectable in post-mortem brains of patients, suggesting that this mutation does destabilise the protein (Pitcher *et al*, 2015).

In hemizygous male inbred mice with little genetic diversity the phenotypic severity directly correlates with genotype. However, in genetically diverse mosaic humans genotype does not solely explain the range of phenotypic variability observed in RTT. The full range of common mutations observed in typical RTT are also observed in atypical RTT individuals (Percy *et al*, 2010a; Cuddapah *et al*, 2014). In the most comprehensive genotype-phenotype study done to date, 38% of individuals with atypical RTT had one of the most common 8 point mutations (R106W, R133C, T158M, R168X, R255X, R270X, R294X, R306C), compared to 58% for typical RTT (Cuddapah *et al*, 2014). Overall, mutations associated with more severe cases of

typical RTT were even more severe in atypical RTT and those that were less severe in typical RTT were even less severe in atypical RTT (Figure 1.4.1)(Cuddapah *et al*, 2014). Thus, atypical RTT was found to represent either end of the phenotypic severity spectrum of RTT. These findings illustrate that an atypical presentation of RTT is not determined by a certain type of mutation, other factors besides genotype must influence this phenotypic variability.

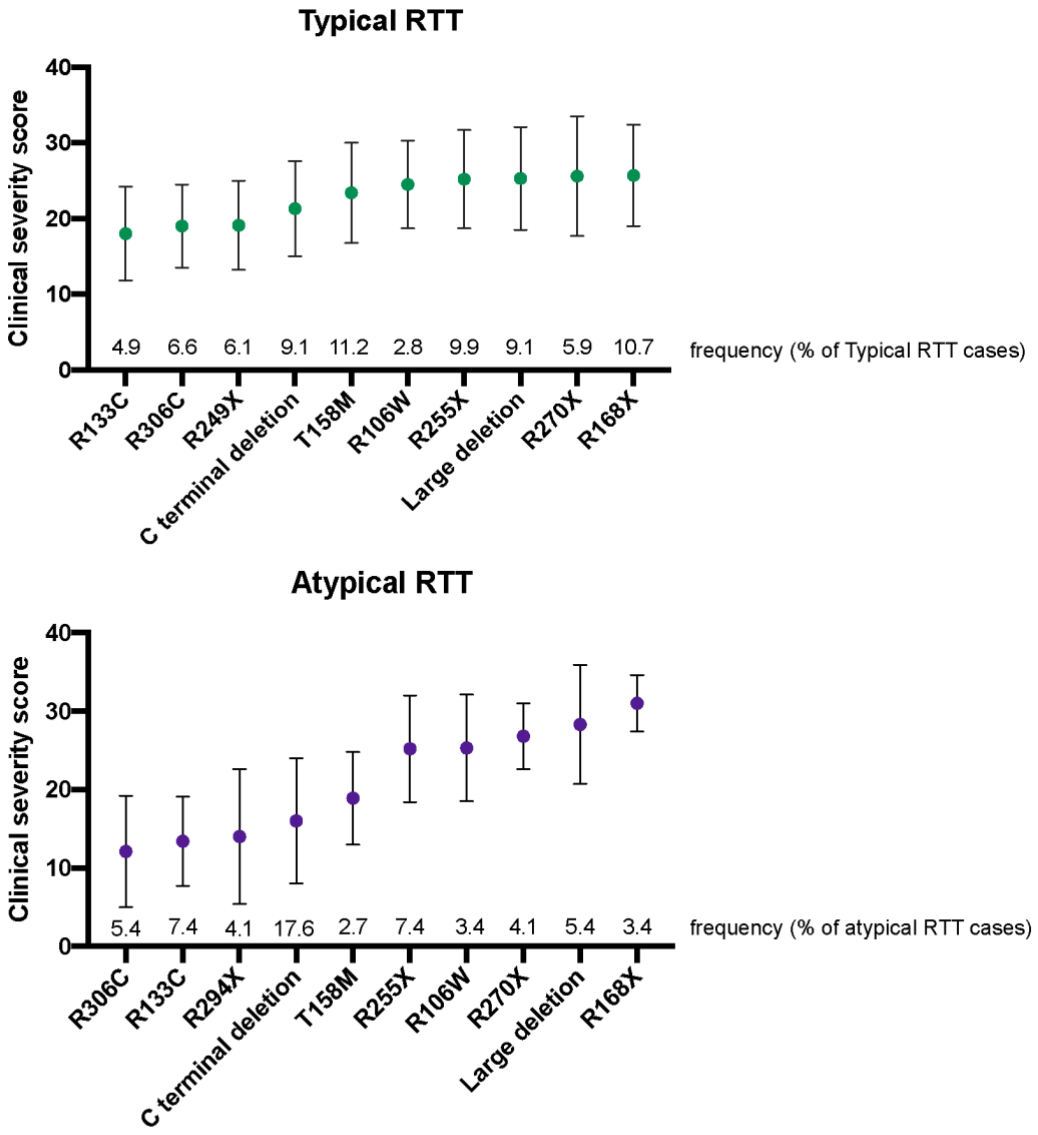

Figure 1.4.1. Rett Syndrome severity and mutation type. Association between clinical severity and mutation type in individuals with typical RTT (above n=815) and atypical RTT (below n=148). Data is taken from Cuddapah et al., (2014). Plotted are the mean scores with SD.

1.4.2 X-inactivation pattern

A second driver of phenotypic variability in RTT is X chromosome inactivation (XCI). To equalize the X-linked gene dosage between XY males and XX females, one X chromosome is transcriptionally silenced in females (Lyon, 1961). One X chromosome per cell is inactivated at random during early embryogenesis following implantation as pluripotent epiblast cells start to undergo lineage-specific differentiation (Monk & Harper, 1979; Tan *et al*, 1993). XCI is stably maintained in subsequent cell divisions and throughout life, and due to cell mixing and migration, adult females are mosaic for populations of cells with either the paternal or maternal X inactivated. Detrimental functional consequences of mutations in X-linked genes subject to X-inactivation, such as *MECP2*, are easily unmasked as they are unbuffered by contributions from the silenced WT allele. Mosaic females heterozygous for X-linked mutations generally benefit from having an admixture of WT and mutant cell populations and the disease phenotype often worsens in the hemizygous males which is indeed the case for *MECP2* mutations.

Generally random-XCI results in an approximately equal (50%) distribution of cells which have inactivated either the paternal or maternal X-chromosomes. A deviation from an equal ratio of inactivation of each parental allele is known as skewing. In apparently normal females, the frequency of skewing (80:20) was estimated at ~9% and extreme skewing (95:5) in <1% (Amos-Landgraf *et al*, 2006). Skewed XCI patterns can arise at the onset of XCI from chance events or genetic variants in XCI machinery (Brown & Robinson, 2000). Preferential inactivation of the X chromosome carrying a mutation in the *XIST* gene (essential driver of XCI) promoter was identified in several unrelated females with apparently inherited skewed XCI (Plenge *et al*, 1997). At the time of XCI commitment, the precursor pool which gives rise to the entire organism is small, therefore, stochastic variation can lead to unequal XCI patterns despite the randomness of the mechanism (Minks *et al*, 2008).

XCI skewing is commonly acquired after XCI is established through cell selection during development (Brown & Robinson, 2000). Large X-chromosome rearrangements can lead to selection to alleviate disruption in gene dosage, or single

gene mutations can infer either selective advantage or disadvantage in growth or survival. The incidence of skewing has been found to increase with age in hematopoietic cells where proliferation continues throughout life and mild selective advantages, or depletion of the stem cell pool can eventually lead to skewing (Busque *et al*, 1996; Gale *et al*, 1997; Fey *et al*, 1994). Skewing can be tissues specific, effecting only the tissues which express the mutant gene (e.g. X-linked severe combined immunodeficiency (XLSCID) (Puck *et al*, 1987). Selection against cells with mutant X active has been suggested to occur in carriers of neurological disorders such as X-linked mental retardation (XLMR) and Fragile-X Syndrome (Plenge *et al*, 2002; Sun & Baumer, 1999). The extent of post-inactivation skewing will depend on the selection pressure, which in turn reflects, the type of mutation, how crucial the genes' role is in cell proliferation, maturation and cell survival, and at what developmental stage or in which tissue is the gene required.

In X-linked disorders where there is no strong selection, the extent of skewing whether purely stochastic, or due to a second genetic variant biasing XCI, can influence the disease phenotype. For example; skewed XCI can lead to the expression of X-linked recessive traits in females which would usually only affect males such as Duchenne muscular dystrophy (Azofeifa *et al*, 1995; Pegoraro *et al*, 1994). For X-linked dominant disorders such as RTT the proportion of cells which have the mutant *MECP2* gene on the active X, has been suggested to correlate with disease severity (see below).

MeCP2 does not seem to have an essential role in neurogenesis nor neuron survival, therefore, selection against MeCP2-deficient neurons in the developing brain seems unlikely. There are conflicted views as to whether the XCI pattern in RTT individuals is typically random. Some studies emphasise that the XCI is balanced in the majority of RTT individuals (Zoghbi *et al*, 1990; Shahbazian *et al*, 2002b; Amir *et al*, 2000; Hoffbuhr *et al*, 2001). Other studies in RTT patient samples and *Mecp2*$^{-/+}$ mice argue that the XCI pattern is typically unbalanced with a tendency for XCI to favour the expression of the WT allele (Archer *et al*, 2007; Braunschweig *et al*, 2004; Young & Zoghbi, 2004). Consistent with this, the incidence of XCI skewing (75 or 80% inactivation of the same X chromosome) is thought to be increased in RTT compared to the unaffected population (Camus *et al*, 1996; Weaving *et al*, 2003; Knudsen *et al*,

2006). In most cases of skewed XCI, the paternal allele was preferentially silenced. The predominant inheritance of *MECP2* mutations on the paternal X (Trappe *et al*, 2001), raises the possibility that XCI skewing in RTT is caused by post-inactivation selection against mutant cells. The difference in reported frequencies of skewed X inactivation may partly be attributed to different definitions of the 'skewed' state (ranging from >65 to >85%). Additionally, XCI is commonly measured from circulating leukocytes which some studies suggest can be an inaccurate representation of XCI pattern in the brain (Shahbazian *et al*, 2002b). XCI skewing has been shown to differ between different brain regions and between brain and peripheral tissues in RTT individuals (Gibson *et al*, 2005). Other studies in larger sample sizes of RTT patients have found good correlations between the XCI pattern in peripheral leucocytes and clinical severity (Archer *et al*, 2007).

XCI can profoundly influence the clinical phenotype associated with heterozygous *MECP2* mutations in females depending on which X chromosome is preferentially active and the degree of skewing. Extreme skewing where the mutant *MECP2* allele is predominantly silenced has been reported in rare asymptomatic carrier mothers, who were protected from the disorder and transmitted the pathogenic mutations to their offspring who had random XCI and RTT if female or neonatal encephalopathy if male (Sirianni *et al*, 1998; Schanen *et al*, 1997; Wan *et al*, 1999; Amir *et al*, 2000; Zoghbi *et al*, 1990; Bienvenu *et al*, 2000; Villard *et al*, 2000; Hoffbuhr *et al*, 2001). Some authors hypothesise that in individuals with such extreme skewing (>90%), the RTT mutation must also coincide with a second genetic trait which causes non-random XCI (Sirianni *et al*, 1998; Hoffbuhr *et al*, 2001). Another striking example is a report of a pair of monozygotic twins discordant for the RTT phenotype (Migeon *et al*, 1995). One identical twin suffered from typical RTT and the other was completely unaffected due to extreme XCI favouring the WT allele, attributed to uneven distribution of XCI between each half of the epiblast during twinning. A further factor to consider when assessing the frequency of skewing in RTT, is that patients with substantial skewed inactivation might not obtain a RTT diagnosis and therefore not included in the study cohort.

It has been hypothesised that the range of phenotypic variability in individuals diagnosed with RTT is caused by the XCI pattern. Thorough examination of effects of X-chromosome inactivation in individuals with the same *MECP2* mutation R168X or T158M, found a significant increase in clinical severity correlated with percentage of cells expressing the mutant allele (Archer *et al*, 2007). It was estimated that the direction of XCI accounted for 19% of the phenotypic variance. As the type of *MECP2* mutation does not seem to distinguish atypical RTT from typical RTT, skewed XCI pattern has been hypothesised to be the cause of an atypical presentation. In single cases of milder atypical RTT, skewing towards the WT allele has been reported (Hoffbuhr *et al*, 2001; Zappella *et al*, 2001; Bienvenu *et al*, 2000), although analysis of XCI in patients diagnosed with typical and atypical RTT found equal amounts of skewing in both groups (Weaving *et al*, 2003), suggesting the effect of XCI on phenotype is not ubiquitous. Overall, it is unclear whether RTT patients are more prone to skewed XCI. Nonetheless, XCI skewing can influence phenotypic severity. As the role of MeCP2 seems to be largely cell autonomous, the higher the proportion of mutant neurons compared to WT neurons in the brain, the greater the expected neurological dysfunction.

1.5 Therapeutic approaches for Rett Syndrome

The RTT mouse model has been instrumental in therapeutic research, allowing testing of genetic and pharmacological interventions and providing a clear read out of the phenotypic effects. The pivotal mouse experiment which identified that the neurological features of RTT are reversible upon restoration of functional MeCP2 in the adult *Mecp2-null* mouse (Guy *et al*, 2007), revealed the exciting prospect that RTT could be curable and that the therapeutic window for RTT is not restricted to a certain stage in development. At the molecular level, loss of MeCP2 in neurons results in the dysregulation of many genes globally. The lack of a dominant downstream molecular pathway has made it challenging to find druggable targets and suggests that combinations of treatments would be needed to effectively treat the full spectrum of RTT symptoms. Despite this, ameliorating one of the core symptoms of RTT such as breathing abnormalities would significantly improve the quality of life of a patient. The pathways that have been targeted so far by drugs showing some promise in mouse

models and gone onto clinical trials fall into the following categories: 1) neurotransmitter signalling; 2) growth factor signalling; 3) metabolism (reviewed by Katz *et al*, 2016; Vashi & Justice, 2019). Although some progress has been made in improving clinical management, treatment options that resolve or substantially reduce the debilitating symptoms of RTT are yet to be identified. Therapeutic approaches that target the root cause of RTT, the loss of MeCP2 function, are appealing given the broad acting role of MeCP2 and the potential for profound amelioration of symptoms. The Rett Syndrome research trust's (RSRT) research plan - CURE 360 – funds a coordinated attack of academic labs and biopharma tasked with driving forward six therapeutic strategies with the combined objective of restoring levels of MeCP2 protein: gene replacement, protein replacement, gene editing, RNA editing, RNA trans-splicing and MECP2 reactivation (https://research.reverserett.org/).

1.5.1 Gene therapy

One way to restore MeCP2 levels in mutant cells is through viral delivery of a functional copy of the *MECP2* gene to mutant cells using viral delivery. The discovery of adeno-associated virus (AAV) vectors, especially AAV9, has opened up the possibility of a gene therapy for RTT and other targetable neurological disorders (Wang *et al*, 2019). AAV9 vectors can cross the blood-brain barrier, achieve widespread gene transfer throughout the nervous system and provide long-term transgene expression. A recent huge advancement in the gene therapy field, was the extremely successful gene therapy for spinal muscular atrophy (SMA), a devastating progressive neurodegenerative disorder caused by the disruption of the survival motor neuron (*SMN1*) gene and the loss of the SMN protein (Coovert *et al*, 1997). The SMA gene therapy (Zolgensma®), a one-time dose of an AAV9 viral vector delivering the *SMN* gene, has treated over 700 patients, including some who are now more than five years post-treatment and more than five years old (Mendell *et al*, 2017)(www.zolgensma.com). Children with the most common and severe form of SMA, type-1, would usually die or require mechanical ventilation before the age of 2 (Kolb, 2001; Finkel *et al*, 2014). The success of the SMA gene therapy has provided hope that in the near future a gene therapy for RTT will become available.

For optimal efficacy and safety of gene therapy approaches to treat RTT, there are two major considerations: 1) sufficient numbers of target cells must be transduced to have a therapeutic benefit; 2) the level of transgene expression per cell must be tightly regulated to avoid overexpression of exogenous *MECP2* (Gadalla *et al*, 2015). So far, multiple groups have demonstrated phenotypic amelioration including prolonged survival following administration of AAV vectors expressing *Mecp2/MECP2* cDNA to *Mecp2-null* and heterozygous mice (Gadalla *et al*, 2013, 2017; Sinnett *et al*, 2017; Tillotson *et al*, 2017; Matagne *et al*, 2017; Garg *et al*, 2013). The extent of the phenotypic amelioration correlated with the transduction efficiency which was shown to vary depending on the delivery route used. Systemic delivery of the vector (e.g. intravenous injection), which perhaps is the more clinically desirable option, was shown to result in low transduction efficiency in the brain and preferential transduction in the peripheral tissues, especially the liver (Gadalla *et al*, 2013, 2017). Surprisingly, low transduction efficiency (2-4% of neurons) slightly increased the survival of *Mecp2-null* mice (Gadalla *et al*, 2013). Administering higher doses of virus systemically did result in higher brain transduction and greater phenotypic improvement in *Mecp2-null* mice and heterozygous mice (Garg *et al*, 2013), but in other studies led to early lethality due to toxic overexpression in the periphery (Gadalla *et al*, 2017). Direct CNS delivery of AAV vectors (e.g., intrathecal, intracisterna magna or direct injection into the neuropil) which have been approved for clinical trials for other neurological disorders, might be necessary to achieve the widespread coverage needed for an efficacious *MECP2* gene therapy (Gadalla *et al*, 2015). In mice, AAV delivery directly to the brain of *Mecp2-null* neonatal pups has demonstrated the best phenotypic rescue to date, as a result of the higher transduction efficiency (Gadalla *et al*, 2017; Tillotson *et al*, 2017). Administration of a 'second-generation' AAV9 vector expressing *MECP2* cDNA to *Mecp2-null* neonates achieved 10-40% transduction efficiency across brain regions and resulted in significantly improved RTT like phenotypes and greatly prolonged lifespan (~26 weeks)(Gadalla *et al*, 2017). However, encouraging, a higher transduction efficiency is likely to be required to achieve a complete phenotypic reversal.

One of the most challenging aspects of treating RTT with gene therapy is maintaining MeCP2 levels within physiological limits. We know that both reduced MeCP2

expression and overexpression lead to neurological disease (section 1.1.3.4). A high dose of virus will be required to achieve a good coverage, but equally, infection of cells with multiple viral particles could lead to overexpression. In female RTT patients, mosaicism further complicates the picture, as gene therapy targets all cells regardless of their XCI status. In half of all neurons, exogenous *MECP2* will be expressed on top of the endogenous WT copy and could exceed what is tolerated by the cell. In the other half of all neurons, exogenous *MECP2* will be expressed on top of the mutant copy. Many mutations cause a dramatic reduction in the level of MeCP2 protein, but for other missense mutations, a dysfunctional MeCP2 protein persists in the cell. Multiple studies have tested whether mutant MeCP2 can act in a dominant negative manner in the presence of WT MeCP2 protein (Heckman *et al*, 2014; Koerner *et al*, 2018; Pitcher *et al*, 2015; Merritt *et al*, 2020). Expression of transgenic WT *MECP2* rescued RTT-like phenotypes in *Mecp2*^{R255X} and *Mecp2*^{R294X} mutant mice. Mice which expressed the R306C NID mutant protein on top of WT were indistinguishable from WT littermates (Heckman *et al*, 2014; Koerner *et al*, 2018). Conversely, expression of the common MBD mutations T158M and R133C on top of WT did not severely effect survival but did result in hindlimb clasping indicative of significant neurological defects, despite there being only a modest increase in total MeCP2 levels (~1.8 times WT levels for T158M and ~2.6 times for R133C (2.4 times overexpression of WT MeCP2 in mice had no obvious phenotype)) (Koerner *et al*, 2018). The latter results suggest that for some mutations, expression above a certain level of exogenous WT MeCP2 in mutant cells could have deleterious neurological consequences.

Earlier gene therapy attempts in mice identified adverse effects of MeCP2 overexpression both in the brain and in peripheral tissues using an AAV9 vector expressing human *MECP2* cDNA from a truncated mouse *Mecp2* promoter (Gadalla *et al*, 2013; Sinnett *et al*, 2017; Gadalla *et al*, 2017). Cerebrospinal fluid (CSF) delivery of this 'first-generation' vector worsened the phenotypic score of *Mecp2-null* mice and also induced hind-limb clasping and abnormal gait phenotypes, weight loss and significantly reduced survival in WT mice (Sinnett *et al*, 2017). Systemic delivery of this vector also led to high transduction of the liver which at high doses caused acute toxicity and early lethality in both *Mecp2-null* and WT mice (Gadalla *et al*, 2017, 2013). These effects were a direct consequence MeCP2 overexpression as identical

treatments with control vectors expressing GFP instead of *MECP2* did not cause adverse neurological phenotypes or liver toxicity (Sinnett *et al,* 2017; Gadalla *et al,* 2017). To combat overexpression phenotypes, the second-generation AAV9 vector was developed which included additional *Mecp2* promoter regulatory elements, the conserved distal polyadenylation signal of *Mecp2* and microRNA binding sites known to be involved in posttranscriptional regulation of *Mecp2* (Sinnett *et al*, 2017; Gadalla *et al,* 2017). Systemic delivery of the second-generation vector led to tighter regulation of expression levels in transduced cells and none of the liver damage observed following the same treatment with the first-generation vector (Gadalla *et al*, 2017). Direct brain injection resulted in substantially prolonged lifespan and improved neurological phenotypes (Gadalla *et al,* 2017). Finally, a recent study designed a radically truncated *Mecp2* allele, ΔNIC, which consists of the MBD and the NID domains and an intervening linker sequence (discussed in section 1.3.3)(Tillotson *et al,* 2017). *Mecp2-null* mice and WT neonatal pups treated with AAV9 vector encoding the humanised ΔNIC (hΔNIC)(direct brain injection) showed greatly extended survival and reduced symptom severity compared to controls. No adverse effects due to overexpression were observed even in WT animals. The moderate instability of hΔNIC compared to WT protein was hypothesised to mitigate toxic effects associated with overexpression, suggesting that using a destabilised version of MeCP2 might widen the dosage window (Tillotson *et al,* 2017).

So far, the gene therapy experiments in mice have yielded promising results. There is still optimisation to be done to improve the transduction efficiency so that a higher proportion of cells in the mature brain are corrected to achieve complete phenotypic reversal. The majority of tests in mice have involved *Mecp2-null* and WT pre-symptomatic mice. Future experiments in heterozygous females and post-symptomatic mice will be needed to more accurately assess effects of transduction of the mosaic brain and whether virally delivered *MECP2* can reverse RTT-like symptoms. Optimisation of vector design going forward includes employing strategies to restrict the expression of exogenous *MECP2* to mutant neurons despite the virus infecting neuronal and non-neuronal tissue. Exploiting microRNAs which promote expression of exogenous MeCP2 in neurons and inhibit its expression in non-target tissue is one method that has shown promise with the second-generation vector (Vashi & Justice,

2019; Gadalla *et al*, 2011). Feedback mechanisms which assess the level of MeCP2 in a given cell and downregulate the viral MeCP2 in response to high cellular levels would be a good mechanism to prevent overexpression in neurons with the WT MeCP2 on the active X.

1.5.2 DNA editing

Given the challenges associated with gene therapy an ideal alternative would be to avoid the introduction of exogenous MeCP2 into cells and instead restore the expression of endogenous MeCP2. Correction of the DNA mutation would provide a one step, permanent cure. Combining the revolutionary CRISPR/Cas9 gene editing technology with an AAV delivery system has made gene editing therapies possible. Many of the RTT causing mutations are single-base changes and precise editing back to the WT sequences is the most attractive solution. The very low activity of the homology directed repair (HDR) pathway in non-dividing cells means that precise editing using CRISPR-Cas9 and a homology template is not a viable option for RTT. A recent addition to the DNA editing tool box are base editors which can be used to correct disease-causing point mutations in both dividing and non-dividing cells (reviewed by Rees & Liu, 2018). Put simply, base editing machinery consist of a Cytosine Deaminase or Adenine Deaminase enzyme which convert C-G base pair to an T-A, or A-T base pair to G-C respectively, fused to modified Cas9 enzyme which target the editing enzyme to specific sequences using a guide RNA. Base-editing generally exhibits high on-target editing efficiency and low INDEL rate but bystander editing can occur on nearby bases which can have undesirable consequences. Beam Therapeutics, a leading gene editing biotech company, is currently working on base editing solutions to treat RTT (https://research.reverserett.org/cures/). A second DNA editing angle being explored for RTT is the replacement of exon 3 and 4 of *MECP2* where 97% of the RTT-causing mutations reside with unmutated exons (see Figure 1.3.1). A further editing approach that the Bird lab is exploring is the conversion of disease-causing C-terminal truncation mutations that account into benign deletions or truncations which are tolerated by MeCP2, by inducing small INDELs at the mutation site (Laura Fitzpatrick unpublished data). The advancement of AAV-CRISPR therapeutics faces the same obstacles that AAV-based gene therapy faces, such as pre-

existing or treatment induced immunity against AAV components and Cas9, and delivery efficiency and specificity (Wang *et al*, 2020). AAV-CRISPR therapeutics have additional challenges which include: low efficiencies of homology-directed repair in post-mitotic cells, potential off-target editing, undesired on-target editing events and the packaging size limit AAV vectors (Wang *et al*, 2020). Discoveries to overcome the challenges that the field faces are being made at an astonishingly fast pace, such as the discovery of small Cas proteins which can fit into a single AAV along with its guide RNA and identification of anti-CRISPR (Acr) proteins that can inhibit DNA cleavage making the system inducible (Wang *et al*, 2020). AAV-CRISPR therapeutics hold great promise for the future therapeutics for RTT.

1.5.3 RNA editing

Unlike DNA editing which is a one-shot permanent modification, mRNA editing requires continuous production of the editing machinery and editing of newly synthesised mutant RNA throughout the lifetime of the patient. The advantage to editing short lived mRNA is that unwanted bystander editing or off-target editing will potentially have less deleterious consequences than if it were to occur at the DNA level. An RNA editing system being developed in mouse models of RTT consists of the catalytic domain of Adenosine Deaminase that Acts on RNA 2 (ADAR2), a naturally occurring RNA editing enzyme which convert adenine to inosine (read as guanine), fused to a RNA binding peptide from bacteriophage lambda (λN) which binds to a specific short hairpin RNA (Sinnamon *et al*, 2017, 2020). Targeted editing is achieved by expression of the ADAR2 fusion protein with a guide RNA which has the λN-recognized stem loops and sequence complementary to the target mRNA sequence. These components can easily fit in a single AAV vector. Adenosine deamination has the potential to edit 36% of RTT causing mutations to repair protein function, these mutations include G>A mutations that can be repaired, or C>T mutations that create premature stop codons which can be edited to tryptophan allowing read-through of the mRNA to the WT stop codon of *Mecp2* (Sinnamon *et al*, 2020). *In vivo* delivery of RNA editing machinery in AAV vectors by localised injection to the hippocampus, achieved ~50% on target mRNA editing which resulted in an enrichment of MeCP2 localised to heterochromatin (increased to 50% of the WT

level)(Sinnamon *et al*, 2020). Further experiments need to be done to determine if widespread transduction of the mouse brain will achieve enough editing to reverse RTT-like phenotypes.

1.5.4 Reactivation of the inactive X-chromosome

In RTT females heterozygous for an *MECP2* mutation, the diseased subset of neurons are expressing the mutant copy of the *MECP2* gene from their active X-chromosomes (Xa) whilst the healthy intact copy of the *MECP2* gene is dormant on the inactive X-chromosome (Xi). Xi reactivation occurs naturally during mouse development in the epiblast of the pre-implantation embryo and in the germline (Ohhata & Wutz, 2013). Xi reactivation is also induced during reprograming of somatic cells to pluripotent stem cells (Pasque & Plath, 2015). If achievable without pluripotency, reactivation of the WT copy of *MECP2* on the Xi to overcome the dysfunction associated with the mutated *MECP2* allele is an attractive therapeutic avenue for RTT. Its main appeal is that once active the expression level of *MECP2* will be under the control of endogenous regulatory elements. Another advantage is that Xi-reactivation might be achievable using small molecules, avoiding the need to use viral transduction to deliver the therapy. Ideally, the reactivation strategy would target the *MECP2* gene or its vicinity specifically. However, attempting to disengage the multiple mechanisms of epigenetic silencing on the inactive X, might lead to reactivation of surrounding genes or the entire inactive X-chromosome and could also have long-range off-target effects on epigenetic control throughout the genome (Vashi & Justice, 2019). As XCI evolved as a mechanism to prevent twice the dosage of X-linked genes in females, off-target reactivation might result in pathological levels of expression of other loci. Furthermore, as mentioned previously, although RTT mutations are loss-of-function mutations and there is little evidence of dominant negative action of these mutations, expression of *MECP2* on top of the mutant allele could lead to an *MECP2*-overexpression phenotype if the mutation reduces MeCP2 function rather that completely destroying it. A mechanism to target reactivation to mutant cells would avoid needless reactivation of the mutant *MECP2* copy in already WT expressing cells.

High-throughput siRNA or small-molecule screens have been used to identify candidate XCI factors that can reactivate silent X-linked reporter transgenes (Bhatnagar *et al*, 2014; Minkovsky *et al*, 2015; Sripathy *et al*, 2017; Lessing *et al*, 2016). Two XCI factors were identified: 3-phosphoinositide-dependent protein kinase 1 (PDPK1) and activin A receptor type 1 (ACVR1), components of the PI3K/AKT and bone morphogenetic protein (BMP) cell-signalling pathways respectively (Bhatnagar *et al*, 2014). Treatment of human induced pluripotent stem cell-derived postmitotic RTT (T158M) neurons with small-molecule inhibitors of ACVRI and downstream effectors of PDPKI achieved reactivation of the Xi-linked WT *MECP2*, obtaining an expression level of ~10% of that in control neurons with the WT allele on the Xa (Przanowski *et al*, 2018). This level of expression of reactivated WT *MECP2* resulted in increased soma size and dendritic branch points compared to control neurons. Pharmacological activation of the XCI was found to be reversible when the drug was washed out (Przanowski *et al*, 2018), suggesting that X-reactivation therapy would require constant administration of the drug. Another XCI factor identified in the same X-reactivation screen was the glycoprotein Stanniocalcin 1 (*Stc1*) (Bhatnagar *et al*, 2014). *Stc1*$^{-/-}$ knock-out mice were reported to have defective XCI and biallelic expression of a handful of genes including *Mecp2,* according to RNA fluorescence *in situ* hybridization (FISH) (Bhatnagar *et al*, 2014). Interestingly, these mice are reported to be phenotypically normal which can be explained by the finding that the X-linked genes are not overexpressed, potentially revealing the existence of compensatory mechanisms which regulate the total level of expression of X-linked genes when XCI fails. On the one hand dosage compensation when the Xi is reactivated is encouraging as it suggests that reactivation of multiple genes on the Xi would not lead to pathological levels of expression. It also raises the possibility that it might not allow the expression of the reactivated WT *MECP2* to reach high enough total levels to have a sufficient therapeutic benefit. A further mixed modulatory approach where DNA methylation was inhibited on top of *Xist* depletion (*Xist* is the non-coding RNA which initiates X-inactivation and coats the Xi from which it is produced) led to a modest expression of the inactive *Mecp2* (2-5% of the protein level expressed from the Xa)(Carrette *et al*, 2017).

Studies so far suggest that although the expression of Xi-linked reporter protein is detectable following Xi-reactivation attempts, the level of expression obtained from the inactive *Mecp2* compared to the active allele is low. Recently, a heterozygous female mouse model was engineered which carried a *Tsix* (Tsix RNA blocks Xist upregulation on the Xa) gene mutation on one X-chromosome and an *Mecp2-null* allele on the other to ensure preferential activation of the *Mecp2-null* allele (Carrette *et al*, 2018). This mouse model has reduced cellular mosaicism and a severe neurological phenotype similar to the *Mecp2-null* male making them a good model to test the therapeutic benefit of Xi-reactivation drugs going forward.

1.6 Aim of the PhD project: to develop an *in vivo* ablation system for selective and inducible ablation of MeCP2-deficient neurons in heterozygous mice

As I have discussed so far, the RTT brain consists of neurons expressing the unmutated copy of *MECP2* which have the capacity to mature and function as unaffected WT neurons, interspersed with diseased neurons which express a mutated copy of *MECP2* and function inappropriately compromising the whole neuronal network. The therapeutic avenues explored so far for RTT focus on attempting to correct the diseased cells which lack a functional MeCP2 protein (referred to as MeCP2– cells from here onwards). The removal or silencing of the diseased neurons from the mosaic neuronal network in an attempt to ameliorate RTT symptoms has not yet been explored. In theory if one could remove MeCP2– neurons from the network, and the remaining MeCP2+ neurons (neurons expressing the WT copy of *Mecp2*) could compensate for their loss and contribute to the entire neuronal network the disorder would be cured.

This PhD project aims to explore this somewhat bold idea by developing a novel mouse model to allow selective ablation of cells at various stages in the development of the heterozygous female mouse model of RTT. The project objective also addresses a general developmental biology question: is the removal of 50% of neurons in the developing brain viable with normal development at any developmental stage? A

second RTT related question addressed is: do the MeCP2+ neurons compensate for the loss of the MeCP2– neurons and does their removal prevent the mice from developing RTT-like neurological symptoms. There is little scope for the removal of diseased neurons from the RTT brain to be translated into a therapy for RTT. This project is a proof of principle project exploring the plasticity of the developing brain.

A study conducted by Minocha and colleagues, (2016) showed that all the cells in the developing female embryo which have inactivated a certain X-chromosome can be removed from the embryo by embryonic day 8.5 (E8.5) to give rise to normal fetal development of a female mouse made up of cells which all have the same X-chromosome inactivated. This was achieved by inducing the conditional deletion of one copy of the X-linked *Hcfc1* gene encoding the host-cell factor (HCF-1), a transcriptional co-regulator involved in cell proliferation (Minocha *et al*, 2016). Epiblast specific heterozygous deletion of *Hcfc1* around E5.5 lead to the gradual disappearance of HCF-1-negative cells (cells with the *Hcfc1* deletion allele on the active X chromosome) by E8.5 owing to cell-cycle exit and apoptosis. The loss of HCF-1-negative cells was tolerated by the developing embryo leading to viable heterozygous offspring with 100% skewed X-inactivation of the epiblast knock-out *Hcfc1* allele. I plan to explore the loss of post-mitotic neurons which have inactivated a particular X-chromosome as opposed to all cells, at stages in development later than that explored in this study.

1.6.1 Naturally occurring programmed cell death and synaptic pruning during neurodevelopment

During neurodevelopment there is an excessive overproduction of neurons and axonal connections followed by considerable programmed cell death (PCD) and synaptic pruning. Naturally occurring, widespread cell death is an important feature of neuronal development, blocking PCD by deleting apoptosis activators: *caspase-3, -9*, or *Apaf1* in mice, leads to massive overgrowth of the brain and perinatal lethality (Kuida *et al*, 1996, 1998; Hakem *et al*, 1998; Yoshida *et al*, 1998; Cecconi *et al*, 1998). Three main functions of PCD during brain development have been proposed: 1) regulating the proliferative pool size during neurogenesis; 2) removing developmentally transient

cell populations and correcting errors; and 3) achieving optimal quantitative connectivity between neurons and their efferent targets and afferent inputs (reviewed by Buss *et al*, 2006). Neuronal precursors in the ventricular proliferative zones are eliminated during embryogenesis soon after they are generated to regulate the size of the proliferating pool of cells (Blaschke *et al*, 1998, 1996; Thomaidou *et al*, 1997). The second wave of PCD occurs during synaptogenesis where roughly 50% of the post-mitotic neurons initially produced are eliminated (Oppenheim, 1985, 1991; Buss *et al*, 2006; Cowan *et al*, 1984). This form of cell death is thought to be explained by the neurotrophic hypothesis: where neurons compete for a limited amount of target-derived neurotrophic signal required for their survival (Oppenheim, 1989, 2001; Cowan, 2001). The bulk of post-mitotic cell death occurs following birth in the first week of postnatal development in mice (Ahern *et al*, 2013; Mosley *et al*, 2017). Considerable regional differences in the magnitude and timing of PCD was observed. Further refinement of the neuronal circuits occurs through pruning of supernumerary synapses: the selective elimination of synapses in the absence of cell death (Lichtman & Colman, 2000; Goda & Davis, 2003; Kantor & Kolodkin, 2003). This allows the removal of exuberant or misguided axons whilst maintaining appropriate connections from the same neuron. Naturally occurring refinement of the neural circuitry could mean that there is a developmental time window where the overabundance of neurons and connections might compensate for the artificially induced elimination of MeCP2– neurons.

1.6.2 Cellular ablation techniques for induced cell death during development

Targeted *in vivo* cellular ablation is a powerful strategy to study the cell-type specific functions in tissues, cell differentiation and regeneration. Several methods have been established to delete a cell population of interest. Early approaches involved the physical removal of target cells using surgical tools such as laser ablation and microdissection (Huang & Moody, 1992; Serbedzija *et al*, 1998). These methods have toxic effects on the surrounding cells and are limited to targeted groups that can be visualised by microscopy, so are better suited to model systems such as *C-elegans* and Zebrafish or for studying embryogenesis. Other techniques are based on the disruption

of a gene required for the development or survival of a particular cell lineage (Kitamura *et al*, 1991)(see above). Alternatively, cells can be killed using cell-lineage restricted expression of a cytotoxic protein, the most widely used toxin being Diphtheria Toxin subunit-A (Palmiter *et al*, 1987; Breitman *et al*, 1987). In these latter examples, the timing of ablation tends to coincide with the onset of expression of the disrupted gene or the promoter in control of the cytotoxic protein.

Temporally inducible cell ablation can be achieved by administration of cytotoxic antibodies or chemicals which specifically target the cell type of interest (see review Liu 2019). The vulnerability of certain cell types to specific chemical agents has been exploited to model human diseases caused by deficiency of a single cell-lineage. For example: Streptozotocin (STZ)-induced diabetes (Furman, 2015), and neurotoxin-induced Parkinson's disease (Schober, 2004; Bové *et al*, 2005). A commonly used inducible ablation technique which can be applied to a wider range of cell types is to render a cell-type susceptible to prodrugs by transgenics. This involves the lineage-specific expression of sensitising genes encoding the enzymes Herpes Simplex Virus thymidine Kinase (HSV-tk) or Nitroreductase (Ntr) which convert prodrugs into their cytotoxic derivatives (Clark *et al*, 1997; Borrelli *et al*, 1988). Prodrug treatment determines the timing of cell death. HSV-tk action is limited to actively dividing cells whereas Ntr-mediated ablation can target both dividing and non-dividing cells. These techniques have the following limitations: 1) bystander effects through the transportation of the metabolite to nearby cells, and 2) the sensitising genes are frequently subject to transgene silencing resulting in incomplete ablation of the target tissue (Palmiter, 2001; Liu *et al*, 2019). The Ntr prodrug CB1954 system was used to ablate olfactory neurons and lead to "patches" of neurons surviving ablation, thought to be due to mosaic expression of the Ntr transgene (Isles *et al*, 2001). To reduce the damage to surrounding tissue following ablation, multiple groups have achieved inducible, targeted cell ablation by exploiting the physiological intracellular signalling pathway of apoptosis rather than delivering a cytotoxic product. This has been achieved by inducible activation of modified Caspases (key activators of apoptosis) through chemically inducible dimerization (Mallet *et al*, 2002). Methods which induce cell ablation by activating apoptosis, achieve cell ablation over a relatively slow period from several hours up to a day. To achieve rapid cell ablation, the Intermedilysin

(ILY)/human CD59 (hCD59)-mediated cell ablation system was developed where ILY specifically lyses cells by binding to hCD59 and forming a transmembrane pore (Hu *et al*, 2008). This method was shown to be well suited to ablating erythrocytes which are not actively synthesising proteins.

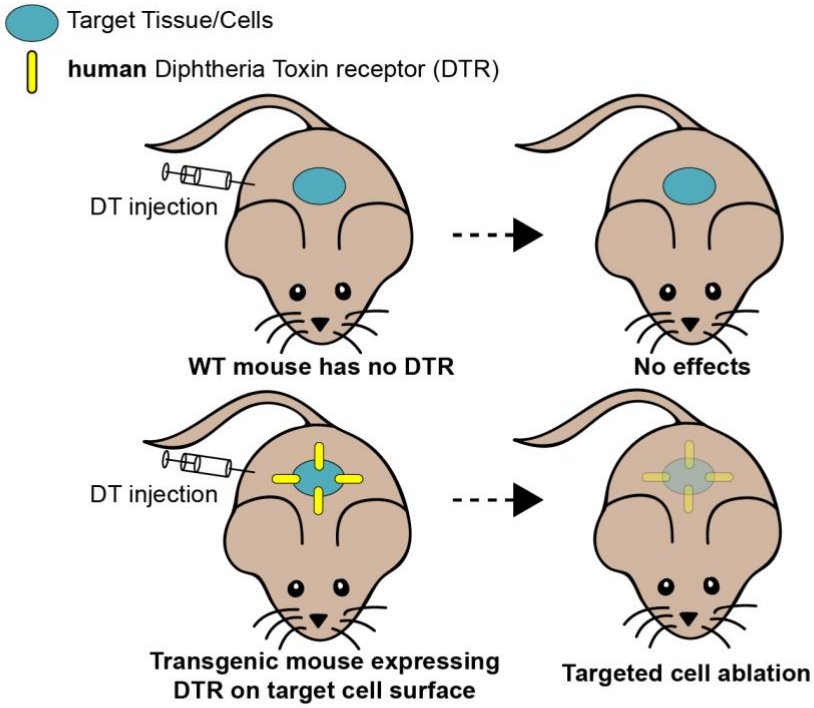

Figure 1.6.2.1 DTR-mediated *in vivo* cell ablation in mice. Mice are naturally resistant to Diphtheria Toxin (DT) as they lack the Diphtheria Toxin Receptor (DTR). Selective expression of the human DTR in a cell-type of interest facilitates the ablation of those target cells upon administration of DT.

A highly efficient, widely used inducible cell ablation technique which can be used to target dividing and non-dividing cells is the Toxin Receptor-mediated Cell knockout (TRECK) system (Saito *et al*, 2001). This involves the transgenic expression of the receptor for Diphtheria Toxin (DT) coupled to the injection of DT to the animal (Saito *et al*, 2001; Jung *et al*, 2002)(Figure 1.6.2.1). The receptor for the DT in toxin-sensitive species is the membrane bound precursor form of heparin-binding epidermal growth factor-like growth factor (proHB-EGF)(Naglich *et al*, 1992)(referred to as the Diphtheria Toxin Receptor (DTR) throughout). This method relies on the fact that mice are naturally resistant to the DT unlike humans (Pappenheimer *et al*, 1982;

Middlebrook & Dorland, 1977) as their homolog of the DTR is unable to bind the toxin due to amino acid substitutions (Mitamura *et al*, 1995). Expression of the human or primate DTR in mice makes them sensitive to DT (Cha *et al*, 2003; Saito *et al*, 2001; Jung *et al*, 2002). WT mice are resistant to even high doses of DT (100µg/kg - lethal dose to human is 0.1µg/kg)(Cha *et al*, 2003). The spatial specificity of cell ablation in DTR transgenic mice can be determined by cell type-specific promoter/enhancer elements used to express the DTR and the temporal specificity of ablation is determined by the timing of administration of DT. Unlike other inducible cell ablation methods, DT-mediated cell ablation can be extremely efficient. Thorel and collegues (2010) used the system to ablate pancreatic ß-cells to model extreme insulin loss achieving 98-99% ablation.

Toxicogenic strains of *Corynebacterium diphtheria* bacteria synthesise and secrete DT as a single polypeptide (reviewed in Collier, 1975; Pappenheimer, 1977). The toxin protein consists of the enzymatically active domain DT-A which catalyses the lethal reaction and the transport domain DT-B which facilitates entry into toxin susceptible cells (Gill & Dinius, 1971; Drazin *et al*, 1971; Collier & Kandel, 1971). The toxin binds to the DTR via the receptor binding domain of DT-B and is internalized by receptor-mediated endocytosis (reviewed in Murphy, 2011)(Figure 1.6.2.2). In acidic conditions in the endosome, DT-A becomes translocated into the cytosol through a transmembrane pore formed by the transmembrane domain of DT-B. Once in the cytosol DT-A catalyses the NAD^+ dependent ADP-ribosylation of the eukaryotic polypeptide elongation factor 2 (EF-2) a crucial component of the protein synthesis machinery (Honjo *et al*, 1968). Upon cessation of protein synthesis, cells undergo apoptosis. The DT-A is highly toxic and one molecule of the toxin has been suggested as enough to kill a cell (Yamaizumi *et al*, 1978). Administration of Fragment A alone is not toxic as it cannot pass the cell membrane, the expression of this fragment from a cell type specific promoter (as mentioned above) has been used to mediate cellular ablation (Palmiter *et al*, 1987; Breitman *et al*, 1987), however, this is very dependent on the specificity of the promoter as only a trace of non-specific DT-A expression can lead to adverse phenotypes. An attenuated form of DT-A has been generated to combat this problem (Breitman *et al*, 1990). This method is not inherently inducible unless made so using the Cre/Lox recombination system. A Cre-dependent ubiquitous DT-A

transgenic mouse line has been developed which can be crossed to Cre driver lines to specify cell-lineage expression (Plummer *et al*, 2017; Brockschnieder *et al*, 2006). The TRECK system not only lessens the risk of off-target cell ablation but also means the timing of ablation is inducible upon DT administration to the mice.

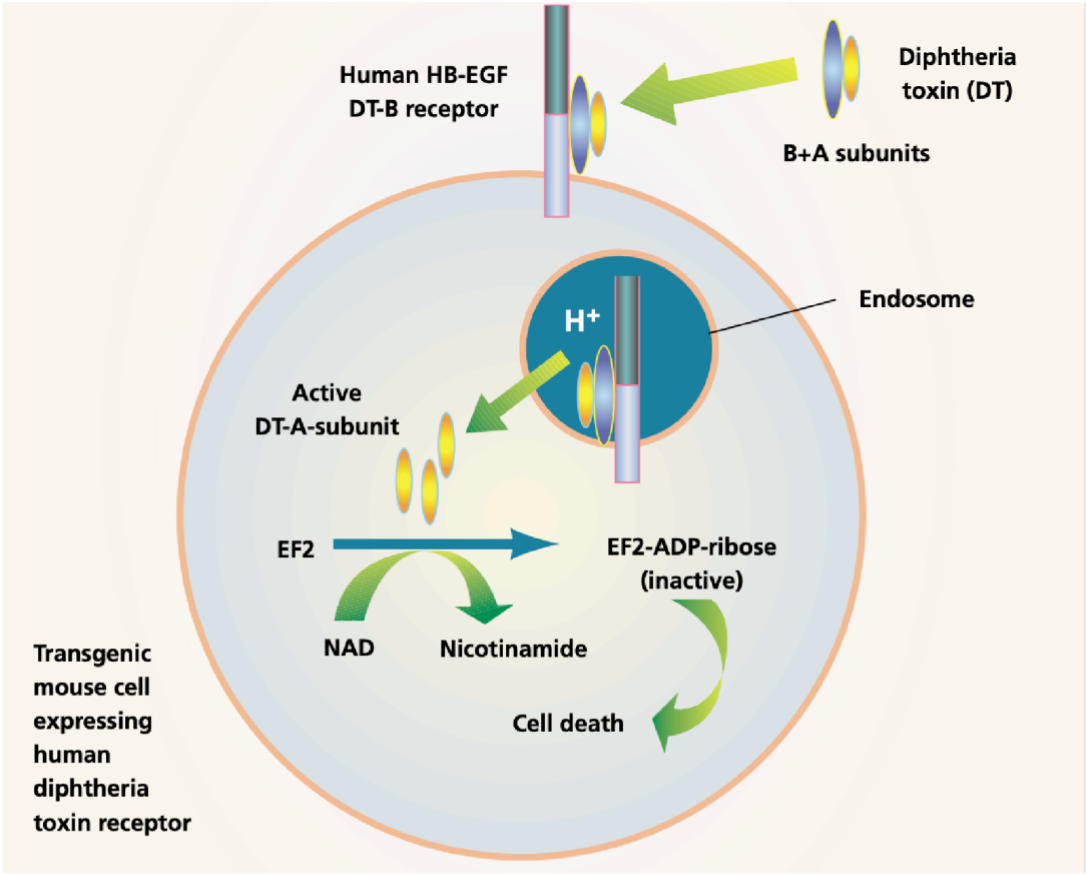

Figure 1.6.2.2. The intoxication process: cell entry and catalytic action of Diphtheria Toxin. Diphtheria Toxin (DT) binds to the human heparin-binding EGF-like growth factor (HB-EGF) receptor (the Diptheria Toxin receptor) via the receptor-binding domain of the DT B-subunit (DT-B). Receptor-mediated endocytosis internalizes the toxin. Acidic conditions in the early endosome allows the translocation of the catalytically active DT-A subunit into the cytoplasm. DT-A catalyses the NAD+ dependent ADP-ribosylation of the eukaryotic polypeptide elongation factor 2 (EF-2), inhibiting protein synthesis. Upon cessation of protein synthesis apoptosis is induced. (Schematic taken from review: Palmiter R. (2001): *Nature Biotechnology* 19: 731-732).

The TRECK system has been used extensively in mouse models to facilitate inducible *in vivo* ablation of populations of cell types in a range of tissues including the central nervous system (Buch *et al*, 2005). This targeted ablation technique has been commonly used to remove subtypes of post-mitotic neurons to study their role in behaviours such as: anxiety (Yamada *et al*, 2020; Révy *et al*, 2014), sleep/wake

behaviour (Iwasaki *et al*, 2018), and feeding behaviours (Gropp *et al*, 2005; Luquet *et al*, 2005). A collection of papers have used the DTR/DT system to ablate adult-generated neurons in the hippocampus, to study their role in learning and memory (Arruda-Carvalho *et al*, 2011; Arruda-carvalho *et al*, 2014; Vukovic *et al*, 2013). The system has enabled researchers to study the role in neuronal subtypes in neurodegenerative and neuropsychiatric disorders including Alzhiemers disease (Hsiao *et al*, 2014), Schizophrenia (Vawter *et al*, 2020), Epilepsy (Hosford *et al*, 2016, 2017), neuropathic pain (Cheng *et al*, 2017), and drug addiction (Durieux *et al*, 2009). Finally, the system has been used to study neuronal regeneration and circuit remodelling (Petrenko *et al*, 2015; Chen *et al*, 2005; Sonntag *et al*, 2012). One notable study used irradiation and the DTR/DT system to show that the developing cerebellum undergoes near full growth and functional recovery following major depletion of granule cell precursors (which give rise to the most plentiful neuron population in the brain) (Wojcinski *et al*, 2017). Nestin-expressing progenitors, which are specified to produce astroglia and interneurons, switch their fate to replenish granule neurons, illustrating the unappreciated progenitor plasticity of the developing cerebellum.

Neuronal ablation studies have used cell type specific promoters to restrict the expression of the DTR to a neuronal subtype for example the olfactory marker protein (OMP) promoter for mature olfactory sensory neuron ablation (Chen *et al*, 2005). Alternatively, to widen the use of the DTR approach and to avoid the requirement of generating a new transgenic DTR mouse strain for every cell-ablation study, a transgenic line with a Cre recombinase inducible DTR knock-in allele at the ubiquitous Rosa26 locus was generated (Buch *et al*, 2005). DTR expression is induced in the cell type of interest given that there is an appropriate Cre-expressing transgenic mouse strain available. A third method to achieved localised DTR expression is through viral delivery of an AAV encoded Cre-inducible DTR to transgenic mice with cell-type specific Cre expression (Fink *et al*, 2014; Azim *et al*, 2014).

1.6.3 Diphtheria toxin-mediated ablation of MeCP2-deficent neurons

To address the objective of this PhD project: to ablate MeCP2-deficient neurons in the female heterozygous mouse model of RTT. I chose to use the DTR-mediated ablation

system. Key aspects of the system outlined above which justified my decision included: the blood brain barrier permeability of DT, the control over the timing of ablation, the ease of genetically modifying mice to express the DTR, and the many examples of it being used to ablate neurons in the CNS.

This thesis describes the generation and characterisation of mouse models which conditionally express the DTR in *Mecp2*-deficient neurons. Two mouse lines were generated: $Mecp2^{StopDTR}$ and $Mecp2^{FLExDTR(OFF)}$, which facilitate Cre-dependent expression of the DTR from the *Mecp2* locus in place of the *Mecp2* gene. In both cases crucial coding sequence of *Mecp2* was replaced with the DTR to produce a *Mecp2* knock-out, DTR knock-in allele. DTR expression was made inducible following Cre-recombination so that the localisation of the DTR can be further specified. In the first mouse line, the $Mecp2^{StopDTR}$ line (discussed in Chapter 3), a *loxP*-flanked transcriptional *Stop* cassette did not fully silence the DTR expression in *cre*-negative cells, resulting in sensitivity of unrecombined mice and cells in culture to DT. The second $Mecp2^{FLExDTR(OFF)}$ mouse line (discussed in Chapter 4) was generated to combat the problem of leaky DTR expression in Cre negative cells. The use of a Cre-dependent Flip-Excision (FLEx) Switch to induce the DTR expression overcame the problem with leaky DTR expression. $Mecp2^{FLExDTR(OFF)}$ (*cre*-negative) mice were resistant to high doses of DT and comparable to WT littermates. DTR expression was shown to be activated only in the presence of Cre recombinase. Chapter 5 discusses the characterisation of the *Snap25-IRES2-cre* and *Synapsin1-cre* transgenic Cre driver lines in order to identify an appropriate line to use to activate DTR expression in neurons. Finally, Chapter 6 describes a preliminary *in vivo* ablation experiment carried out to explore the ablation of MeCP2-deficient neurons in neonatal development. The associated challenges and future applications of this system are discussed.

Chapter 2 Materials and Methods

2.1 Reagents

Name	Recipe
1M HEPES	1M HEPES (4-(2-hydroxyethyl)-1-piperazineethanesulfonic acid) (Sigma #H3375) pH to 7.9 with KOH
3M KCL	Potassium Chloride (Fisher Scientific P/4280/60)
1M $MgCl_2$	Magnesium Chloride hexahydrate (Sigma M9272)
1M Tris/HCL pH7.5/8.0	UltraPure Tris (Invitrogen 15504-020) adjusted to pH using concentrated HCl
0.5M EDTA	Ethylenediaminetetraacetic acid disodium salt dihydrate (VMR 20302.236) pH to 8.0 with 10M NaOH
5M NaCl	Sodium Chloride (Fisher Scientific 5/3160/63)
3M NaOAc	Sodium Acetate pH 5.2 (Sigma #S7899)
1M $CaCl_2$	Calcium Chloride (Sigma #C1016)
1M MgAc	Magnesium tetrahydrate (Sigma #M5661)
NaOH	Sodium hydroxide (Fisher Scientific S/4880/53)
KOH	Potassium hydroxide (Sigma #P1767)
20% SDS	Sigma #L4509
liquid broth (LB)	1% (w/v) Bacto tryptone, 0.5% (w/v) Bacto yeast extract, 1% (w/v) NaCl (adjusted to pH 7.0 with 5M NaOH)
Super Optimal broth with Catabolite repression (SOC)	2% (w/v) Bacto tryptone, 0.5% (w/v) Bacto yeast extract, 10mM NaCl, 10mM $MgCl_2$, 10mM $MgSO_4$, 2.5 mM KCl, 20 mM Glucose (Sigma #G8270)
Ampicillin	Stock 50 mg/ml in water (Fisher Scientific T-22943)
Kanamycin	Stock 20 mg/ml in water (Gibco 11815-024)
TE	10 mM Tris/HCl pH 7.5 stock, 1mM EDTA
Orange G	12% (w/v) ficoll (Sigma G8790), 1% (w/v) Orange G (Sigma O3756-25G) in TE
1 X TAE	40 mM Tris, 1.142% (v/v) acetic acid (Fisher Scientific A/0400/PB17), 1 mM EDTA
1X SDS running buffer	24.8 mM Tris, 192 mM glycine (Sigma G8790), 1% (w/v) SDS (Sigma L4509)
1 X Transfer buffer	25 mM Tris, 190 mM glycine
TBS (Tris buffered saline)	Dissolve 0.5 M Tris and pH to 8.0 with HCl, add 1.5M NaCl
PBS	1 tablet (Fisher BR14a) per 100ml
20 X SSC	24.8 mM Tris, 192 mM glycine,1% (w/v) SDS
1M NaPi	Di-sodium hydrogen phosphate (Fisher Scientific S/4440/60), pH to 7.2 using orthophosphoric acid (Fluka 79617)
Church Buffer	0.5 M NaPi, 1mM EDTA, 7% (w/v) SDS,1% (w/v) BSA (Sigma A9418)
PBS-gelatine	1 tablet (Fisher BR14a) per 100ml, 0.1% (w/v) gelatin (Sigma #G2500)
Ponseau	0.1% (w/v) ponceau (Sigma P 7767) in 5% acetic acid

Table 2.1.1. List of lab stock buffers and solutions.

Reagent	Manufacturer and catalogue number
Oligonucleotides	Sigma-Aldrich UK
Agarose	Merck 11388991001
Ethidium Bromide solution	Sigma E1510
Triton X-100	Sigma T9284
complete EDTA-free Protease Inhibitors cocktail	(Roche/Sigma large: 11873580001 mini: 11836170001)
DTT	Sigma D9779
2x Laemmli Sample Buffer	Sigma S3401
Oxoid skimmed milk powder	Thermo Fisher LP0031B
Tween-20	Sigma P1379
Paraformaldehyde	Sigma 158127
ProLong Diamond	Life Technologies P36961
Phenyl:chloroform:Isoamyl Alcohol	Sigma P3803 Invitrogen 15593-031
Isopropanol (Propan-2-ol)	Fisher Scientific P/7500/17
Hydrochloric acid	Fisher Scientific H/1200/PB17
Herring Sperm DNA	Sigma D7290
[α^{32}]dCTP	Perkin Elmer NEG513H250
[γ^{32}]dATP	Perkin Elmer NEG502A
KARYOMAX® Colcemid™	Gibco 15212012
Methanol	Fisher Scientific M/4000/PC17
Acetic acid Glacial	Fisher Scientific A/0400/PB17
Vectashield® mounting medium with DAPI	Vector laboratories H-1200
TRI Reagent®	Sigma T9424
MOPS (3-(N-morpholino) propanesulfonic acid	Sigma M1254
Formaldehyde	Sigma F8775
Formamide	Roche 11814320001
Nuclease-free H_20	Ambion AM9937
Diphtheria Toxin	Sigma D0564
Incucyte® Cytotox Red dye	Essen Bioscience #717
Sucrose	Fisher Scientific S/8560/60
NP40 IGEPAL® CA-630	Sigma 18896
PMSF (Phenylmethanesulfonyl fluoride)	Sigma P7626
B-Mercaptoethanol	Sigma M6250
OptiPrep™ Density Gradient Medium	Sigma D1556
Bovine Serum Albumin (BSA)	Sigma A9418
Glycerol	Fisher Scientific G/0600/17
Isopentane (2-Methylbutane)	Honeywell research chemicals 270342

Table 2.1.2. List of other reagents and manufacturer information.

Enzyme	Manufacturer and catalogue number
Restriction enzymes	New England Biolabs
Antarctic Phosphatase	New England Biolabs M0289
Exonuclease	New England Biolabs M0293
Benzonase	Sigma E1014
Proteinase K	Bioline BIO-37085
RNAse A	Thermo Scientific EN0531
NEBuffer™ 2	New England Biolabs B7002S

Table 2.1.3. List of enzymes and manufacturer information.

Cell culture reagent	Manufacturer and catalogue number
Cell culture dishes / flasks	Greiner/Corning
DMEM	Gibco 41966-029
Foetal Bovine Serum (FBS)	Gibco- batch tested
TryplE Express	Gibco 12604-013
DPBS	Gibco 14190-094
Pen/Strep	Gibco 15140-122
Lipofectamine-2000	Invitrogen 11668019
Opti-MEM	Gibco 31985062
GMEM medium	Gibco 21710-025
Non-essential amino acids	Gibco 11140-035
Sodium pyruvate	Gibco 11360-039
β-mecaptoethanol (tissue culture)	Gibco 31350-010
Leukemia Inhibitory Factor	ESGRO® #ESG1107
Trypsin-EDTA	Gibco 15400-054
Retinoic Acid (RA)	Sigma R2625
Poly-D-Lysine	Sigma P-7280
Laminin	Sigma L2020
Nucleon® treated dishes / plates	Thermo Scientific
Trypsin 2.5% (for 4 X TES)	Gibco 15090-046
Chicken serum	Gibco 16110-082
EDTA (cell culture)	Gibco 15575-020
Advanced DMEM/F12	Gibco 12634-028
N-2 supplement	Gibco 17502-048
L-Glutamine	Gibco 25030-081
Neurobasal medium	Gibco 21103-049
1x B-27 supplement	Gibco 17504-044
G418 antibiotic	Gibco 108321-42-2
DMSO	Sigma D2650
H_20 sterile, cell culture suitable	Sigma W3500

Table 2.1.4. List of cell culture reagents and manufacturer information.

Equipment	Manufacturer and catalogue number
Gene Pulser Electroporation cuvette 0.4 cm gap	Bio-Rad 1652081
cell lifter	Corning 3008
cell sieve	FALCON 352340
G50 column	GE Healthcare #27533001
Precast Mini-PROTEAN TGX 4-20% gels	Bio-Rad 4561095 4561093
3 MM CHR Whatman™ blotting papers	GE Healthcare 3030-917
Whatman™ gel blotting paper (Grade GB003)	WHA10427812
0.2μM nitrocellulose membrane	Bio-Rad 1620112
Zetaprobe	BioRad 1620159
Amersham™ Hybond-XL	GE Healthcare RPN303 S
Ultra-clear centrifuge tubes (SW28 rotor)	Beckman Coulter 344058
Ultra-clear centrifuge tubes (SW40ti rotor)	Beckman Coulter 344060
Superfrost Plus microscope slides	VWR 631-0108

Table 2.1.5. List of equipment and manufacturer information.

Kit name	Manufacturer and catalogue number
Phusion® High-Fidelity DNA Polymerase	New England Biolabs M0530
Q5® Hot Start High-Fidelity DNA Polymerase	New England Biolabs M0493
NEBulider® HiFi DNA assembly master mix	New England Biolabs E2621
Zymoclean™ Gel DNA recovery kit	Zymo Research D4007
MSB® Spin PCRapace kit	Stratec 1020220200
Quick ligation kit™	New England Biolabs M2200S
Miniprep kit	QIAGEN 27106
Maxiprep kit	QIAGEN 12262
BigDye® Terminator v3.1 Cycle Reaction	Thermo Fisher Scientific 4337455
In situ cell death kit TMRE red	Roche/Sigma 12156792910
Prime-a-Gene Labelling System	Promega U1100
Gentra Puregene Cell Kit	Qiagen 158767
QuantiTect® Reverse Transcription kit	Qiagen 205310
Sensimix™ SYBR® and Fluorescein Kit	Bioline QT615-05
StrataClone PCR blunt cloning kit	Agilent Technologies 240207
T4 Polynucleotide Kinase (PNK)	New England Biolabs M0201
DreamTaq Green PCR Master mix 2X	Thermo Fisher K1081
APEX™ Alexa Fluor™ 647 Antibody labelling Kit	Thermo Fisher #A10475
APEX™ Alexa Fluor™ 568 Antibody labelling Kit	Thermo Fisher #A10494

Table 2.1.6. List of kits used and their manufacturer information.

2.2 Primers

Primer name	5' - 3' Sequence	Experiment
Exon_1_fwd	taccgcgggcccgggatccaAAAACCC GTCCGGAAAATGG	*pMecp2^{DTR}* cloning
Exon_1_rev	cttttcctccAGTCTCTCCTCCTCGC CTC	*pMecp2^{DTR}* cloning
DTR-P2A-GFP_fwd	aggagagactGGAGGAAAAGAAG CTGCTG	*pMecp2^{DTR}* cloning
DTR-P2A-GFP_rev	tgattatgatctagagtcgcTTACTTGTA CAGCTCGTCC	*pMecp2^{DTR}* cloning
F_DTR_Age1(2)	GGATCCACCGGTCGCCACCAT GAAGCTGCTGCCGTCGGTG	*pDTR* cloning
R_DTR_Not1(2)	AGAGTCGCGGCCGCTTCAGTG GGAATTAGTCATGCCCAACTT	*pDTR* cloning
pCMV-DTR_Gib_fwrd	CAAGCTTGGTACCGAGCTCGG ATCCACCGGTCGCCACC	pDTR-IRES-GFP cloning
pCMV-DTR_Gib_rev	AGGGGCGGAATTCGTTAACCG CCGCTTCAGTGGGAATTAGTC	pDTR-IRES-GFP cloning
SEQ_1	TATTTCCCTGAGTTAGCAAT	pBS-Me2-STOP-DTR sequencing
SEQ_2	TAGACTCCAGCAACCAGTA	pBS-Me2-STOP-DTR sequencing
SEQ_3	TGTTCTCCTCTTCCTCATCT	pBS-Me2-STOP-DTR sequencing
SEQ_4	AGGATGATCTGGACGAAG	pBS-Me2-STOP-DTR sequencing
SEQ_5	AGGTGTCATTCTATTCTGGG	pBS-Me2-STOP-DTR sequencing
SEQ_6	AATACCACTTGCCACCTATC	pBS-Me2-STOP-DTR sequencing
SEQ_7	GCTTTGCTATTTACACCACA	pBS-Me2-STOP-DTR sequencing

SEQ_8	TGACATGGTAAGTAAGCTAGC	pBS-Me2-STOP-DTR sequencing
SEQ_9	GCACTCAAGCTCACCTATACT	pBS-Me2-STOP-DTR sequencing
SEQ_10	TACCTATGACCACACAACC	pBS-Me2-STOP-DTR sequencing
SEQ_11	GCACCATCTTCTTCAAGG	pBS-Me2-STOP-DTR sequencing
SEQ_12	AGAATAAAGGCAGCTGTTGT	pBS-Me2-STOP-DTR sequencing
P5	TGGTAAAGACCCATGTGACCCA	pBS-Me2-FLEx-DTR sequencing
R_Neo	TACCCGCTTCCATTGCTCA	pBS-Me2-FLEx-DTR sequencing
SEQ_3	TGTTCTCCTCTTCCTCATCT	pBS-Me2-FLEx-DTR sequencing
SEQ_4	AGGATGATCTGGACGAAG	pBS-Me2-FLEx-DTR sequencing
SEQ_5	AGGTGTCATTCTATTCTGGG	pBS-Me2-FLEx-DTR sequencing
SEQ_10	TACCTATGACCACACAACC	pBS-Me2-FLEx-DTR sequencing
SEQ_9	GCACTCAAGCTCACCTATACT	pBS-Me2-FLEx-DTR sequencing
pbsSeqfor2	CAGCCATACCACATTTGTAGAG	pBS-Me2-FLEx-DTR sequencing
pbsSeqRev2	AGAGTCCCATAGTTTCTCCTG	pBS-Me2-FLEx-DTR sequencing
SEQ_12	AGAATAAAGGCAGCTGTTGT	pBS-Me2-FLEx-DTR sequencing
U6 promoter	GAGGGCCTATTTCCCATGATTCC	CRISPR gRNA sequencing
R_DTR	GTGCTCCTCCTTGTTTGGTG	cDNA expression vector sequencing
F_5'UTR	GGAGAGAGGGCTGTGGTAAA	cDNA expression vector sequencing
SEQ_10	TACCTATGACCACACAACC	cDNA expression vector sequencing
1157del41 screen F4	TCACCATAACCAGCCTGCTCGC	5' PCR screen *Mecp2*^{StopDTR} targeting
R_PCRscreen_5b	GATGGATTGGCAGATGTAGCTAAAAGGC	5' PCR screen *Mecp2*^{StopDTR} targeting
F_PCRscreen_3	GCAAAGACCCCAACGAGAAG	3' PCR screen *Mecp2*^{StopDTR} targeting
EGFP PCR screen R2	TCAAAAGCAGAGCAGGCAAAAG	3' PCR screen *Mecp2*^{StopDTR} targeting
1157del41 screen F4	TCACCATAACCAGCCTGCTCGC	5' PCR screen *Mecp2*$^{FLExDTR(OFF)}$ targeting
1157del41 screen R3	ATTCGATGACCTCGAGGATCCG	5' PCR screen *Mecp2*$^{FLExDTR(OFF)}$ targeting
P5	TGGTAAAGACCCATGTGACCCA	5’ PCR *Mecp2*^{StopDTR} amplicon - sequencing
R_Neo	TACCCGCTTCCATTGCTCA	5’ PCR *Mecp2*^{StopDTR} amplicon - sequencing
pbsSeqFor1	CAGCCATACCACATTTGTAGAG	3’ PCR *Mecp2*^{StopDTR} amplicon - sequencing
pbsSeqRev1	AGAGTCCCATAGTTTCTCCTG	3’ PCR *Mecp2*^{StopDTR} amplicon - sequencing
F_Me2FLExDTR_SQ	GTGCCACTCCCACTGTCCTT	PCR *Mecp2*$^{FLExDTR(OFF)}$ amplicon - sequencing
R_Me2FLExDTR_SQ	GCTCCAACTACTCCCACCCC	PCR *Mecp2*$^{FLExDTR(OFF)}$ amplicon - sequencing
SEQ_1B	AAGGCTCACAAGTTAACAGT	Sequencing *Mecp2*^{StopDTR} locus
SEQ_1C	GCCCAGCCTCAAGTTTATAT	Sequencing the *Mecp2*^{StopDTR} locus
SEQ_1	TATTTCCCTGAGTTAGCAAT	Sequencing the *Mecp2*^{StopDTR} locus
SEQ_2	TAGACTCCAGCAACCAGTA	Sequencing the *Mecp2*^{StopDTR} locus

pbsSeqFor 1	CAGCCATACCACATTTGTAGAG	Sequencing the *Mecp2*^{StopDTR} locus
SEQ_8	TGACATGGTAAGTAAGCTAGC	Sequencing the *Mecp2*^{StopDTR} locus
SEQ_9	GCACTCAAGCTCACCTATACT	Sequencing the *Mecp2*^{StopDTR} locus
SEQ_10	TACCTATGACCACACAACC	Sequencing the *Mecp2*^{StopDTR} locus
SEQ_11	GCACCATCTTCTTCAAGG	Sequencing the *Mecp2*^{StopDTR} locus
SEQ_12	AGAATAAAGGCAGCTGTTGT	Sequencing the *Mecp2*^{StopDTR} locus
F_PCRscreen_3	GCAAAGACCCCAACGAGAAG	Sequencing the *Mecp2*^{StopDTR} locus
SEQ_5	AGGTGTCATTCTATTCTGGG	Sequencing the *Mecp2*$^{FLExDTR(OFF)}$ locus
SEQ_10	TACCTATGACCACACAACC	Sequencing the *Mecp2*$^{FLExDTR(OFF)}$ locus
SEQ_9	GCACTCAAGCTCACCTATACT	Sequencing the *Mecp2*$^{FLExDTR(OFF)}$ locus
pbsSeqfor2	CAGCCATACCACATTTGTAGAG	Sequencing the *Mecp2*$^{FLExDTR(OFF)}$ locus
pbsSeqrev2	AGAGTCCCATAGTTTCTCCTG	Sequencing the *Mecp2*$^{FLExDTR(OFF)}$ locus
F_qPCR1	CCTCGCACAGCCTTCACT	RT-qPCR forward *Mecp2*
R_qPCR1	CTGAGCAGCTCCAGAGGC	RT-qPCR reverse *Mecp2*
GAPDH_F	CCTGCACCACCAACTGCTTAG	RT-qPCR forward GAPDH
GAPDH_R	GTCTTCTGGGTGGCAGTGATG	RT-qPCR reverse GAPDH
F_5'UTR	GGAGAGAGGGCTGTGGTAAA	RT-PCR of entire coding seq cDNA
pbsSeqRev2	AGAGTCCCATAGTTTCTCCTG	RT-PCR of entire coding seq cDNA
F_5'UTR	GGAGAGAGGGCTGTGGTAAA	RT-PCR of across splice boundary
R_DTR	GTGCTCCTCCTTGTTTGGTG	RT-PCR of across splice boundary
M13 Seq Fwd	GTTTTCCCAGTCACGAC	Colony PCR cDNA amplicons
M13 Seq Rev	CAGGAAACAGCTATGAC	Colony PCR cDNA amplicons
T3	GCAATTAACCCTCACTAAAGG	Sequencing cDNA
R_DTR	GTGCTCCTCCTTGTTTGGTG	Sequencing cDNA
F_5'UTR	GGAGAGAGGGCTGTGGTAAA	Sequencing cDNA
P3 fwd	GACCCCTTGGACTGAAGTT	Genotyping mice
P3 RV	CCACCCTCCAGTTTGTTTTA	Genotyping mice
NeoF	AGGATCTCCTGTCATCTCACCTTGCTCCTG	Genotyping mice
NeoR	AAGAACTCGTCAAGAAGGCGATAGAAGGCG	Genotyping mice
CreF	GACCGTACACCAAAATTTGCCTGC	Genotyping mice
CreR	TTACGTATATCCTGGCAGCGATC	Genotyping mice
common-snap	AACGTCGAACAAAGATGCTG	Genotyping mice
wt rv-snap	AATGGGGGTGACTGACTCTG	Genotyping mice
mutant rv-snap	CTGCAAAGGGTCGCTACAG	Genotyping mice
Ex1-DTR	GCGAGGAGGAGAGACTGGAGGAAAAGAAGCTG	RT-PCR Southern probe

Table 2.2. List of primers and the experiments they were used in.

2.3 Antibodies

	Name	Source	Company
Primary antibodies			
DTR	Human HB-EGF	goat IgG polyclonal	R&D systems AF-259-NA
GFP	Living Colors® A.v. Monoclonal Antibody (JL-8) GFP antibody	mouse IgG monoclonal	Takara Bio Clontech 632381
H3	Anti-Histone H3	rabbit polyclonal	Abcam ab1791
mCherry	Anti-mCherry	rabbit polyclonal	Abcam ab167453
MeCP2	Anti-MeCP2	mouse monoclonal	Sigma M7443
NeuN	Anti-NeuN clone A60	mouse monoclonal	Millipore MAB377
NeuN-fitc488	Anti-NeuN clone A60, Alexa Fluor®488 conjugated	mouse monoclonal	Millipore MAB377X
Secondary antibodies			
anti-goat 800CW	IRDye® 800CW	donkey anti-Goat IgG	LICOR Biosciences 926-32214
anti-rabbit 680LT	IRDye® 680LT	donkey anti-Rabbit IgG	LICOR Biosciences 926-68023
anti-mouse 800CW	IRDye® 800CW	donkey anti-Mouse IgG	LICOR Biosciences 926-32212
anti-mouse 680LT	IRDye® 680LT	donkey anti-Mouse IgG	LICOR Biosciences 926-68022
anti-goat-633	Alexa Fluor® 633	polyclonal donkey anti-Goat IgG	Invitrogen A-21082

Table 2.3 List of antibodies and the manufacturer information.

2.4 Cloning

The pBS-Me2-STOP-DTR targeting vector sequence was assembled in two sequential restriction enzyme digestion and ligation steps introducing two synthesised DNA fragments (GeneArtTM Thermofisher Scientific), into the pBS-Me2-NeoStop vector (Guy et al, 2007)(sequence components in Appendix Table 1.). Firstly, the synthesised MfeI-HF fragment containing the DTR-P2A-EGFP sequence was ligated into the MfeI-HF digested pBS-Me2-NeoStop vector backbone to produce the intermediate vector. Secondly, the HpaI, AgeI-HF fragment containing SA-pApA was ligated into the HpaI and AgeI-HF digested intermediate vector.

The pBS-Me2-FLEx-DTR targeting vector was produced by replacing the HpaI to MfeI-HF fragment of the pBS_Me2_Bam7.2 (Guy *et al*, 2001) containing the exon 3 and 4 coding sequence of *Mecp2*, with the FRT-Neo-FLEx-DTR synthesised DNA fragment containing the FRT-floxed PGK-neo resistance cassette and the lox2272/loxP-floxed inverted DTR (GeneArt™ Thermofisher Scientific)(Sequence components in Appendix Table 1.).

The CRISPR-Cas9 guide target sequence was cloned into the PX330-U6-Chimeric_BB-CBh-hSpCas9 (Addgene ID: 42230) Cas9 expressing plasmid via the BbsI-HF restriction enzyme sites, in frame with the sgRNA scaffold (Appendix Table. 1). The forward and reverse oligonucleotides including the 20nt guide target sequence plus overhangs required for the cloning reaction were annealed in NEBuffer™ 2 using the thermocycler (parameters: 37°C for 30 mins, 95°C for 5 mins followed by a ramp down to 25°C at 5°C/min) before being ligated into the digested PX330 plasmid backbone.

To clone the pDTR cDNA expression vector, the DTR was PCR amplified from the pBS-Me2-STOP-DTR targeting vector using primers containing AgeI-HF and NotI-HF restriction sites to allow ligation into the AgeI-HF and NotI-HF digested pEGFP-NI plasmid replacing EGFP (Addgene 6085-1)(primers: F_DTR_Age1(2), R_DTR_Not1(2)). An ATG transcription start sequence and a TGA stop codon were also added to the primers. Phusion® High-Fidelity DNA Polymerase was performed according to manufacturer's protocol.

Restriction enzyme digestions were performed using the appropriate buffers and temperature according to the New England Biolabs guidelines. Digested fragments were run on a 1% agarose gels containing Ethidium Bromide (EtBr) and the desired fragments were purified using Zymoclean™ Gel DNA recovery kit according to kit manual. The digested PX330 Cas9 plasmid was purified using MSB® Spin PCRapace kit. Dephosphorylation of the vector backbone was done using Antarctic Phosphatase at 37°C for 30 minutes. Ligation reactions were performed at an insert to vector ratio of 3:1 using the Quick ligation kit™.

NEBuilder® HiFI DNA assembly was used to clone the *pMecp2^{DTR}* and the pDTR-IRES-EGFP cDNA expression vectors. PCR amplicons containing the coding sequence of exon 1 of *Mecp2* and the DTR-P2A-EGFP cDNA were assembled into the AgeI-HF® and NotI-HF® digested backbone of the pEGFP-N1 plasmid to produce the *pMecp2^{DTR}* vector. The *Mecp2* exon 1 fragment was amplified from an existing plasmid in the Bird lab; pCDNA3-MoMe2E1-IRES-GFP-2 which contained the *Mecp2* cDNA e1 isoform (primers: Exon_1_fwd, Exon_1_rev). The DTR-P2A-EGFP cDNA (with the first 3 amino acids of *Mecp2* exon 3) sequence was amplified from the pBS-Me2-STOP-DTR targeting vector (primers: DTR-P2A-GFP_fwd, DTR-P2A-GFP_rev). To make the pDTR-IRES-EGFP vector the intact DTR coding sequence was amplified from the pDTR cDNA expression vector and cloned into the BamHI-HF® and XhoI digested pCDNA3-MoMe2E1-IRES-GFP plasmid (digest removed *Mecp2* cDNA MoMe2E1) primers: pCMV-DTR_Gib_fwrd, pCMV-DTR_Gib_rev). Primers were designed using the NEBuilder® assembly tool and Q5® Hot Start High-Fidelity DNA Polymerase reactions were performed to amplify the fragments according to manufacturer's protocol. PCR amplified fragments and digested vector backbone were purified by gel extraction or PCR clean up as described above. Plasmids were assembled using the NEBulider® HiFi DNA assembly master mix according to the NEB protocol.

Plasmids were transformed into DH5α cells according to following conditions: 5 µl of ligation reaction or 20 ng DNA was added to 50-100µl DH5α cells and incubated on ice for 30 minutes, heat shocked for 45 seconds in 42°C water bath, put on ice for 2 minutes before 500-900µl of Super Optimal broth with Catabolite repression (SOC) medium was added and transformed cells were put at 37°C with agitation for 1 hour to recover. Transformed cells were then plated on liquid broth (LB) plates with Kanamycin or Ampicillin resistance and grown up overnight at 37°C. Plasmids were grown up further and purified using QIAGEN Miniprep or Maxiprep kits according to manufacturer's protocol.

Diagnostic restriction enzyme digestions were done to identify correctly assembled plasmids. Plasmids were sanger sequencing (Edinburgh Genomics) using the BigDye® Terminator v3.1 Cycle Reaction (Primers: Table 2.2). The BigDye®

Terminator v3.1 Cycle reaction was prepared as follows; 3.5µl of Enzymatic clean up reaction, 3.2 pmol sequencing primer, 2µl BigDye® Terminator v3.1 ready reaction mix and 3.5µl distilled H_20. Thermocycler reaction conditions: initial DNA denaturation 96°C 1 min followed by 25 cycles of DNA denaturation 96°C 10 secs, primer annealing 50°C 5 secs and extension 60°C for 4 mins.

2.5 NIH3T3 transfection experiments

2.5.1 NIH3T3 cell culture

Mouse NIH3T3 cells were cultured in DMEM medium supplemented with 10% foetal bovine serum (FBS) on cell culture dishes and flasks. Cells were regularly split using TryplE Express and DPBS. To split NIH3T3 cells: culture medium was removed, cells were washed briefly with pre-warmed PBS, then incubated for ~3 minutes in TryplE Express at 37°C. Cells were agitated to remove them from the bottom of the dish and visualised down the microscope to check they were sufficiently detached. TryplE Express was quenched with 3 volumes of medium. Cells were resuspended and moved to a universal/falcon tube. Cells were spun down at 1,300 rpm. The cell pellets were resuspended and a fraction of the cells were plated into fresh culture dishes containing pre-warmed medium.

2.5.2 Western blot analysis on NIH3T3 cell pellets

NIH3T3 cells were seeded into 6 well plates at a density of $1x10^6$ cells/well 24 hours before transfection to achieve 70-80% confluency at time of transfection. For each transfection (each well); 12 µl Lipofectamine-2000 was diluted in 150 µl Opti-MEM and incubated for 5 minutes at room temperature, 2.5 µg of plasmid DNA was diluted in 150µl of Opti-MEM before the Lipofectamine/Opti-MEM mix was added dropwise to the DNA/Opti-MEM mix and incubated for 20 minutes at room temperature. The DNA/ Lipofectamine/ Opti-MEM solution was added onto wells of 6-well plate containing freshly changed medium. Transfection was stopped by changing the medium 5 hours later. 3 wells of cells per were transfected per cDNA vector. Cells were harvested 24 hours later by trypsinisation, cell pellets were washed in DPBS

before being frozen at -80°C. Frozen pellets of cells were thawed on ice, any PBS was removed and pellets (confluent well of 6 well plate) were resuspended in 100µl ice cold NE1 buffer (20mM HEPES pH 7.9, 10mM KCL, 1mM $MgCl_2$, 0.1% Triton X-100, 20% glycerol, 0.5 mM DTT, Benzonase 1000U/ml and protease inhibitors cocktail) and incubated at room temperature for 10 mins. 125µl of 2x Laemmli Sample Buffer was added and solution vortexed, boiled for 3 minutes, snap frozen on dry ice then boiled for a further 3 minutes. Protein samples were aliquoted and snap frozen on dry ice before being stored at -80°C.

For western analysis on protein samples from transfected NIH3T3 cells; 5-10µl of the whole cell protein preps were run on Bio-Rad Mini-PROTEAN TGX precast gradient gel (4-20%) at 200V and blotted onto 0.2µM nitrocellulose membrane by 3 hours wet transfer in transfer buffer (25mM Tris, 192mM glycine) at 60V and 4°C. Membranes were blocked with 5% skimmed milk powder in 1X TBS + 0.1% Tween-20 and incubated overnight at 4°C with primary antibodies diluted in the same blocking solution (1:500 DTR, 1:1000 GFP, 1:10,000 H3). Membranes were washed 3 times for 5-20 mins each wash in 1X PBS + 0.1% Tween-20, blocked for 30 minutes before being incubated for 1-3 hours at room temperature with secondary antibodies diluted 1:10,000 in blocking solution (anti-goat 800CW, anti-mouse 800CW, anti-mouse 680LT, anti-rabbit 680LT Table 2.3). Membranes were washed again before being imaged on the LI-COR® Odyssey CLx imaging system and images analysed using Image Studio Lite software (LI-COR biosciences).

2.5.3 Immunofluorescence on transfected NIH3T3 cells

Day 1: NIH3T3 cells were seeded onto sterile 19 mm and 25 mm glass coverslips in 6 well plates at a density of 50,000 cells per well. Coverslips were sterilized using concentrated nitric acid, thoroughly washed with H_20 and 100% ethanol before use. Day 2: Cells were transfected with cDNA expression vectors; 2µg DNA, 10 µl lipofectamine-2000 and a total of 400 µl OptiMEM was used per transfection (each well) using same method described in section 2.5.2. Day 3: Cells were fixed. Medium was removed and replaced with 4% paraformaldehyde (in 1X PBS pH to 7.4) incubated for 15 minutes, washed in PBS, and stored at 4°C overnight in PBS before

staining. Cells were permeablised in 0.5% Triton X-100 in PBS, blocked for 1hr in 1.5% donkey serum, incubated for 2 hours with primary antibody (1:13 human DTR) and incubated for 1 hour with secondary antibody (1:1000 or 1:500 anti-goat 633). After each step cells were washed 3 times for 5 minutes in PBS. For the final set of washes: cells were washed 5 mins in PBS, incubated for 10 mins in 1µg/ml DAPI in PBS and washed again 5 mins in PBS. Coverslips of cells were mounted in ProLong Diamond onto slides, set overnight in the dark at RT before visualising and imaging using confocal microscopy (ZEISS LSM 880 with Airyscan).

2.5.4 Working with Diphtheria Toxin in cell culture

In order to use Diphtheria Toxin in cell culture I put together a risk assessment which was approved by the School of Biological Sciences Health and Safety Committee (see Appendix Document 1 for further details). Before working with DT, people working with DT ensured they had an up-to-date tetanus- diphtheria toxoid (Td) or equivalent immunization. Working with the toxin was to be done under Biological Containment level 2 conditions in Class II microbiological safety cabinet (MSC). Personal protective equipment including face mask, double gloving, disposable gown and lab coat were worn. Surfaces and equipment were cleaned with 10% bleach (1% Sodium hypochlorite) and 70% ethanol after use and DT containing liquid waste was inactivated with bleach for 30 minutes before disposing of. All disposable waste was autoclaved on a hotter cycle than the normal cycle used for lab waste in the building (134°C for 5 minutes). DT lyophilised power was reconstituted in 1 ml sterile cell culture H_20 (1mg/ml stock solution) which was then aliquoted into 10 µl-100µl aliquots and stored at in a locked container at -20°C.

2.5.5 DT-mediated ablation assay for transfected NIH3T3 cells

NIH3T3 cells were transfected with cDNA expression vectors, GFP positive cells were sorted using Fluorescence-activated cell sorting (FACS) and then treated with Diphtheria Toxin (DT) and analysed using the Incucyte® live-cell analysis system. Day 1: $5x10^6$ cells per 10 cm dish were seeded 2 dishes per genotype. Day 2: Cell were transfected with cDNA expression vector DNA using Lipofectamine-2000: 12 µg

DNA, 36 µl Lipofectamine-2000 and a total of 3 ml Opti-MEM using the same method as outlined in section 2.5.2. Day 3: Transfected cells were trypsinised and 2 dishes per plasmid were pooled and resuspended in 2 ml of normal NIH3T3 medium supplemented with 1% Pen/Strep and taken for FACS. FACs sorting was performed by Martin Waterfall using the FACS Aria II cell sorter (IIR Flow Cytometry Core Facility, UoE). 30,000 cells with high GFP fluorescence per well were sorted into 24 well plate containing pre-warmed medium with antibiotic. Sorted cells were put straight into the Incucyte® and imaged every 3 hours. Day 4: 24 hours after sorting NIH3T3 cells transfected with cDNA expression vectors were treated with medium containing 100 ng/ml DT and 200nM Incucyte® Cytotox Red dye. DT was diluted in normal growth medium and added to cells in a Class II Microbiology Safety Cabinet (MSC) in the Biological containment level 2 tissue culture room. Cells were imaged by the Incucyte® every 3 hours for a further 5 days. DT-containing medium and plates were discarded safely after imaging, contaminated medium was collected and inactivated with bleach (see 2.5.4 and Appendix Document 1.) before plates were disposed of for autoclaving. Quantification of percentage confluence and red cell count per well at each time point was done using the Incucyte® live-cell analysis software. A collection of images of NIH3T3 cells stained with Incucyte® cytotoxic red dye at different levels of confluence, were used to set up a Basic Processing Definition which was then applied to all images in the dataset. The parameters were set to ensure that the analysis software recognised the NIH3T3 cells and the red cell staining correctly compared to background (see confluence processing technical note and fluorescent processing technical note for details www.essenbioscience.com/en/resources/incucyte-zoom-resources-support/). For a 24-well plate, 4 phase and fluorescent images per well were taken at each time point. The Incucyte® analysis software then quantified the percentage confluence per phase image - the percentage of the image that is occupied by cells – and produces a value per well which is the average confluence of the 4 images. The number of red cells per image is then calculated from the fluorescent images and again given as a single value per well (the average count for 4 images).

2.6 Generation of targeted mouse ESCs

2.6.1 General ESC tissue culture

Mouse Ju09 embryonic stem cells (ESCs) (129/Ola mouse genetic background) were derived from E14TG2a ESCs (Hooper *et al*, 1987) by Jan Ure (Centre for Genome Research University of Edinburgh) and were gifted to the lab by Joe Mee from the Centre for Regenerative Medicine (University of Edinburgh). ESCs were cultured on gelatinized culture dishes and flasks in Glasgow MEM medium (GMEM) supplemented with recombinant mouse Leukemia Inhibitory Factor (LIF), 10% FBS, 1% Non-essential amino acids, 1% Sodium pyruvate, and 0.1% β-mecaptoethanol. Cells were routinely split between 1/8 and 1/16 every two to three days into a new gelatinised vessel using 1 X Trypsin-EDTA and on the intermediate days cells were given fresh media. To split ESCs, culture medium was removed, cells were washed briefly with pre-warmed Trypsin-EDTA, then incubated for ~3 minutes with fresh Trypsin-EDTA at 37°C. Cells were agitated to remove them from the bottom of the dish and visualised down the microscope to check they were sufficiently detached. Trypsin-EDTA was quenched in 3 volumes of medium. Cells were resuspended and moved to a universal/falcon tube. Cells were spun down at 1,300 rpm. The cell pellets were resuspended and 1/8-1/16 of the cells were plated into fresh gelatinised culture dishes containing pre-warmed medium.

2.6.2 Targeting ESCs

Linearized targeting vector was electroporated into low passage WT JuO9 ES cells and subjected to G418 selection. The targeting vector (50 µg) was linearized by digestion with restriction enzymes: EcoRV-HF for pBS-Me2-STOP-DTR, and NotI-HF for pBS-Me2-FLEx-DTR. Linearized vector DNA and CRISPR-cas9 plasmid DNA (50 µg) was extracted and sterilised using phenyl/chloroform extraction: an equal volume of phenyl/chloroform and 0.1 volume of NaOAc (3 M pH 5.2) was added to digestion reaction or plasmid Maxiprep, vortexed and centrifuged (5 minutes, 13,000 rpm). The aqueous layer was then removed and added to 1 volume of 100% ethanol before being incubated at -20°C overnight. The next day, linearized DNA was

centrifuged (5 minutes, 13,000 rpm) washed with 80% ethanol and pellets were stored at -20°C until ready to electroporate.

Extracted DNA was dissolved in filter sterilized TE, before 15μg of targeting vector and 5 μg CRISPR-Cas9 plasmid respectively were added to $20x10^6$ ES cells in 600 μl 1X PBS, transferred to a GenePulser Electroporation cuvette (0.4 cm gap) and electroporated using the Gene Pulser XCell™ machine (conditions; 240V, 500μF, ∞ resistance). Cells were allowed to recover for 10 minutes at room temperature before being plated at a density of $1\text{-}2x10^6$ in 10cm dishes in normal ES medium and 24 hours later G418 antibiotic (350μg/ml) selection was applied. Medium was changed every 2 days or more if needed. Resistant colonies were picked into 96-well round bottomed plates, Trypsinised and plated out in gelatinized 96-well plates in selection medium (150μg/ml G148). Once confluent, clones were Trypsinised, Trypsin was quenched with 50% selection medium, 50% FBS and half of the cells were transferred to 96-well plates containing selection media for continued growth for genomic DNA extraction, and to the other half cold 2x Freeze medium (20% DMSO in medium) was added, the plate were sealed and frozen at -80°C in a polystyrene container. Once confluent ,the plates of clones that were grown on further were lysed for genomic DNA extraction (see below).

Potential positively targeted clones identified by PCR (section 2.6.4) were later thawed in the 37°C water bath and transferred to 24-well plates. Confluent cells were then moved to 6-well plates and then split into two T25 flasks per clone. One confluent, T25 was cryopreserved in 3 aliquots (1X Freeze medium: Growth medium supplemented with 12% FBS and 10% DMSO) and from the other flask, cells were pelleted and stored at -80°C for genomic DNA extraction (see below).

2.6.3 Genomic DNA extraction from cultured cells

Confluent clones in 96-well plates were lysed overnight at 37°C in lysis buffer (100mM Tris pH8.5, 5 mM EDTA, 0.2% SDS, 200 mM NaCl, 100 μg/ml Proteinase K, 50 μg/ml RNase A). DNA was precipitated by the addition of 100μl Isopropanol and centrifuged at 3,000 rpm for 15 mins at RT. DNA pellets were washed in 100μl

Ethanol and centrifuged at 3,000rpm for 15 mins. DNA pellets were air-dried before being dissolved in 100 µl TE. For Southern blot analysis; genomic DNA was extracted from ES cell pellets harvested from confluent T25 flasks using the Gentra Puregene Cell Kit (QIAGEN) according to the kit manual.

2.6.4 PCR screening for targeting vector integration

Positively targeted clones were screened by PCR for targeted integration of the 5' and 3' end of the targeting vector. Primer pairs were used where one anneals just outside the homology arm in the *Mecp2* locus and the other one binds in the closest region 5' or 3' within the targeting vector which is not homologous to the unmodified locus (Primers see Table 2.2). Phusion® High Fidelity polymerase reactions were set up according to the manufacturers protocol. PCR reactions were run on 1% agarose gels containing EtBr.

2.6.5 Southern blot screening for targeted integration

Genomic DNA (10 µg per Southern blot) was digested with 3µl of restriction enzyme (Bsu361 and/or SacI) in appropriate NEB buffer in a total volume of 40 µl for around 8 hours at 37°C. Digested DNA was run on 0.8% agarose gel containing EtBr overnight at 36V (~18 hours). Gels were incubated in 0.25M HCL for 15 minutes and 0.4M NaOH for 45 minutes. Membranes (Zetaprobe or AmershamTM Hybond N+) were prewetted with ddH20 and 0.4M NaOH before dry transfer was assembled. Gel was blotted with prewetted membrane 2x wetted Whatman® 3MM papers, 2x dry Whatman® 3MM papers, a stack of tissues, a glass sheet and a weight. The gel was transferred for 4 hours before being disassembled. Membrane was washed in 2x SSC buffer before being air dried. Each membrane was blocked with 25 ml Church buffer containing 125 µl Herring Sperm DNA for 1-2 hours at 65°C. Per blot; 20-30 ng of a DNA probe homologous to the 3'UTR of Mecp2 (1.2-kb NcoI–BamHI fragment within the 3'UTR (Guy *et al*, 2001)) radioactively labelled with 5 µl [α32]dCTP using the Prime-a-Gene Labelling System according to manufacturer's protocol. Labelled probe was purified using G50 column, boiled at 100°C for 5 minutes, rapidly cooled on ice and added to membranes in blocking solution. Probes were left to hybridise at

65°C, overnight, with rotation. The next day membranes were washed once in room temperature RT 2xSSC briefly followed by two 20 minute washes in 2x SSC + 1% SDS at 65°C. The membrane was sealed between sheets of polythene and exposed in a Phosphor Imager Cassette. The phosphor screens were imaged after 24 hours' or 3 days' exposure using the Typhoon FLA 7000.

2.6.6 Sequencing the targeted locus in ESCs

PCR amplicons of DNA were generated encompassing the important modifications in the *Mecp2*^{StopDTR} and *Mecp2*$^{FLExDTR(OFF)}$ targeted loci where mutations would be deleterious (Primers: Table 2.2). Phusion® High Fidelity polymerase reactions were performed according to manufacturer's protocol. PCR reactions were run on 1% agarose gels containing EtBr. PCR reactions were cleaned up by incubation with Exonuclease 1 and Antarctic phosphatase (0.5µl of enzyme per 15µl of PCR reaction plus 12.5µl dd$H_2$0) at 37°C for 15 mins before inactivating the enzymes at 80°C for 15 mins. Alternatively, the desired product was purified by gel extraction using Zymoclean™ Gel DNA recovery kit. The PCR amplicons were Sanger sequenced (Edinburgh Genomics) using the BigDye® Terminator v3.1 Cycle Reaction (Primers: Table 2.2) .

2.6.7 Karyotyping

One 10 cm dish of proliferating ES cells (~50% confluency) per clone were treated with 0.1 µg/ml KARYOMAX® Colcemid™ and incubated at 37°C for 3 hours to arrest the cells in metaphase. Medium was removed and cells were washed twice with PBS, Trypsinised and harvested. Pellets of cells were resuspended in 300µl and 5ml of 0.4% KCl and incubated at 37°C for 10 minutes. Fixative (100µl MeOH: Acetic acid 3:1) was then added to cells at room temperature and mixed gently by inversion. Cells were centrifuged at 300 x g for 5 mins, supernatant removed and resuspended in 5 ml of fixative. Cells were incubated at room temperature for 20 mins before being centrifuged again at 300 x g for 5 mins. Supernatant was removed and cells resuspended in 200 µl of fixative. Cell suspension (20 µl) was dropped from approximately 30 cm onto pre-chilled slides. Slides were allowed to dry overnight at

room temperature before being mounted in Vectashield® mounting medium with DAPI and coverslips were sealed with nail polish.

2.7 Characterisation of knock-in ESCs and mice

2.7.1 Transient transfection with Cre expressing plasmid

ES cells (10 x 10^6) were transfected with 15 µg pCAGGS-CRE plasmid (Araki *et al*, 1995) by Electroporation (Gene Pulser XCell^{TM} machine; 240V, 500µF, ∞ resistance). Transfected cells were grown on for 2 days before being split at clonal density (~1000 cells per 10 cm dish). Colonies were picked into a 96 - well round bottomed plate, Trypsinised and half of the cells were plated into a gelatinized master wells in normal medium and the other half were plated into duplicate wells in selection medium: 350 µg/ml G148 (*Mecp2*^{StopDTR} targeting) or 100 ng/ml Diphtheria Toxin containing medium (*Mecp2*$^{FLExDTR(OFF)}$ targeting). Master clones which were killed by G418 or DT in the duplicate wells were grown on further.

2.7.2 Differentiation of ESCs into neurons

Rapidly proliferating ESCs are plated into non - tissue culture treated deep bacterial dishes (6 x 10^6 cells per dish, two dishes per genotype) in 10ml Embryoid Bodies (EB) medium (normal ESC medium without LIF: GMEM supplemented with 10% FBS, 1% Non-essential amino acids, 1% Sodium pyruvate). Medium was changed on EBs 2 days later: EBs were collected in falcon tubes allowed to settle at the bottom before medium aspirated, EBs were resuspended in fresh EB medium and plated in a new deep bacterial dish. Volume of medium was increased to 13 mls. On day 4 and 6 medium was changed again, this time 10µM Retinoic Acid (RA) was added to the medium and volume was increased to 15mls. After 4 days in RA, EBs are trypsinised and plated out onto Poly-D-Lysine and Laminin coated Nucleon® treated 6 cm dishes or 6 well plates. Dishes/plates were treated with 10µg/ml PDL dissolved in PBS and incubated at room temperature for 20 minutes before being washed twice with PBS. Dishes/plates were directly treated with 4µg/ml Laminin in PBS or washed dishes/plates were aspirated and allowed to dry and stored at RT in sealed container to

be Laminin treated later. Laminin treated plates were incubated for 4 hours at room temperature or at 4°C overnight before laminin was aspirated and neuronal precursors were seeded immediately into dishes/plates. For trypsinisation of EBs; two plates of EBs per genotype were collected in 50 ml falcon tubes and EBs were washed three times with 20 mls PBS. Between washes EBs were allowed to settle before most of the medium or PBS was aspirated. After third wash as much PBS as possible was removed before 1 ml of 4x TES (1%Trypsin (from 2.5% Trypsin stock see table 2.1.4), 4% Chicken serum, and 4mM EDTA(cell culture) in DPBS) was added and cells incubated at 37°C with gentle agitation for 5 minutes. Trypsinisation was stopped with 10ml EB medium. Cells were centrifuged for 5 mins at 1100 rpm, medium aspirated and cells resuspended in 10ml EB medium by gentle pipetting. Cells were left for 5 minutes for undigested EBs to settle before upper medium was passed through a 40µm Cell Sieve into a new flacon tube. Cells were counted and an appropriate volume of cell suspension was centrifuged for 5 minutes at 1100 rpm before being resuspended in plating medium (Advanced DMEM/F12, 1xN-2 supplement, 1x Pen/Strep and 1x L-Glutamine). Cells were plated at a density of $2x10^5$ cells/cm^2 on coated dishes and plates. The next day dishes/plates were shaken firmly to remove dead cells and half the medium was replaced with Neuronal differentiation medium (Neurobasal medium, 1x B-27 supplement, 1x Pen/Strep, and L-Glutamine). Every 3 days, half of medium was replaced with Neuronal differentiation medium and 6 or 7 days after plating the EBs out cells were harvested. To harvest neurons, medium was removed cells washed in ice cold PBS before layer of neurons was removed using a cell lifter into fresh cold PBS. Cells were centrifuged for 1 min at 13,000 rpm, PBS removed, centrifuged again for 15 minutes at 13,000 rpm, PBS removed and finally pellets were snap frozen on dry ice.

2.7.3 Protein extraction and western blot analysis of ESC-derived neurons

Frozen pellets of neurons were thawed on ice, any PBS was removed and pellets (from 6cm dish ~$10x10^6$ cells) were resuspended in 125µl ice cold NE1 (20mM HEPES pH 7.9, 10mM KCL, 1mM $MgCl_2$, 0.1% Triton X-100, 20% glycerol, 0.5 mM DTT, Benzonase 1000U/ml and protease inhibitors cocktail) and incubated at room

temperature for 10 mins. 150µl of 2x Laemmli sample buffer was added and solution vortexed, boiled for 3 mins, snap frozen on dry ice then boiled for 3 mins. Samples were either ran out on gel directly or aliquoted and snap frozen on dry ice before being stored at -80°C.

For western analysis on protein samples from ESC derived neurons: 10µl of the whole cell protein preps were run on Bio-Rad TGX gradient gel (4-20%) at 220V in 1 X SDS running buffer and blotted onto 0.2µM nitrocellulose membrane by overnight wet transfer in 1 X Transfer Buffer at 25V and 4°C. Membranes were blocked with 5% skimmed milk powder in 1X TBS + 0.1% Tween-20 and incubated overnight at 4°C with primary antibodies diluted in the same blocking solution (primary antibodies; 1:500 DTR, 1:1000 GFP, 1:10,000 H3). Membranes were washed 3 x 5 - 20 minutes in 1X PBS + 0.1% Tween-20, blocked for 30 minutes before being incubated for 1-3 hours at room temperature with secondary antibodies diluted 1:10,000 (secondary antibodies; anti-goat 800CW, anti-mouse 800CW, anti-mouse 680LT, anti-rabbit 680LT). Membranes were washed 3 x 5 - 20 minutes in PBS and imaged on the LI-COR® Odyssey CLx imaging system and images quantified using Image Studio Lite software (LI-COR biosciences).

2.7.4 RNA extraction from ESC-derived neurons and mouse brain

RNA was extracted from frozen pellets of ESC-derived neurons (6 cm dish ~1 $x10^6$ neurons) and frozen mouse brain (half brain per prep) using the TRI Reagent® protocol. RNA was dissolved in nuclease free H_20 and stored at -20°C.

2.7.5 Northern blot analysis of RNA extracted from ESC-derived neurons or mouse brain

Northern blot buffers: 10X MESA buffer: 0.2M MOPS (3-(N-morpholino)propanesulfonic acid), 50 mM NaOAc and 10 mM EDTA. RNA sample buffer: 375 µl deionised formamide, 75 µl 10x MESA buffer, 120 µl 37% formaldehyde, 50 µl nuclease free H_20.

RNA (20 µg) was precipitated in 0.1 volume of NaOAc (3M pH 5.2), and 2 volumes of ~100% Ethanol overnight at -20°C. RNA was centrifuged (15 mins, 13,000 rpm at 4°C), washed in 75% Ethanol, centrifuged (5 mins, 13,000 rpm at 4°C). Pellet was dried briefly and dissolved in 5 µl nuclease free H_20. RNA sample buffer (20µl per sample) was added and RNA was run on gel immediately of stored temporarily at -20°C. Before loading the gel samples were incubated at 65°C for 15 minutes, centrifuged briefly before 5 µl 1 X Orange G/ 0.2 mg/ml EtBr loading buffer was added. Samples were run on a 15 by 20 cm 1% agarose, 1X MESA buffer and 2% formaldehyde gel in 1X MESA running buffer overnight at 36V.

The RNA was transferred onto a nylon blotting membrane (Amersham™ Hybond N+) by capillary transfer. The gel was incubated twice for 20 minutes in 10 x SSC with gentle shaking. The membrane was prewetted in distilled H_20 for 5 mins followed by a 10 minutes soak in 10 x SSC. The transfer was assembled as follows: the gel was suspended above a tray of 10 x SSC buffer, on top of two 3MM Whatman® papers and a 3MM Whatman® paper wick where the edged of the paper were soaking in the buffer below so that it draws the buffer into the gel by capillary action. On top of the gel is the membrane followed by two 3MM CHR Whatman™ blotting papers, a thick piece of Whatman™ gel blotting paper (Grade GB003), a stack of paper towels, a glass plate and finally a weight. The RNA was allowed to transfer overnight. The blot was disassembled and the membrane was washed in 2 x SSC. The RNA was fixed to the membrane by U.V crosslinking and baking at 80°C for 2 hours. The hybridisation, washes and exposure was done the same as for the Southern blot (described in 2.6.5). Hybridisation probes used were the 1.2kb NcoI-BamHI fragment of the 3'UTR of mouse *Mecp2* (Guy *et al*, 2001) or the DTR cDNA fragment (prepared by digesting the pDTR vector with AgeI-HF and NotI-HF and gel extraction using Zymoclean™ Gel DNA recovery kit). Quantification of the signal intensity on northern blots was performed using Fiji-ImageJ.

2.7.6 RT-qPCR analysis on ESC-derived neurons

The QuantiTect® Reverse Transcription kit was used to synthesis cDNA from isolated RNA according to manufacturer's protocol which included a genomic DNA Wipeout

step. Negative control reactions with no reverse transcriptase enzyme were carried out for all samples. cDNA samples were diluted 1:10 in nuclease free H_20 and stored at -20°C.

Sensimix^{TM} SYBR® and Fluorescein Kit was used for Real - Time quantitative PCR (RT-qPCR). Each reaction included: 1X Sensimix^{TM} reagent, 500 nM of each primer (*Mecp2*: F_qPCR1 and R_qPCR1 GAPDH: F and R) and 2.5 µl of cDNA made up to 12.5 µl with nuclease free H_20. Serial dilutions of cDNA were used to produce standard curves for each primer set. For each primer pair, 3 technical replicate reactions were run for each cDNA sample including the serial dilutions. RT-qPCR reactions were ran in a 384-well plate on the Lightcycler 480 (Roche): thermocycler conditions: 95°C for 10 min, followed by 40 cycles of: 95°C 15s, 60°C 15s, 72°C 15s. Melting curves were generated following amplification to determine the specificity of each primer pair: thermocycler conditions: ramp up from 60°C to 95°C (ramp 0.11, 5 acquisition per °C. The relative expression of the modified *Mecp2* alleles compared to the house keeping gene GAPDH was quantified using the relative standard curve method. Briefly, standard curves for each primer pair were plotted (Cp values vs. log dilution factor) and fitted to a straight line. The gradient of this line was used to estimate the PCR efficiency for each primer pair. This plot was then used to normalise each experimental value. The normalised values calculated for *Mecp2* (WT or modified *Mecp2* alleles both recognised by primers) were then divided by the those normalised values for the house keeping gene GAPDH, to get the relative expression level. The relative expression values were then averaged for the technical triplicates. As three biological replicates were performed (three neuronal differentiations), the values presented is the mean of the technical replicates for each biological replicate.

2.7.7 Sequencing cDNA from ESC-derived neurons and mouse brain

For all RT-PCR reactions: 2.5 µl cDNA (preparation described in 2.7.6) was used per 50 µl Phusion® High-Fidelity DNA Polymerase reaction. Primers which annealed in the unmodified UTRs of *Mecp2* were used to amplify the entire coding sequence of cDNA in all ESC-derived neurons or mouse brain (primers: F_5'UTR, pbsSeqRev2). PCR amplicons were cleaned up with the MSB® Spin PCRapace kit and blunt cloned

using the StrataClone PCR blunt cloning kit according to kit protocols. Blue, white screening was used to identify colonies with plasmid that had incorporated the insert.

For cDNA amplicons from ESC-derived neurons: 10 white colonies per genotype *Mecp2*^{DTR}, *Mecp2*^{StopDTR} were picked, grown up and purified using QIAGEN Miniprep kit. The cloned inserts were Sanger sequenced (Edinburgh Genomics) from the extracted plasmids using the BigDye® Terminator v3.1 Cycle Reaction (primers: T3 and R_DTR). Sequencing data was retrieved for 6 - 8 cDNA clones per genotype to get an idea of the species of mRNA formed from each allele.

Colony PCR was performed on a larger number of colonies for cDNA amplicons from *Mecp2*$^{StopDTR/y}$ and *Mecp2*^{mCherryStop} mouse brain. The DreamTaq PCR master mix 2X was used according to manufacturer's instructions with an extended denaturation step of 5 minutes to lyse the bacteria. Primers in the backbone of the vector were used to amplify the entire insert (M13 Seq Fwd and Rev). PCR reactions were cleaned up by incubation with Exonuclease 1 and Antarctic phosphatase (0.5µl of enzyme per 15µl of PCR reaction plus 12.5µl ddH_20) at 37°C for 15 mins before inactivating the enzymes at 80°C for 15 mins. The splice boundary of the cDNA clones were Sanger sequenced (Edinburgh Genomics) using the BigDye® Terminator v3.1 Cycle Reaction (Primer: F_5'UTR). PCR reactions were performed and sequenced from DNA from two biological replicates (mouse brains from two separate animals). 30 aligned sequences were analysed per biological replicate.

2.7.8 RT-PCR and Southern blot analysis

RT-PCR was performed as described above (section 2.7.7) using primers which amplify across the exon-to-exon splice boundaries (F_5'UTR and R_DTR). 25 µl of the PCR reaction was ran on a 2% agarose/EtBr gel. The gel was soaked in 0.4 M NaOH for 20 minutes. The Southern blot transfer was assembled as described in 2.6.5 and DNA was left to transfer overnight. The membrane was probed with a 32 nt Ex1-DTR single stranded radiolabelled oligo probe which anneals across the exon 1 – exon 3 (DTR) boundary (sequence in primers Table 2.2.). The melting temperature of the entire oligo is 78°C and the melting temperature of each half which has homology to

either side of the splice boundary is below 65°C. The membrane was blocked as described previously (section 2.6.5). The 32 nt probe was end labelled using a T4 Polynucleotide Kinase (PNK): 10 pmol of oligo was incubated with 2 µl [γ^{32}]dATP and PNK buffer for 1 minute at 37°C, before 2.5 µl T4 PNK was added and incubated for 30 minutes at 37°C. The probe was Column purified using Zymoclean™ Gel DNA recovery kit: 300 µl Agarose Dissolving Buffer (ADB) was added, solution centrifuged at 10,000 rpm, washed with kit wash buffer twice and eluted in 50 µl elution buffer. Probe was boiled for 5 mins and added to membrane in blocking buffer and allowed to hybridise overnight at 65°C with rotation. The membrane was washed in 6 x SSC, 1% SDS for 20 minutes at 65°C followed by another 10 minute wash. The membrane was sealed between sheets of polythene and exposed in a Phosphor Imager Cassette for 1.5 hours before imaging using the Typhoon FLA 7000.

2.7.9 DT-mediated ablation assay for mouse ESCs

ESCs were plated at a density of 50,000 - 80,000 cells per well into 24-well gelatinized plates in 0.5 ml normal growth medium. Plates of cells were taken to Biological containment level 2 tissue culture room for Diphtheria toxin to be added. DT and Incucyte® Cytotox Red dye were diluted in normal growth medium to concentrations 2x the final concentration: 0 - 2 µg/ml DT and 200 µM Incucyte® Cytotox Red dye. DT and Incucyte® Cytotox Red containing medium was added on top of seeded ESCs (0.5 ml per well) to give final concentrations of 0 - 1 µg/ml DT and 100 µM Incucyte® Cytotox Red dye. Cells were imaged by the Incucyte®, 4 images per well every 2 or 3 hours for up to 72 hours. DT-containing medium and plates were discarded safely after imaging. Quantification of percentage confluence per well at each time point was measured using the Incucyte® analysis software as described previously in section 2.5.5. A new Basic analysis Processing Definition was set up for ESCs to run the analysis.

2.7.10 TUNEL analysis on DT-treated ESCs

ESCs were seeded into 6 well plates at a density of 100,000 cells per well. Three replicate wells of each genotype per condition (No DT or +DT) were seeded and two

wells for unstained controls. Two days later (cells ~50% confluent) medium was changed on cells to normal ESC medium containing 0 or 100 ng/ml DT. 24 hours later cells were harvested by Trysinisation. The medium from all wells, 1st Trypsin wash and Trypsinised cells were all collected, no cells were discarded. Cells were centrifuged (5 mins 500 x g), washed in 1 ml PBS and centrifuged (5 mins 500 x g). To fix cells: cells were resuspended in 200 µl PBS, 1 ml 2% paraformaldehyde in PBS was added dropwise with gentle swirling and incubated 15 - 30 minute at room temperature. Fixed cells were centrifuged (5 mins 500 x g) and washed 3 x 1 ml PBS. For permeabilization: cells were incubated in 500 µl PBTB (0.1%Triton, 5%BSA in PBS) for 15 minutes on ice then centrifuged (5 mins 500 x g). Cell pellets were resuspended in 50 µl of TUNEL reaction mix (*In situ* cell death kit TMR red)(or labelling solution for unstained controls) and incubated for 1 hour in dark at 37°C with gentle pipetting every 15 mins. After incubation, 1 ml PBTB was added and solution centrifuged (5 min 500 x g). Stained cells were washed 2x in 1ml PBTB and centrifuged (5 min 500 x g). Stained cells were resuspended in 500 µl PBTB, stored at 4°C overnight and analysed by flow cytometry by Martin Waterfall the next day (IIR Flow Cytometry Core Facility, UoE).

2.7.11 DT-mediated ablation assay for ESC-derived neurons

ESCs were differentiated using the protocol described in section 2.7.2. The DT and Incucyte® Cytotox Red Dye treatment was incorporated into the first half medium change after Trypsinising the Embryoid Bodies (EBs) and plating out the neuronal precursors into 6-well plates. Three replicate wells of each genotype were seeded per DT concentration. Plates of cells were taken to Biological Containment Level 2 tissue culture room for DT to be added. DT and Incucyte® Cytotox Red dye were diluted in neuronal differentiation medium (section 2.7.2) to 2x the final concentrations: 0 - 200 ng/ml DT and 200 µM Incucyte® Cytotox Red dye. Half of the medium was removed from each well of differentiating neurons and replaced with DT and Incucyte® Cytotox Red containing medium (1 ml per well) to give final concentrations of: 0 - 100 ng/ml DT and 100 µM Incucyte® Cytotox Red dye. Neurons were imaged by the Incucyte®, 16 images per well every 3 hours for a total of 72 or 96 hours. DT-containing medium and plates were discarded safely after imaging. Quantification of

red cell count per mm^2, per well, at each time point was measured using the Incucyte® analysis software. A NeuroTrack analysis Processing Definition was set up using a representative collection of images of the mESC-derived neurons under different experimental conditions, at different time points (see NeuroTrack Fluorescence Processing Technical Note https://www.essenbioscience.com/en/resources/incucyte-zoom-resources-support/). Parameters were set to ensure that analysis software recognised the fluorescent cell bodies correctly compared to the background. The red cell count per mm^2 was quantified per image and an average value per well (average of 16 images) was generated.

2.8 Generation and experiments with *Mecp2*^{StopDTR} and *Mecp2*$^{FLExDTR(OFF)}$ mice

2.8.1 Mouse experiments

All mice used in this study were bred and maintained at the University of Edinburgh animal facilities under standard conditions, and procedures were carried out by certified persons, licensed by the UK Home Office and according to the Animals (Scientific Procedures) Act 1986. All experiments were performed in accordance with the project license authorised by the UK Home Office.

2.8.2 Genotyping of mice

Mice were ear biopsied for genotyping. DNA was extracted from ear notches as follows: 25 or 50 µl of 'ear biopsy buffer' (50 mM KCl, 1.5 mM $MgCl_2$, 10mM Tris HCl pH8.5, 0.01% PBS-gelatine, 0.45% NP-40, 0.45% Tween 20, 0.45% Triton X-100, 100 µg/ml Proteinase K) was added to each ear notch. Samples were then run in the following thermocycler programme: 65°C 15 min, 96°C 2 min, 65°C 4 min, 96°C 1 min, 65°C 1 min, 96°C 2 30 s. Genotypes were determined by DreamTaq PCR using 2 X DreamTaq polymerase Master mix, according to manufactures protocol. All PCR reactions were ran at the same annealing temperature 58 °C.

For the *Mecp2*^{StopDTR} and *Mecp2*$^{FLExDTR(OFF)}$ lines, the NeoF/NeoR primers which amplified within the *PGK-neo* gene present in both lines detected the presence of the *Mecp2*^{StopDTR} and the *Mecp2*$^{FLExDTR(OFF)}$ modified allele. A second PCR which used the P3 forward and reverse primers which anneal in the *Mecp2* intron 2 were used to identify the WT *Mecp2* allele (the amplicon is disrupted in the modified alleles). Genotypes of transgenic Cre driver lines were determined using primers located within the *cre* transgene (see Table 2.2). Genotyping was performed by Dina De Sousa, Verdiana Steccanella and for a short time Justyna Cholewa-Waclaw.

2.8.3 Generation of the knock-in mouse lines by blastocyst injection

Mecp2^{StopDTR} and *Mecp2*$^{FLExDTR(OFF)}$ knock-in low passage mouse Ju09 ES cells (129/Ola) were used for blastocyst injection. Blastocyst injections to generate the *Mecp2*^{StopDTR} mouse line were carried out by Jim Selfridge from the Bird lab. The generation of the *Mecp2*$^{FLExDTR(OFF)}$ mouse line was carried out by the Bioresearch and Veterinary Services (BVS) Central Transgenic Core (CTC) facility. Typically: ~15 ES cells were injected per blastocyst and ~12 injected blastocysts were transferred by unilateral embryo transfer (Jim Selfridge) or ~20 were transferred by bilateral transfer (CTC) to pseudo-pregnant recipient females (B6CBA/F1). For the *Mecp2*^{StopDTR} line: 7 recipient females received blastocysts, all became pregnant and 42 pups were born. For the *Mecp2*$^{FLExDTR(OFF)}$ line: 6 recipient females received embryos, 5 became pregnant and 17 pups were born. Chimeric offspring were identified by their varied coat colour due to the contribution of both the chinchilla (129/Ola) ESC and black (C57BL/6J) embryos. Interestingly, in both separate transgenic generation experiments, a total of 5 chimaeras were identified which were all test mated to C57BL/6J mice. For both the *Mecp2*^{StopDTR} and *Mecp2*$^{FLExDTR(OFF)}$ lines, one male chimaera had 2 litters with 100% germline transmission (identified by the agouti coat colour). Female germline pups, heterozygous for the knock-in allele were bred on to C57BL/6J males to establish the line.

2.8.4 Administration of DT to mice

In order to administer DT to mice I put together a risk assessment which was approved by the GM and Biological Safety Committee for Easter Bush (see Appendix Document

2 for details). All laboratory members working with DT (Jim Selfridge and myself) ensured they had an up-to-date tetanus-diphtheria toxoid (Td) or equivalent immunization. All work with DT was done under Biological Containment level 2 conditions in a Class II microbiological safety cabinet (MSC) including mouse injections and tissue harvesting. DT activity is not found in the urine or faeces of rodents receiving doses of less than 50 μg/kg, therefore animals treated with DT, bedding, cages etc.. in contact with treated animals were not a risk to the handler. Personal protective equipment including, disposable lab coat or gown with long sleeves and elasticated cuffs and double gloving was worn. All syringes and needles were disposed of in a small sharps box which was disposed of in autoclave waste along with all other disposable waste. All disposable waste was autoclaved for 1 hour at 136°C. Surfaces and equipment were cleaned with 10% bleach (1% Sodium hypochlorite) and 70% ethanol after use. Excess DT was kept to a minimum and inactivated by autoclave.

DT was stored at Kings Building (KB) in the Bird lab (as outlined in section 2.5.4 and Appendix Document 1.) and thawed and diluted at KB before being transported to the animal facility on the day of injections. Alternatively for some experiments DT was provided by Prof. Neil Mabbott's lab at Roslin Institute due to ease of transportation. Rachel Young prepared and transported DT safely according to local risk assessment to the animal facility on the day of injections. For transportation from KB: DT was transported in 1ml plastic vials with leak proof lids at a maximum concentration of 5ug/ml. Plastic vials were within two further layers of packaging. Outer package consisted of a Nalgene® screw cap, rigid plastic container (500mL), lined with sufficient absorbent material to absorb the entire contents of the inner packaging. Outer package was appropriately labelled as with a copy of the safety data sheet secured to the container and the associated hazard symbols clearly marked.

Training for Intraperitoneal injection (IP) into mice was carried out by designated trainers within the animal facility recognized by the Named Training Competency Officer (NTCO) for Bioresearch and Veterinary Services (BVS). This training was carried out within the guidelines of the Standard Operating Procedure (SOP) for administering an IP injection into mice. The injection volume of DT depended on the

animal weight but the DT concentration was calculated to ensure that the injection volume was less <20 ml/kg to comply with the UofE BVS guidelines. Consecutive injections (where performed) were administered to alternative sides of the abdomen.

2.8.5 Administration of DT to Mecp2^{StopDTR} male mice

Homozygous male *Mecp2*^{StopDTR} mice and their WT littermates (3 or 4 of each genotype) were administered DT dissolved in PBS by intraperitoneal (IP) injection. One daily injection of 50 µg/kg on two consecutive day or a single injection of 0.5 µg/kg or 5 µg/kg was administered to 3 separate cohorts at 3 – 5 weeks of age. The first set of injections (using 50 µg/kg) were carried out by Jim Selfridge. All other IP injections were carried out by me. Mice were checked twice daily for general condition and weighed once daily by animal unit staff (BVS). Injected mice were culled by cervical dislocation if they reached their humane endpoints (see below) or 1 week after the first injection. A gross post-mortem was done on each animal and tissues were harvested including brain, liver, kidney and gut and snap frozen in liquid nitrogen (LN_2).

Humane endpoints due to adverse effects of DT injection included: weight loss (~20%), loss of general condition (pinched at rear and hunched) and contents of the gut appeared black on post-mortem. Humane endpoints due to an MeCP2 deficiency phenotype include: weight loss of more than 20% of bodyweight, a tremor score of higher than 2, a general appearance score of higher than 2 or breathing score of 2. MeCP2 null mice on a mixed background typically reach their humane endpoint between 6-20 weeks of life without intervention.

2.8.6 Administration of DT to Mecp2$^{FLExDTR(OFF)}$ male and female mice

Male and female mice harboring the *Mecp2*$^{FLExDTR(OFF)}$ allele and WT control mice were administered DT dissolved in PBS by IP injection. To begin with 3 mice of each genotype: *Mecp2*$^{FLExDTR(OFF)/y}$ males, *Mecp2*$^{+/y}$ males, *Mecp2*$^{FLExDTR(OFF)/+}$ females and *Mecp2*$^{+/+}$ females were injected with one IP injection of 5ug/kg at 3 weeks of age. I carried out all the IP injections for the *Mecp2*$^{FLExDTR(OFF)}$ animals. Animals were weighed every day and assessed visually twice daily for one week followed by once

daily for any signs of adverse effects by animal unit staff (BVS). Mice were culled by cervical dislocation 3 weeks for males and 4 weeks for females after the date of injection and their gross anatomy was assessed post-mortem. Following this experiment 3 *Mecp2*$^{FLExDTR(OFF)/y}$ and 3 *Mecp2*$^{+/y}$ males, were injected with one IP injection of 50 ug/kg at 3 weeks of age. Following injections mice were monitored closely as above and culled 3 weeks following injection.

2.9 Characterisation of the *Syn1-cre* and *Snap25-IRES2-cre* transgenic lines

2.9.1 Transgenic Cre driver mice

The three following transgenic Cre driver mice lines were acquired from Jackson Laboratory and maintained in the animal facility: B6.Cg-Tg(Nes-cre)1Kln/J (JAX stock no: 003771); B6;129S-*Snap25*$^{tm2.1(cre)Hze}$/J (JAX stock no: 023525) and B6.Cg-Tg(Syn1-cre)671Jxm/J (JAX stock no: 003966). These mice were crossed to the *Mecp2* Cre reporter line: *Mecp2*^{mCherryStop}, generated by Jim Selfridge in the Bird lab. The *Mecp2*^{mCherry} line with constitutive MeCP2^{mCherry} expression was generated by crossing *Mecp2*^{mCherryStop} mice with B6.C-Tg(CMV-cre)1Cgn/J (JAX stock no: 006054). Tissues were harvested from 6-8 week old mice. I performed the majority of tissue collections and perfusion fixations. Some tissue collections were performed by Bioresearch Veterinary Services (BVS) animal facility staff.

2.9.2 Protein extraction from mouse tissues

Protein samples were prepared for western blotting by homogenizing tissues (half a brain, section of lung and liver, entire tissue for other tissues) using an Ultra-Turrax T25 homogeniser in NE1 buffer (20mM HEPES pH 7.9, 10mM KCL, 1mM $MgCl_2$, 0.1% Triton X-100, 20% glycerol, 0.5 mM DTT, protease Inhibitors cocktail). The homogenates were incubated with 1000U/ml Benzonase for 15 minutes at room temperature before an equal volume of 2 x Laemmli Sample Buffer was added. Samples were boiled for 5 minutes, snap frozen on dry ice, boiled again before

centrifuging (13,000rpm 5 minutes 4°C) and taking the supernatant. Protein samples were aliquoted and snap frozen before being stored at -80°C.

2.9.3 Western blot analysis on protein extracts from mouse tissues

For western analysis protein samples were firstly diluted in 1x Laemmli Sample Buffer; Brain, heart, kidney, lung and spleen were diluted 1:4 and liver and testis were diluted 1:2, before being boiled for 3 minutes. 10µl of the dilutions were run on Bio-Rad TGX gradient gel (4-20%) at 220V in 1XSDS running buffer and blotted onto 0.2µM nitrocellulose membrane by overnight wet transfer in 1 X Transfer Buffer at 25V and 4°C. Membranes were blocked with 5% skimmed milk powder in 1X TBS + 0.1% Tween-20 and incubated overnight at 4°C with primary antibodies diluted in the same blocking solution (1:1000 MeCP2, 1:5000 mCherry and 1:10,000 H3 rabbit Table 2.3.). Membranes were washed in 1X PBS + 0.1% Tween-20, blocked for 30 minutes before being incubated for 1-3 hours at room temperature with secondary antibodies diluted 1:10,000 (anti-mouse 800CW, anti-rabbit 680LT, 800CW anti-rabbit). Membranes were imaged on the LI-COR® Odyssey CLx imaging system. Quantification of the signal intensity of bands on the western blot images was performed using Image Studio Lite software (LI-COR biosciences).

2.9.4 Nuclei extraction from mouse brain tissue

Whole brain was gently homogenized using small loose dounces for 20 strokes in 2ml ice cold homogenization buffer (HB) (320mM Sucrose, 5mM CaCl, 3mM MgAc, 10mM Tris pH8.0, 0.1nM EDTA, 0.1% NP40, 0.1 mM PMSF, 1mM B-Mercaptoethanol, 1x Protease inhibitors). Homogenate was transfered to falcon tube containing 3ml HB, mixed and kept on ice for 5min. 10ml ice cold 29% iso osmolar OptiPrep solution (29% OPTIPREP in dH_20) was loaded into 30ml Ultracentrifuge tubes (Ultra clear Beckman Coulter SW28 rotor) on ice. 5ml of ice cold 50% OptiPrep gradient centrifugation medium (50% OPTIPREP, 5mM CaCl, 3mM MgAc, 10mM Tris-HCl pH8.0, 0.1mM PMSF, 1mM Beta-mecaptoethanol in dH_20) was added to the lysate and solution was mixed by inverting the tube. Lysate plus 50% OptiPrep was very slowly added on top of 10ml 29% iso osmolar OptiPrep solution in centrifuge

tubes and samples were centrifuged at 10.100 x g (7500 rpm) for 30 min at 4°C in Ultracentrifuge. Nuclei were resuspend in 2 ml resuspension buffer (5% Glycerol, 1x protease inhibitors in PBS), aliquoted into 4 cryovials per sample, flash frozen in liquid nitrogen and stored at -80°C.

2.9.5 Flow cytometry on nuclei from mouse brain tissue

Nuclei were thawed on ice and centrifuged at 600g for 5 mins at 4°C. Supernatant was removed, nuclei pellet resuspended in 500µl of PBTB (2.5g Bovine Serum Albumin (BSA), 0.1% Triton, 1x protease inhibitors in PBS filter sterilized) by gentle pipetting and suspension was again centrifuged at 600 g for 5 mins at 4°C. Supernatant was removed and nuclei pellet gently resuspended in 250µl PBTB. NeuN primary antibody (10µl) was conjugated to Alexa Fluor™ 647 using APEX™ Alexa Fluor™ Antibody labelling Kit according to kit manual. The final eluate volume of the labelling reaction is ~50µl. 2µl of labelled antibody was added to the resuspended nuclei (2µl per nuclei aliquot corresponding to ~1/4 brain). Nuclei were incubated for 45 mins at 4°C on rotating wheel protected from light. After incubation stained nuclei were taken to flow cytometer (IIR Flow Cytometry Core Facility, UoE) for analysis on ice. Martin Waterfall performed Flow Cytometry analysis.

2.9.6 Perfusion fixation and sectioning mouse brain

Mice were perfused with 4% paraformaldehyde (PFA)(in 1X PBS pH to 7.4) following culling before dissection of the brain. Mice were culled using CO_2 according to UoE Biological Veterinary Services (BVS) standard operating procedures. Death was confirmed by palpation or the heart, before the chest cavity was opened and heart exposed. A perfusion needle was placed in the left ventricle and PFA was pumped at 7mls/min through circulatory system before exciting through incision in the right atrium. Brain was dissected and stored in PFA overnight at 4°C. The following day brains are dehydrated in 30% sucrose in PBS overnight at 4°C on rocker. Brains were then flash frozen in Isopentane and stored at -80°C before sectioning. Brains were sectioned into 10µM sections using Cryostat (Leica CM1900) and mounted onto

Superfrost Plus microscope slides. Sections were air-dried briefly then stored immediately stored at -80°C.

2.9.7 Immunofluorescence on mouse brain sections

Brain sections were thawed and allowed to dry completely before being washed in PBS by immersing the slides into coplin jars filled with ~45ml of PBS (1 rinse and 2x 10 minute washes). Sections were permeabilised with 0.1% Triton X-100 in PBS for 15 minutes (~70 µl of solution to cover section). Sections were washed again (same as above), blocked in 1.5% normal goat serum for 60 minutes and then incubated overnight at 4°C in the dark in a humidified atmosphere with conjugated NeuN-fitc488 antibody diluted (1:200) in blocking buffer. The next day sections were washed in PBS (1 x 10 mins), incubated for 10mins in 1µg/ml DAPI in PBS in coplin jar and washed again (2 x 10 min). Sections were mounted in ProLongDiamond, set overnight in the dark at RT before observing sections using confocal microscopy (ZEISS LSM 880 with Airyscan).

2.9.8 DNA extraction from mouse brain tissue

Brain tissue was dissected from mice, cut into two hemispheres and flash frozen in liquid nitrogen and stored at -80°C. Brain tissue (1 hemisphere) was homogenised using a large loose Dounce homogeniser in 3 ml lysis buffer (50mM Tris.Cl pH7.5, 100mM NaCl, 5mM EDTA) to form a uniform suspension. Homogenates were transferred to falcon tubes, 1% SDS and 4 mg/ml Proteinase K were added and samples incubated overnight at 55°C. Homogenates were incubated for a further 1-2 hours at 37°C with 0.1 mg/ml RNaseA. DNA was then extracted with an equal volume of phenyl:chloroform:isoamyl Alcohol, mixed gently and centrifuged for 15 minutes 3000 rpm at room temperature. The aqueous phase was removed and 0.1 volume of NaOAc) and 2.5 volume of ~100% EtOH was added to precipitate the DNA. Knots of DNA were fished out using a heat-sealed pasture pipette, rinsed in 80% EtOH and resuspended in 400µl TE. DNA was left to dissolve overnight at 4°C overnight to dissolve slowly before being mixed with wide bore tips. Genomic DNA was stored at 4°C. Genomic DNA was digested with EcoRI-HF restriction enzyme and Southern

blot analysis was performed as described in section 2.3.5. Quantification of the signal intensity on Southern blots was performed using Fiji-ImageJ.

2.10 *In vivo* ablation experiments

2.10.1 Subcutaneous DT injections of P0-2 mice

Subcutaneous DT injection into P0-2 pups were performed by Jim Selfridge according to the UofE BVS Standard Operating Procedure (SOP) for administering an SC injections into mice. A single SC injection of 30 µg/kg was administered to each pup on P0-2.

2.10.2 Flow cytometry to distinguish MeCP2+ and MeCP2– nuclei

Nuclei were isolated from half brains of 5 or 7 week old female mice following DT injection at P0-2. Nuclei preps were performed according to protocol outlined in section 2.9.4. For half brain, volumes were halved and 15 ml Ultracentrifuge tubes (Ultra clear Beckman Coulter SW40ti rotor) were used. Nuclei were resuspended in 1 ml resuspension buffer and snap frozen in 4 aliquots of 250µl (each aliquot corresponded to ~1/8 brain). Nuclei were stained following the protocol described in section 2.9.5. MeCP2 and NeuN primary antibodies were conjugated to Alexa Fluor™ 568 and 647 respectively using the APEX™ Alexa Fluor™ Antibody labelling Kits. Volumes of labelled antibodies used to stain nuclei were 1µl of NeuN-647 and 5µl MeCP2-568 of the ~50µl eluate (based on optimisation experiments using different staining conditions see Appendix Figure 10.).

Chapter 3 Generation and characterisation of *Mecp2*^{StopDTR} mice

3.1 Introduction

To genetically engineer the *MeCP2*-deficient neurons of the female heterozygote mouse model of Rett Syndrome (RTT) to be sensitive to Diphtheria Toxin (DT), the Diphtheria Toxin Receptor (DTR) expression must be both linked to the *Mecp2*-null allele (*Mecp2*$^{\Delta}$) and be restricted to neurons (Figure 3.1). To restrict the expression of the DTR to the *Mecp2*$^{\Delta}$ cells of the female heterozygous mouse, the human HB-EGF (DTR) coding sequence was knocked into one copy of the X-linked *Mecp2* gene, replacing the endogenous sequence and putting the DTR expression under the control of the endogenous *Mecp2* promoter. This modification relies on random X-chromosome inactivation to silence the expression of the DTR in *Mecp2*$^{+}$ cells where the WT allele is on the active X-chromosome and the *Mecp2*^{DTR} knock in allele is on the inactive X-chromosome. In the other half of the cells, where the WT allele is on the inactive X-chromosome and silenced, the *Mecp2*^{DTR} knock in allele will be expressed from the active allele, resulting in these cells being both deficient for MeCP2 and selectively expressing the DTR.

As endogenous *Mecp2* is ubiquitously expressed (Ross *et al*, 2016; Shahbazian *et al*, 2002a; Song *et al*, 2014; Zhou *et al*, 2006), it was crucial to localise the DTR expression to neurons or the CNS to avoid inducing ablation of 50% of all cells in the body upon DT administration. In mice, the Cre/loxP mutagenesis tool has become the most effective way to control gene expression spatially and temporally by conditional gene activation (Lakso *et al*, 1992), or deletion (Gu *et al*, 1994; Orban *et al*, 1992). Cre recombinase is a Type 1 topoisomerase from bacteriophage P1 which catalyses the efficient site-directed recombination between short 34-bp DNA sequences called *loxP* sites in bacteria (Sternberg & Hamilton, 1981) and eukaryotes (Sauer, 1987; Sauer & Henderson, 1988). Cre recombinase expression from a tissue or developmental stage–specific promoter can invert or excise a target gene or DNA sequence flanked by *loxP* sites (*floxed*) with spatial or temporal specificity (Rajewsky *et al*, 1996; Sauer, 1998). There are many readily available transgenic Cre driver

mouse lines with defined patterns of Cre expression. The choice of neuron-specific or CNS-specific Cre drivers for this project will be discussed in Chapter 5.

Dragatsis and Zeitlin (2001), described a method to mediate the Cre dependent gene repair using a *floxed* selectable marker and a transcriptional *Stop* cassette (*loxP-NeoStop*) inserted into an early intron to disrupt the expression of the downstream gene sequence. Cre-mediated excision of the transcriptional road block allows uninterrupted transcription and reactivation of the expression of the allele. Guy and coworkers (2007) generated a re-activatable *Mecp2*^{Stop} allele to study whether reintroducing functional MeCP2 in the adult brain would reverse the Rett Syndrome-like phenotype. The insertion of the *Stop* cassette into intron two of *Mecp2* efficiently knocked down the gene. The common *floxed Stop* method was exploited to conditionally express the DTR from the *Mecp2* locus (Figure 3.1).

To achieve DTR expression and *in vivo* ablation selectively in MeCP2-deficient neurons in the female heterozygote, female mice heterozygous for the *Mecp2* deletion, conditional *DTR* knock-in allele (*Mecp2*^{StopDTR}) would be crossed to transgenic neuron-specific Cre driver male mice (Figure 3.1). In female progeny of this cross who inherit both the *Mecp2*^{StopDTR} allele and the Cre transgene, neurons where the *Mecp2*^{StopDTR} allele is on the active X chromosome, would be deficient for MeCP2 and selectively express the DTR due to Cre expression and recombination. In the other half of neurons, the *Mecp2*^{StopDTR} is on the inactive X-chromosome and repressed, and the WT allele is on the active X-chromosome and expressed. In these WT *Mecp2* expressing neurons, although Cre recombination and removal of the *Stop* cassette might occur, the DTR should not be expressed due to X-inactivation. In non-neuronal cells, Cre should not be expressed and DTR expression should be silenced by the *Stop* cassette. DT administration to mice will determine the timing of ablation of the susceptible DTR+ neurons.

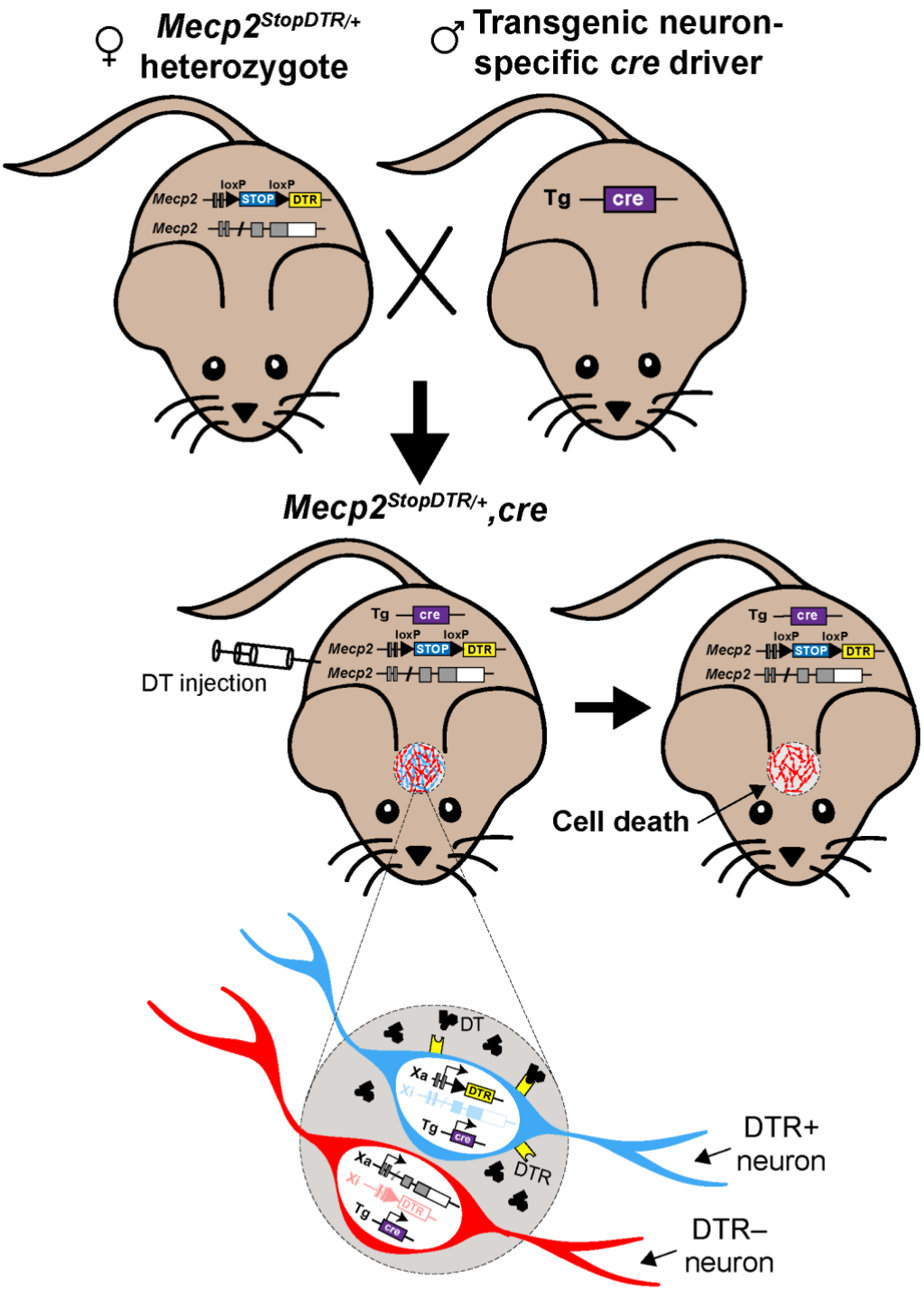

Figure 3.1. The DT-mediated ablation of MeCP2-deficient neurons in the female heterozygous mouse model of RTT. Female mice, heterozygous for the *Mecp2*^{StopDTR} allele are crossed to male mice which express a *cre* transgene from a neuron-specific promoter. In female progeny of this cross who are heterozygous for the modified *Mecp2*^{StopDTR} allele and inherit the *cre* transgene (*Mecp2*$^{StopDTR/+}$*,cre)*: due to X-inactivation and localised *cre* expression, only those neurons expressing the DTR knock-in allele on their active X-chromosome will express the DTR. DT-administration to mice by intraperitoneal injection will ablate the DTR+ neurons specifically. Neurons which have silenced the DTR knock-in allele by X-chromosome inactivation should not express the DTR and be resistant to DT.

I generated the *Mecp2*^{StopDTR} allele where a modified *Stop* cassette was inserted upstream of the DTR transcript within the *Mecp2* locus to produce a Cre inducible DTR gene (Figure 3.2.2.1). To produce the *Mecp2*^{StopDTR} mouse line, due to the size of the DNA modification the most appropriate genetic engineering method to use was to target the single *Mecp2* allele in male mouse Embryonic Stem Cells (ESCs) using CRISPR-Cas9-assisted homologous recombination. Correctly targeted cells were then injected into blastocysts of mice to ultimately generate female mice heterozygous for the *Mecp2*^{StopDTR} allele. The generation of modified mouse ESCs allowed characterisation of this modification in a cell culture system to ensure that it behaves as designed. This chapter describes the generation and characterisation of *Mecp2*^{StopDTR} and *Mecp2*^{DTR} ESCs and mice.

3.2 The *Mecp2*^{StopDTR} targeting vector design

3.2.1 The type of homology targeting vector used

The mouse *Mecp2* locus contains 4 exons, the last two exons contain the majority of the coding sequence and the characterized functional domains of *Mecp2*. Exons 1 and 2 are relatively small, over 40 kb upstream and are alternatively spliced to form the two isoforms of *Mecp2* (Figure 3.2.1). The major isoform of MeCP2, MeCP2-e1 (or MeCP2-α), is 10 times more abundant than the alternative isoform MeCP2-e2 in neurons (Kriaucionis & Bird, 2004). The MeCP2-e1 transcript includes exons 1, 3 and 4 and uses the translation start site in exon 1 (Kriaucionis & Bird, 2004; Mnatzakanian *et al*, 2004)(Figure 3.2.1). MeCP2-e2 is produced by sequentially splicing all four exons and uses the translation start site in exon 2. The lower abundance of the MeCP2-e2 protein is due to a small upstream ORF in the 5'UTR of MeCP2-e2 mRNA which interferes with the translation from the bona fide AUG of MeCP2-e2 (Kriaucionis & Bird, 2004). Due to the repetitive nature of the region surrounding exons 1 and 2, the small size of these exons, the fact that these exons are alternatively spiced and the distance they are from the majority of the coding sequence, the *Mecp2* KO mouse models were both generated by disrupting the crucial coding exons 3 and 4 (Guy *et al*, 2001; Chen *et al*, 2001). The *Mecp2*^{Stop} mouse model was produced by inserting the

Stop cassette into intron 2 just upstream of exon 3 (Guy *et al*, 2007). A similar approach was adopted here to generate the desired modification (Figure 3.2.2.1).

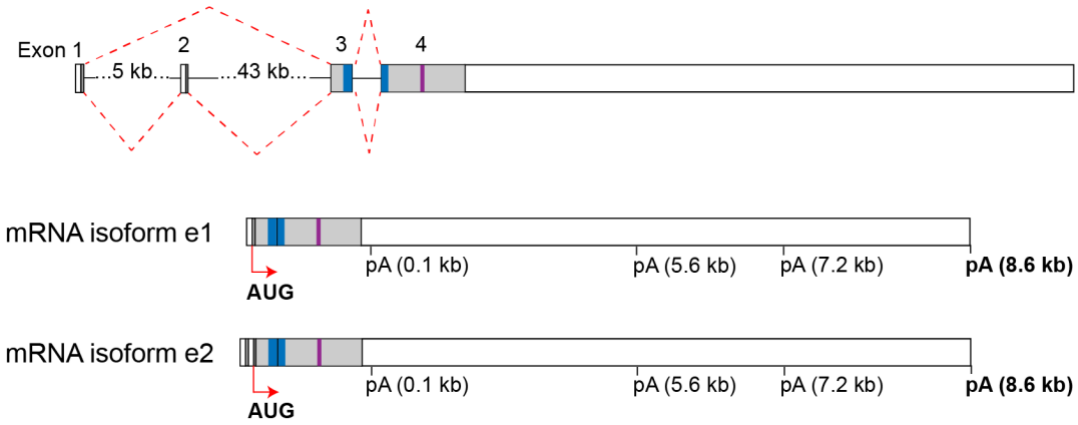

Figure 3.2.1 Schematic diagram of the *Mecp2* gene structure. The *Mecp2* gene has 4 exons which are alternatively spliced to give two mRNA isoforms e1 and e2. *Mecp2-e1* contains exons 1, 3 and 4. *Mecp2-e2* contains exon 1, 2, 3 and 4. In the e1 isoform, translation initiates from the AUG in exon 1. In the e2 isoform, translation inititates from the AUG in exon 2. Exon 1 and exon 2 encode 26 and 9 amino acids respectively. The long 3'UTR has 4 alternative polyadenylation (pA) sites. The major transcript expressed in the brain is the long ~10.2 kb transcript which uses the 8.6 kb 3'UTR. Boxes: exons; lines: introns; grey: open reading frame; blue: Methyl CpG-binding domain (MBD); purple: NCOR interaction domain (NID); red dotted line: splicing pattern; red arrow: translation initiation.

The *Mecp2*^{Stop} mice were produced by targeting mouse ESCs with the *pBS-Me2-NeoStop* targeting vector (Guy *et al*, 2007). This vector consists of a 7.2 kb sequence homologous to the sequence surrounding exon 3 and 4 of the mouse *Mecp2* gene with a *floxed* PGK-neo gene cassette and a transcriptional *Stop* cassette in intron 2. I adapted this targeting vector to create the *pBS-Me2-STOP-DTR* targeting vector (Figure 3.2.2.2, 3.3.1).

3.2.2 The DTR was expressed from the Mecp2 knock-out allele

To knock out *Mecp2* and make the expression of the DTR linked to the KO allele, the major protein coding exons 3 and 4 of *Mecp2* were removed and replaced with the human HBEGF (DTR) coding sequence (Figure 3.2.2.1.). The DTR coding sequence was inserted in-frame following the first 3 codons of exon 3 so that it will be expressed from the *Mecp2* promoter as a fusion protein with the N terminal amino acids of MeCP2 (29 amino acids in the major isoform or 12 amino acids in the minor isoform).

A similar approach was used when producing truncated versions of MeCP2 protein ΔN, ΔNC, and ΔNIC, where the first 3 codons of exon 3 were retained in order to preserve correct splicing (Tillotson *et al*, 2017). These truncated proteins were transcribed and translated correctly. The N-terminus of *Mecp2* is a short non-structured region unlikely to interfere with the function of the DTR transmembrane protein. The N-terminus of the DTR can be fused to GFP without altering its function as a transmembrane receptor (Chen *et al*, 2005)(Whether the fusion of the N-terminus of MeCP2 disrupts the function of the DTR is addressed in section 3.4).

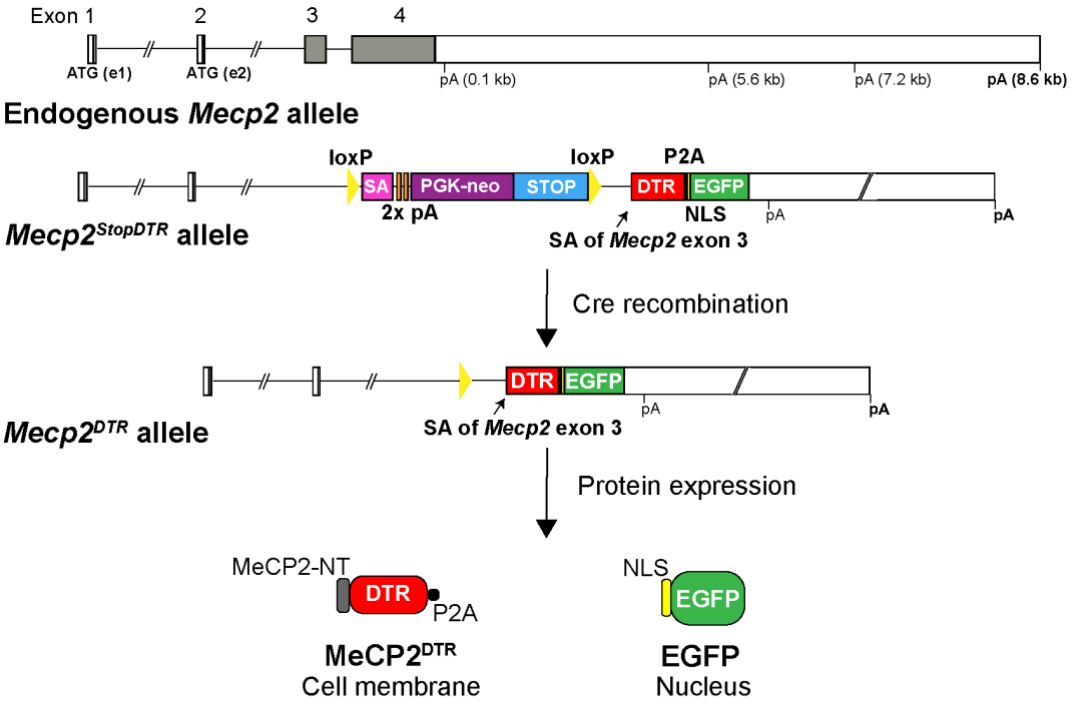

Figure 3.2.2.1 Cre-dependent expression of the DTR from the *Mecp2* locus using a *loxP-SA-pApA-NeoStop* cassette. A diagram of the endogenous *Mecp2* allele is shown at the top. Boxes: exons; grey boxes: protein coding sequence. The alternative start codons (ATGs) and polyadenylation termination sites (pAs) are annotated. Those sites used by the major isoforms in the brain are shown in bold. Below endogenous *Mecp2* is the genetically modified *Mecp2*^{StopDTR} allele before Cre recombination, and after recombination (*Mecp2*^{DTR}). SA (pink): splice acceptor sequence from the mouse *Engrailed-2* (En-2) gene; pA: polyadenylation termination sequences, one SV40 pA sequence and one bGH pA sequence; PGK-neo: The neomycin resistance gene expressed from the mouse phosphoglycerate kinase 1 (PGK) promoter; STOP: transcriptional *Stop* cassette (Lakso *et al.,* 1992); DTR: human HB-EGF coding sequence; P2A (black rectangle or circle): P2A self-cleaving peptide; NLS (Yellow rectangle): SV40 nuclear localization sequence; EGFP: enhanced GFP coding sequence. The endogenous splice acceptor (SA) of *Mecp2* which is retained inframe with the DTR coding sequence is labelled in the modified alleles. At the bottom are the proteins expected to be translated from the modified recombined *Mecp2*^{DTR} locus. MeCP2-NT: N-terminus of MeCP2. Sequence components are listed in Appendix table 1.

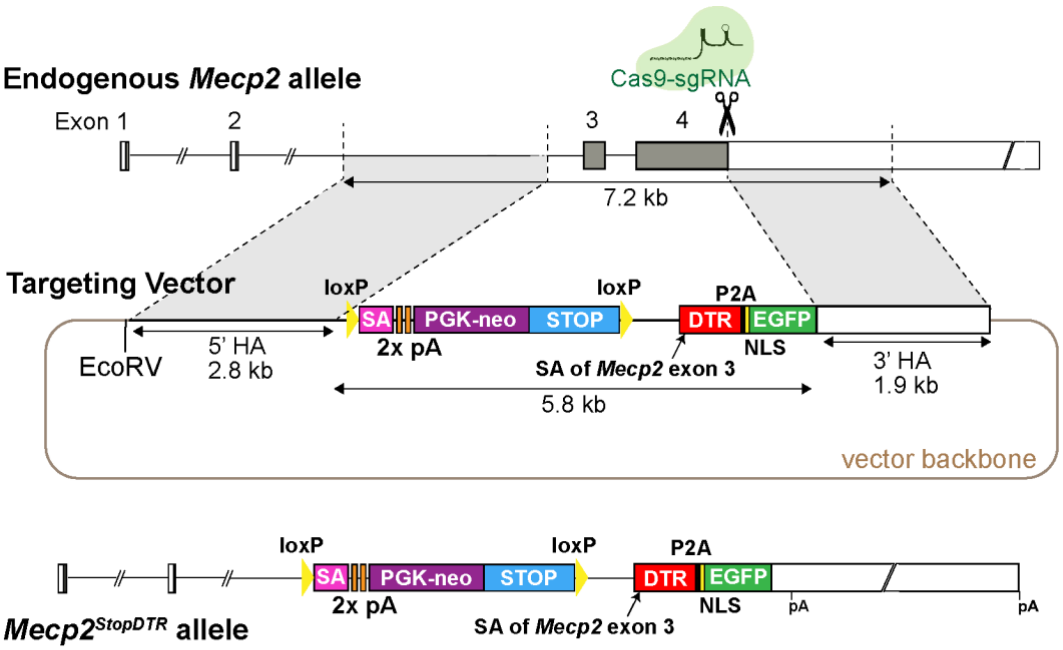

Figure 3.2.2.2. Genetically engineering mESCs to express the *Mecp2*^{StopDTR} allele. The desired modification of the *Mecp2* locus was produced by CRISPR-Cas9 assisted homologous recombination using a large linearised plasmid targeting vector. Sizes of DNA sequences are indicated below arrows. HA: homology arm; EcoRV: unique restriction enzyme cut site used to linearise the targeting vector. Sequence components are listed in Appendix table 1.

3.2.3 Bicistronic expression of the transmembrane DTR and a nuclear localised reporter

To report the expression of the transmembrane DTR protein and in order to visualize individual DTR positive neurons in the mosaic brain, I decided to use the bicistronic co-expression of a reporter protein with a nuclear localisation signal (NLS) sequence instead of tagging the DTR. There are two well established ways to achieve bicistronic co-expression of two proteins from one transcript: 1) the use of an Internal Ribosome Entry Site (IRES); or 2) a self-cleaving 2A peptide. The IRES was discovered in poliovirus and encephalomyocarditis (EMCV) RNA as a method to highjack the eukaryotic translation machinery to initiate cap-independent translation by providing internal sequences which bind ribosomes (Pelletier & Sonenberg, 1988; Jang *et al*, 1988). The main disadvantages of the IRES are its large size (500-600 bp) and lower expression of the downstream cistron due to inefficient translation of its coding sequence (de Felipe *et al*, 2006; Szymczak & Vignali, 2005). The self-cleaving 2A

peptide has been adapted into multicistronic vectors to overcome the disadvantages of the IRES. Ryan *et al*, (1991) identified the 16 amino acid self-cleaving peptide within the foot-and-mouth virus (FMDV) polyprotein which is responsible for mediating co-translational cleavage separating the 2A peptide from its immediate downstream peptide. It has now been identified that the separation of the peptides is the result of the ribosome skipping the synthesis of a peptide bond between glycine and proline at the C terminus of the peptide sequence (Donnelly *et al*, 2001a, 2001b; Ryan *et al*, 1999; De Felipe *et al*, 2003). Several 2A peptides have since been identified and widely used in biomedical research including the equine rhinitis A virus (ERAV) 2A (E2A), porcine teschovirus-1 2A (P2A) and the *Thoseaasigna* virus 2A (T2A)(Szymczak & Vignali, 2005). The porcine teschovirus-1(P2A) has the highest cleavage efficiency according to *in vivo* studies both in human cell lines and in mice (Kim *et al*, 2011)

I decided to use the P2A peptide due to its high efficiency in producing the downstream reporter and small size. The use of the P2A meant that an additional C-terminal fusion of the 21 amino acids was added to the upstream DTR and an N-Terminal addition of 1 proline was added to the downstream reporter. This is a potential disadvantage of the use of a 2A that is avoided when using an IRES. Like the N-terminal fusion of the DTR with GFP mentioned above (Chen *et al*, 2005), the DTR has been fused to a C-terminal reporter, which did not alter its function as a DT receptor (Duffield *et al*, 2005; Jung *et al*, 2002). This suggests that the additional C-terminal fusion of the P2A peptide would not disrupt the DTRs ability to transport DT across the cell membrane but it is a factor that needed to be tested (addressed in section 3.4).

To report the expression of the DTR transmembrane protein, I chose to use enhanced GFP (EGFP) with an N-terminal NLS. EGFP is frequently used in the Bird lab, where we have good antibodies for western blotting, and protocols to visualize the endogenous GFP signal by immunofluorescence and flow cytometry in samples from both ESC derived neurons and in mouse tissue. The simian virus 40 (SV40) NLS was chosen because it is a widely used strong NLS.

3.2.4 The floxed transcriptional Stop cassette was modified to improve its recognition

The use of the *loxP*-flanked "*NeoStop*" sequence as a means of preventing the expression of your gene of interest until activation by Cre recombinase mediated removal of the *NeoStop* sequence was described by (Dragatsis & Zeitlin, 2001). The Neo sequence is a PGK-neo resistance gene expressed from a PGK promoter (PGK-neo) used for selection of targeted ESCs and the *Stop* sequence is composed of the C-terminal sequence of yeast His3 gene, a SV40 polyadenylation signal sequence and a synthetic oligonucleotide containing a false translation initiation codon and a 5' splice donor which serves to terminate transcription (Lakso *et al*, 1992). In the original *Mecp2*^{Stop} allele the *loxP-NeoStop* cassette (referred to as *Stop1* from here onwards) was inserted into intron 2 of *Mecp2* and mediated ~97.5% reduction in MeCP2 protein production (Guy *et al*, 2007; Robinson *et al*, 2012). There was a small amount of leaky MeCP2 detectable in the *Mecp2*^{Stop} brain (~2.5% of the wild type level) produced by a small proportion of functional, mature *Mecp2* transcripts which spliced around the *Stop* cassette and evaded the transcriptional roadblock. Leaky expression of the DTR would hinder this project as it could lead to off-target cellular ablation in *Mecp2* expressing cell types, other than neurons. In an attempt to increase the recognition of the transcriptional road block and prevent splicing around it, a strong splice acceptor sequence from the mouse *engrailed* 2 gene (En-2) and two polyadenylation terminator signal sequences specialised for terminating transcription in eukaryotic cells: the SV40 and bovine growth hormone bGH PolyA, were inserted upstream of the PGK-neo resistance gene cassette to produce the *loxP-SA-pApA-NeoStop* cassette (referred to as *Stop2* from here onwards). These modifications make this *floxed Stop* cassette similar to one described in the literature to conditionally repress expression of the DTR from the ubiquitously expressed ROSA26 locus (Buch *et al*, 2005). The En-2 splice acceptor is frequently used in gene trap constructs and one study quantified the splicing around the gene trap sequences to be <0.1% (Skarnes *et al*, 1992). However, the frequency of splice acceptor usage will depend on the strength of the competing splice acceptor.

3.3 The *Mecp2*^{StopDTR} targeting vector assembly

The *pBS-Me2-STOP-DTR* targeting vector was assembled by two sequential restriction enzyme digestion and ligation cloning steps, that inserted two synthesized DNA fragments into the original *pBS-Me2-NeoStop* vector (Figure 3.3.1). In the first cloning step: the MfeI fragment of the targeting vector spanning exon 3 and 4 was replaced by a synthesised DNA fragment which retained the intron 2 and 3'UTR sequence of *Mecp2*, but with the sequences of exon 3, 4 and the intervening intron 3 replaced with the DTR-P2A-EGFP coding sequence. The DTR protein coding sequence had the first 3 codons of exon 3 immediately upstream, in-frame and had no translation start and stop codon. The P2A, the SV40 NLS and the EGFP coding sequence followed in frame. The stop codon of EGFP replaced the stop codon of *Mecp2* and the full 3'UTR of *Mecp2* immediately downstream was intact. The HpaI restriction enzyme site in the *Stop* cassette was mutated to remove it in order to clone the second fragment in the correct position. In the second cloning step, the HpaI, AgeI fragment containing the 5' *loxP* site and the start of the PGK-neo resistance gene was replaced with a synthesized DNA fragment with the En-2 splice acceptor consisting of ~400 bp sequence surrounding the intron - exon boundary of the mouse *Engrailed 2* gene and the two polyA terminator sequences in between the *loxP* site and the PGK-neo resistance gene (see Appendix Table 1. for sequence components of the *pBS-Me2-STOP-DTR* targeting vector). Validation of the correctly cloned plasmid product was confirmed by a panel of diagnostic restriction digests to check for large DNA rearrangements and the entire modified region of the vector was sequenced to check for smaller mutations.

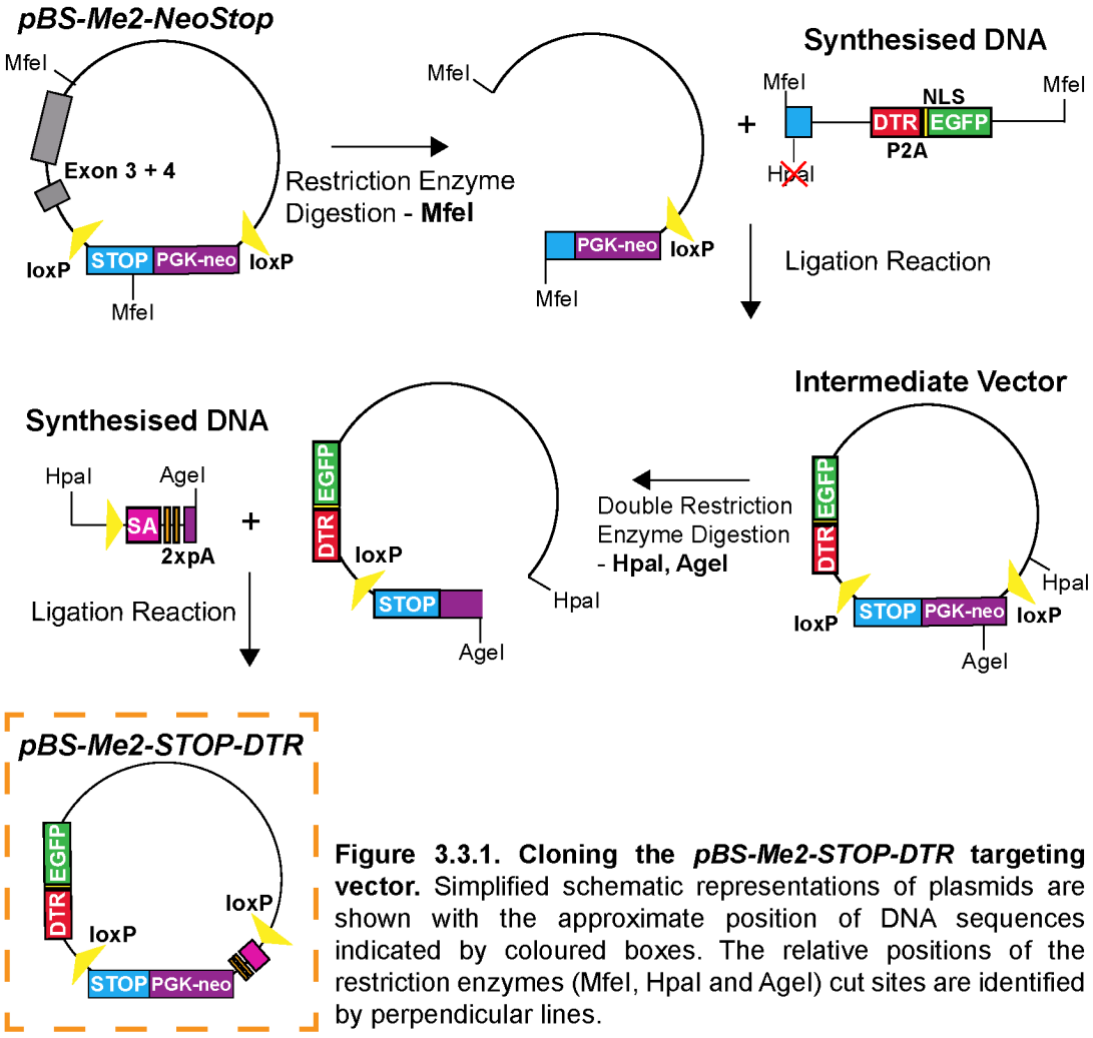

Figure 3.3.1. Cloning the *pBS-Me2-STOP-DTR* targeting vector. Simplified schematic representations of plasmids are shown with the approximate position of DNA sequences indicated by coloured boxes. The relative positions of the restriction enzymes (MfeI, HpaI and AgeI) cut sites are identified by perpendicular lines.

A CRISPR-Cas9 mediated DSB in the 3'UTR of *Mecp2* was used to encourage homologous recombination and insertion of the entire modification. The CRISPOR Design Tool (crispor.tefor.net) was used to identify an appropriate guide sequence which could anneal to the endogenous *Mecp2* locus, but was unlikely to bind to the vector DNA or the targeted locus and with few off-target sites in the rest of the mouse genome. A guide sequence which annealed over the 3'UTR and exon 4 coding sequence boundary was chosen (Figure 3.3.2). Successful integration of the targeting vector would result in replacement of the coding sequence of exon 4 with EGFP which would block the guide RNA from annealing and prevent further Cas9 cleavage. Between the *floxed* cassette and the DTR-P2A-EGFP there is ~400 bps of homology to the endogenous *Mecp2* gene which could mean that only one half of the modification including the PGK-neo selection cassette without the DTR-P2A-EGFP

could be integrated. I chose to cut at the start of the 3' homology arm in an attempt to encourage the integration of the entire non-homologous sequence from the 5' PGK-neo selection cassette to the 3' EGFP. The 20-nt guide sequence was cloned into a Cas9 expressing plasmid.

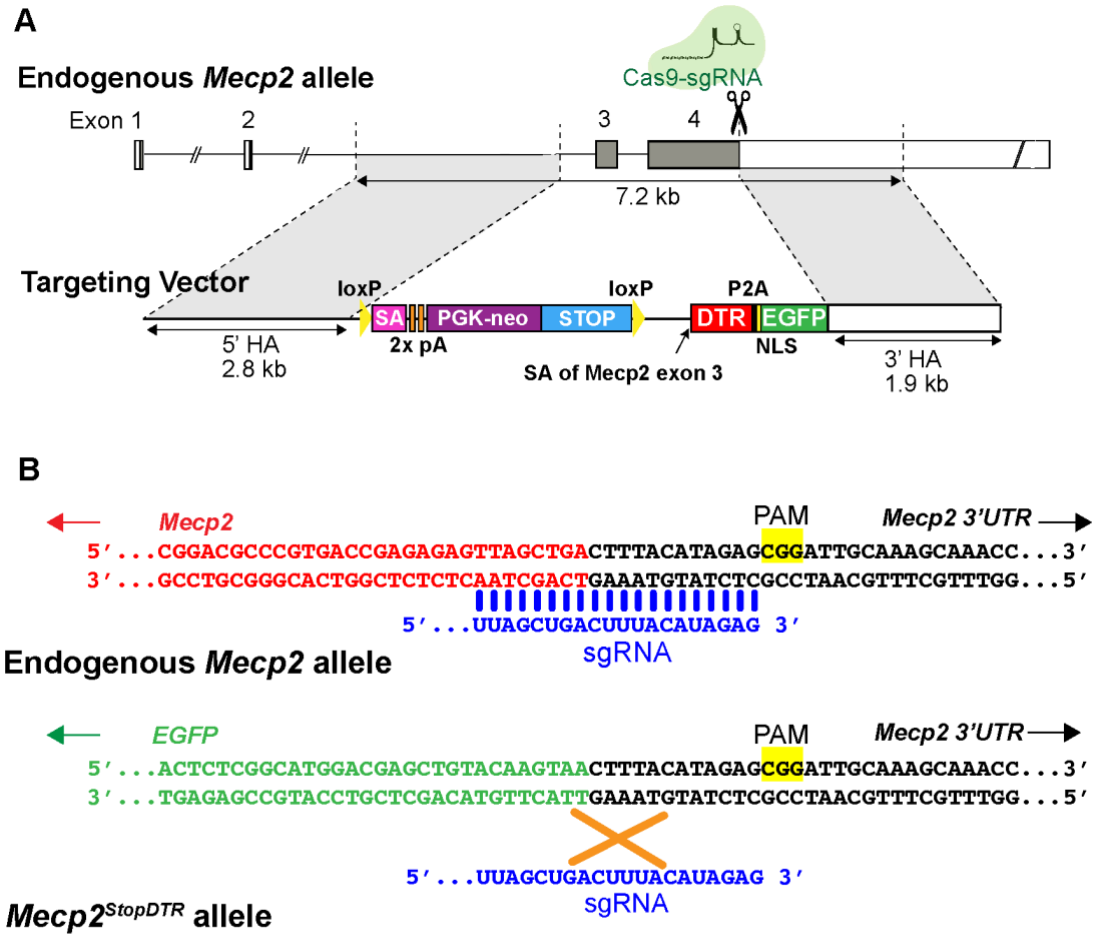

Figure 3.3.2. Design of the CRISPR-Cas9 targeting for the generation of the *Mecp2*^{StopDTR} allele. A) Position of the Cas9 cut site (scissors) within the endogenous *Mecp2* gene. B) Schematic representation of how the guide RNA target sequence is disrupted in the targeted *Mecp2*^{StopDTR} allele. Blue: the 20-nt guide RNA sequence; yellow: the PAM motif; green: EGFP coding sequence; red: *Mecp2* coding sequence; black: *Mecp2* 3'UTR sequence.

3.4 Expression of the *Mecp2^{DTR}* cDNA in mouse NIH3T3 cells

3.4.1 The design and cloning of the cDNA expression vectors

The *Mecp2^{StopDTR}* knock-in allele designed and discussed above to mediated inducible DTR expression from the *Mecp2* locus is complex and there are multiple aspects of the modification which could function insufficiently. One such aspect is: the 5' N-terminus of MeCP2 and the P2A peptide fused to the DTR could alter its function as a transmembrane receptor for DT. In order to determine whether the mRNA transcribed from the proposed *Mecp2^{DTR}* knock-in allele following Cre activation via removal of the *Stop* cassette would be translated correctly into functional DTR and EGFP proteins, a plasmid expressing the *Mecp2^{DTR}* cDNA and control expression vectors were cloned and used in transfection experiments in mouse NIH3T3 fibroblast cells (Figure 3.4.1). Mouse cells were used to ensure that there was no expression of an endogenous functional DTR which might obscure the results of the experiments (the mouse homolog of the DTR (HB-EGF) is insensitive to the toxin unlike the human homolog). I used the cDNA sequence corresponding to the major e1 isoform of *Mecp2^{DTR}* for the expression vector construct (denoted *pMecp2^{DTR})* which includes: exon 1 spliced onto the first 3 codons of exon 3 of *Mecp2*, followed by an in-frame fusion of the *DTR* ORF (without an ATG or stop codon), a P2A sequence and the *EGFP* ORF with an N-terminal NLS. As discussed previously (section 3.2.2), the DTR protein will have an N-terminal fusion of 29 amino acids (e1 isoform) of the start of MeCP2 and a C-terminal fusion of 21 amino acids of the P2A peptide following P2A mediated ribosome skipping. The EGFP will have a N-terminal fusion of an NLS sequence with an additional proline remaining from the end of the P2A following the ribosome skipping. To determine if the additional sequences added to the DTR or EGFP altered the function or localisation of these proteins, expression vectors which expressed the *DTR* cDNA only (*pDTR*) and the *EGFP* cDNA only (*pEGFP-N1*), and which expressed the DTR and EGFP bicistronically using an IRES (*pDTR-IRES-EGFP*) were cloned and used for positive controls for DTR and EGFP expression (Figure 3.4.1).

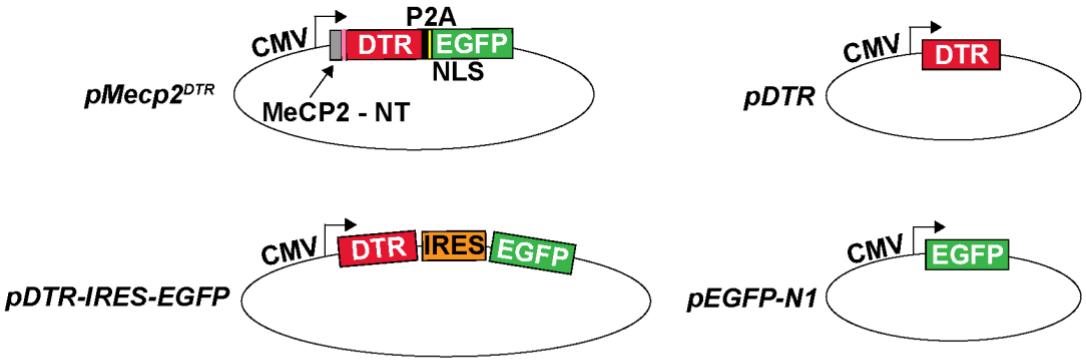

Figure 3.4.1. Schematic of the expression vectors used in the NIH3T3 transfection experiments. CMV: cytomegalovirus promoter; grey box: coding sequence of exon 1 of *Mecp2*; pink: coding sequence of first 3 amino acids of exon 3 of *Mecp2*; red: the DTR (human HBEGF) coding sequence; black: P2A; yellow: SV40 NLS; green: EGFP coding sequence; orange: Internal ribosome entry site (IRES); line: plasmid backbone.

3.4.2 The DTR and EGFP proteins were expressed from Mecp2^{DTR} cDNA

Mouse NIH3T3 fibroblast cells were transfected with the three vectors: *pEGFP-N1*, *pDTR*, *pMecp2^{DTR}* and visualized in the Incucyte live-cell analysis system which is an incubator with a fully-automated compact microscope which operates within it. Cells in both the *pEGFP-N1* and *pMecp2^{DTR}* transfected populations expressed GFP, whereas the *pDTR* and mock transfected cells did not. Western blots were performed on protein extracts from transfected cells using GFP and DTR antibodies and histone H3 antibody for a loading control (Figure 3.4.2). Importantly, the DTR and EGFP were both detected in the *pMecp2^{DTR}* transfected cells, two bands were detected for both the DTR and GFP antibodies. It is reasonable to deduce that the larger band is the "uncleaved" MeCP2-DTR-P2A-NLS-EGFP fusion protein and the smaller bands are "cleaved" MeCP2-DTR-P2A and the NLS-EGFP proteins. The DTR alone or EGFP alone expressed in *pDTR, pDTR-IRES-EGFP* or *pEGFP-N1* transfected cells are smaller than the "cleaved" products as they are missing the fusions of the N-terminus of MeCP2, the P2A or the NLS. The estimated molecular weight of each of the proteins from the peptide sequences are: 55.48 kDa for MeCP2-DTR-P2A-NLS-EGFP, 27.6 kDa for MeCP2-DTR-P2A, 27.91 kDa for NLS-EGFP, 23.07 kDa for DTR and 26.95 kDa for EGFP. The size of each protein on the western blot gel agree approximately with the estimates from protein sequences (Figure 3.4.2).

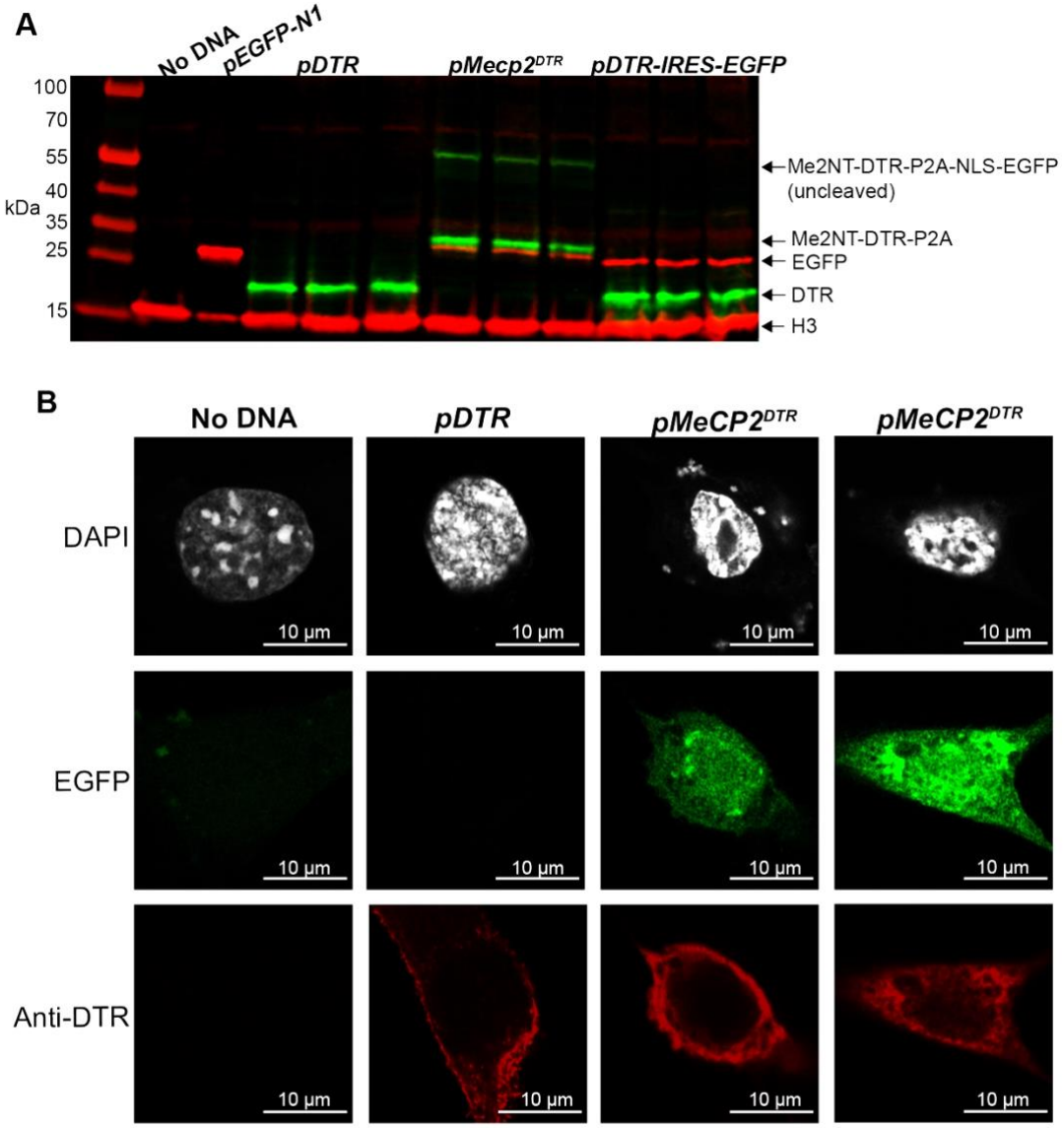

Figure 3.4.2.The DTR and eGFP proteins are expressed from the *Mecp2*^{DTR} cDNA transfected into NIH3T3 cells A) Western blot of protein extracts from transfected NIH3T3 cells. Three technical replicates were blotted for each genotype except for No DNA and *pEGFP-N1* controls. Arrows highlight what each band corresponds to. Anti-H3 was used as a loading control. B) Immunofluorescence for DTR and endogenous fluorescence of EGFP in transfected NIH3T3 cells.

In order to visualise the localisation of the DTR and EGFP proteins within the cell, immunofluorescence was performed on transfected cells grown on coverslips using the DTR antibody and visualizing endogenous EGFP (Figure 3.4.2). The DTR was readily detectable and was localised to the cytoplasm and cell membrane, staining was excluded from the nucleus. The EGFP protein expressed from the *pMecp2*^{DTR} vector, has an N-terminal SV40 NLS signal so is designed to be localised in the nucleus. The

EGFP signal is in the nucleus but it is also diffuse in the cytoplasm. The cytoplasmic EGFP could be the "uncleaved" form fused to the DTR, or EGFP alone might diffuse out of the nucleus when overexpressed. For the ultimate purposes of reporting neurons in the brain which express the DTR, the localisation of GFP to both the nucleus and cytoplasm is sufficient. This analysis identified that the DTR and GFP localise to the correct cellular compartments when over expressed from the *Mecp2^{DTR}* cDNA.

3.4.3 Mecp2^{DTR} cDNA expression in NIH3T3 cells mediated sensitivity to Diphtheria Toxin

Diphtheria toxin is extremely potent and highly toxic to humans, great care needs to be taken when conducting experiments with it. An extensive risk assessment was put together by me and reviewed by the School of Biological Sciences Health and Safety Officers to ensure that safe practices were being used (see Appendix Document 1). Due to the high level of risk with this work, experiments were designed to ensure handling of DT was kept to a minimum. The Incucyte live-cell analysis system was used to visualise and image cells treated with DT overtime. The addition of a dead cell stain, the Incuctye Cytotox Red dye was used to identify and quantify the number of dead cells. The dye is added to the cell culture medium and is taken up through disrupted membranes of dead or dying cells where it binds to DNA and fluoresces red. Fluorescent images taken on the Incucyte can be quantified by the built in Incuctye software to give a measure of cell death.

To achieve a population where the majority of cells were transfected, *pEGFP-N1*, *pMecp2^{DTR}* and *pDTR-IRES-EGFP* transfected cells were sorted for EGFP fluorescence by fluorescence-activated cell sorting (FACS) before being treated with DT and Incuctye Cytotox Red and visualised in the Incucyte. Using the Incucyte analysis software the percentage confluence per well and the red object count per image were calculated for each condition (Figure 3.4.3 Appendix Figure 7). The DTR expressing cells treated with DT experienced a lag in confluence before reaching ~100% confluency by 100 – 130 hours compared to 72 – 76 hours for untreated DTR expressing cells. The total number of red objects per image (i.e. dead cells) increased substantially for cells expressing the DTR and treated with DT compared to untreated

cells and treated control *pEGFP-N1* cells. The lag in percentage confluence of *DTR* cDNA transfected cells can be explained by the transient expression of the DTR plasmids and their dilution as the cells continue to divide. Cells which manage to lose the plasmid will escape being killed by the toxin and will go on to populate the well, but, due to the loss of a lot of cells which took up the toxin, they will take longer to reach confluency.

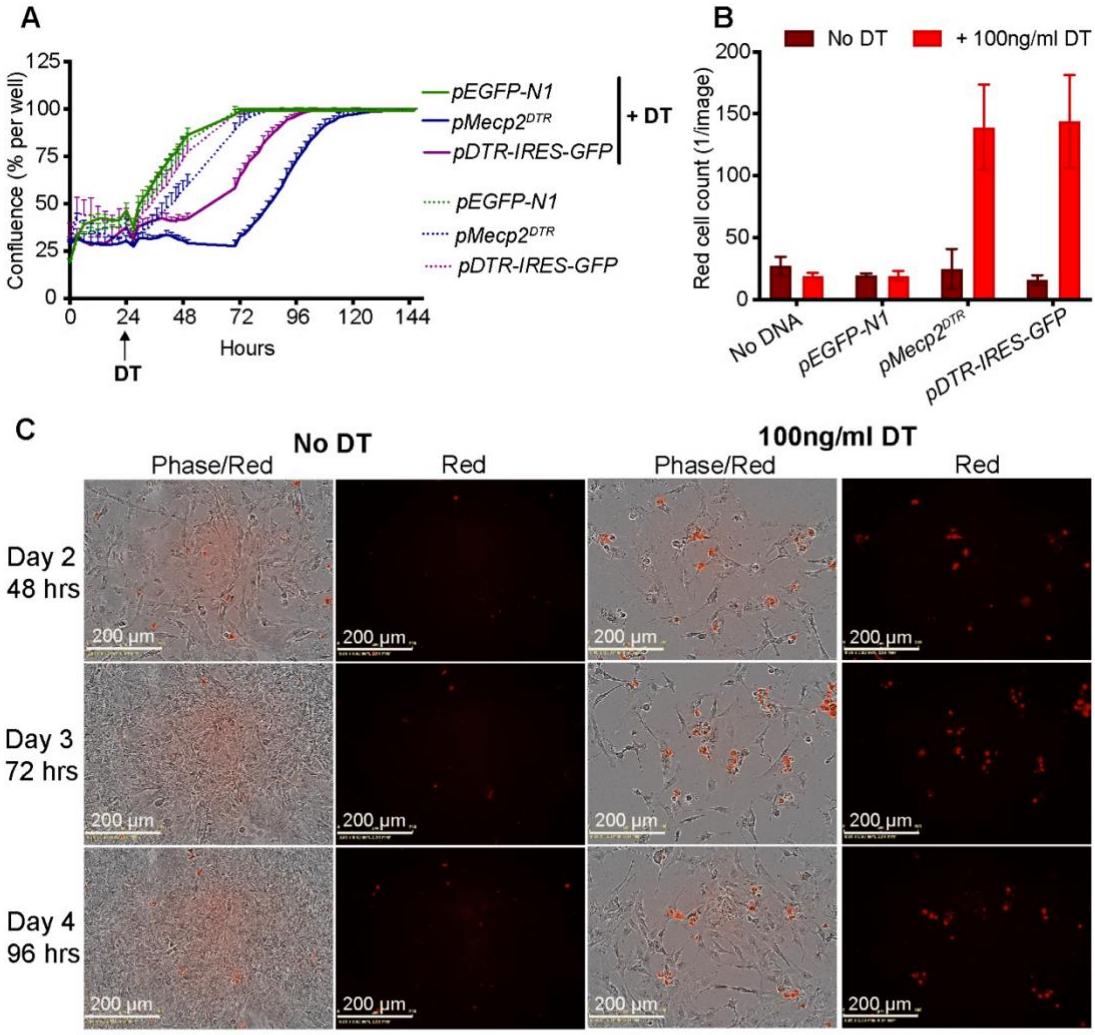

Figure 3.4.3 *Mecp2*^{DTR} cDNA expression in transfected NIH3T3 cells mediates sensitivity to DT. A) Percentage confluence of NIH3T3 cells transfected with different expression vectors, treated or not treated with 100ng/ml Diphtheria Toxin (DT). DT was added to cells 24 hours after FACS sorting for EGFP expression. Shown here is mean and standard deviation for 3 wells of transfected cells per genotype and condition. B) Red cell count (dead cell count) per image 48 hours after DT treatment for NIH3T3 cells transfected with different expression vectors. Shown here is mean and standard deviation for 3 replicate wells of transfected cells per genotype and condition. C) Phase and fluorescent images of DT treated and untreated *pMeCP2*^{DTR} transfected NIH3T3 cells taken on the Incucyte® at 48, 72 and 96 hours after FACS sorting.

The NIH3T3 transfection experiments allowed me to conclude that the mRNA which should be expressed from the *Mecp2*^{DTR} (Δ*Stop*) knock-in allele (designed in section 3.2) can be translated correctly to form the DTR and EGFP. The MeCP2^{DTR} fusion protein forms a functional transmembrane receptor which mediates sensitivity of otherwise resistant mouse fibroblast cells to DT.

3.5 The generation of *Mecp2*^{StopDTR} knock-in mouse ESCs

To generate modified mouse ES cells harbouring the *Mecp2*^{StopDTR} allele as designed above in sections 3.2. Mouse ES cells were targeted by CRISPR assisted homologous recombination following electroporation of cells with linearized vector DNA and CRISPR plasmid. Those cells with the PGK-neo selection cassette of the targeting vector integrated into their genomes were selected for using G418 antibiotic resistance. Resistant clones were screened by PCR using primer pairs which specifically amplified DNA only present when a targeted integration of the 5' and 3' end of the targeting vector into the *Mecp2* locus had occurred. Out of 192 clones screened by PCR, 10 potentially targeted clones were identified. These 10 clones were grown up, genomic DNA was extracted, and Southern blot analysis was performed using two different restriction enzyme digests which identified 4 clones that were correctly targeted 3 of these had no random integrations of the vector DNA elsewhere in the genome (Figure 3.5.1). The overall targeting efficiency of generating the *Mecp2*^{StopDTR} knock-in allele was 2.08%.

The modified locus was sequenced, and no mutations were identified in any of the targeted clones. All three clones also appeared to have a normal karyotype of 40 chromosomes (Figure 3.5.2). Clone 1H6 was therefore used to generate the *Mecp2*^{StopDTR} mouse line by blastocyst injection.

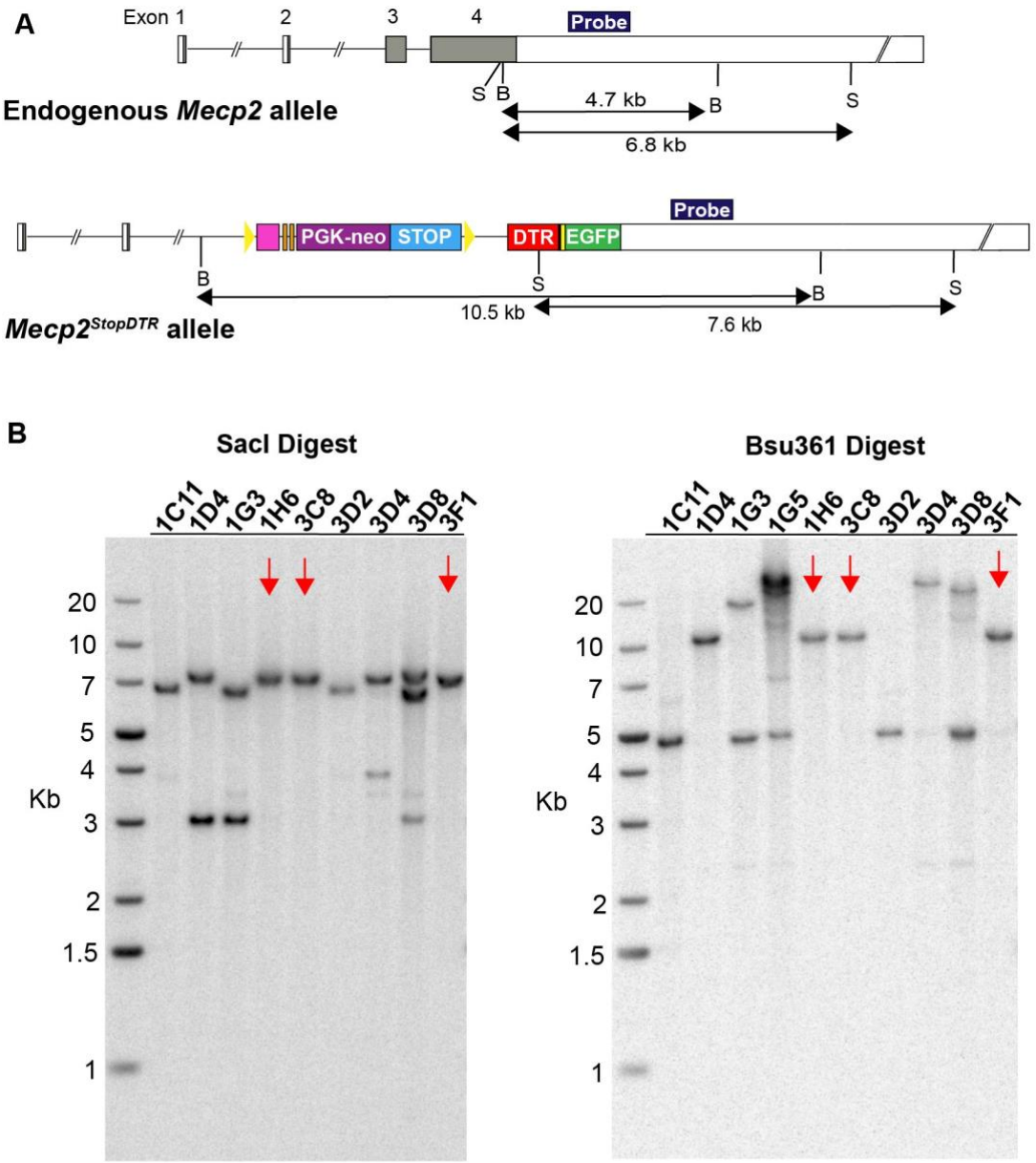

Figure 3.5.1. Southern blot analysis identified *Mecp2*^{StopDTR} targeted ESC clones with no random integrants. A) Southern Blot screening strategy for identifying positively targeted ESC clones. The 3'UTR hybridization probe is indicated in dark blue and S and B indicate the position of the SacI and Bsu361 restriction enzyme cut sites respectively within the *Mecp2* locus. B) Southern blot analysis after SacI and Bsu361 digestion identified positively targeted clones with no random integrations of vector DNA (red arrows).

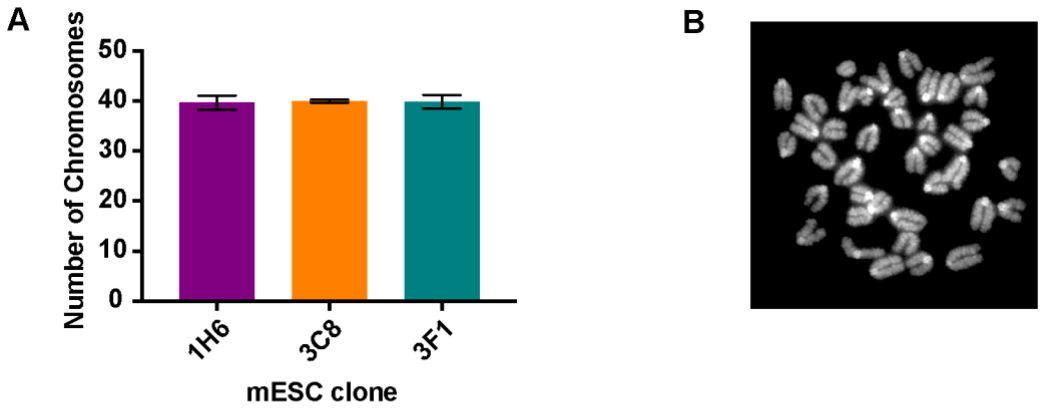

Figure 3.5.2. *Mecp2*^{StopDTR} targeted ESCs had a normal karyotype. A) The number of chromosomes per metaphase spread for each *Mecp2*^{StopDTR} ESC clone. Total metaphase spreads counted per genotype: 25 (plotted: mean and SD). B) An example a microscopy image of a DAPI stained metaphase spread.

3.6 Characterisation of the *Mecp2*^{StopDTR} and *Mecp2*^{DTR} ESCs and neurons

3.6.1 Transient Cre expression removed the Stop cassette in Mecp2^{StopDTR} *ESCs*

To characterise the *Mecp2*^{StopDTR} genetic modification in cell culture, I firstly had to produce clones where the DTR expression had been activated by Cre-mediated removal of the *Stop* cassette. The three clones of targeted *Mecp2*^{StopDTR} ESCs were transiently transfected with a Cre expressing plasmid and cloned out. Clones which were no longer resistant to G418 and had potentially lost the PGK-neo selection gene (inserted between the loxP sites) were identified (Figure 3.6.1). Cre recombination was verified at the DNA level by Southern blot (Figure 3.6.1). The Southern probe was located in the 3'UTR and the EcoRI digestion of DNA allowed the clear distinction between a fragment from an unrecombined locus and a recombined locus. The Southern blot analysis also allowed the identification of mixed clones where recombination hadn't occurred in all cells in the population. This was evident for 1H6 c1 where there was a small fraction of contaminating unrecombined cells (Figure 3.6.1). I could conclude from this analysis that the Cre recombination of loxP sites

within the *Mecp2*^{StopDTR} allele works efficiently in cell culture following transient expression of Cre recombinase.

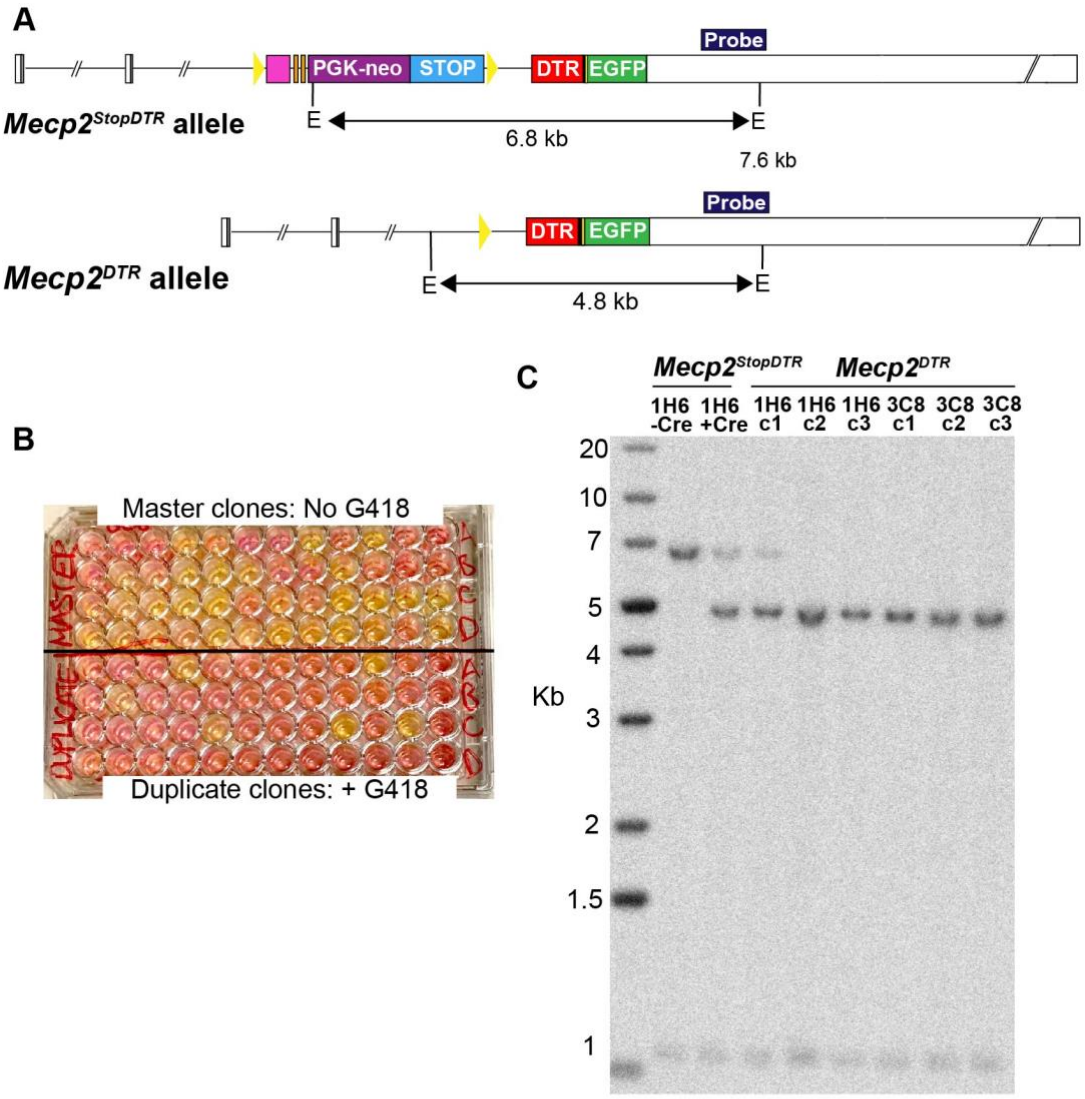

Figure 3.6.1. Cre-mediated removal of the *loxP-SA-pApA-NeoStop* cassette in *Mecp2*^{StopDTR} ESCs. A) Southern Blot screening strategy for identifying recombined ESC clones. The 3'UTR hybridization probe is indicated in dark blue and E indicates the position of the EcoRI restriction enzyme cut sites. B) The colour change of medium on wells of master and duplicate clones treated and not treated with G418 respectively. Pink wells indicate the clones which don't grow or die and yellow medium indicate clones which do grow and are resistant to G418. C) Southern blot analysis of a number of isolated clones which did not grow in the presence of G418 and therefore potentially no longer contained the *NeoStop* cassette (*Mecp2*^{DTR} clones). 1H6+Cre: bulk population of the parental *Mecp2*^{StopDTR} 1H6 clone transiently transfected with a Cre recombinase expressing plasmid.

3.6.2 DTR and EGFP protein was not detectable in neurons derived from recombined Mecp2^{DTR} ESCs

The *Mecp2* locus is lowly expressed in ESCs and as a result MeCP2 protein is difficult to detect. Therefore, in order to study the gene expression of the modified locus, the ESCs were differentiated into neurons. In ESC-derived neurons MeCP2 protein is readily detectable 5-6 days after plating out Embryoid bodies (Figure 3.6.2.1). The *Mecp2^{StopDTR}* targeted ESC clones 1H6 and 3C8, recombined *Mecp2^{DTR}* subclones of 1H6c2 and 3C8c2, a WT JuO9 bulk population of cells and a WT-GFP clone where WT *Mecp2* is tagged with a C-terminal GFP were differentiated into neurons. Differentiating neurons were visualized and imaged in the Incucyte (Figure 3.6.2.1). Neurons were harvested at day 6 or 7 and processed for protein and RNA or fixed and stained for immunofluorescence.

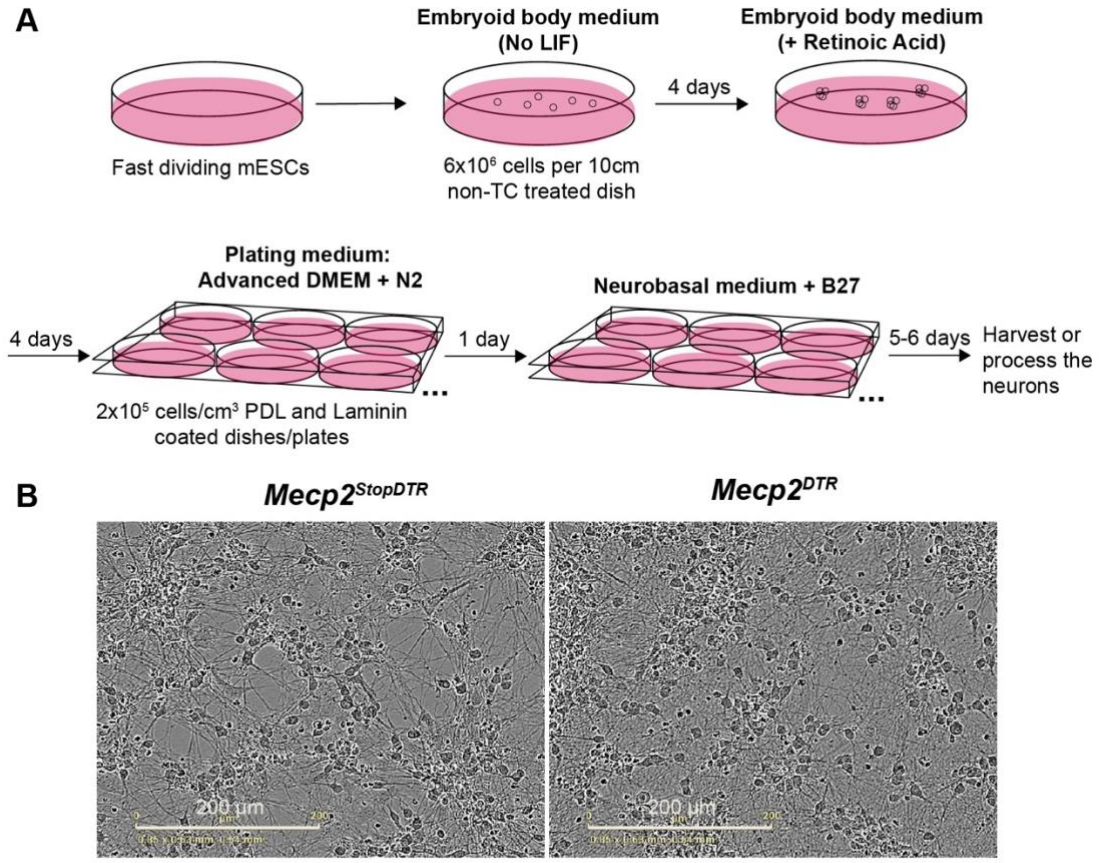

Figure 3.6.2.1. Differentiation of *Mecp2^{StopDTR}* and *Mecp2^{DTR}* ESCs into neurons. A) Schematic representation of the neuronal differentiation protocol. B) Phase images of neurons derived from *Mecp2^{StopDTR}* and *Mecp2^{DTR}* ESCs taken on the Incucyte.

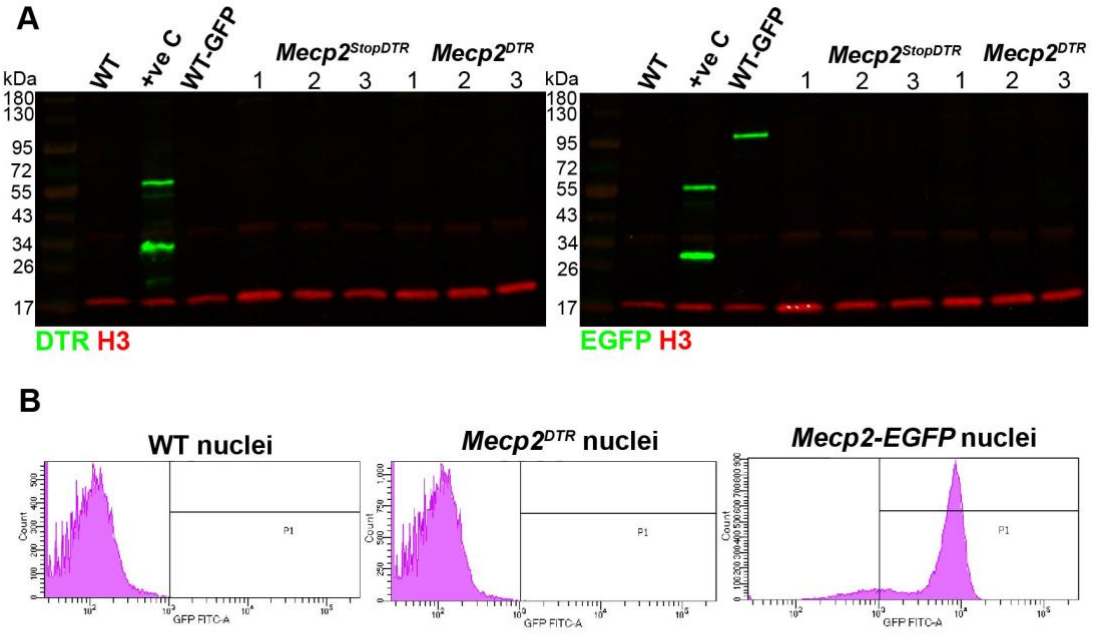

Figure 3.6.2.2. Absence of detectable EGFP and DTR protein in *Mecp2*^{StopDTR} and *Mecp2*^{DTR} neurons. A) Western blot using anti-DTR and anti-H3 (left) and anti-GFP and anti-H3 (right) antibodies; WT: WT neurons; WT-EGFP: neurons derived from ESCs where WT MeCP2 is tagged with EGFP; +veC: NIH3T3 cells transfected with plasmid expressing *Mecp2*^{DTR} cDNA; *Mecp2*^{StopDTR} (1,2,3): 3 different differentiations of *Mecp2*^{StopDTR} ESC clone 1H6; *Mecp2*^{DTR} (1,2,3): 3 different differentiations of *Mecp2*^{DTR} ESC clone 1H6c2. B) Flow cytometry analysis of GFP fluorescence of nuclei extracted from WT, *Mecp2*^{DTR} and *Mecp2-EGFP* ESC-derived neurons. Plotted is the cell count (y axis) versus GFP fluorescence intensity (x axis).

No EGFP fluorescence could be detected in images taken by the Incucyte during differentiation for recombined *Mecp2*^{DTR} neurons which should express EGFP. WT-GFP neurons however did fluoresce green. Western blot analysis was performed to try and detect the DTR and EGFP protein. Protein extracts for the WT-GFP neurons were used as a positive control for MeCP2-EGFP in neurons, and protein extracts from mouse fibroblast cells (NIH3T3 cells) transfected with the *Mecp2*^{DTR} cDNA were used as a positive control for the DTR (see section 3.4 for the NIH3T3 transfection experiments) (Figure 3.6.2.2). I could not detect the EGFP or DTR protein extracts from *Mecp2*^{DTR} neurons by western blot. I also performed immunofluorescence on fixed *Mecp2*^{DTR} neurons, using the DTR antibody and tried to detect endogenous EGFP by fluorescence or using an EGFP antibody (Data not shown). Signal could not be detected for EGFP or DTR compared to my controls. In another attempt to detect protein, nuclei were extracted from *Mecp2*^{DTR} neurons and analysed by flow

cytometry, again, I could not detect any EGFP fluorescence (Figure 3.6.2.2). In the literature, the presence of the DTR mRNA in transgenic lines is commonly shown by *in situ* hybridisation or northern blot analysis rather than the presence of DTR protein itself (Saito *et al*, 2001; Chen *et al*, 2005). This suggests that others also experience a difficulty to detect the DTR protein. It is suggested that special measures to solubilise the plasma membrane are needed to isolate and detect the DTR protein (Mekada *et al*, 1991, 1988). Neither the difficulty to solubilise the DTR nor the potential that the antibody is not sensitive enough to detect the DTR in ESC derived neurons explains why the bicistronically expressed EGFP is also undetectable.

3.6.3 Leaky expression of the DTR mRNA was detectable in Mecp2^{StopDTR} cells

I set out to determine if mRNA of the correct sequence is produced from the *Mecp2^{DTR}* locus and whether it is expressed at a similar level as WT *Mecp2* mRNA. I performed real-time quantitative PCR (RT-qPCR) using primers that amplify a region in the 3'UTR of *Mecp2* and northern blot analysis using a probe which bound in the 3'UTR to compare between the levels of WT *Mecp2* mRNA, *Mecp2^{DTR}* mRNA and *Mecp2^{StopDTR}* mRNA (Figure 3.6.3.1). *Mecp2* has multiple polyadenylation sites which give rise to alternative transcripts of ~1.8 kb, 5.4 kb, 7.5 kb and 10.2 kb which vary in abundance between tissues and stages of development (Figure 3.2.1)(Coy *et al*, 1999; Shahbazian *et al*, 2002a; Reichwald *et al*, 2000; Pelka *et al*, 2005; D'Esposito *et al*, 1996). The major transcript expressed in neurons is the long ~10.2 kb transcript which has an 8.6 kb 3'UTR. The expected size of mRNA expressed in *Mecp2^{DTR}* neurons is the same approximate size as WT *Mecp2* mRNA. From both analyses I could determine that mRNA of the correct size was produced in the *Mecp2^{DTR}* neurons (Figure 3.6.3.1). According to RT-qPCR this was actually higher than the level in the WT neurons, however, there was more variation in the level of mRNA between the separate differentiations for the WT neurons. A pool of WT ESCs was differentiated into neurons whereas *Mecp2^{DTR}* ESCs were derived from a single clone, which might account for the increased variation in WT samples.

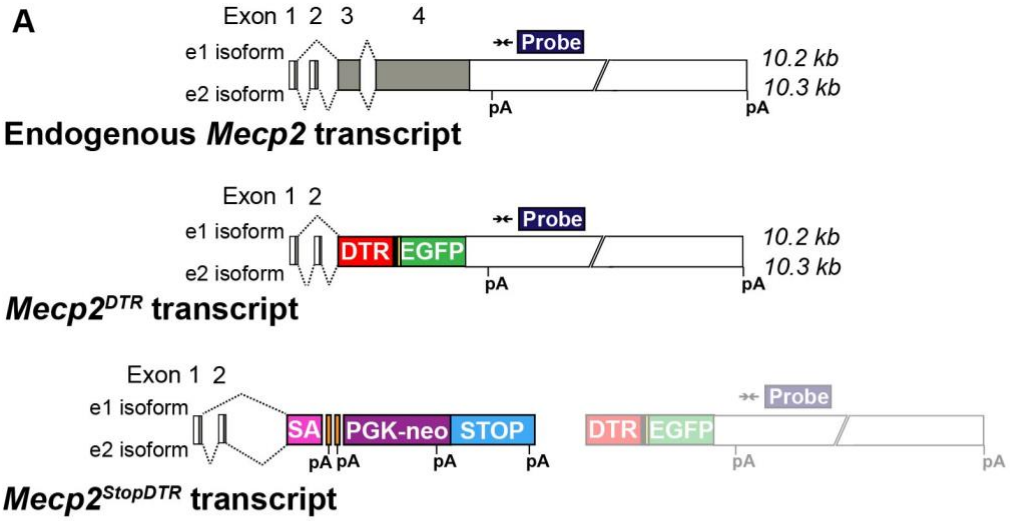

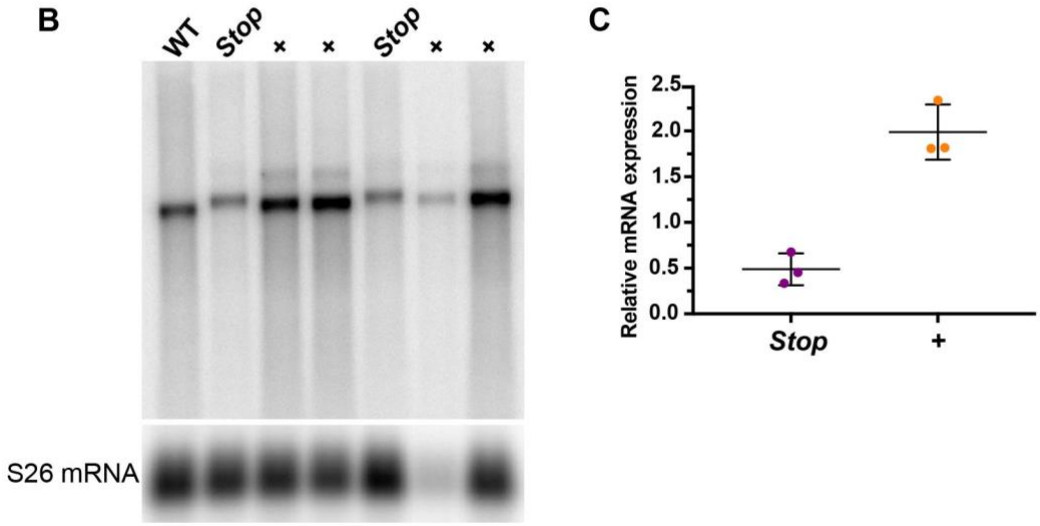

Figure 3.6.3.1. Northern blot and RT-qPCR analysis of mRNA expression in *Mecp2*^{DTR} and *Mecp2*^{StopDTR} ESC-derived neurons. A) Diagram of the sizes of the different mRNA isoforms expected to be produced from each allele. The annealing position of the Northern blot probe and the RT-qPCR primers (black arrowheads) within the 3'UTR are highlighted. B) Northern blot analysis of mRNA extracts from a differentiated pool of WT ESCs, two *Mecp2*^{StopDTR} (Stop) clones: 1H6 and 3C8, and 4 *Mecp2*^{DTR} (+) clones: 1H6 c1, 1H6 c2, 3C8 c1 and 3C8 c2. S26 ribosomal protein mRNA was probed to act as a loading control. C) RT-qPCR analysis of mRNA produced from the *Mecp2* locus in extracts from 3 differentiations of WT (pool), *Mecp2*^{StopDTR} (Stop) 1H6, *Mecp2*^{DTR} (+) 1H6 c2 neurons. The mRNA level is shown relative to the the level of GAPDH mRNA. Each point represents the average of 3 technical replicates per differentiation.(Error bars: SD).

Analysis of the mRNA in the different genotypes of neurons also showed a considerable amount of mRNA produced in *Mecp2*^{StopDTR} neurons (Figure 3.6.3.1). This was alarming because in theory the *Stop* cassette should terminate transcription

before it reaches the 3'UTR of *Mecp2*. Quantification of the level of mRNA by RT-qPCR shows that the mRNA containing the 3'UTR of *Mecp2* in *Mecp2*^{StopDTR} neurons is ~24% of that produced in *Mecp2*^{DTR} neurons. On the northern blot the mRNA band migrates more slowly than that produced in *Mecp2*^{DTR} neurons indicating a sequence difference.

To further investigate what mRNA sequence is being transcribed in the *Mecp2*^{StopDTR} neurons. RNA was reverse transcribed into cDNA, cDNA was then PCR amplified using primers that anneal in the 5'UTR and the 3'UTR to amplify the entire coding region as well as primers in the 5'UTR and the DTR to amplify across the splice boundaries. In samples from *Mecp2*^{DTR} neurons fragments of the expected sizes corresponding to the e1 and e2 isoforms were detected suggesting that correctly spliced mRNA is produced from the *Mecp2*^{DTR} locus. In samples from *Mecp2*^{StopDTR} neurons there were 2 fragments for each primer set which were ~300 and ~400 bps larger than those in *Mecp2*^{DTR} samples (Figure 3.6.3.3). RT-PCR amplicons were blunt cloned and sequenced. The e1 and e2 isoforms of the *Mecp2*^{DTR} mRNA of the correct sequence were identified. Within the *Mecp2*^{StopDTR} cDNA blunt clones, the predominant sequences contained different combinations of segments of sequences originating from components within the *Stop* (Figure 3.6.3.2). These mRNA species were formed by splice events in and out of the Engrailed 2 (En-2) splice acceptor sequence and the *Stop* cassette sequence and as a result were bigger in size than the mRNA produced in *Mecp2*^{DTR} neurons, explaining the increased size of *Mecp2*^{StopDTR} mRNA on the northern blot and RT-PCR. Interestingly, in each cDNA clone sequenced, the segments of sequence were exactly the same but in different combinations, suggesting that there are certain sequences which act as splice acceptors and splice donors within the En-2 exon and the *Stop* cassette sequences. If the AUG of *Mecp2* is used, translation would be terminated at an in frame stop codon within the spliced En-2 sequence and should not give rise to an in frame DTR. Intrestingly, there are a number of downstream AUGs in the larger aberrantly spliced fragment of the *Stop* cassette which happen to now be in frame with the DTR coding sequence. If these alternative AUGs are used as translation start codons then this could in theory give rise to DTR protein expression. It is unknown whether these alternative AUGs are ever used and whether the DTR

translated in this way with the extended N-terminal tail comprising of the peptide sequence encoded by these aberrantly spliced sequences is functional.

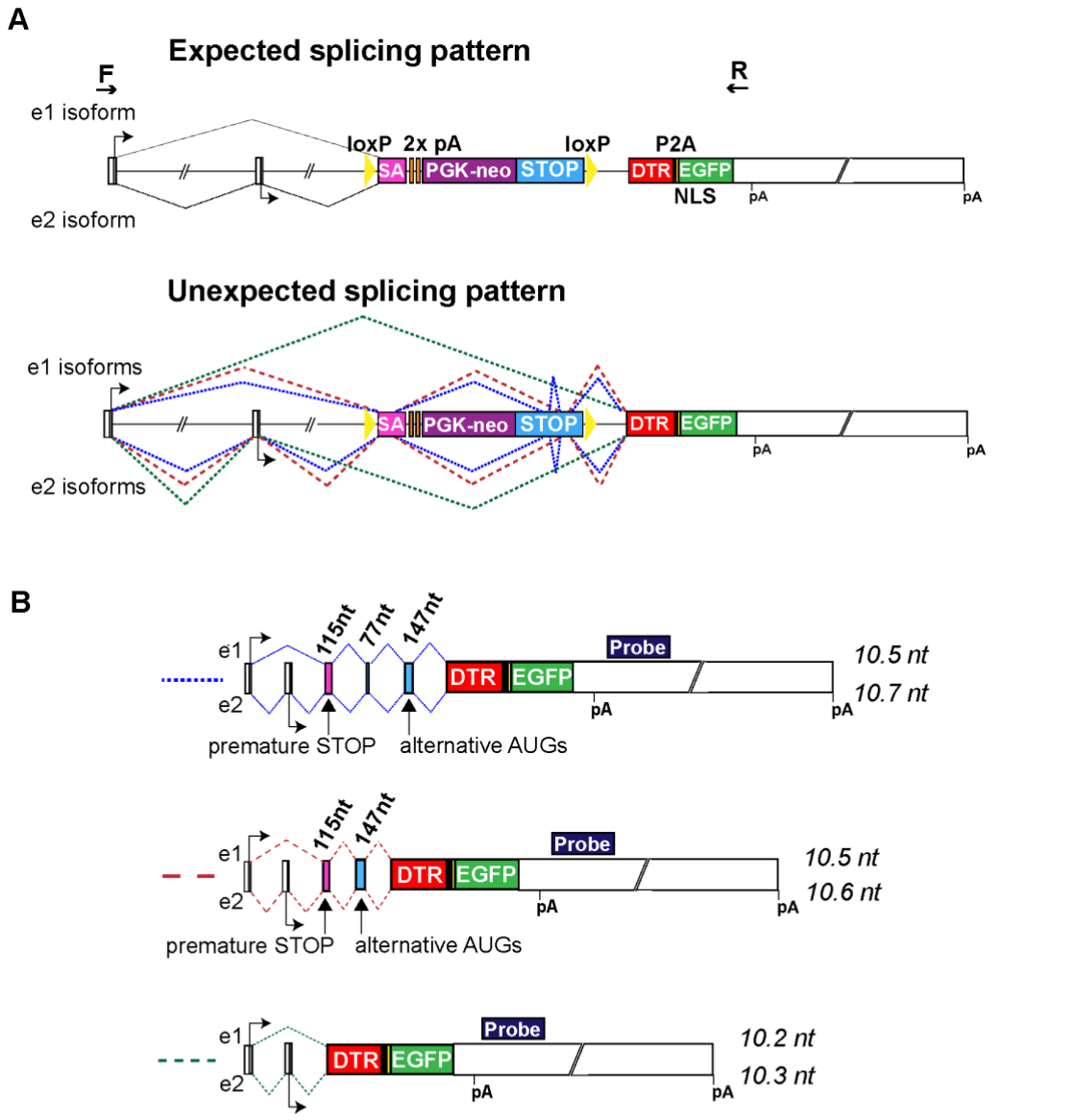

Figure 3.6.3.2. Aberrantly spliced transcripts were identified by sequencing the cDNA from *Mecp2*^{StopDTR} neurons and mice. Schematic representation of the three different cDNA products sequenced from mRNA samples from *Mecp2*^{StopDTR} neurons and mice. A) Describes the *Mecp2*^{StopDTR} gene and the expected and unexpected splicing patterns which take place. Primers used for amplifying the cDNA are shown by black arrows (F: forward, R: reverse). Dotted lines represent the splicing pattern for each mRNA species shown in B. Above is the splicing pattern for the e1 isoform of each transcript and below are the e2 isoforms. B) Shows the three transcript products produced by the abberant splicing patterns. The size of each spliced fragment is annotated and the total size of the major mRNA isoforms (e1 isoform above, e2 below) detected on the Northern blot (Figure 3.6.3.1) are in italics at the 3' end of the transcript.

A small fraction of the sequenced *Mecp2*^{StopDTR} mRNA products were formed by splicing around the *Stop* cassette entirely (Figure 3.6.3.2). This transcript would encode an in-frame DTR. To get an idea of how often the *Stop* cassette is missed by splicing around it, I carried out Southern blot analysis on amplified cDNA using a radiolabeled probe which bound across the exon 1 to exon 3 (DTR containing exon) splice boundary (Figure 3.6.3.3). Non-specific binding of the probe should not occur because the melting temperature of the sequences that have homology to either side of the splice boundary are much lower than the temperature used for the Southern blot hybridisation and wash steps. I could not detect bands of the size corresponding to the product formed by splicing around the *Stop* cassette sequence in the *Mecp2*^{StopDTR} samples on an Ethidium Bromide gel (Figure 3.6.3.3). These products were easily identified in *Mecp2*^{DTR} samples where the *Stop* cassette has been removed by Cre recombination. Southern blot of the RT-PCR gel did highlight a tiny amount of the product of the size expected when the *Stop* cassette is missed in the *Mecp2*^{StopDTR} samples. This was barely detectable compared to the whopping signal for the activated *Mecp2*^{DTR} neurons.

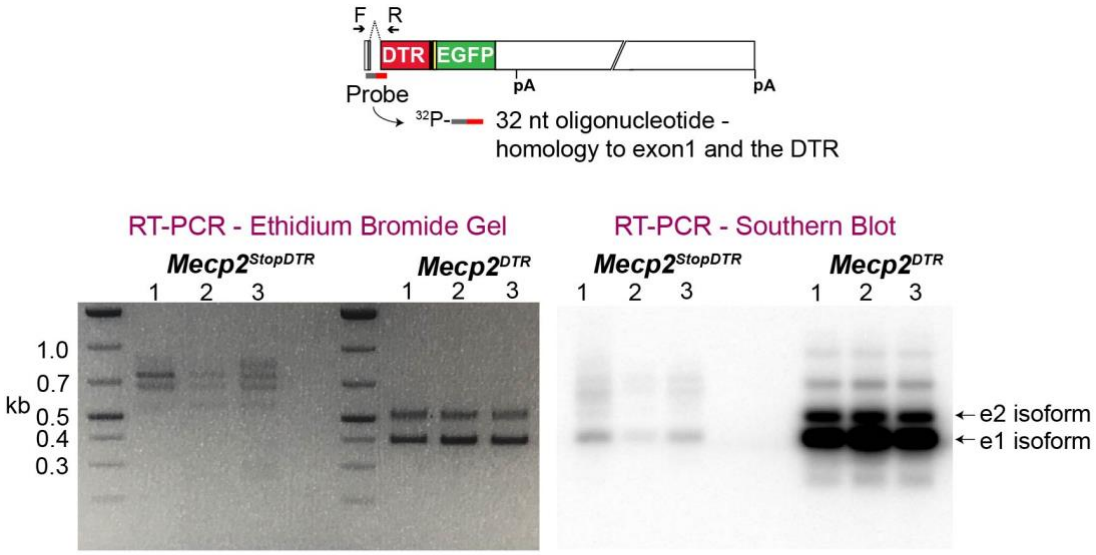

Figure 3.6.3.3. A very small amount of in-frame DTR-containing mRNA was detectable in *Mecp2*^{StopDTR} neurons. Above) Diagram of where the radiolabeled probe used for the Southern blot anneals within the in-frame transcript expressed from the *Mecp2*^{StopDTR} locus (e1 isoform specific). The primers used to amplify the cDNA are shown by black arrows (F: forward, R: reverse). Below) Left: RT-PCR reactions from *Mecp2*^{StopDTR} and *Mecp2*^{DTR} cDNA samples run on an Ethidium Bromide agarose gel; Right: Southern blot of the RT-PCR gel probing specifically for the cDNA product formed by splicing around the *loxP-SA-pApA-NeoStop* cassette in *Mecp2*^{StopDTR} neurons and splicing as expected in *Mecp2*^{DTR} neurons.

Taken all together, there was a near to WT level of mRNA produced in *Mecp2*^{DTR} neurons of the correct sequence indicating that the mRNA level does not explain the inability to detect DTR protein in these neurons. Worryingly, there is a small but detectable level of mRNA produced in *Mecp2*^{StopDTR} neurons which will encode an in-frame DTR. This "leaky" expression of the DTR from the *Mecp2*^{StopDTR} has the potential to make these cells sensitive to DT if enough functional receptors are inserted into the cell membrane to permit entry of DT. Sensitivity of these cells to DT would be deleterious to the ultimate *in vivo* ablation experiments as it would lead to off-target non-neuronal ablation.

3.7 Administration of Diphtheria toxin to *Mecp2*^{StopDTR} and *Mecp2*^{DTR} cells in culture

3.7.1 Mecp2^{DTR} *ESCs were sensitive and Mecp2*^{StopDTR} *ESCs were resistant to Diphtheria Toxin*

To determine whether the targeted *Mecp2*^{DTR} ESCs are sensitive to DT and importantly whether the *Mecp2*^{StopDTR} ESCs are resistant, I treated the different genotypes of ESCs with a moderate dose of DT. I plated out two different clones of *Mecp2*^{DTR} and *Mecp2*^{StopDTR} and a pool of WT control ESCs at a relatively low density then treated the cells with DT and measured their confluence over time in the Incucyte. Treated or untreated WT and *Mecp2*^{StopDTR} cells divided rapidly and reached ~100% confluency by ~30 hours (Figure 3.7.1.1). Untreated *Mecp2*^{DTR} cells also showed this rapid division, however, DT treated *Mecp2*^{DTR} cells which should express the DTR, failed to divide after being treated with DT and died (Figure 3.7.1.1). *Mecp2*^{StopDTR} cells remained resistant when the dose of DT was increased to 1 µg/ml.

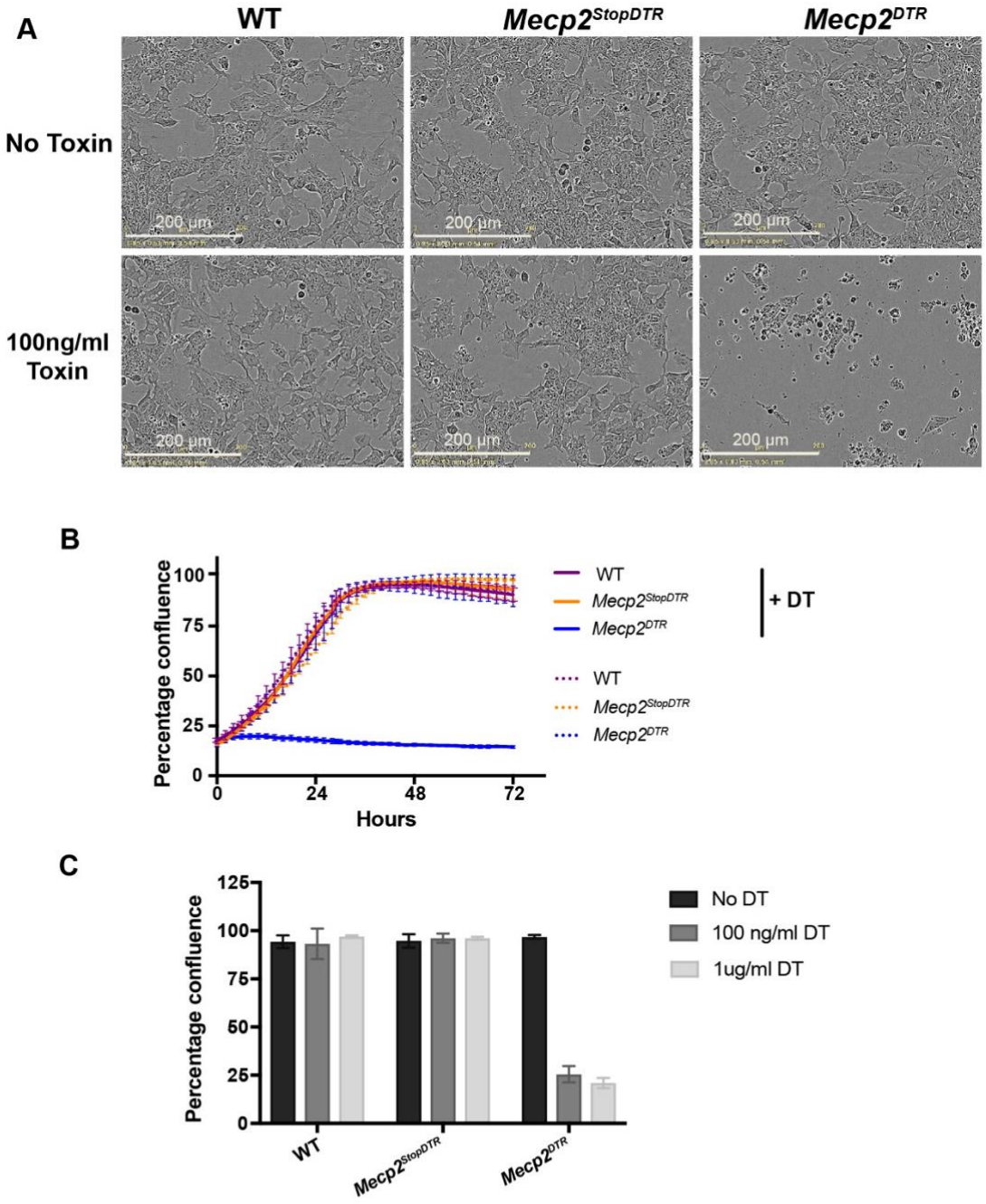

Figure 3.7.1.1. *Mecp2*^{StopDTR} mESCs are resistant to DT and *Mecp2*^{DTR} ESCs are sensitive. A) Representative phase images taken by the Incucyte of *Mecp2*^{StopDTR} 1H6, *Mecp2*^{DTR} 1H6c2 and the WT pool of ESCs, treated or not treated with 100ng/ml DT, 24 hours after treatment. B) The percentage confluence of cells following the addition of 100ng/ml DT to the culture medium at 0 hours. Plotted here is the mean and SD of the percentage confluence per well for 3 wells of ESCs per genotype and condition. Data sets for two clones of *Mecp2*^{StopDTR}, 1H6 and 3C8 and 2 clones of *Mecp2*^{DTR} 1H6c2 and 3C8c2 are grouped together. C) The percentage confluence 48 hours after the addition of no, 100 and 1µg/ml DT to the culture medium. Plotted is the mean and SD for 3 wells of cells per genotype and condition and as above, the data sets for 2 clones of *Mecp2*^{StopDTR} and *Mecp2*^{DTR} are grouped together.

Terminal deoxynucleotidyl transferase dUTP nick end labelling (TUNEL) analysis was performed on the ESCs following DT administration to determine if apoptosis of *Mecp2*^{DTR} + DT cells could be detected using an alternative method (Figure 3.7.1.2). TUNEL analysis is a commonly used assay which detects DNA fragmentation, a hallmark of apoptosis, at a single-cell level. DNA is cleaved to form double-stranded breaks or nicks during the early stages of DNA degradation, the free 3'-hydroxyl termini of these breaks can be labelled with modified deoxyribonucleotides, by template-independent polymerization catalysed by Terminal deoxynucleotidyl transferase (TdT)(Gavrieli *et al*, 1992). Fluorescently labelled nucleotides are particularly useful for analysis by flow cytometry.

Mecp2^{DTR} and *Mecp2*^{StopDTR} ESCs along with WT control cells were treated with DT and 24 hours later cells were harvested, fixed and stained with TUNEL labelling reagents. Cells were analysed by flow cytometry to determine the proportion of the population which were TUNEL positive. Forward scatter versus side scatter cell density plots show that untreated cells and *Mecp2*^{StopDTR} and WT cells treated with toxin have similar morphology, however, *Mecp2*^{DTR} + DT cells are smaller in size and show a higher complexity or granularity, suggesting that these cells are apoptosing (Figure 3.7.1.2). *Mecp2*^{DTR} + DT clearly show a substantial increase in fluorescence (TUNEL positive staining), compared to untreated controls and toxin treated *Mecp2*^{StopDTR} and WT ESCs.

At the concentrations tested, *Mecp2*^{DTR} ESCs are selectively sensitive to DT compared to *Mecp2*^{StopDTR} and WT cells. Encouragingly, despite the slight leaky expression of DTR transcripts detected in neurons, ESCs retaining the *Stop* cassette were resistant to DT.

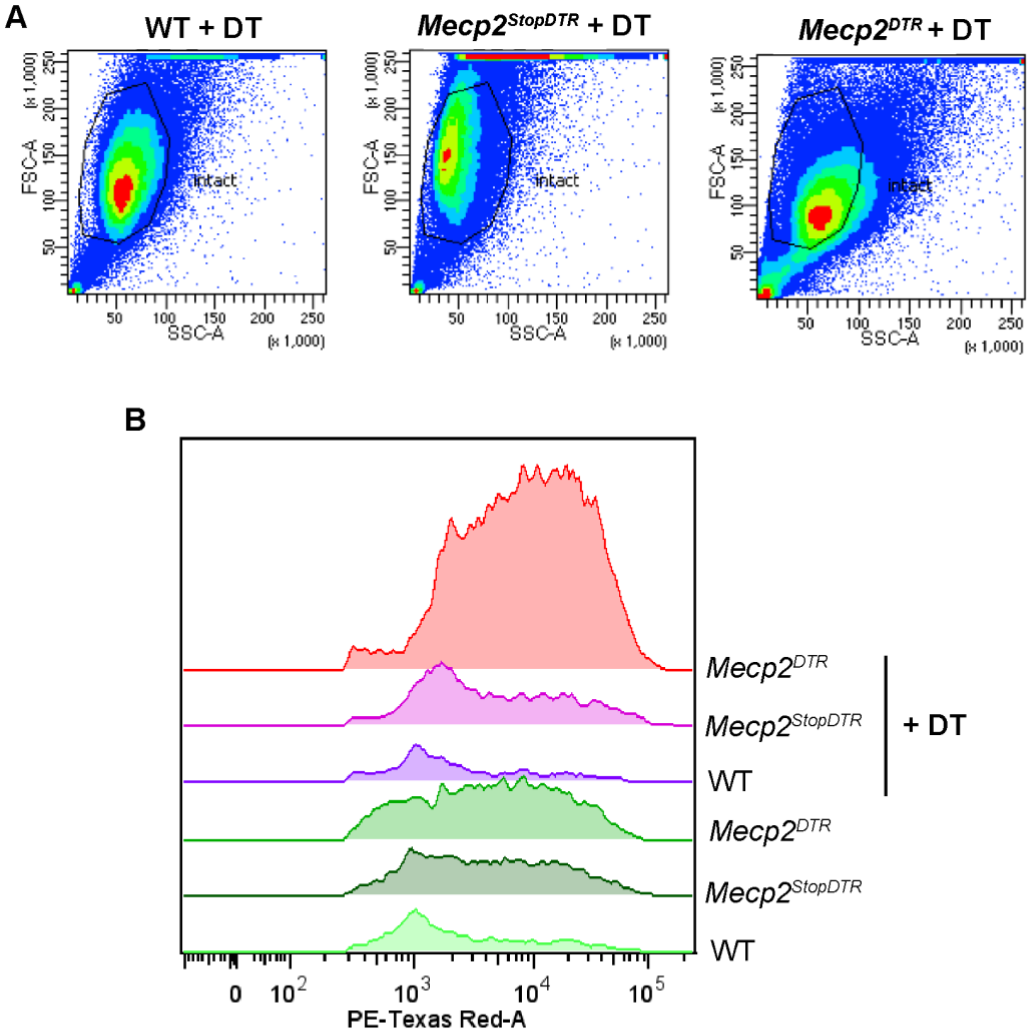

Figure 3.7.1.2. Apoptosis of *Mecp2*^{DTR} ESCs treated with DT could be visualised using TUNEL analysis. Flow cytometry data of mESCs treated or not treated with 100 ng/ml Diphtheria Toxin (DT) folowing TUNEL staining using TMR red labelled dUTPs. A) Forward scatter (FSC-A) versus side scatter (SSC-A) plots of WT, *Mecp2*^{StopDTR} and *Mecp2*^{DTR} cells treated with DT. Apoptosing cells are smaller (FSC-A) in size and have a more complex morphology (SSC-A) and so become shifted down and right as shown in the *Mecp2*^{DTR} + DT condition. B) Overlay of cell count versus fluorescence intensity for each genotype treated or not treated with DT.

3.7.2 Mecp2^{DTR} *and Mecp2*^{StopDTR} *neurons were both sensitive to Diphtheria Toxin*

The *Mecp2*^{StopDTR} mouse model was designed to be used to carry out *in vivo* neuronal ablation experiments at different stages in development. *Mecp2* is expressed much more highly in neurons so it is plausible that neurons expressing the DTR from the

Mecp2 locus are more sensitive to DT than ESCs. Accordingly, I treated neurons in cell culture with DT to see how neurons behaved compared to ESCs.

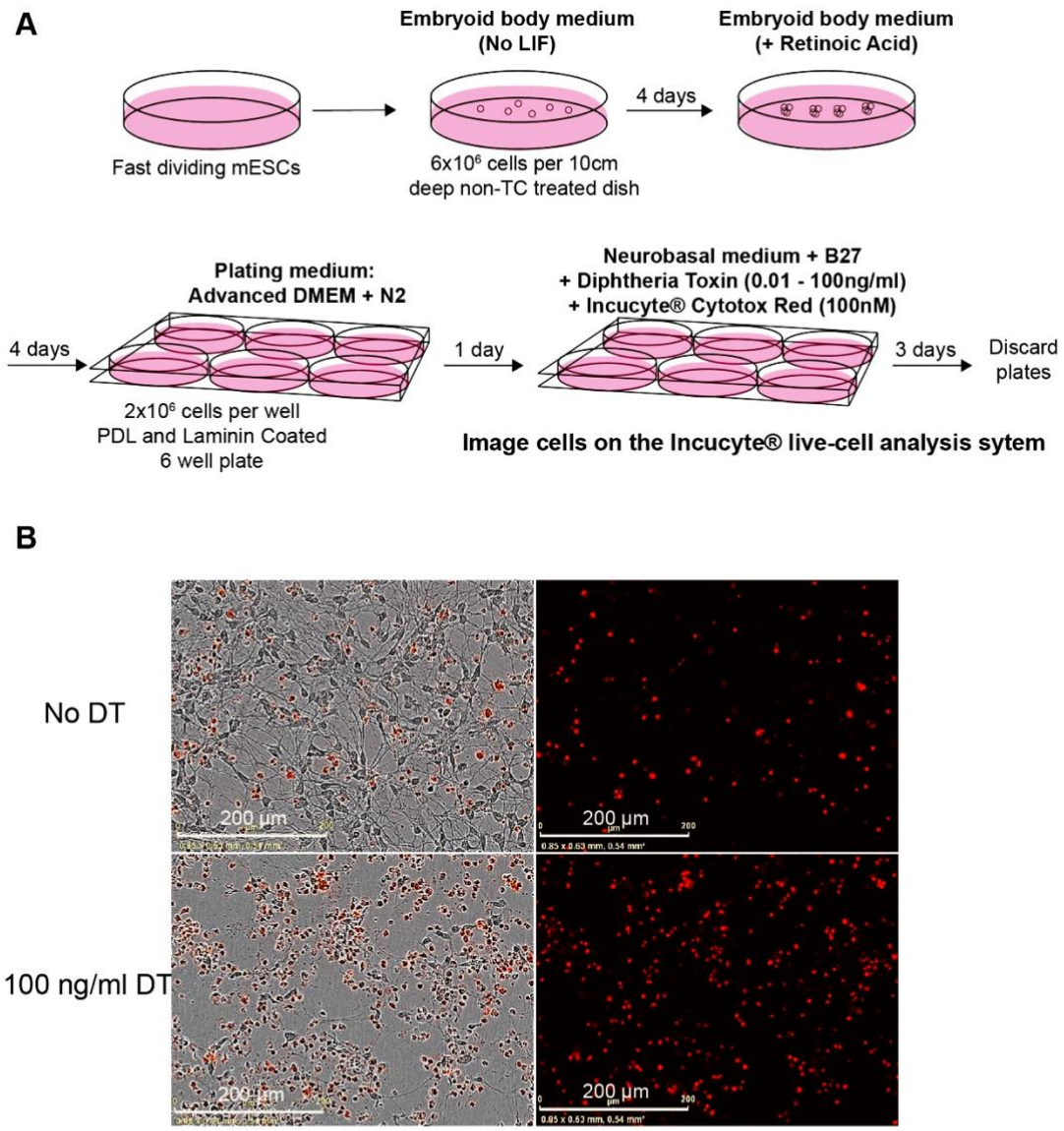

Figure 3.7.2.1. DT-mediated ablation assay for ESC-derived neurons. A) Diagram of the protocol used for the DT-ablation of mESC derived neurons. B) Example phase and fluorescent images taken on the Incucyte showing untreated and treated *Mecp2*^{DTR} neurons. Incucyte Cytotox Red fluorescent dye identifies dead cells.

Mecp2^{StopDTR}, *Mecp2*^{DTR} and WT ESCs were differentiated into neurons and DT and Incucyte Cytotoxic Red dye treatments were incorporated into the first half medium change after plating out the embryoid bodies (EBs)(Figure 3.7.2.1). The accumulation of dead cells (those fluorescing red) over time was measured by the Incucyte. During

neuronal differentiation there is a basal level of cell death among cells which fail to differentiate into neurons. This is shown by the accumulation of dead cells for WT and untreated *Mecp2*^{StopDTR} and *Mecp2*^{DTR} neurons over time (Figure 3.7.2.1). It is clear when analysing images taken on the Incucyte at which time all neurons have died, as the neurites disintegrate, and the cell bodies become condensed.

DT-induced cell death for a given genotype was assayed by a significant accumulation of red cells over time compared to the basal accumulation of red cells observed in the untreated condition. A clear increase in the accumulation of dead cells over time was observed for activated *Mecp2*^{DTR} neurons treated with 1-100 ng/ml DT compared to untreated cells (Figure 3.7.2.2). The number of red cells per area plateaued at ~30 hours and at this point all of the neurons in the images taken by the Incucyte were evidently dead compared to images of untreated neurons at the same time point (Appendix Figure 8.). Importantly, untreated *Mecp2*^{DTR} neurons were visually comparable to WT neurons treated or untreated with DT.

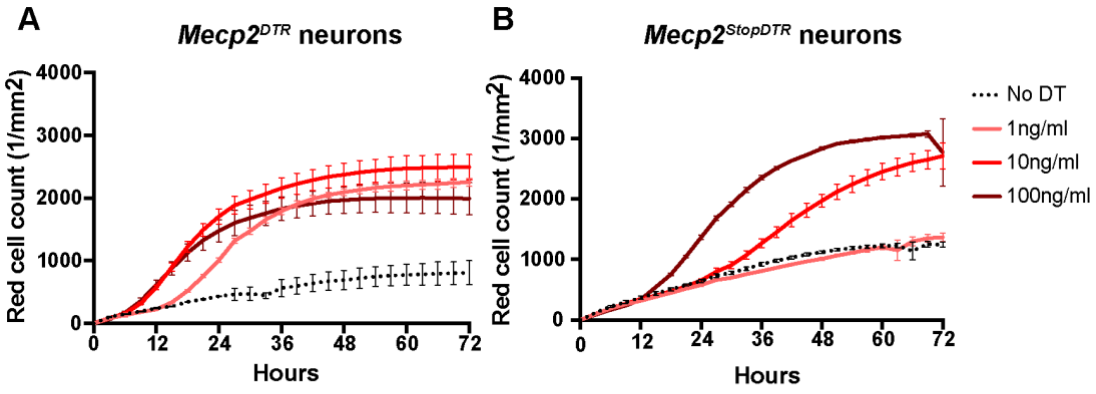

Figure 3.7.2.2. *Mecp2*^{StopDTR} and *Mecp2*^{DTR} neurons were both sensitive to Diphtheria Toxin in cell culture. A) The red cell count (dead cell count) per mm^2 for *Mecp2*^{DTR} neurons over time following administration of different doses of DT. B) The red cell count (dead cell count) per mm^2 for *Mecp2*^{StopDTR} neurons over time following administration of different doses of DT. A+B) DT toxin was administered at 0 hours. Plotted is the mean and SD for 3 wells of cells per condition.

Treating *Mecp2*^{StopDTR} ESC-derived neurons with DT was the key experiment which changed the trajectory of this project. Unfortunately, the leaky expression of the DTR detected at the mRNA level in *Mecp2*^{StopDTR} neurons was enough to make neurons

sensitive to certain doses of DT shown by the accumulation of the number of red cells over time as well as the clear death of neurons in Incucyte images (Figure 3.7.2.2 and Appendix Figure 8.). A difference in sensitivity between the activated *Mecp2*^{DTR} neurons and the stopped *Mecp2*^{StopDTR} neurons was identified, 1 ng/ml induced cell death of *Mecp2*^{DTR} neurons but did not kill *Mecp2*^{StopDTR} neurons. To determine how much more sensitive *Mecp2*^{DTR} neurons were compared to *Mecp2*^{StopDTR} neurons, lower doses of toxin were tested. *Mecp2*^{DTR} neurons were clearly sensitive to 0.1 ng/ml DT but were resistant to 0.01 ng/ml DT whereas *Mecp2*^{StopDTR} were resistant to both doses (Figure 3.7.2.3).

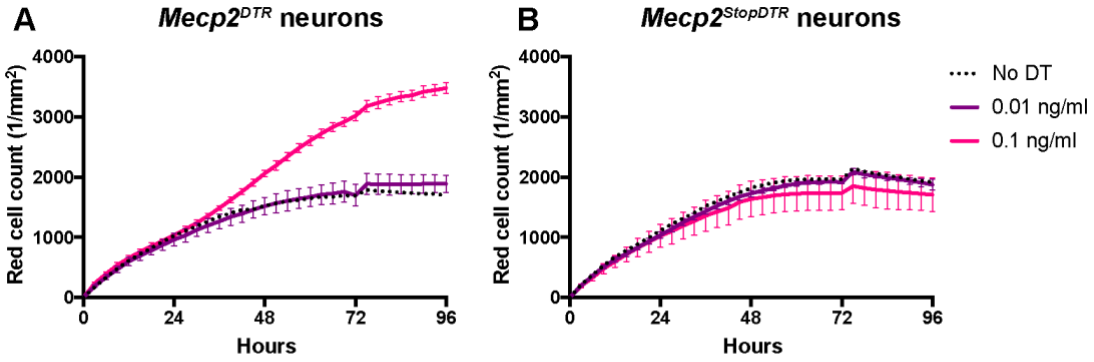

Figure 3.7.2.3. *Mecp2*^{DTR} neurons were 100 times more sensitive to Diphtheria Toxin than *Mecp2*^{StopDTR} neurons in cell culture. A) The red cell count (dead cell count) per mm^2 for A) *Mecp2*^{DTR} neurons and B) *Mecp2*^{StopDTR} neurons over time following administration of different doses of DT. A+B) DT toxin was administered at 0 hours. Plotted is the mean and SD for 3 wells of cells per condition.

The DT-assay on ESC-derived neurons in culture determined that activated *Mecp2*^{DTR} could be efficiently ablated by broad a range of DT doses and that unfortunately *Mecp2*^{StopDTR} neurons were sensitive to higher doses of DT. *Mecp2*^{DTR} activated neurons were 100 times more sensitive to DT in cell culture than *Mecp2*^{StopDTR}.

3.8 The efficiency of the modified *Stop2* cassette was improved compared to the original *Stop1* cassette

Mice were generated in parallel to the cell culture experiments. This was done in the interests of time, in order to ensure that *Mecp2*^{StopDTR} mice were available. For this reason, we were unaware of the problem with sensitivity of *Mecp2*^{StopDTR} ESC-derived

neurons to DT until mouse generation was well advanced. It was important to determine how the expression from the modified locus in the mouse brain compared with the ESC-derived neurons.

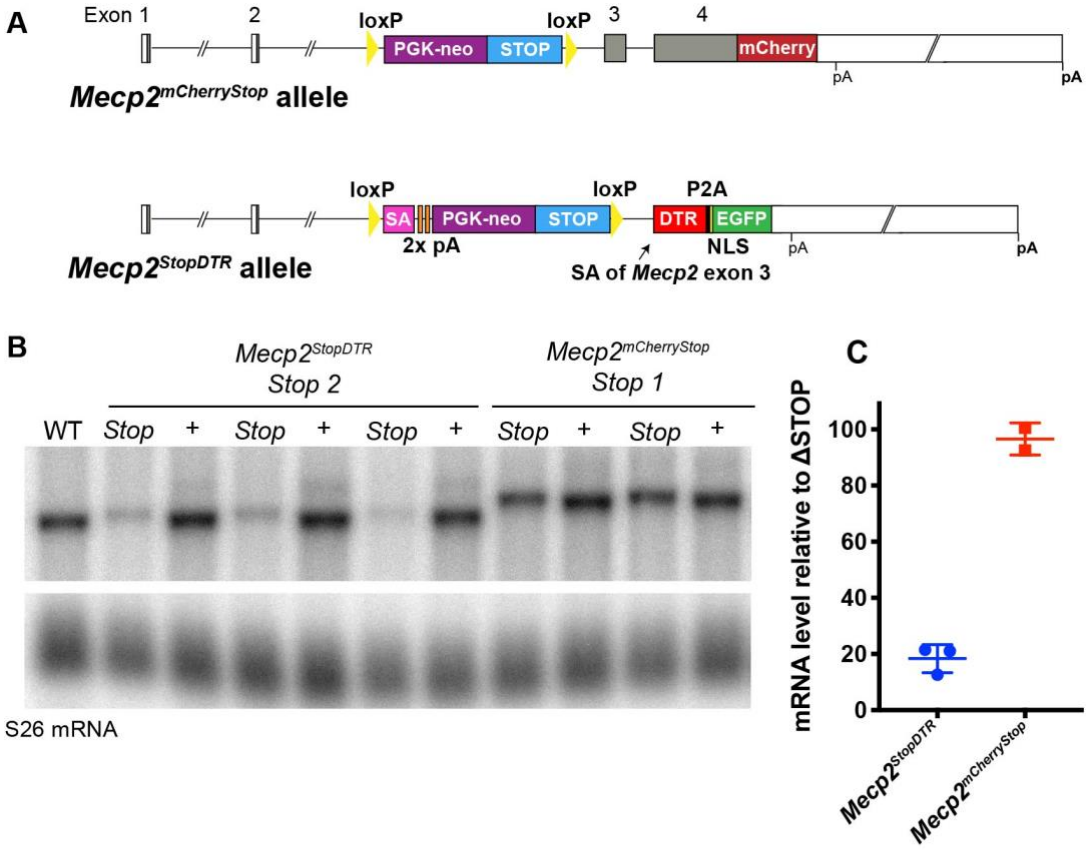

Figure 3.8. Northern blot analysis identified substantial improvement in termination of transcription by the modified *Stop2* cassette compared to the original *Stop1* cassette. A) Schematic diagrams of the *Mecp2*^{mCherryStop} allele which contains the original unmodified *Stop1* cassette used in the conditional reactivation *Mecp2*^{Stop} allele (Guy et al., 2007) and the *Mecp2*^{StopDTR} allele which contains the modified Stop2 cassette. B) Northern blot analysis of RNA extracted from brains of WT mice, mice +/- the modified *Stop2* cassette: *Mecp2*$^{StopDTR/y}$ *(Stop)*, or *Mecp2*$^{StopDTR/y}$*,Nes-cre* (+), and mice +/- the original *Stop1* cassette: *Mecp2*$^{mCherryStop/y}$ (*Stop*) or *Mecp2*$^{mCherry+/y}$ (+). Each lane corresponds to a different mouse and all mice are hemizygous males. The hybridisation probe anneals in the 3'UTR of *Mecp2*. C) The mRNA level in *Mecp2*$^{StopDTR/y}$ and *Mecp2*$^{mCherryStop/y}$ brains as a percentage of the level in their corresponding ΔStop (+) line the *Mecp2*$^{\Delta}$*DTR*$^{Stop/y}$*,Nes-cre* (+) and *Mecp2*$^{mCherry+/y}$ (+) respectively. Quantification of the signal intensity of each band in the Northern blot was achieved using ImageJ-Fiji. The level of mRNA detected in each sample is normalised to the S26 ribosomal protein mRNA loading control and is expressed as a percentage of the average level in the corresponding ΔStop (+) line. (Error bars: SD)

Northern blot analysis of RNA extracted from brains from male *Mecp2*$^{StopDTR/y}$ mice and *Mecp2*$^{StopDTR/y}$*,Nes-cre* mice was performed to determine the level of leaky expression of DTR containing mRNA in the *Mecp2*$^{StopDTR/y}$ brain (Figure 3.8.). The

Nes-cre (*cre*) driver can achieve approximately >90% recombination efficiency at the *Mecp2* locus in whole brain according to Southern blot analysis (Ross *et al*, 2016). Therefore *Mecp2*$^{StopDTR/y}$*,cre* mice were used as a positive control for activated DTR expression in the brain. The mRNA level in the *Mecp2*$^{StopDTR/y}$ brain was 18.4% of the level in *Mecp2*$^{StopDTR/y}$*,cre* brain. This mRNA includes all mature transcripts produced from the *Mecp2*^{StopDTR} allele which contain the endogenous 3'UTR of *Mecp2*, only a fraction of which encodes an in-frame DTR (as discussed in section 3.6.3).

To determine whether the efficiency of the modified *Stop2* cassette (*loxP-SA-pApA-NeoStop*) was improved compared to the original *Stop1* cassette (*loxP-NeoStop*) (discussed in section 3.2.4): the mRNA expression in mice with either cassette was directly compared. RNA samples from two other mouse lines generated by Jim Selfridge in the Bird lab: *Mecp2*^{mCherryStop} and *Mecp2*^{mCherry} were included in the northern blot analysis (Figure 3.8.). The *Mecp2*^{mCherryStop} line is an *Mecp2* reporter mouse line where the C terminus of MeCP2 is tagged with mCherry and the *Stop1* cassette is inserted into intron 2. This allele is identical to the original conditional reactivation allele (Guy *et al.*, 2007), apart from the addition of an mCherry tag. The *Mecp2*^{mCherry} *(*Δ*Stop)* line was generated by crossing the *Mecp2*^{mCherryStop} line to a transgenic CMV-Cre driver to achieve ubiquitous expression of MeCP2^{mCherry}. This line was included as a positive control for *Mecp2*^{mCherryStop} activation. The northern blot probe anneals in the 3'UTR of *Mecp2* which is intact in all of the different genotypes, therefore, the levels of mRNA can be directly compared. It is clear from the blot that there is substantially less leaky mRNA in the *Mecp2*$^{StopDTR/y}$ brain compared to the *Mecp2*$^{mCherryStop/y}$ brain (Figure 3.8.). The mRNA level in the *Mecp2*$^{mCherryStop/y}$ brain is indistinguishable (96.6%) from the level *Mecp2*$^{mCherry/y}$ brain whereas the mRNA level in the *Mecp2*$^{StopDTR/y}$ brain is 18.4% of the *Mecp2*$^{DTR/y}$ brain. This result shows that the mRNA which evaded premature termination at the *Stop* cassette was >5 fold more within the *Stop1* allele compared to the *Stop2* allele.

The northern blot result alone makes it seem as though there should be 18.4% DTR mRNA expressed in the *Mecp2*$^{StopDTR/y}$ brain and 96.6% *Mecp2*^{mCherry} mRNA expressed in the *Mecp2*$^{mCherryStop/y}$ brain. Protein analysis in *Mecp2*$^{mCherryStop/y}$ brains shows that there is only ~4.5% of MeCP2^{mCherry} protein produced from the *Stop* allele

(see section 5.2.2). Therefore, despite high levels of transcript from this stopped allele, the majority of mRNA products detected on the northern blot do not encode functional protein. To approximately quantify how much in frame DTR containing mRNA is produced in the *Mecp2*$^{StopDTR/y}$ brain and how this level of leaky expression compares to that in the *Mecp2*$^{mCherryStop/y}$ brain, I blunt cloned PCR amplicons of cDNA and sequenced them in order to know what proportion should encode a functional protein (see Table 3.8.). The total amount of in-frame transcript produced in the *Mecp2*$^{StopDTR/y}$ brain that is capable of being translated into functional DTR protein is 0.61% of the total mRNA level in the reactivated *Mecp2*$^{DTR/y}$ brain. The additional modifications made to the *Stop1* cassette reduced the amount of leaky in-frame transcript by approximately 13-fold.

	Stop1	***Stop2***
Total mRNA (% of reactivated)	96.6	18.4
In-frame mRNA (% of total sequenced)	8.3	3.33
Total leaky in frame mRNA (% of reactivated)	8.02	0.61

Table 3.8. The efficiency of the modified *Stop2* cassette was improved by 13 fold compared to the original *Stop1* cassette. Total mRNA level was quantified from the northern blot analysis shown in Figure 3.8: the level of mRNA detected in each biological replicate (N=2) was normalised to the S26 ribosomal protein mRNA loading control and expressed as a percentage of the average level in the corresponding reactivated brains (ΔStop or +). The total mRNA value in the table is the average for two biological replicates (two separate mouse brains). The amount of in-frame mRNA is calculated from sequencing the PCR amplicons of cDNA from mRNA extracted from mouse brain. The average percentage of in-frame mRNA sequences out of the total number of aligned sequences analysed for two biological replicates is shown here. A total of 30 aligned sequences were analysed per biological replicate. Total leaky in-frame mRNA is then calculated by combining the total mRNA detected by northern blot with the in-frame mRNA fraction according to sequencing.

3.9 *Mecp2*^{StopDTR} mice were sensitive to Diphtheria Toxin

DT administration to unrecombined *Mecp2*^{StopDTR} neurons in culture suggested that at higher doses of toxin these neurons were susceptible to DT-induced cell death. In comparison with *Mecp2*^{DTR} neurons, where the *Stop* cassette has been removed by Cre, the dose needed to kill *Mecp2*^{StopDTR} neurons was ~100 times higher than that needed

to kill *Mecp2*^{DTR} cells. As there was a dose which induced death of *Mecp2*^{DTR} neurons but not for *Mecp2*^{StopDTR} neurons in cell culture, we hypothesised that there might be a usable dose in *Mecp2*$^{StopDTR/+}$*,cre* mice which would lead to ablation of recombined *Mecp2*^{DTR} neurons but not lead to unwanted off-target cell ablation of unrecombined *Mecp2*^{StopDTR} non-neuronal cells (which do not express Cre). Hemizgous *Mecp2*$^{StopDTR/y}$ males express the X-linked DTR knock-in allele in 100% of their cells compared to heterozygous females which express this allele in only 50% of their cells due to random X-chromosome inactivation. Accordingly, males should be more susceptible to adverse effects of sensitivity to DT and so are a more stringent test for DT susceptibility than females. *Mecp2*$^{StopDTR/y}$ male mice were treated with different doses of DT to determine whether these mice were susceptible to the toxin.

Another difference between hemizygous *Mecp2*$^{StopDTR/y}$ males and heterozygous *Mecp2*$^{StopDTR/+}$ females is the severity of the MeCP2-deficiency phenotype. Males that express an *Mecp2*^{StopDTR} allele are *Mecp2*-null and develop a neurological phenotype associated with MeCP2 deficiency after ~6 weeks and reach their humane endpoints at ~6-20 weeks. Females who are heterozygous for *Mecp2*^{StopDTR} allele are also heterozygous for the functional *Mecp2* gene. These animals develop a much milder, sometimes undetectable, neurological phenotype associated with MeCP2 deficiency after ~6 months and have a normal life-span. The male *Mecp2*$^{StopDTR/y}$ mice were treated with DT before 6 weeks in an attempt to distinguish a phenotype attributed to DT toxicity from *MeCP2* deficiency.

Numerous injection regimes have been published in literature for *in vivo* ablation of DTR expressing cells. Single or multiple injections of a high dose of 40-50 µg/kg have been commonly used to ablate cells in the CNS (Chen *et al*, 2005; Hatori *et al*, 2008; Gropp *et al*, 2005; Luquet *et al*, 2005; Yamada *et al*, 2020; Cheng *et al*, 2017; Hosford *et al*, 2017, 2016). We hypothesized that using a high dose of toxin that could efficiently kill DTR+ target cells, without having toxic effects in WT mice should clearly identify if the small amount of leaky expression of the DTR in the mouse is enough to cause a substantial problem. We decided to administer two injections on consecutive days of 50 µg/kg DT to 3 week-old *Mecp2*$^{StopDTR/y}$ mice and WT controls. Injection of 40-50µg/kg DT on two consecutive days has been used in other studies

(Chen *et al*, 2005; Gropp *et al*, 2005; Yamada *et al*, 2020). The general condition of the mice was checked daily and 5 days after the first injection it was clear that all *Mecp2*$^{StopDTR/y}$ mice administered the toxin were showing signs of adverse effects of DT injection, they had undergone a >20% reduction in weight, showed little activity, were pinched at the rear and hunched. WT mice injected with the toxin showed no abnormal phenotype. The experiment was terminated here at the first sign of adverse effects and mice were culled humanely. On postmortem, the contents of the intestine of *Mecp2*$^{StopDTR/y}$ mice was black which the vet advised was a sign of DT toxicity. This experiment made it alarmingly clear that leaky expression of the DTR in *Mecp2*$^{StopDTR/y}$ mice caused lethality when a high dose of toxin was administered.

We decided to dramatically reduce the dose of toxin and carried out a single injection of 0.5 µg/kg or 5 µg/kg on two smaller cohorts of *Mecp2*$^{StopDTR/y}$ and WT 4 or 5 week old mice respectively (Table 3.9). Mice were insensitive to 0.5 µg/kg of DT, showed no significant difference in weight gain compared to WT mice and no abormal phenotype. On postmortem there were no differences between treated *Mecp2*$^{StopDTR/y}$ mice and WT mice. Mice treated with doses of 5ug/kg did display signs of adverse effects. This time the adverse effects were different. There was no substantial weight loss (<20% BW) and sudden decline in health occurred resulting one animal being culled for health concerns and one suddenly dying a day later. In both cases mice showed no sign of adverse effects in previous check of the day. These mice were older and closer to being pathogenic due to MeCP2 deficiency compared to previous animals treated with a much higher dose which might contribute to the difference in phenotype associated with adverse effects of toxin. The mice didn't score for a MeCP2 deficiency phenotype at each check. We decided not to do any further experiments with these mice as, based on the doses of DT used in literature for *in vivo* cell ablation of DTR expressing cells, a dose of 0.5ug/kg is likely to be too low to mediate efficient ablation of such a large population of target cells.

Dose	50 µg/kg	5 µg/kg	0.5 µg/kg
Number of injections	1 daily, 2 consecutive days	1 injection	1 injection
Cohort	4 STOP, 4 WT	3 STOP, 3 WT	3 STOP, 3 WT
Age	3 weeks	5 weeks	4 weeks
End point reached	5 days after 1st injection	3 - 4 days after 1st injection	N/A
Adverse Phenotype	Lost >20% BW, pinched at rear, hunched	No significant weight loss, sudden decline in health status	N/A
Pathology	Contents of intestine black	N/A	N/A

Table 3.9. *Mecp2*$^{StopDTR/y}$ mice were resistant to 0.5 µg/kg but sensitive to 5 µg/kg DT and higher. N/A: not applicable because no difference was observed compared to WT animals.

3.10 Discussion

The overall aim of this PhD project was to develop a novel mouse model to enable selective and inducible ablation of MeCP2 deficient cells in the female heterozygote. This chapter described the production and characterisation of the *Mecp2*^{StopDTR} ESCs and the subsequent mouse model. *Mecp2*^{StopDTR} knock-in ESCs were successfully generated and used to generate the mouse line through blastocyst injection. In both ESCs and mice, Cre recombinase efficiently removed the *Stop* cassette to activate the DTR expression. Expressing the DTR in place of the endogenous *Mecp2* gene as a fusion protein with the N-terminus of MeCP2 in *Mecp2*^{DTR} (Δ*Stop*) cells mediated efficient ablation. Even very low expression from the *Mecp2* locus in embryonic stem cells was enough to mediate DT sensitivity.

The main downfall of the *Mecp2*^{StopDTR} modification is the fact that the modified *Stop* cassette inserted into intron 2 upstream of the DTR coding sequence does not sufficiently inactivate the expression of the DTR in the absence of Cre recombinase. This is thought to be caused by the expression of a tiny amount of *Mecp2*^{DTR} mRNA products formed by splicing around the *Stop* cassette entirely, which would encode an inframe DTR protein. Compared to the original *Stop1* cassette, the recognition of the

modified *Stop2* cassette was increased by ~13 fold, but the remaining ~0.6% of leaky *Mecp2*^{DTR} mRNA expression from the *Mecp2*^{StopDTR} allele was enough to cause death of neurons in culture as well as sensitivity in *Mecp2*$^{StopDTR/y}$ mice following DT treatment. MeCP2 is very highly expressed in neurons, it has been estimated that there are 16 x 10^6 molecules per neuronal nuclei in the brain (Skene *et al*, 2010)**.** Unlike other lowlier expressed genes, 0.6% of WT levels of mRNA from the *Mecp2* gene, likely gives rise to a substantial amount of protein. *Mecp2* is lowly expressed in mouse ESCs and is upregulated during neuronal differentiation. The resistance of *Mecp2*^{StopDTR} mouse ESCs to even very high concentrations of Diphtheria Toxin shows that the upregulated expression of *Mecp2* in neurons is needed to generate enough leaky in-frame transcripts to mediate sensitivity to DT. This also suggests that it is the expression from the *Mecp2* promoter which is driving the leaky expression of the DTR as another alternative would be expression driven from the PGK promoter in the PGK-neo selection cassette inserted upstream of the DTR. Transcripts expressed from the PGK promoter should be terminated at the polyadenylation (polyA) sequence of the PGK-neo gene cassette or if missed would likely be terminated at the downstream transcriptional *Stop* cassette sequence. There is no inframe AUG in the intron sequence upstream of the DTR which would allow the DTR to be translated from transcripts erroneously not terminated at these polyA sites. It is possible that cryptic splice donors in the neo cDNA allow splicing around the polyA sequence onto the 3' DTR. These cryptically spliced transcripts would need to encode an in frame DTR to contribute to the leaky DTR expression observed here. There was no evidence of cryptic splice events occurring within the PGK-neo cassette when the aberrantly spliced transcripts produced in the *Mecp2*^{StopDTR} neurons were sequenced (Figure 3.6.3.2.). Northern blot analysis of RNA extracted from *Mecp2*^{StopDTR} mouse brain using a fragment of the DTR coding sequence as a probe (discussed in Chapter 4.4.3) did not detect any other species of mRNA of different sizes apart from the one discrete band corresponding to the size of the spliced *Mecp2*^{DTR} fusion mRNA.

With hindsight, instead of trying to improve an already leaky system, I should have started from scratch with a new approach. One such approach using a Cre dependent Flip - Excision (FLEx) Switch instead of a modified *Stop* cassette is described in Chapter 4. The essential problem with the *Mecp2*^{StopDTR} allele is that any splicing

around the *Stop* that occurs will lead to the expression of the DTR as it has been inserted in-frame with the start of the third exon. A way I could have prevented this would have been to shift the DTR out of frame with exon 1 and 2 of *Mecp2* and put the splice acceptor upstream of the 5' loxP site (Figure 3.10.). The DTR would be positioned such that the deletion of the *Stop* cassette would result in the splice acceptor now being in frame with the DTR. Splicing around the *floxed Stop* cassette in this hypothetical allele would not give rise to an in-frame DTR. Buch *et al*, (2005) used this exact method to develop the Cre inducible DTR (iSTOP) allele, where the *floxed Stop* cassette and the DTR is inserted into the ubiquitously expressed Gt(ROSA)26Sor locus.

There were a number of reasons why we went ahead with the design of the *Mecp2*^{StopDTR} allele. Previous studies had shown that the *loxP-NeoStop* cassette inserted into the same position of intron 2 of *Mecp2* could reduce the expression of the downstream exon by 97.5% (Robinson *et al*, 2012; Guy *et al*, 2007). We were confident that the addition of a strong splice acceptor could increase the recognition further. There is evidence in literature that repeated injections of DT is required to ablate the entire target tissue and that the dose needed to achieve efficient ablation correlates with the level of expression of the DTR, suggesting that the dose of DT is titratable (Saito et al, 2001; Buch et al, 2005; Chen et al, 2005; Durieux et al, 2009). Transgenic lines where the DTR transgene expression is controlled only by a cell-type specific promoter have been used for successful targeted *in vivo* cell ablation with no reported adverse effects from off-target ablation, again raising no red flags about the importance of a completely OFF gene (Chen *et al*, 2005; Duffield *et al*, 2005; Jung *et al*, 2002; Luquet *et al*, 2005; Saito *et al*, 2001). Groups have also used models where the DT fragment A, the toxic component itself, has been expressed specifically in the desired cell type using a cell type specific promoter (Palmiter et al, 1987; Breitman et al, 1987, 1990; Lem et al, 1991; Ross et al, 1993; Lowell et al, 1993; Behringer et al, 1988). The expression of the DTR to potentiate the effect of the injected harmful toxin was thought of as a method to lessen the chance of nonspecific cell damage and allow inducible ablation (Saito et al, 2001).

A relatively small number of experiments in mice showed that using the *Mecp2*^{StopDTR} line might not be straightforward. Those experiments were imperfect in that we were administering DT to *Mecp2*-null animals which were soon to develop a RTT-like neurological phenotype and reach their humane endpoints. This was thought to be the most stringent test for toxicity as these mice expressed the *Mecp2*^{StopDTR} allele in 100% of their cells. Ultimately, we are more interested in whether the heterozygous *Mecp2*$^{StopDTR/+}$ females, which express the *Mecp2*^{StopDTR} allele in 50% of their cells, would experience adverse effects of DT administration. It is possible that heterozygous *Mecp2*$^{StopDTR/+}$ females would not experience adverse effects from 5 µg/kg or higher, however, the absence of phenotypic adverse effects would not be an assurance that there is no off-target ablation. Off-target ablation might confound the outcome of *in vivo* neuronal ablation experiments. A dose that would be efficacious without leading to unwanted off-target ablation might have been obtainable in *Mecp2*$^{StopDTR/+}$*,cre* mice due to the very high expression level of *Mecp2* (and by extension the *Mecp2*^{StopDTR} allele) in target neurons. As mentioned above the efficiency of ablation of target cells has been shown to correlate with DTR expression level (Saito *et al*, 2001). The target tissue is a large population of neurons in the brain so the dose of DT would need to be high enough to cross the blood-brain-barrier sufficiently. Tissues susceptible to off-target ablation might be those peripheral tissues that are more accessible to toxin administered by intraperitoneal injection.

The major conclusion to this chapter was that leaky expression of the DTR in inactivated, Cre negative *Mecp2*^{StopDTR} cells is likely to have deleterious effects on *in vivo* ablation and a new model should be generated to combat this problem. A clean *in vivo* ablation model with localised expression of the DTR to Cre positive cells only will allow flexibility in the dose of DT that can be used.

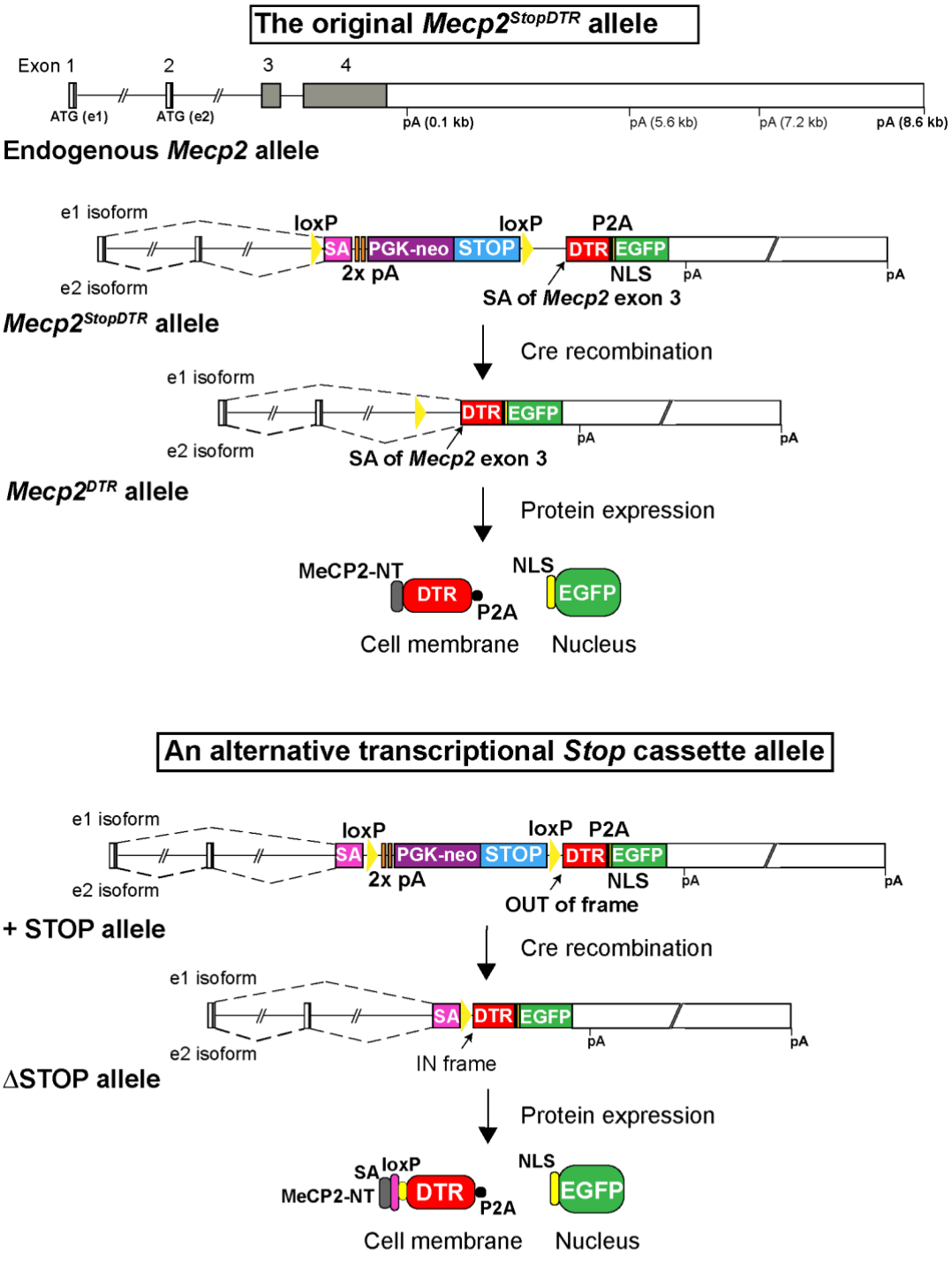

Figure 3.10. An alternative method using a transcriptional *Stop* cassette to silence the DTR expression in the absence of Cre. Boxes: exons; grey boxes: protein coding sequence of *Mecp2*; SA: splice acceptor sequence from the mouse engrailed-2 (En-2) gene; pA: polyadenylation termination sequence, one SV40 pA sequence and one bGH pA sequence; Neo: Neomycin resistance gene (PGK-neo); STOP: transcriptional stop cassette; DTR: human HB-EGF coding sequence; P2A (black rectangle or circle): P2A self-cleaving peptide; NLS (yellow rectangle): SV40 nuclear localization sequence; EGFP: enhanced GFP coding sequence; aa: amino acids; MeCP2-NT: N-terminus of MeCP2.

Chapter 4 Generation and characterisation of *Mecp2*$^{FLExDTR(OFF)}$ mice

4.1 Introduction

Chapter 3 described the generation and characterisation of *Mecp2*^{StopDTR} mice, which were designed as a system to allow targeted *in vivo* ablation of MeCP2-deficient neurons in the female heterozygous mouse model of Rett Syndrome (RTT). The *Mecp2*^{StopDTR} allele was a Diphtheria Toxin Receptor (DTR) knock-in, *Mecp2* knock-out allele designed to allow Cre recombinase dependent expression of the DTR from the endogenous *Mecp2* promoter, replacing the *Mecp2* gene. Unfortunately, in the absence of Cre recombinase, the *Stop* cassette did not sufficiently inactivate the expression of the DTR. Leaky expression of the DTR in stopped *Mecp2*^{StopDTR} cells resulted in the death of these neurons when treated with certain doses of Diphtheria Toxin (DT) in cell culture as well as sensitivity of *Mecp2*^{StopDTR} mice to DT compared to resistant WT mice. As discussed in section 3.10, I decided to re-design the inducible DTR knock-in allele, and generate a new mouse line to combat the problem of leaky expression of the DTR in cells not expressing Cre recombinase.

The alternative approach I decided to use to induce the expression of the DTR from the *Mecp2* locus was the Cre dependent Flip-Excision switch (FLEx) method (also called the DIO: Double-floxed Inverted Open reading frame). The FLEx switch allows the permanent inversion of a DNA sequence of interest (Schnütgen *et al*, 2003)(Figure 4.1.1). It takes advantage of heterotypic *lox* sites which are variant forms of *lox* sites that differ in their recombination specificities. *Lox* sites are 34-bp sequences of DNA consisting of two 13-bp inverted repeats which are individually bound by a Cre recombinase monomer (Guo *et al*, 1997), and an intervening 8-bp core region where DNA cleavage and strand-exchange occurs (Gopaul *et al*, 1998). Variant forms of *lox* sites have been identified which contain mutations in their core region and can efficiently recombine with another identical *lox* site but inefficiently recombine with *loxP* sites or other non-identical heterotypic *lox* sites (Hoess *et al*, 1986; Lee & Saito, 1998; Sauer, 1996; Siegel *et al*, 2001; Hoess *et al*, 1982; Branda & Dymecki, 2004). In the FLEx switch: an open reading frame sequence is flanked by two pairs of

heterotypic *lox* sites in an alternative organisation, with each compatible pair being in a head-to-head orientation. Cre-mediated recombination with one compatible pair of sites (e.g. *loxP*), leads to the inversion of the intervening DNA sequence which yields a direct repeat of the second pair of *lox* sites (e.g. *lox2272*), flanking a single heterotypic site (e.g. *loxP*)(Schnütgen *et al*, 2003)(Figure 4.1.1). Further recombination of the pair of compatible sites in the head-to-tail orientation (e.g. *lox2272*), excises the intervening *lox* site (e.g. *loxP*), yielding the inverted ORF sequence flanked by single heterotypic *lox* sites. The incompatibility of these sites means that the ORF is permanently locked in the sense orientation. Due to the reversibility of the Cre-mediated inversion reaction, equilibrium between the normal and inverted DNA will be achieved until excision occurs to lock the DNA sequence in place. The direct comparison between the same gene modified with a FLEx switch and single *loxP* sites in mice, showed that they were functionally indistinguishable, recombination was as efficient for the FLEx switch as it was for the single *loxP* sites (Schnütgen *et al*, 2003). The FLEx switch has been used in AAV viruses to activate the expression of the viral transgene specifically in Cre expressing cells in the brain (Atasoy *et al*, 2008; Sohal *et al*, 2009), it has been integrated into genomic loci to generate conditional FLEx alleles by *floxing* crucial exons to invert them upon Cre recombination (Schnütgen *et al*, 2003), in conditional gene trap knock-in alleles (Schnütgen *et al*, 2005), and finally, it has been used to conditionally express the highly cytotoxic Diphtheria Toxin fragment A from the Rosa26 locus for targeted *in vivo* cell ablation experiments (Plummer *et al*, 2017).

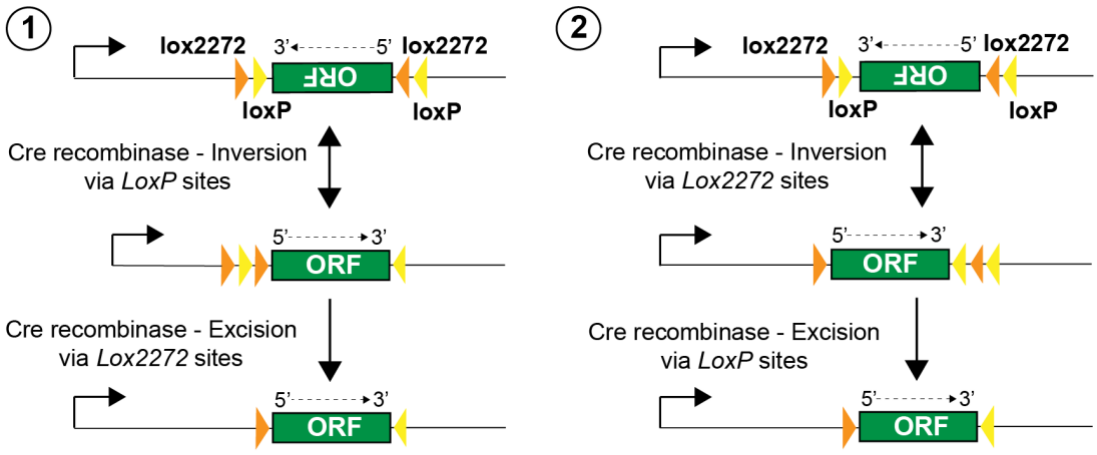

Figure 4.1.1. Flip - Excision (FLEx) switch induction of gene expression. There are two possible mechanisms of permanent inversion of the *floxed* open reading frame (ORF) sequence: 1) Inversion via recombination of the *loxP* sites followed by excision of the upstream *loxP* site via recombination of the *lox2272* sites; 2) Inversion via recombination of the *lox2272* sites followed by excision of the downstream *lox2272* via recombination of *loxP* sites. In both cases inversion and excision locks the gene cassette into the correct orientation and prevents further inversion as the cassette becomes *floxed* by heterotypic *lox* sites which cannot efficiently recombine with one another.

To use the FLEx-switch to conditionally express the DTR from the *Mecp2* locus, I aimed to replace the *Mecp2* coding sequence with the inverted DTR coding sequence flanked by heterotypic *lox* sites. In the OFF orientation the DTR will be in the incorrect antisense 3' to 5' orientation, rendering it inaccessible to splicing or translation. To activate the DTR expression, Cre recombination will invert the DTR into the sense orientation. *In vivo* ablation using the *Mecp2*$^{FLExDTR(OFF)}$ line can be achieved in the same way as proposed for the previous *Mecp2*^{StopDTR} line, by administering DT to heterozygous *Mecp2*$^{FLExDTR(OFF)/+}$,*cre* female mice (Figure 4.1.2). This chapter describes the generation and characterisation of *Mecp2*$^{FLExDTR(OFF)}$ embryonic stem cells (ESCs) and mice.

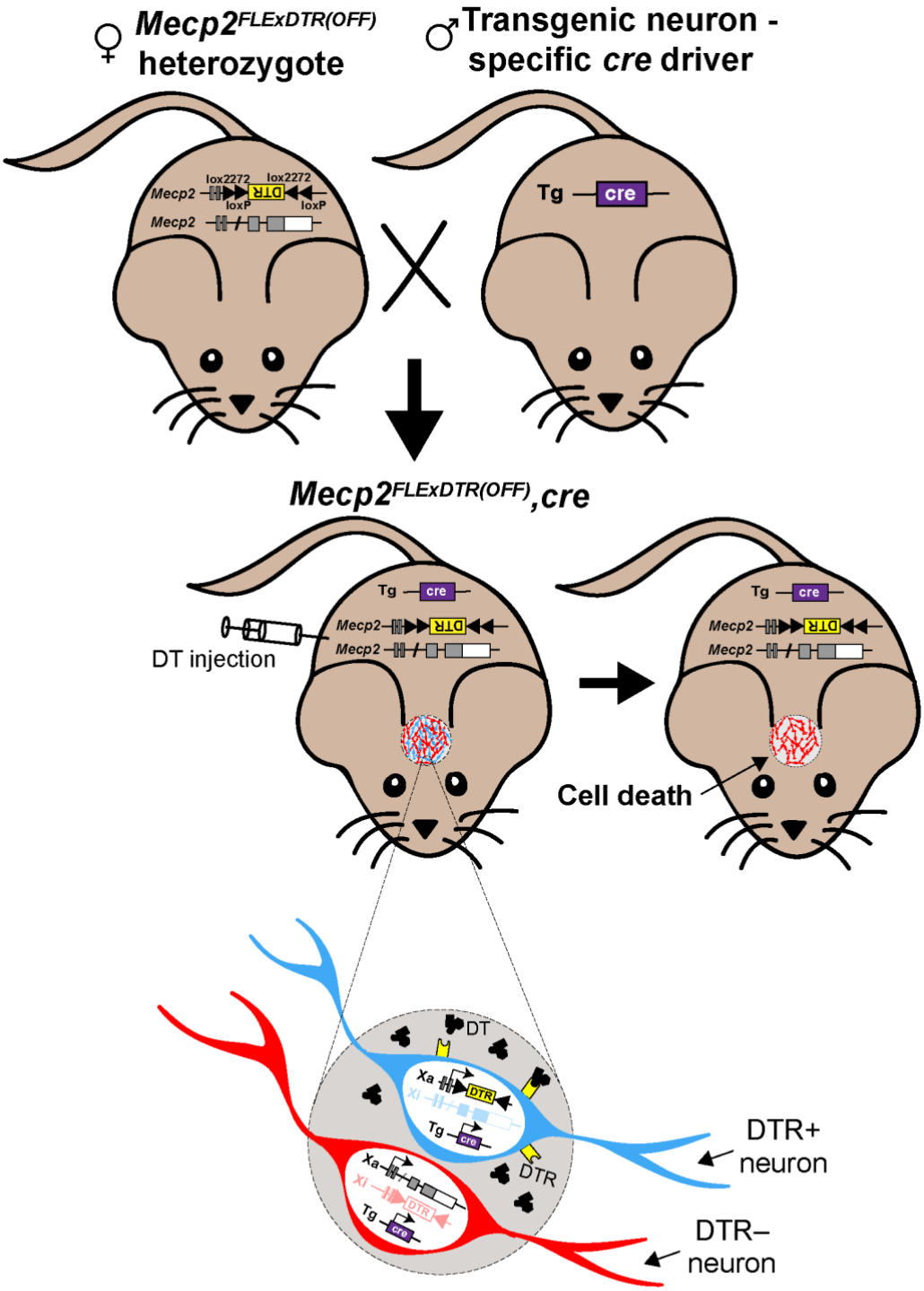

Figure 4.1.2. The DT-mediated ablation of MeCP2-deficient neurons in the female heterozygous mouse model of RTT. Female mice heterozygous for the *Mecp2*$^{FLExDTR(OFF)}$ allele are crossed to male mice which express a *cre* transgene from a neuron-specific promoter. In female progeny of this cross who are heterozygous for modified *Mecp2*$^{FLExDTR(OFF)}$ allele and inherit the *cre* transgene (*Mecp2*$^{FLExDTR(OFF)/+}$,*cre*): due to X-inactivation and localised Cre expression, only those neurons expressing the DTR knock-in allele on their active X-chromosome will express the DTR. DT-administration to mice by intraperitoneal injection will ablate the DTR+ neurons specifically. Neurons which have silenced the DTR knock-in allele by X-chromosome inactivation should not express the DTR and be resistant to DT.

4.2 Design and assembly of the *Mecp2*$^{FLExDTR(OFF)}$ targeting vector

When designing the new *Mecp2*$^{FLExDTR(OFF)}$ allele, I used the previous *Mecp2*^{StopDTR} allele to inform which aspects of the genetic modification to keep and which aspects needed improving. Replacing exons 3 and 4 of *Mecp2* with the DTR to knockout the gene and at the same time express the DTR as a fusion protein with the first exons of *Mecp2*, worked sufficiently well in the *Mecp2*^{StopDTR} line. The MeCP2^{DTR} fusion protein formed a functional receptor and expression of this protein from the *Mecp2* locus made cells sensitive to DT. Even very low expression from the *Mecp2* locus in ESCs was enough to mediate DT sensitivity. Accordingly, in the *Mecp2*$^{FLExDTR(OFF)}$ line, the DTR coding sequence was again inserted in-frame with the first 3 amino acids of exon 3 of *Mecp2* so that when the DTR expression is activated by Cre-mediated inversion the DTR is expressed as a fusion protein with the first exons of *Mecp2*, exactly as in the *Mecp2*^{StopDTR} allele (Figure 4.2.1). Included in the inversion is ~400 bp of intron 2 of *Mecp2*, the same sequence that is between the *loxP* site and start of exon 3 in the *Mecp2*^{StopDTR} locus.

In addition to leaky DTR expression, a second more minor aspect of the modification which did not work as designed, was the bicistronically expressed EGFP reporter. EGFP fluorescence was not easily detectable in recombined *Mecp2*^{DTR} neurons, therefore, served no purpose as a reporter of DTR expression. The fluorescent reporter was not included in the design of the *Mecp2*$^{FLExDTR(OFF)}$ allele. Instead the presence or absence of MeCP2 can be used to distinguish neurons expressing WT MeCP2 from the active X chromosome from those which express the *Mecp2* knockout, *Mecp2*$^{FLExDTR(ON)}$ allele.

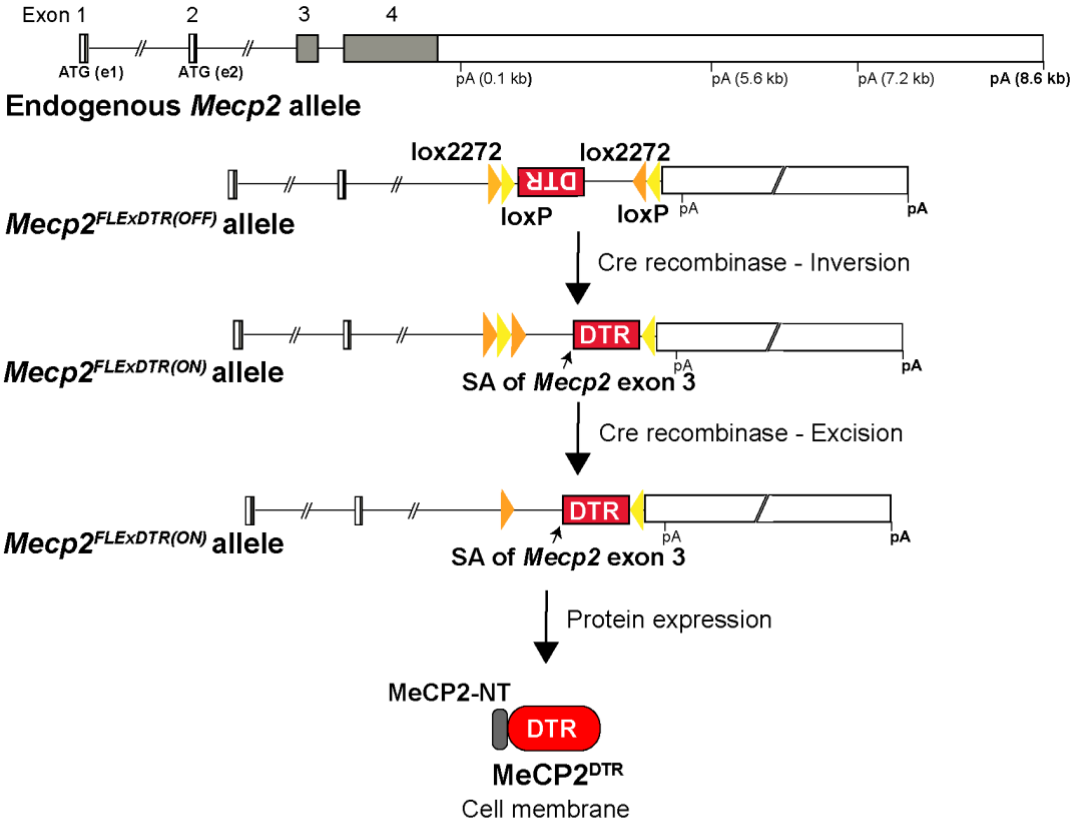

Figure 4.2.1. Cre-dependent expression of the DTR from the *Mecp2* locus using the Flip - Excision (FLEx) switch. A diagram of the endogenous *Mecp2* allele is shown at the top. Boxes: exons; grey boxes: protein coding sequence. The alternative start codons (ATGs) and polyadenylation termination sites (pAs) are annotated. Those sites used by the major isoforms in the brain are shown in bold. Below endogenous *Mecp2* is the genetically modified *Mecp2*$^{FLExDTR(OFF)}$ allele before Cre recombination, and after recombination (*Mecp2*$^{FLExDTR(ON)}$). DTR: human HB-EGF coding sequence. The endogenous splice acceptor (SA) of *Mecp2* which is retained inframe with the DTR coding sequence is labelled in the modified alleles. At the bottom is the MeCP2^{DTR} protein expected to be translated from the modified recombined *Mecp2*$^{FLExDTR(ON)}$ locus. MeCP2-NT: N-terminus of MeCP2. Sequence components are listed in Appendix table 1.

For the FLEx switch, I chose to use the combination of *lox2272* and *loxP* heterotypic sites. *Lox2272* has been reported to be more efficient (Kolb, 2001) and less permissive than other commonly used heterotypic *lox* sites, which have been shown to occasionally recombine with *loxP* sites (Siegel *et al*, 2001). The FLEx switch using *loxP* and *lox2272* has been successfully used in mouse knock-in models (Luche *et al*, 2007; Plummer *et al*, 2017). Notably, a conditional *Mecp2* knock-out model was generated recently where the *loxP/lox2272* FLEx switch was used to invert exon 3 to inactivate gene expression (Liu *et al*, 2020). The sequences of the *loxP* and *lox2272* and the intervening (62 and 70 bp) sequences were taken from a commonly used FLEx construct on Addgene (Appendix Table 1.). Once inverted, the minimum distance

between the compatible *lox* sites should be 82 base pairs to permit efficient excision (Hoess *et al*, 1985). Accordingly, in this construct, once inverted the compatible sites will be 166 base pairs apart. The downstream *lox* sites were inserted between the DTR stop codon and the 3'UTR of *Mecp2*. Small spacers of 10 bp were inserted between the DTR stop codon and the flanking *loxP* site and between the *lox2272* site and the 3'UTR. The 3'UTR was kept completely intact so that the endogenous regulation is not disrupted.

A PGK-neo selection cassette was inserted upstream of the *lox* sites in intron 2 to aid ESC targeting (Figure 4.2.2). The PGK-neo selection cassette was flanked with Flp recombinase recognition target (FRT) sites so that it can be later excised to clean up the allele. The PGK-neo cassette was inserted in the same 5' to 3' orientation as the *Mecp2* gene so removal of the cassette should be done in case the polyadenylation termination sequence of the PGK-neo gene cassette disrupts transcription of the downstream DTR in the activated $Mecp2^{\Delta}DTR^{FLEX}$ ON allele. If I had inserted the PGK-neo gene in the antisense orientation this step might not have been necessary.

In order to construct the $Mecp2^{FLExDTR(OFF)}$ targeting vector I modified an existing homology vector in the Bird lab which consists of a 7.2 kb sequence homologous to the sequence surrounding exon 3 and 4 of the mouse *Mecp2* gene (Figure 4.2.2). The $Mecp2^{FLExDTR(OFF)}$ targeting vector was assembled in one restriction enzyme digestion and ligation cloning step: the HpaI to MfeI fragment of the homology vector encompassing exon 3 and 4 was replaced with a fragment of synthesised DNA containing the FRT flanked selection gene and the *loxP, lox2272* flanked inverted DTR cassette (Appendix Table 1.).

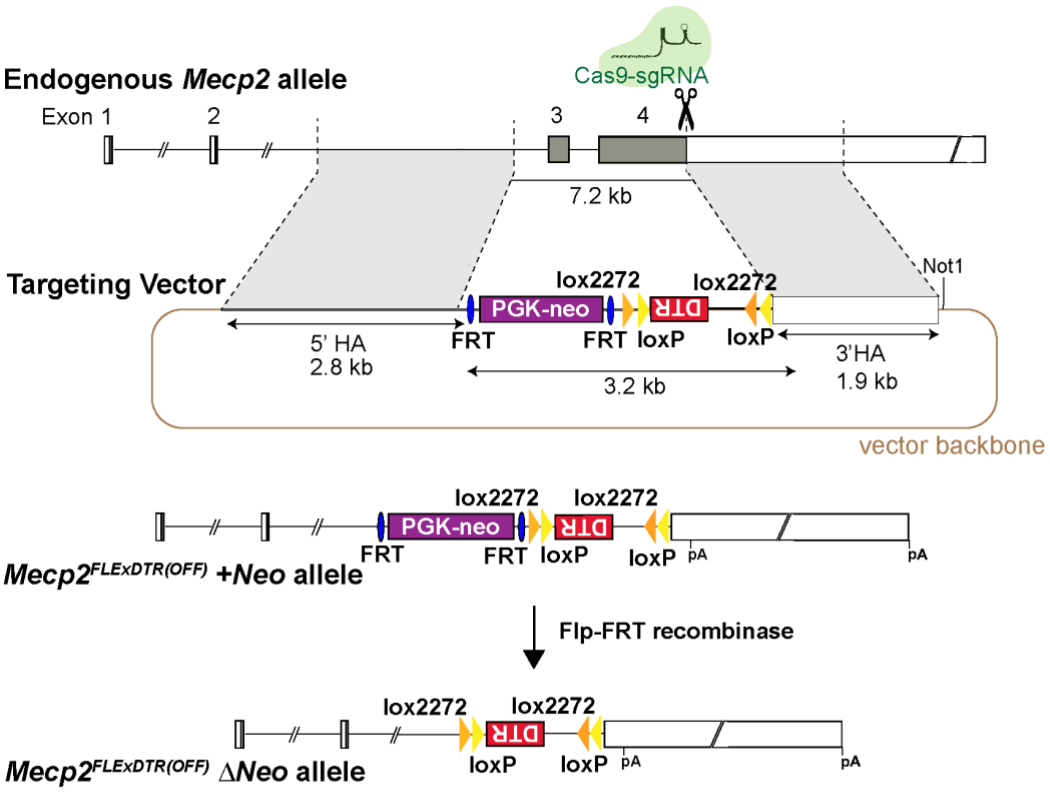

Figure 4.2.2 Genetically engineering mouse ESCs to express the *Mecp2*$^{FLExDTR(OFF)}$ allele. The desired modification of the *Mecp2* locus was produced by CRISPR-Cas9 assisted homologous recombination using a large linearised targeting vector. Sizes of DNA sequences are indicated below arrows. HA: homology arms; PGK-neo: the neomycin resistance gene expressed from the mouse phosphoglycerate kinase 1 (PGK) promoter; FRT: Flippase Recognition Target sites; Not1: unique restriction enzyme cut site used to linearise the targeting vector. Sequence components are listed in Appendix table 1.

4.3 Generation of targeted *Mecp2*$^{FLExDTR(OFF)}$ mouse ESCs

Male mouse ESCs were targeted by CRISPR-assisted homologous recombination following electroporation with linearized targeting vector DNA and CRISPR plasmid to generate ESCs expressing the *Mecp2*$^{FLExDTR(OFF)}$ allele. The CRISPR-Cas9 guide target site used previously to generate the *Mecp2*^{StopDTR} allele was positioned in a good location for the *Mecp2*$^{FLExDTR(OFF)}$ targeting, so the plasmid cloned for the previous targeting experiment was used here too. Cells with the PGK-neo selection cassette of the targeting vector integrated into their genomes were selected for using G418 antibiotic resistance. Resistant clones were screened for targeted integration of the vector DNA by PCR using primers which specifically amplify DNA only present when a targeted integration of the 5' and 3' end of the targeting vector had occurred. Out of

192 clones screened by PCR, 6 potentially targeted clones were identified. These 6 clones were grown up, genomic DNA was extracted, and Southern blot analysis was performed using a Bsu361 restriction enzyme digestion which identified 3 clones that were correctly targeted, 2 of these had no random integrations of the vector DNA elsewhere in the genome (clones 1B4 and 1H5)(Figure 4.3). The overall targeting efficiency of generating the *Mecp2*^{FLExDTR} knock-in allele was 1.56%. Clone 1H5 had a small amount of WT DNA contamination according to Southern blot but the WT contaminated cells were removed by further cloning out these cells. The modified region of *Mecp2* for clone 1B4 was sequenced to check that the entire desired modification was knocked in and no small mutations were present.

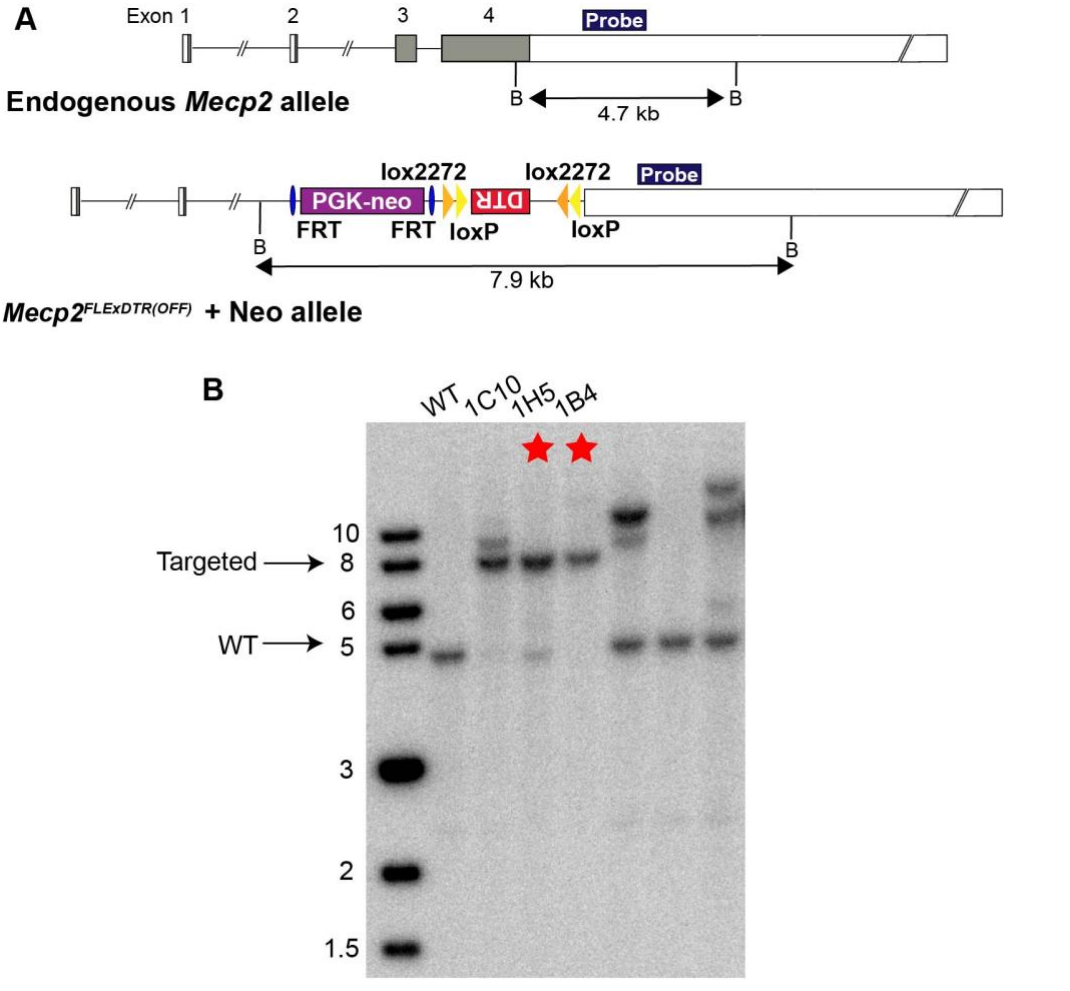

Figure 4.3 Southern blot analysis identified *Mecp2*$^{FLExDTR(OFF)}$ targeted ESC clones with no random integrants. A) Southern Blot screening strategy for identifying positively targeted ESC clones. The 3'UTR hybridization probe is indicated in dark blue and B indicates the position of the Bsu361 restriction enzyme cut sites. B) Southern blot analysis after Bsu361 digestion identified positively targeted clones with no random integrations of vector DNA (red stars).

4.4 Characterisation of the *Mecp2$^{FLExDTR(OFF)}$* targeted mouse ESCs

4.4.1 Cre recombinase–mediated activation of the DTR expression in targeted Mecp2$^{FLExDTR(OFF)}$ ESCs

In order to assess if the Cre–mediated inducibility of the DTR expression in the modified *Mecp2$^{FLExDTR(OFF)}$* allele works, and to determine how these cells respond to DT treatment compared to the *Mecp2^{StopDTR}* cells, the targeted *Mecp2$^{FLExDTR(OFF)}$* ESCs were transiently transfected with a Cre expressing plasmid. Transfected clones were picked in duplicate and DT was added to one set of clones and normal ESC culture medium was added to the duplicate clones. A number of clones that failed to grow on the plate treated with DT but grew in normal culture medium, as assayed by the colour change of the medium, were selected and grown on further (Figure 4.4.1.1). These clones were plated in a 24-well plate and again treated with DT, but this time confluence was measured in the Incucyte live-cell imaging system to get a more sensitive measure of cell death. It was clear from this analysis that most of the clones carried forward were sensitive to DT as when treated with DT they failed to divide and increase in confluence compared to untreated cells (Figure 4.4.1.1). There were clones that were clearly resistant to DT and increased in confluence at the same rate as untreated cells (1H5-3 and 1H5-5). Southern blot analysis was performed on genomic DNA extracts from these clones to confirm recombination had occurred to invert the DTR coding sequence at the DNA level (Figure 4.4.1.2). The Southern blot mostly agreed with the Incucyte analysis: those clones that failed to grow when treated with DT had inverted the DTR coding sequence. Clone 1H5-3 which did grow in the presence of DT and had not inverted the DTR sequence (Figure 4.4.1.2). For clone 1H5-5 the Southern blot and DT assay did not agree. According to Southern blot this clone should be susceptible to DT (Figure 4.4.1.2), however, DT treatment did not efficiently inhibit growth (Figure 4.4.1.1). I am unsure of an explanation for this result other than uneven distribution of DT to each well of cells. Overall, this analysis showed two things: 1) Cre-mediated inversion of the DTR coding sequence into the

sense orientation was successfully achieved following transient Cre expression, and 2) the expression of the inverted DTR mediated DT sensitivity in ESCs.

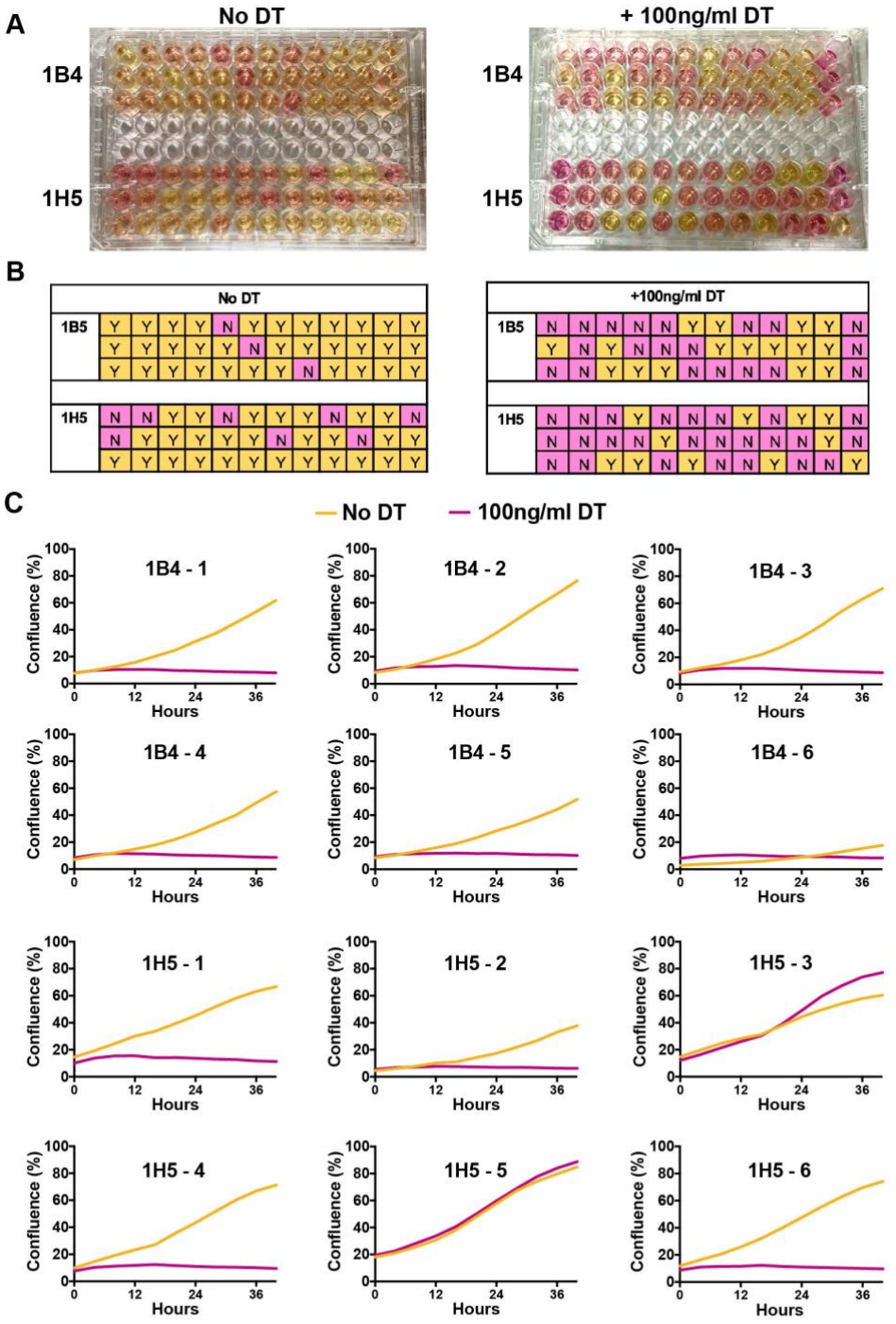

Figure 4.4.1.1 Cre-mediated activation of the DTR expression in *Mecp2*$^{FLExDTR(OFF)}$ ESCs. A) Colour change of medium in wells of replicate clones treated and not treated with DT. Pink wells indicate the clones which do not grow or die and yellow medium indicates clones which do grow and do not die. B) Tables summarising the images shown in A. Y (yellow): yes cells did grow; N (pink): no cells did not grow. C) Graphs of the percentage confluence quantified by the Incucyte live-cell imaging system for DT treated (pink) and untreated (orange) cells for 6 subclones of each parent clone transfected with Cre expressing plasmid.

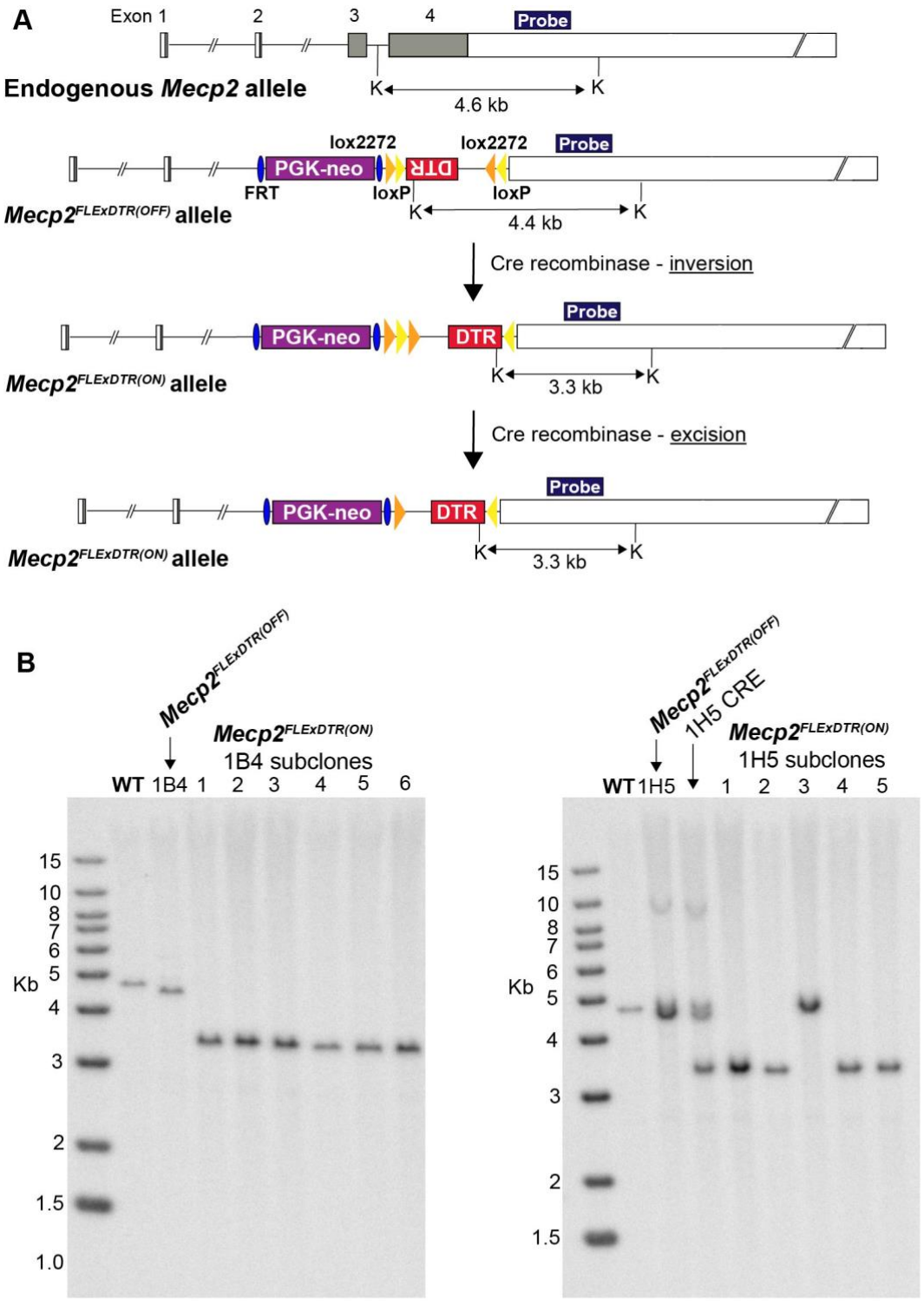

Figure 4.4.1.2 Southern blot analysis identified *Mecp2*$^{FLExDTR(ON)}$ clones which had inverted the DTR coding sequence. A) Southern Blot screening strategy for identifying the DTR inverted, *Mecp2*$^{FLExDTR(ON)}$ allele. The 3'UTR hybridization probe is indicated in dark blue and K indicates the position of the KpnI restriction enzyme cut sites. B) Southern blot analysis of a number of isolated clones which did not grow in the presence of DT and had potentially inverted the DTR to activate its expression. 1H5 CRE: DNA extracted from a mixed population of clone 1H5 cells transfected with the Cre-expressing plasmid.

To determine whether the excision of the intervening *lox* site following the inversion of the DTR occured upon transient Cre expression, therefore locking the DTR in the sense orientation, I PCR amplified across the upstream *lox* sites in *Mecp2*$^{FLExDTR(ON)}$ cells (Figure 4.4.1.3). In all four *Mecp2*$^{FLExDTR(ON)}$ clones the smaller band corresponding to the excised *lox* site was produced rather than a larger band which would correspond to the inverted and not excised allele. This PCR reaction showed that both inversion and excision had occurred in these clones and identified that both the *loxP* and *lox2272* sites are recombinogenic.

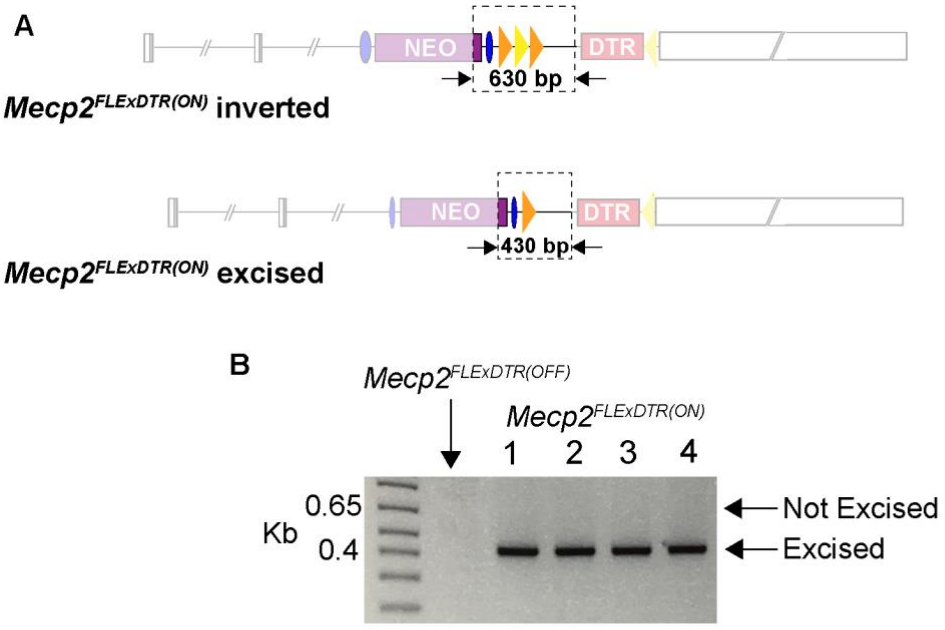

Figure 4.4.1.3. The *lox2272* and *loxP* sites are both recombinogenic and mediate Cre-dependent inversion and excision. A) The expected sizes of DNA fragments produced by PCR amplifying across the lox sites in the inverted *Mecp2*$^{FLExDTR(ON)}$ allele before and after excision. Arrows: position of PCR primers. B) PCR amplified genomic DNA from *Mecp2*$^{FLExDTR(OFF)}$ and 4 clones of *Mecp2*$^{FLExDTR(ON)}$ cells.

4.4.2 Sensitivity of Mecp2$^{FLExDTR(ON)}$ *and resistance of Mecp2*$^{FLExDTR(OFF)}$ *ESCs and neurons to Diphtheria Toxin*

DT administration to ESCs showed that *Mecp2*$^{FLExDTR(ON)}$ ESCs were sensitive to DT (Figure 4.4.1.1). When treated with a range of DT doses *Mecp2*$^{FLExDTR(ON)}$ ESCs were resistant to 5ng/ml DT and the percentage confluence increased exponentially similarly to untreated cells (Figure 4.4.2.1). *Mecp2*$^{FLExDTR(ON)}$ ESCs were killed by DT doses of 50 and 500 ng/ml shown by a failure to increase in confluence.

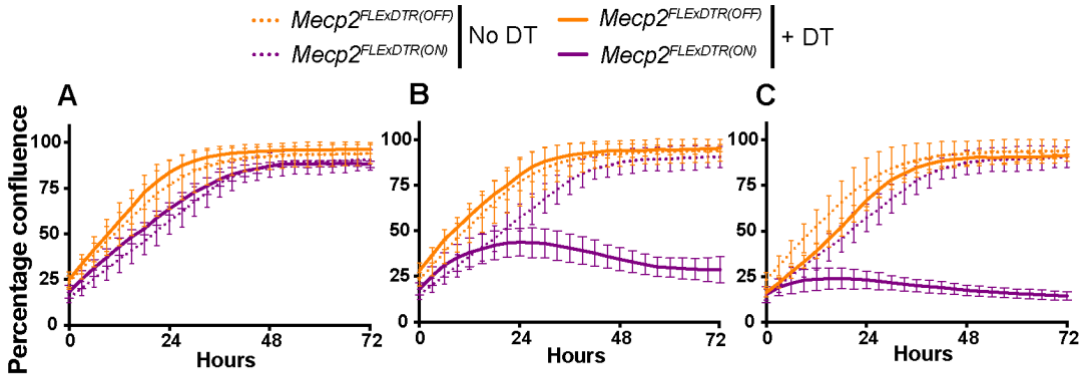

Figure 4.4.2.1. *Mecp2*$^{FLExDTR(ON)}$ ESCs are sensitive to Diphtheria Toxin whereas *Mecp2*$^{FLExDTR(OFF)}$ ESCs are resistant. The percentage confluence of ESCs quantified by the Incucyte live-imaging software analysis following the addition of A) 5 ng/ml, B) 50 ng/ml and C) 500 ng/ml DT to the culture medium at 0 hours. Plotted is the mean and SD for 3 wells per genotype, per conditon.

The low level of expression from the *Mecp2* locus in ESCs suppressed the effects of leaky expression of the DTR produced from the previous *Mecp2*^{StopDTR} locus (discussed in section 3.7.1). *Mecp2*^{StopDTR} ESCs were resistant to even very high doses of DT (Figure 3.7.1.1). In ESC-derived neurons, however, where *Mecp2* expression is upregulated, the leaky expression of the DTR in *Mecp2*^{StopDTR} neurons reached a high enough level to mediate sufficient DT uptake to induce cell death, when treated with moderate doses of DT (Figure 3.7.2.2). Accordingly, to determine whether the problem with leaky expression of the DTR had been fixed by using the FLEx switch, *Mecp2*$^{FLExDTR(ON)}$ and *Mecp2*$^{FLExDTR(OFF)}$ ESC-derived neurons were treated with DT. *Mecp2*$^{FLExDTR(ON)}$ and *Mecp2*$^{FLExDTR(OFF)}$ ESCs were differentiated into neurons and treated with 100 ng/ml DT, a dose which induced cell death of *Mecp2*^{StopDTR} neurons. The DT and Incucyte Cytotox Red dye were incorporated into the first half medium change, the day after plating out embryoid bodies, and neurons were imaged and fluorescent red cells were counted by the Incucyte exactly as done previously (Figure 3.7.2.1). Importantly, *Mecp2*$^{FLExDTR(OFF)}$ neurons were resistant to 100 ng/ml DT and the increase in number of dead cells were comparable to untreated *Mecp2*$^{FLExDTR(OFF)}$ neurons (Figure 4.4.2.2). Of note, *Mecp2*^{StopDTR} neurons died when treated with 10 ng/ml, a dose ten times lower than that used here.

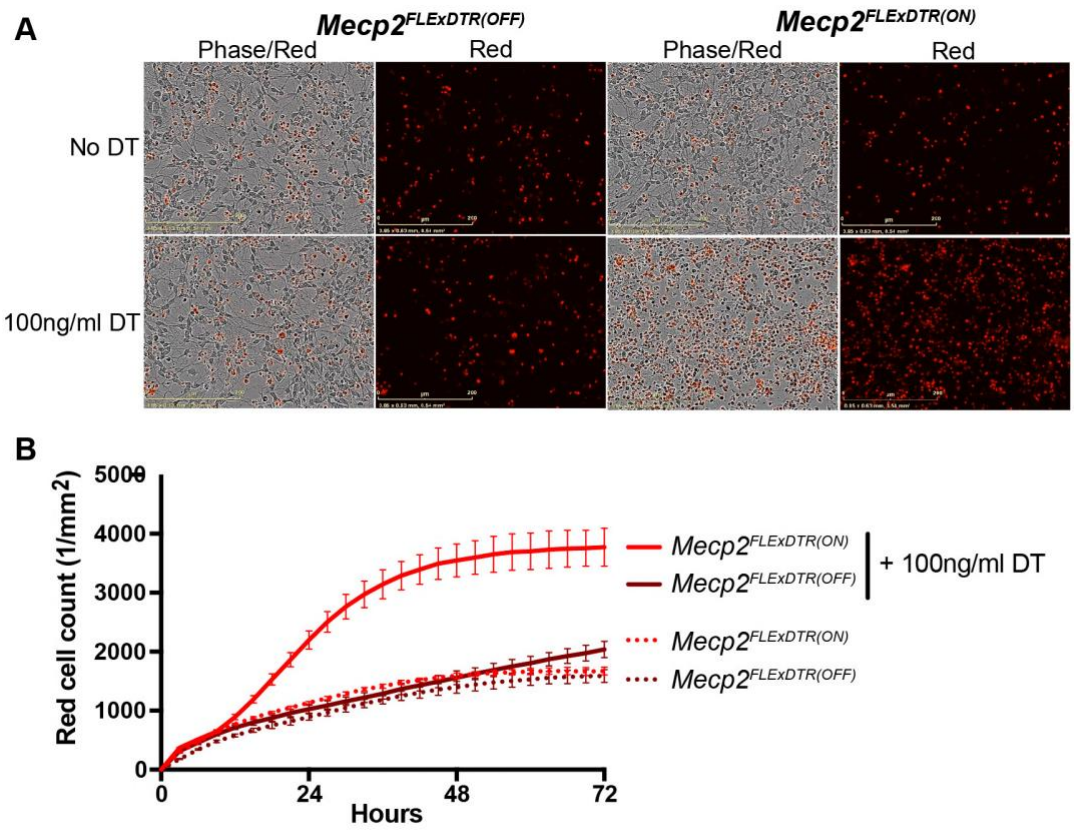

Figure 4.4.2.2. *Mecp2*$^{FLExDTR(OFF)}$ ESC-derived neurons were resistant to Diphtheria Toxin. A) Phase and fluorescent images taken on the Incucyte of *Mecp2*$^{FLExDTR(ON)}$ and *Mecp2*$^{FLExDTR(OFF)}$ neurons 36 hours after DT treatment. B) The increase in red cell count (dead cell count) per mm^2 over time for *Mecp2*$^{FLExDTR(ON)}$ or *Mecp2*$^{FLExDTR(OFF)}$ cells treated or not treated with 100 ng/ml DT. Plotted is the mean and SD for 3 wells per genotype, per condition.

4.4.3 No DTR mRNA expression was detectable in Mecp2$^{FLExDTR(OFF)}$ ESC-derived neurons

To determine whether any mRNA was produced from the *Mecp2*$^{FLExDTR(OFF)}$ locus, northern blot analysis was performed on RNA extracted from *Mecp2*$^{FLExDTR(OFF)}$ and *Mecp2*$^{FLExDTR(ON)}$ ESC-derived neurons (Figure 4.4.3). No mRNA containing the 3'UTR of *Mecp2* (the 3'UTR is intact in the *Mecp2*$^{FLExDTR(OFF)}$ and *Mecp2*$^{FLExDTR(ON)}$ alleles) was detectable on the northern blot showing that the inversion of the sequence encompassing the DTR which includes the splice acceptor of exon 3, efficiently disrupts the expression of the transcript.

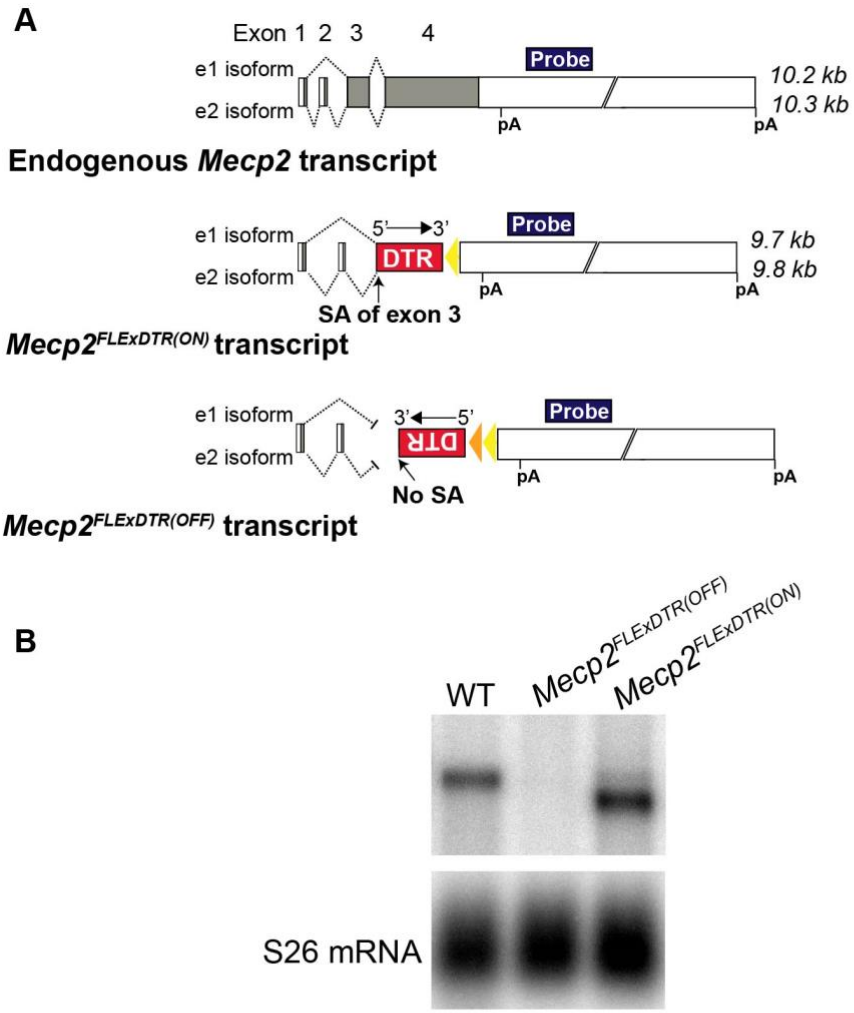

Figure 4.4.3. No DTR mRNA was detectable in *Mecp2*$^{FLExDTR(OFF)}$ ESC-derived neurons. A) Diagram of the sizes of the different mRNA isoforms expected to be produced from each allele. The annealing position of the Northern blot probe within the 3'UTR is highlighted. B) Northern blot analysis of mRNA extracts from a differentiated pool of WT ESCs, and *Mecp2*$^{FLExDTR(OFF)}$ and *Mecp2*$^{FLExDTR(ON)}$ differentiated ESC clones. S26 ribosomal protein mRNA was probed to act as a loading control.

Once it had been established that *Mecp2*$^{FLExDTR(OFF)}$ neurons were resistant to DT and no leaky expression of DTR was detectable, the *Mecp2*$^{FLExDTR(OFF)}$ clone 1B4 was used to generate mice by microinjection of the ESCs into blastocysts. The blastocyst injections for this line were performed by a technician at the Bioresearch and Veterinary Services (BVS) Central Transgenic Core (CTC) facility. The PGK-neo selection cassette used to aid ESC targeting was left in the locus to limit the amount of manipulation these cells had undergone and to lessen the number of passages before injection into blastocysts, to ensure we achieve germline contribution of these cells.

The PGK-neo selection cassette could be removed later in the mice by crossing to a Flp recombinase expressing transgenic line.

4.5 Characterisation of *Mecp2*$^{FLExDTR(OFF)}$ mice

4.5.1 Resistance of Mecp2$^{FLExDTR(OFF)}$ *mice to Diphtheria Toxin*

It was important to achieve a mouse model for *in vivo* cell ablation experiments where in unrecombined Cre-negative cells there was no DTR expression and as a result no unwanted off-target DT-mediated ablation. To determine whether the new *Mecp2*$^{FLExDTR(OFF)}$ mouse line was resistant to DT, as suggested by cell culture experiments, male and female *Mecp2*$^{FLExDTR(OFF)}$ mice were treated with two doses of DT. In previous experiments (discussed in section 3.9), *Mecp2*^{StopDTR} male mice experienced adverse side effects such as loss of general condition, weight and sudden death following the administration of 5 µg/kg DT or higher.

At 3 weeks of age *Mecp2*$^{FLExDTR(OFF)/y}$ hemizygous male and *Mecp2*$^{FLExDTR(OFF)/+}$ heterozygous female mice and WT control mice were administered a single IP injection of 5 µg/kg DT. These mice were weighed once a day and checked twice daily for general condition for one week, followed by daily checks for a further 2-3 weeks. None of the mice experienced adverse effects of toxin administration. All were comparable to WT animals injected with DT in terms of general condition and weight increase (Figure 4.5.1).

To test the system further the dose was increased to 50 µg/kg, a dose suggested in literature to be a high dose which has no toxic effects in WT mice. This time a cohort of *Mecp2*$^{FLExDTR(OFF)/y}$ and WT males were administered a single IP injection of 50 µg/kg DT at 3 weeks of age and monitored closely, same as above. These mice also showed resistance to this high dose of DT. Males are hemizygous for the X-linked *Mecp2*$^{FLExDTR(OFF)}$ allele and express the DTR knock-in allele in 100% of their cells, therefore, serve as a more stringent test for DT sensitivity compared to heterozygous females who express the DTR knock-in allele in 50% of their cells. The fact that males showed no adverse effects upon administration of the high 50 µg/kg DT implies that females will be resistant.

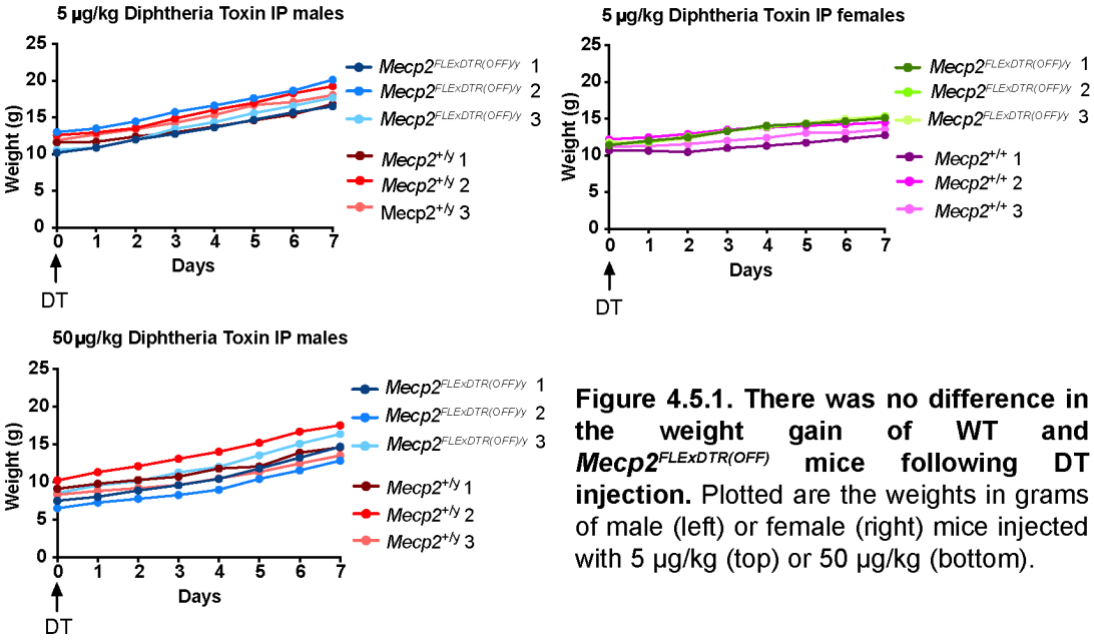

Figure 4.5.1. There was no difference in the weight gain of WT and *Mecp2*$^{FLExDTR(OFF)}$ mice following DT injection. Plotted are the weights in grams of male (left) or female (right) mice injected with 5 µg/kg (top) or 50 µg/kg (bottom).

4.5.2 Recombination efficiency of the Mecp2$^{FLExDTR(OFF)}$ allele in vivo

To characterise the recombination efficiency of the *Mecp2*$^{FLExDTR(OFF)}$ allele *in vivo*, mice carrying the *Mecp2*$^{FLExDTR(OFF)}$ allele and the *Nes-cre* transgene were generated. DNA was extracted from whole brain tissue from *Mecp2*$^{FLExDTR(OFF)/+}$,*Nes-cre* female, *Mecp2*$^{FLExDTR(OFF)/y}$,*Nes-cre* male, *Mecp2*$^{FLExDTR(OFF)/y}$ (*cre* negative) male, and WT control mice. Southern blot analysis was performed for Kpn1 digested genomic DNA using a hybridisation probe which anneals in the 3'UTR of *Mecp2* (Figure 4.5.2). Kpn1 digestion clearly distinguishes between the *Mecp2*$^{FLExDTR(ON)}$ and *Mecp2*$^{FLExDTR(OFF)}$ alleles as well as the WT *Mecp2* allele.

The recombination efficiency of the *Mecp2*$^{FLExDTR(OFF)}$ allele in the brain of *cre* positive male mice was quantified from the Southern blot as 80.2%. The *Nes-cre* (*cre*) driver has been previously reported to achieve >90% recombination efficiency of single *loxP* sites to excise a *Stop* cassette in the *Mecp2* locus in whole brain (Ross *et al*, 2016). This Southern blot here shows that recombination to invert the *Mecp2*$^{FLExDTR(OFF)}$ allele is similarly as efficient as the recombination of the single *loxP* sites at the same locus. To directly compare the two alleles, mice would need to be age matched, on a similar genetic background and samples would need to be run on the same Southern blot. In *cre* positive females, visually, the recombination efficiency was similar to that in males, suggesting that recombination in these mice by 6 weeks of age

efficiently occurs on both the inactive and active X-chromosome. Quantification of the faint lower band corresponding to the unrecombined *Mecp2*$^{FLExDTR(OFF)}$ allele for *Mecp2*$^{FLExDTR(OFF)/+}$,*Nes-cre* samples was not possible due to the WT upper band being too close in proximity to distinguish the two intensities. This problem could be solved by finding a restriction enzyme digestion which will produce a bigger size differences between the WT and *Mecp2*$^{FLExDTR(OFF)}$ alleles. Importantly, there are no additional bands that would correspond to products of cryptic recombination events between *loxP* and *lox2272* sites in the *Mecp2*$^{FLExDTR(ON)}$ allele which would cause the DTR to be inverted back into the antisense orientation and switched OFF in Cre expressing cells (Table 4.5.2).

Allele	Recombination	Size
Mecp2$^{FLExDTR(OFF)}$	None	4390 bp
Mecp2$^{FLExDTR(ON)}$	Inversion via *loxP*	3312 bp
	Inversion via *loxP* and excision via *lox2272*	3312 bp
	Inversion via *lox2272*	3512 bp
	Inversion via *lox2272* and excision via *loxP*	3312 bp
Mecp2$^{FLExDTR(OFF)*}$	Cryptic recombination between *loxP* and *lox2272*	4286 bp

Table 4.5.2. Expected sizes of the KpnI DNA fragments following different recombination events at the *Mecp2*$^{\Delta}$*DTR*^{FLEx} locus. The *Mecp2*$^{FLExDTR(OFF)*}$ allele is in the OFF state following cryptic recombination between *loxP* and *lox2272* in the ON allele which would invert the DTR back into the antisense orientation.

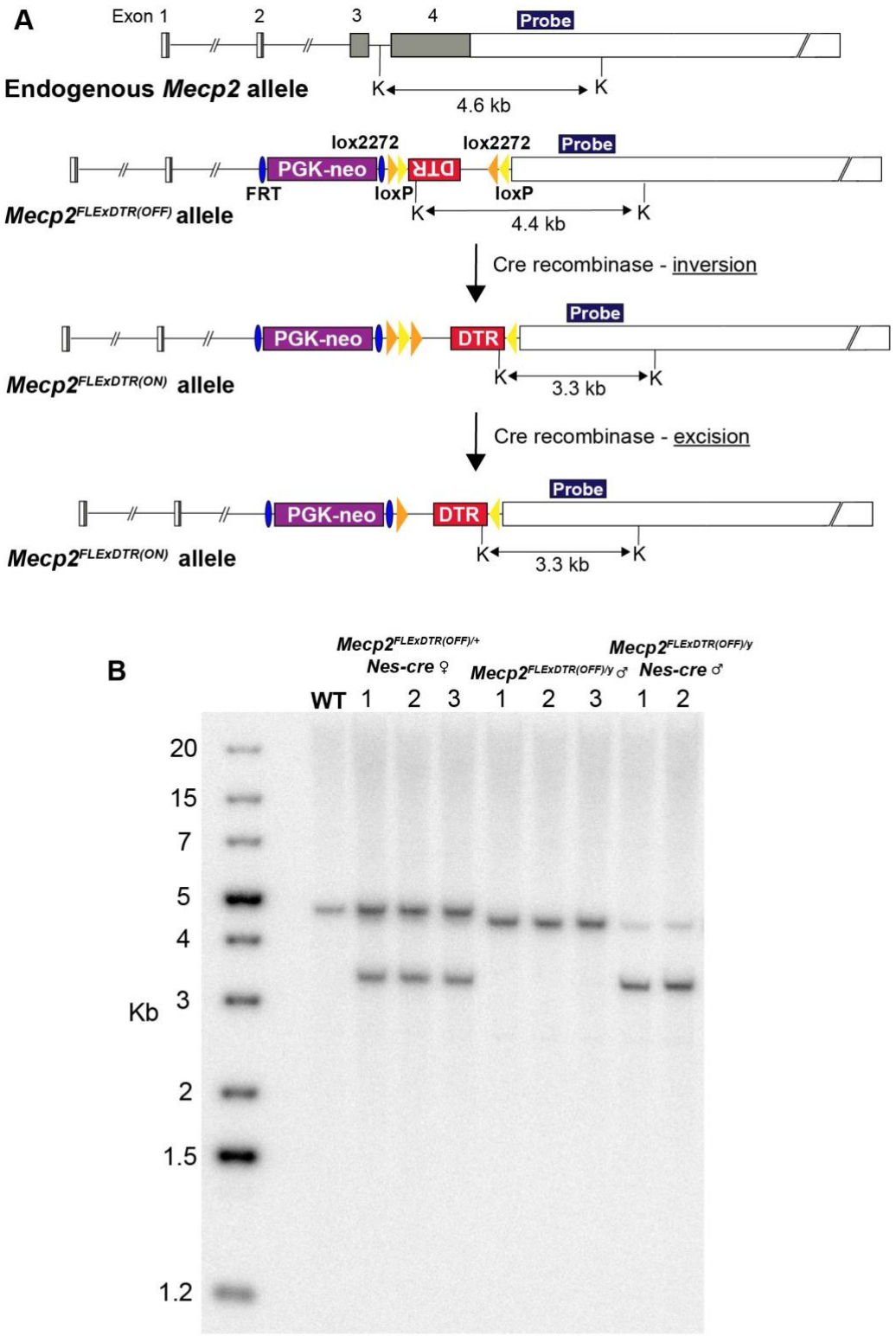

Figure 4.5.2. Recombination efficiency of the *Mecp2*$^{FLExDTR(OFF)}$ allele *in vivo.* A) Southern blot screening strategy for identifying the DTR inverted, *Mecp2*$^{FLExDTR(ON)}$ allele. The 3'UTR hybridization probe is indicated in dark blue and K indicates the position of the KpnI restriction enzyme cut sites. B) Southern blot analysis of DNA extracted from brain tissue from 1 WT, 3 *Mecp2*$^{FLExDTR(OFF)/+}$,*Nes-cre* female, 3 *Mecp2*$^{FLExDTR(OFF)/y}$ male and 2 *Mecp2*$^{FLExDTR(OFF)/y}$,*Nes-cre* male mice.

4.5.3 mRNA expression from the Mecp2$^{FLExDTR(ON)}$ allele in vivo

Northern blot analysis was performed on *Mecp2*$^{FLExDTR(OFF)}$ mice and *Mecp2*$^{FLExDTR(OFF)}$*,Nes-cre* mice to assess the expression level of the DTR mRNA *in vivo*, how it compares to WT *Mecp2* expression and whether, as in ESC-derived neurons, there is no detectable expression from the unrecombined *Mecp2*$^{FLExDTR(OFF)}$ allele (Figure 4.5.3). *Mecp2*$^{FLExDTR(OFF)}$*,Nes-cre* mice were used to analyse the expression of the DTR from the recombined *Mecp2*$^{FLExDTR(ON)}$ allele as recombination to activate DTR expression occurs in the majority of cells in the brain in *cre*-positive mice (see previous section 4.5.2). The hybridisation probe which anneals in the 3'UTR of *Mecp2* was used to compare WT *Mecp2* mRNA and *Mecp2*^{DTR} mRNA levels. A second northern blot was done using the DTR cDNA sequence as a hybridization probe to see whether any species of mRNA containing the DTR was produced in *Mecp2*$^{FLExDTR(OFF)}$ cells (Figure 4.5.3). Samples from the previous *Mecp2*^{StopDTR} line were run alongside the *Mecp2*$^{FLExDTR(OFF)}$ samples as an extra comparison. There was no detectable mRNA containing the 3'UTR of *Mecp2* or the DTR in *Mecp2*$^{FLExDTR(OFF)/y}$ mice, unlike in the *Mecp2*$^{StopDTR/y}$ where there is leaky mRNA expression in the *Stop* mice which, as discussed previously in Chapter 3, contains a mixture of transcripts some of which encode an in-frame DTR. The DTR cDNA sequence was a reliable probe for DTR mRNA as shown by absence of signal in the negative control WT RNA sample, but a strong signal in RNA samples from recombined *Mecp2*$^{FLExDTR(OFF)}$*,Nes-cre* and *Mecp2*^{StopDTR}*,Nes-cre* mice. In conclusion, the absence of mRNA in the *Mecp2*$^{FLExDTR(OFF)/y}$ mice further confirms that these mice should be as resistant to DT as WT mice. The northern blot analysis directly compares the previous *Mecp2*^{StopDTR} allele and the re-designed *Mecp2*$^{FLExDTR(OFF)}$ allele and shows that the leaky expression of DTR in *Stop* mice was fixed by using the FLEx switch approach to induce DTR expression in a Cre-dependent manner.

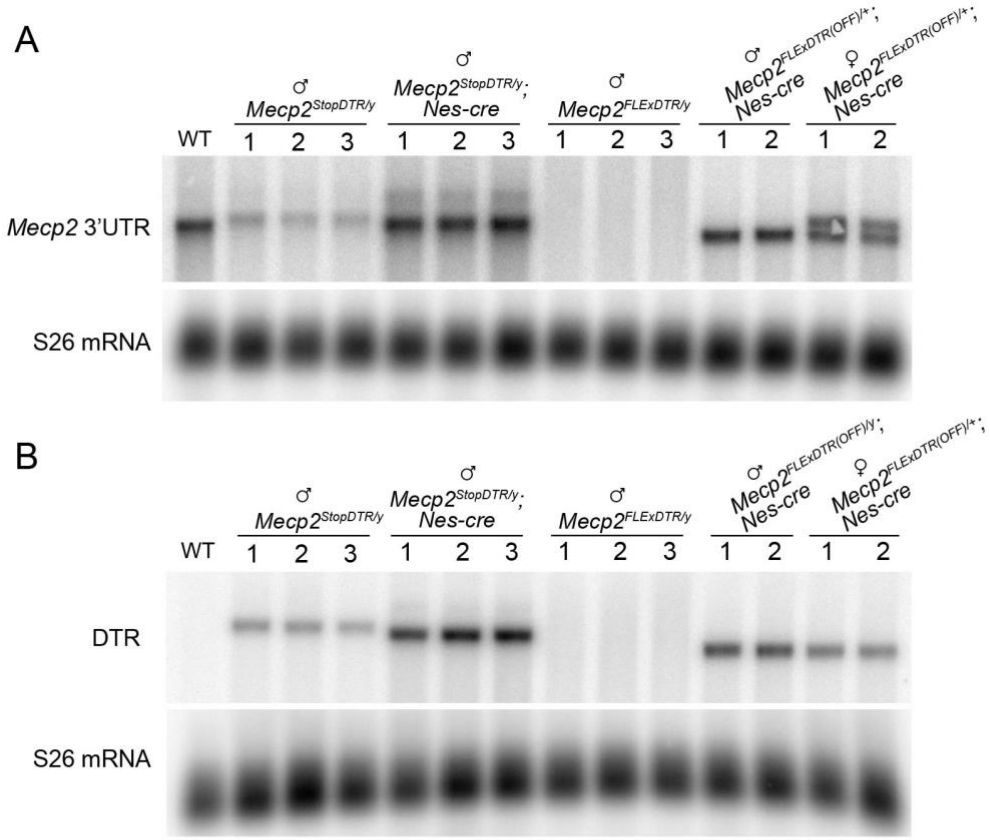

Figure 4.5.3. Northern blot analysis detected no DTR mRNA in *Mecp2*$^{FLExDTR(OFF)}$ mice. Northern blot analysis of RNA extracted from brains of WT mice; *Mecp2*$^{StopDTR/y}$ and *Mecp2*$^{StopDTR/y}$,*Nes-cre* hemizygous male mice; *Mecp2*$^{FLExDTR(OFF)/y}$ and *Mecp2*$^{FLExDTR(OFF)/y}$,*Nes-cre* hemizygous male mice; and *Mecp2*$^{FLExDTR(OFF)/+}$,*Nes-cre* heterozygous female mice. Each lane corresponds to a different mouse. Blot A) The hybridisation probe anneals in the 3'UTR of *Mecp2*. Blot B) The hybridisation probe was a fragment of the DTR coding sequence. For both blots S26 ribosomal protein mRNA was probed to act as a loading control.

To determine the relative amount of mRNA expression in the *Mecp2*$^{FLExDTR(OFF)/y}$,*Nes-cre* brain compared to the WT and *Mecp2*$^{StopDTR/y}$,*Nes-cre* brain the signal intensities of the bands on the northern blots were quantified (Figure 4.5.3). When compared to WT levels there is 65.3% of mRNA expression in *Mecp2*$^{FLExDTR(OFF)/y}$,*Nes-cre* mouse brain and 127.5% in *Mecp2*^{StopDTR},*Nes-cre* mice. As Cre recombination by *Nes-cre* is less than 100% in brain, 100% of WT expression is not expected. Interestingly, however, there is actually more *Mecp2*^{DTR} mRNA in the *Mecp2*$^{StopDTR/y}$,*Nes-cre* brain than the WT brain and the *Mecp2*$^{FLExDTR(OFF)/y}$,*Nes-cre* brain. One reason that there might be more *Mecp2*^{DTR} mRNA in the recombined *Mecp2*^{DTR} (*–Stop*) brain compared to the *Mecp2*$^{FLExDTR(ON)}$ brain is that the PGK-neo gene cassette upstream of the DTR

in the *Mecp2*$^{FLExDTR(ON)}$ allele could prematurely terminate some transcripts before they reach the DTR (discussed further in section 4.2). The PGK-neo cassette is excised with the *Stop* cassette in the recombined *Mecp2*^{DTR} (*–Stop*) allele. When comparing the mRNA level in *Mecp2*$^{FLExDTR(OFF)/y}$*,Nes-cre* relative to the *Mecp2*$^{StopDTR/y}$*,Nes-cre* mouse brain there is 51.2% (3'UTR) and 65.9% (DTR). Apart from the presence or absence of the PGK-neo cassette, the mRNA species in the recombined *Stop* allele and the FLEx allele are otherwise not identical: in addition to the DTR, the *Stop* mRNA also encodes P2A and eGFP, and the FLEx mRNA has no P2A or eGFP but has a *lox* site between the translation stop cassette of the DTR and the 3'UTR. These other modifications could also account for the differences in mRNA level.

A further point to raise for the northern blot analysis is that transcripts produced from the recombined *Mecp2*$^{FLExDTR(ON)}$ allele which contain small aberrantly spliced sequences of the PGK-neo gene cassette would not easily be distinguished from the desired mRNA product formed from splicing exon 1 or 2 of *Mecp2* on to the DTR (splicing around the PGK-neo cassette). If these transcripts encode an out of frame DTR sequence, then the level of functional DTR mRNA expression would be lower than that quantified from the blot. When analysing the splicing patterns which arose in the unrecombined leaky *Mecp2*^{StopDTR} allele which also contained a PGK-neo selection cassette in intron 2, splicing in and out of the PGK-neo cassette sequence did not occur (section 3.6.3 and 3.8). The same sequences within the engrailed splice acceptor and *Stop* cassette sequence acted as splice acceptor and donor sequences in the aberrantly spliced transcripts. Therefore, the DTR mRNA level in the *Mecp2*$^{FLExDTR(OFF)}$*,Nes-cre* brain calculated from the northern blot likely is the true level of functional DTR transcripts.

The reduced amount of *Mecp2*^{DTR} mRNA in the brain according to northern blot analysis (~60% of the level of WT *Mecp2* mRNA) is not a cause for concern as *Mecp2* is extremely abundant in neurons. There is likely to be enough functional DTR protein expressed to facilitate high sensitivity of neurons to DT. Accordingly, recombined *Mecp2*$^{FLExDTR(ON)}$ ESCs, which still contain the PGK-neo selection cassette, are sensitive to moderate doses of DT and ESCs lowly express MeCP2. The FRT flanked

PGK-neo cassette can be removed from intron 2 in the *Mecp2*$^{FLExDTR(OFF)}$ mice by crossing these mice to a Flp recombinase expressing mouse line.

There are several reports that the targeted insertion of PGK-neo selection cassettes can disrupt the expression of neighbouring genes in the mouse (Meier *et al*, 2010; Olson *et al*, 1996; Pham *et al*, 1996; Ramirez-Solis *et al*, 1993; Scacheri *et al*, 2001; Jin *et al*, 2021; West *et al*, 2016). This long-range dysregulation of genes can cause additional adverse phenotypes that reflect more than just the disruption of the targeted gene, muddying the interpretation of the study. The *Mecp2*$^{FLExDTR(OFF)}$ mice do not display any unexpected adverse overt phenotype which could be attributed to PGK-neo cassette-mediated toxicity, however, subtle phenotypes cannot be ruled out. Moving forward with experiments with these mice, removing the PGK-neo selection cassette using Flp recombination will remove any doubt one might have about the adverse effects of the PGK-neo cassette on both the expression level of the *Mecp2*^{DTR} fusion gene and surrounding genes.

4.6 Discussion

The overall conclusion of this chapter is a positive one: the engineered *Mecp2*$^{FLExDTR(OFF)}$ allele allows tightly controlled Cre-dependent expression of the DTR from MeCP2-deficient cells. Cre recombination efficiently activates the expression of the DTR from the *Mecp2* promoter by inverting its coding sequence into the sense orientation. Both Cre-mediated inversion and excision readily occur to lock the DTR coding sequence in place. There is no detectable cryptic recombination between incompatible *loxP* and *lox2272* sites which would cause the DTR to be switched back off in recombined *ON* cells. Importantly, there is no detectable leaky expression of the DTR mRNA in Cre–negative neurons or mice. Furthermore, *Mecp2*$^{FLExDTR(OFF)}$ ESC-derived neurons and mice are resistant to all doses of DT tested, including very high doses in mice. This shows that the FLEx switch is superior to the *Stop* cassette in completely switching off a gene, which can be important in alleles like this where leaky expression has cytotoxic consequences.

4.6.1 Unanswered questions regarding the Mecp2$^{FLExDTR(OFF)}$ allele

The *Mecp2$^{FLExDTR(OFF)}$* mice do not experience any adverse effects when administered a high dose of DT; they are comparable to WT mice. A caveat to the interpretation of these results is that there was no positive control for the efficacy of DT where there is a clear expected outcome. It would have been unethical to include the *Mecp2^{StopDTR}* mice which we know do experience adverse effects following DT administration. It is possibility that the DT used for these injections had reduced activity. DT is very sensitive to freeze thaw cycles. Stock solutions of DT were aliquoted, and care was taken to only thaw the toxin once prior to dilution. An additional concern is that crude observations and measurements done for the injected mice such as general condition, weight gain and gross anatomy post-mortem, cannot rule out that a small amount of DT-induced cell ablation did occur that is tolerated by the mouse. The fact that we cannot detect any DTR expression in these animals encourages us that this is a true result and these mice are indeed resistant to high doses of toxin. The localisation of expression of the DTR using these animals for *in vivo* ablation experiments going forward will be reliant on the tightly controlled expression of the Cre recombinase in the transgenic *cre* driver used (discussed in Chapter 5).

A big assumption made when designing this allele and the previous allele is that, X chromosome inactivation (XCI) will silence the DTR on the inactive X chromosome (Xi) in neurons expressing the WT *Mecp2* allele (MeCP2+ neurons). *Mecp2* is subject to X-inactivation which is why females heterozygous for a loss of function mutation in *Mecp2* suffer from Rett Syndrome due to mosaic expression of the mutated *Mecp2* allele. The XCI pattern and skewing has been shown to influence the phenotype of RTT females (discussed in section 1.4.2.). I was unable to test whether X-inactivation sufficiently silences expression of the DTR from the Xi in ESC-derived neurons as these cells are male and lack the second X chromosome. Northern blot analysis of mRNA in heterozygous female and hemizygous male *Mecp2$^{\Delta}$DTR^{FLEX},cre* mice has shown that male mice have roughly double the amount of DTR mRNA compared with females as expected due to XCI. *Mecp2* has not been reported to be a gene which escapes X-inactivation (Carrel & Willard, 2005; Yang *et al*, 2010; Calabrese *et al*, 2012). A transgenic mouse line with the DTR transgene driven from the insulin

promoter inserted into the X-linked *Hcfc1* gene (which undergoes X-inactivation) has been generated and successfully used to ablate ~50% of ß-cells of the pancreas in heterozygous females (Thorel *et al*, 2010). XCI sufficiently silenced the DTR transgene on the Xi in the other ~50% of ß-cells in this mouse model. *In vivo* ablation experiments in the heterozygous *Mecp2*$^{\Delta}$*DTR*$^{FLEX/+}$*,cre* mice (discussed in Chapter 6) or DT treatment of a primary culture of neurons derived from these mice, would be the most appropriate way to test whether the DTR is sufficiently silenced on the inactive X-chromosome.

4.6.2 Further uses of this allele beyond the scope of this project

The activation of the DTR from the *Mecp2* knock out allele is Cre-dependent and therefore can be localised to any cell type for which there is an appropriate transgenic Cre driver mouse. This means that this line can be used to explore the outcome of ablation of the MeCP2 deficient population of a wide range of different cell types. It can be used in the heterozygous female to ablate only those cells with the *Mecp2*$^{FLExDTR(ON)}$ allele on the Xa. Alternatively, it can be used in the hemizygous KO male to ablate the entire population of a certain cell type.

A potential novel use of this line is to explore DT as a delivery vector for MeCP2 protein transduction therapy. Fusing catalytically inactivated DT to protein cargo has been shown to facilitate the delivery of that cargo into DTR expressing cells (Auger *et al*, 2015). An array of proteins of different sizes, structures and stabilities were successfully transported into DTR expressing cells and were shown to be refolded into an active conformation in the cytoplasm. As humans express the DTR and are sensitive to DT, catalytically inactive DT-mediated delivery of clinically relevant proteins is an attractive therapeutic avenue to be explored. In *Mecp2*$^{FLExDTR(ON)}$ mice the target MeCP2-deficient cells are labelled with the DTR. These mice would be a perfect model to test the therapeutic benefit of DT-mediated MeCP2 protein transduction therapy. *Mecp2*$^{FLExDTR(OFF)/y}$ hemizygous male mice develop severe neurological symptoms comparable to *Mecp2-null* mice. As with gene therapy, testing protein transduction therapy on these mice would give a clear read-out of phenotypic amelioration, through prolonged survival and improved activity, gait, breathing and

tremor. Using heterozygous *Mecp2*$^{FLExDTR(ON)/+}$ female mice would allow only MeCP2– cells to be transduced in the mosaic brain as only these cells would be DTR+. This would negate the potential problem of overexpression of MeCP2 in the cells already expressing WT levels of the protein. This would obviously not be the case in the human brain as the pattern of expression of the human DTR cannot be controlled, but would serve as a proof of principle experiment in mice.

Another potential use of the *Mecp2*$^{FLExDTR(OFF)}$ mouse line would be to target the *Mecp2*$^{FLExDTR(ON)}$ allele as a docking site for further manipulation of the *Mecp2* gene in mice. Using the FLEx switch as opposed to the *loxP-Stop* method means that two heterotypic *lox* sites remain either side of the DTR in the recombined allele which could be further used for recombinase-mediated cassette exchange (RMCE) (Feng *et al*, 1999)(Figure 4.6.2). This would allow the insertion and expression of different sequences from the endogenous *Mecp2* promoter following transfection of ESCs or zygotes with Cre and a donor DNA sequence with your DNA cassette of interest flanked by a *lox2272* and *loxP* site. The *lox2272/loxP* combination has been reported to achieve more efficient RMCE compared to the commonly used *lox511/loxP* pair (Kolb, 2001; Araki *et al*, 2002). As the majority of the coding sequence of *Mecp2* is deleted in the *Mecp2*$^{FLExDTR(ON)}$ allele to knock-out the gene, RMCE using this allele would allow you to express any desired sequence from the *Mecp2* promoter in the place of *Mecp2*. It would also allow generation of *Mecp2* alleles with uncharacterised disease-causing mutations, truncations or different protein tags by replacing the DTR with variant forms of *Mecp2*. It would facilitate the generation of an allelic series of mutant *Mecp2* in ESCs or mice.

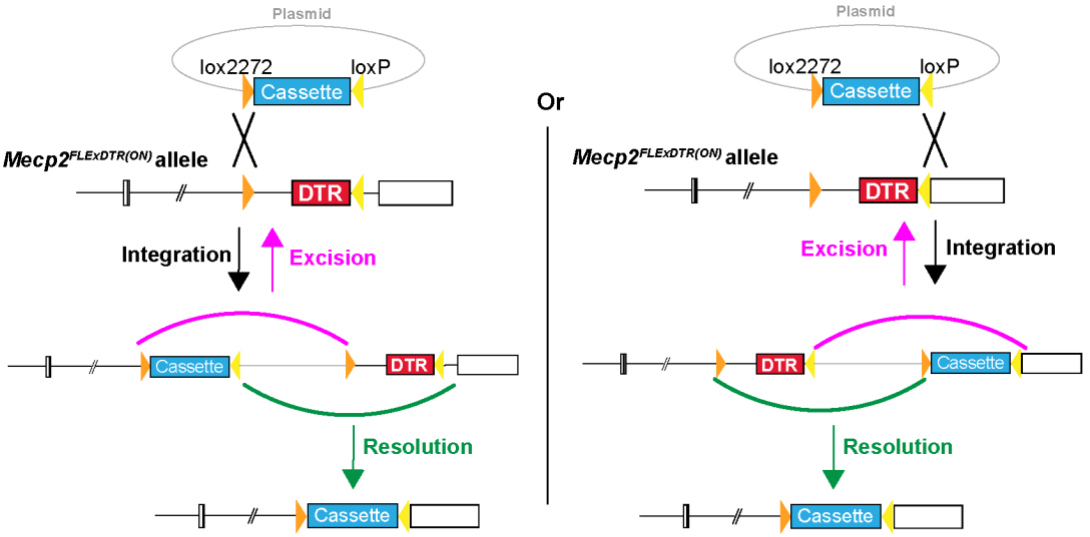

Figure 4.6.2. Recombinase-Mediated Cassette Exchange (RMCE) using the *Mecp2*$^{FLExDTR(ON)}$ allele. Site-specific chromosomal integration can be performed by exchanging the DTR chromosomal sequence with a plasmidic cassette sequence. Recombination via one *lox* site (left: lox2272, right: loxP) leads to plasmid integration. Further recombination via the same site (left: lox2272, right: loxP) leads to excision of the cassette. Recombination via the heterotypic site following integration (left: loxP, right lox2272) leads to resolution of the array created. The end result of the RMCE reaction is an exchange of the DTR with the desired DNA cassette. This exchange is stable because the cassette is flanked by incompatible lox sites that cannot recombine with each other.

Chapter 5 Characterisation of transgenic neuronal Cre drivers

5.1 Introduction

Cre/Lox technology has been used extensively in mice to conditionally knock-out or reactivate a gene of interest in a cell lineage or developmental stage-specific manner. This has led to the generation of many different transgenic Cre driver lines expressing the *cre* recombinase gene in different cell types. These lines have been made available to researchers to purchase from depositories such as the Jackson Laboratory (https://www.jax.org/). Careful characterisation of the pattern of expression of Cre in a chosen line is essential in order to correctly interpret the phenotype resulting from a conditional mutagenesis study. Randomly integrated transgenes with tissue specific exogenous promoters may not faithfully recapitulate the endogenous expression of that promoter. This can be due to the lack of all required regulatory elements needed for tissue specific expression, or the genome environment surrounding the transgene integration site. Knock-in techniques where the *cre* transgene is inserted into an endogenous gene locus using homologous recombination, so that *cre* expression is controlled by the endogenous promoter, are more likely to have the desired cell-type specific expression. Another assumption frequently made for Cre driver lines is that the integration and expression of the *cre* recombinase transgene will be innocuous to the biology of the cell. However, there have been several reports of adverse phenotypes in Cre driver lines attributed to Cre activity or transgene insertion (Schmidt *et al*, 2000; Buerger *et al*, 2006; Lee *et al*, 2006; Forni *et al*, 2006; Naiche & Papaioannou, 2007; Higashi *et al*, 2009). Prolonged Cre overexpression has been shown to trigger DNA rearrangements in the absence of introduced *loxP* sites due to recombination of pseudo-*loxP* sequences present in the mouse genome (Schmidt et al, 2000; Loonstra et al, 2001; Thyagarajan et al, 2000). The integration of the *cre* transgene might also disrupt expression of genes surrounding the integration site, causing adverse phenotypes. The potential pitfalls of Cre driver lines emphasise the importance of both fully characterising the pattern of Cre expression before using the line for conditional mutagenesis experiments as well as using the appropriate *cre+* controls.

The characterisation of a reliable pan-neuronal promoter, which drives efficient neuron-specific transgene expression would provide a valuable tool for studying neurological disease. Neuron-specific conditional knock-out or reactivation of genes implicated in neurological disease allows researchers to study whether symptoms originate solely from the dysfunction of neurons in the brain or whether glial cell dysfunction contributes. *MECP2* cDNA expression from the Tau locus on the *Mecp2* knock-out background was used to test the hypothesis that Rett Syndrome-like phenotypes in the mouse model are solely neuronal (Luikenhuis *et al*, 2004). However, similar *Tau-MECP2* knock-in constructs were later shown to be expressed in both glia and neurons, tracking the endogenous expression pattern of *Mecp2* (Koerner *et al*, 2018), therefore invalidating the earlier conclusion that RTT-like phenotypes are rescued by neuron-specific expression of MeCP2 (Luikenhuis *et al*, 2004). Another important use of a reliable neuronal specific promoter is in devising gene therapies for neurological disorders that involve targeting the expression of viral transgenes specifically to neurons. This would lessen the potential toxic side effects of off-target expression of your gene of interest.

For this project specifically: *in vivo* cellular ablation of MeCP2-negative neurons in the female heterozygote using the Cre-inducible $Mecp2^{FLExDTR(OFF)}$ allele is dependent upon tightly controlled expression of Cre recombinase in the desired cell type, namely neurons. Substantial off-target cellular ablation in undesired tissues would likely be deleterious to the phenotypic outcome and would complicate the interpretation of the results. Three transgenic drivers were established in the animal facility for this project: *Nes-cre* which drives Cre expression throughout the CNS in both glia and neurons and two 'pan-neuronal' transgenic Cre diver lines *Syn1-cre* and *Snap25-IRES2-cre*, reported to drive expression in neurons only)(Harris *et al*, 2014; Zhu *et al*, 2001; Tronche *et al*, 1999).

The commercially available *Nes-cre* line from the Jackson Laboratory (Tronche et al, 1999), is one of the most widely used Cre driver lines in neurobiology. There are over 1000 papers using this line listed in the Mouse Genome database (http://www.informatics.jax.org)(Bult *et al*, 2019). Nestin is a type VI intermediate filament expressed in a variety of tissues, including brain, muscle, kidney,

reproductive organs, adipose and soft tissue, and bone (Human Protein Atlas http://www.proteinatlas.org)(Uhlén *et al*, 2015). Nestin is enriched in progenitors of these tissues, especially skeletal and cardiac muscle precursor cells (Kachinsky *et al*, 1994, 1995; Lendahl *et al*, 1990; Sejersen & Lendahl, 1993). The relatively wide spectrum of expression reflects the presence of multiple regulatory elements within the gene: enhancer elements in the first and second intron have been shown to drive expression in myogenic and neural precursor cells respectively (Zimmerman *et al*, 1994). In the *Nes-cre* line, the randomly inserted *cre* transgene, is expressed from the rat *Nes* promoter and the intron 2 enhancer which drives expression in multipotent neuroepithelial stem cells which give rise to the neurons and glia in the developing central nervous system (Zimmerman *et al*, 1994; Tronche *et al*, 1999). When crossed to the *Mecp2*^{Stop} line where MeCP2 expression is Cre-dependent, Cre-mediated recombination occurs at the *Mecp2* locus in >90% of the entire brain (Ross et al, 2016). Cre-recombination is largely restricted to the nervous system but is detected at low frequencies in the kidney (24%), lung and heart (>20%). Ectopic expression in isolated cells in bone marrow, pancreatic cells and in the germline has been reported in *Nes-GFP* and *Nes-cre* transgenic lines, both using the same *Nes* regulatory elements (Méndez-Ferrer *et al*, 2010; Delacour *et al*, 2004; Carrière *et al*, 2007; Luo *et al*, 2020).

To determine whether the loss of 50% of neurons from the developing or adult brain is compatible with life, we ideally wanted to have a pan-neuronal Cre driver which did not express Cre in glia or in peripheral tissues. The *Syn1-cre* and *Snap25-IRES2-cre* lines were acquired from the Jackson laboratory depository, in the hope that the Cre expression was more restricted to neurons in these lines. This chapter describes experiments to characterise the pattern of Cre expression in these two lines.

Syn1 and *Snap25* gene promoters are good candidates to drive pan-neuronal gene expression. Both proteins have highly neuron-specific roles in the pre-synaptic nerve terminal to facilitate neurotransmission. The best-characterised role of Synapsin-1 is to modulate neurotransmitter release at pre-synaptic nerve terminals by tethering synaptic vesicles to actin filaments in a phosphorylation-dependent manner (reviewed by Cesca *et al*, 2010). Synapsin-1 protein expression is widespread throughout the

central and peripheral nervous system and is not present in significant quantities in non-neuronal cells (reviewed by De Camilli *et al*, 1990). The *Syn1* promoter has been found to contain a sequence motif similar to the neuron-restrictive silencer element (NRSE) which is necessary and sufficient to silence *Syn1* expression in non-neuronal cells (Li *et al*, 1993; Schoch *et al*, 1996; Thiel *et al*, 1998). Synaptosomal-Associated Protein, 25kDa (SNAP-25) is a component of the SNARE (Soluble NSF (N-ethylamaleimide-sensitive factor) Attachment Protein Receptor) complexes which mediate synaptic vesicle docking and fusion during exocytosis (Rizo & Südhof, 2002). Whereas SNAP-25 is expressed almost exclusively in the brain, its homolog SNAP-23, which is ~60% identical to SNAP-25, is expressed ubiquitously (Ranichandran *et al*, 1996; Wang *et al*, 1997).

The *Syn1-cre* transgenic line developed by Zhu et al, (2001), has been described in literature as a 'pan-neuronal' Cre driver and has been used in many studies for neuron-specific deletion of a Cre-inducible gene (Mouse Genome database: www.informatics.jax.org/allele/key/6193). Cre recombinase is expressed from a 4.3 kb fragment of the rat Synapsin-1 gene (*Syn1*) promoter (Hoesche et al, 1993). The pattern of Cre expression was originally characterised using a *loxP-Stop LacZ* Cre-dependent reporter strain (Zhu et al, 2001). LacZ immunoreactivity was reported to be restricted to the brain, spinal cord and Dorsal Root Ganglion (DRG), and detectable from E12.5 onwards. Within the brain, unlike other brain regions, LacZ immunoreactivity was low in the cerebellum, where only few Purkinje cells were positive. No recombination in other tissues was detected using PCR analysis. LacZ immunoreactivity was found to colocalise with the neuronal marker NeuN and not with the astrocyte marker GFAP, suggesting that Cre expression is localised to neurons within the brain.

The second "pan-neuronal" Cre driver acquired for this project, the *Snap25-IRES2-cre* line, was generated by the Allen Institute for Brain Science and described as the having "strong widespread expression throughout the brain" (connectivity.brain-map.org/transgenic)(Harris *et al*, 2014). The *Snap25-IRES2-cre* allele is a *cre* knock in allele where an Internal Ribosome Entry site (IRES) and the *cre* recombinase gene sequence are inserted downstream of the stop codon of the endogenous *Snap25* gene

(www.informatics.jax.org/allele/MGI:5507846). Cre recombinase is bicistronically expressed with endogenous *Snap25* from the same transcript, so its expression pattern should closely follow the pattern of endogenous *Snap25* mRNA. The *Snap25-IRES2-cre* line is the least characterised of the three Cre driver lines discussed in this chapter, as it has only been cited in a few papers.

5.1.1 Allen Institute for Brain Science characterisation of the transgenic Cre driver lines

The Allen Institute for Brain Science has established a high-throughput *in situ* hybridization (ISH), imaging and data processing pipeline to describe whole brain gene expression patterns in Cre driver mice (Harris *et al*, 2014). Their publicly available Transgenic Characterization database (connectivity.brain-map.org/transgenic), has anatomical data from over 100 Cre driver lines, including the *Syn1-cre* and *Snap25-IRES2-cre* lines, which can be used to assist researchers in choosing the appropriate Cre driver for investigation into specific cell-types and networks.

To systematically characterize whole brain *cre* expression patterns, the Cre driver lines are combined with ubiquitously expressed Cre-dependent reporter lines to generate double positive mice for brain collection at up to four postnatal ages (for details see Harris *et al*, 2014 or connectivity.brain-map.org/transgenic). The entire brain is sectioned and tissue subjected to ISH to detect the *cre* reporter mRNA, *cre* mRNA itself, and other marker genes of interest. A high resolution ISH image series throughout the rostral-caudal extent of the brain is provided for each Cre driver line to visualise the expression patterns. An expression mask is produced for each ISH image which shows the areas of detected expression with colour-coding of the expression level. For each ISH image series, whole brain expression summary data for 12 main brain divisions is presented as a histogram.

The average expression value for the 12 major brain structures, the expression pattern classification and whether the Cre reporter expression matches the corresponding endogenous gene is shown for the *Snap25-IRES2-cre* and *Syn1-cre* lines in Table 5.1.1. Representative ISH images and expression masks of brain sections for both lines

are shown in (Allen institute data: Figures 5.1.1 and 5.1.2). Upon enquiry, the Allen institute advised that the *Snap25-IRES2-cre* line was the most pan-neuronal Cre driver line they had characterised which had widespread expression throughout the brain (Allen institute data: Table 5.1.1 Figure 5.1.1). They found it to be superior to the *Syn1-cre* line which had widespread expression throughout the brain but with relatively sparser expression in some areas including the striatum and cerebellum, and enriched expression in the cortex (Allen institute data: Table 5.1, Figure 5.1.2). *Snap25-IRES2-cre* expression faithfully represents the endogenous *Snap25* expression pattern. Data on the correlation of *cre* expression and endogenous *Syn1* expression is not available for the *Syn1-cre* line. From the Allen Institute online ISH data it is difficult to determine whether Cre is expressed in non-neuronal cells in the brain. Upon enquiry, the Allen Institute advised that they had identified *Snap25-IRES2-cre* expression in a small fraction of non-neuronal cells. A further outstanding question not addressed by the Allen Institute characterisation is whether Cre expression in either lines is restricted to the brain or whether there is significant expression in peripheral tissues.

	Snap25-IRES2-cre			*Syn1-cre*		
Major Division	Expression Energy	Expression Pattern	Matches Endogenous	Expression Energy	Expression Pattern	Matches Endogenous
Isocortex	35.335	widespread	yes	19.001	widespread	ND
Olfactory Areas	27.323	widespread	yes	14.289	widespread	ND
Hippocampus	28.646	widespread	yes	13.553	scattered	ND
Cortical Subplate	36.381	widespread	yes	19.157	scattered	ND
Striatum	29.859	widespread	yes	12.862	enriched	ND
Pallidum	22.253	widespread	yes	11.719	scattered	ND
Thalamus	23.687	widespread	yes	19.774	widespread	ND
Hypothalamus	25.383	widespread	yes	13.679	enriched	ND
Midbrain	22.746	widespread	yes	15.177	widespread	ND
Pons	23.042	widespread	yes	15.201	enriched	ND
Medulla	21.459	widespread	yes	14.732	enriched	ND
Cerebellum	19.862	widespread	yes*	10.467	scattered	ND

Table 5.1.1. Expression patterns of Cre reporter mRNA in the 12 major brain divisions in *Snap25-IRES2-cre* or *Syn1-cre* mice. Data was generated by the Allen Brain Institute Transgenic Characterization pipeline (http://connectivity.brain-map.org/transgenic) and taken from Harris et al., (2014) Supplementary data Table 2. Shown here is the average expression energy, expression pattern and correlation of expression with corresponding endogenous gene for 12 major brain divisions. Expression energy = sum of expressing pixel intensity / sum of all pixels in division. Expression patterns are as follows: widespread: very dense expression across neighbouring structures; scattered: less dense expression across neighbouring structures; enriched: some boundary definition of a particular structure from its neighbours.*indicates that expression pattern may not qualitatively match endogenous.

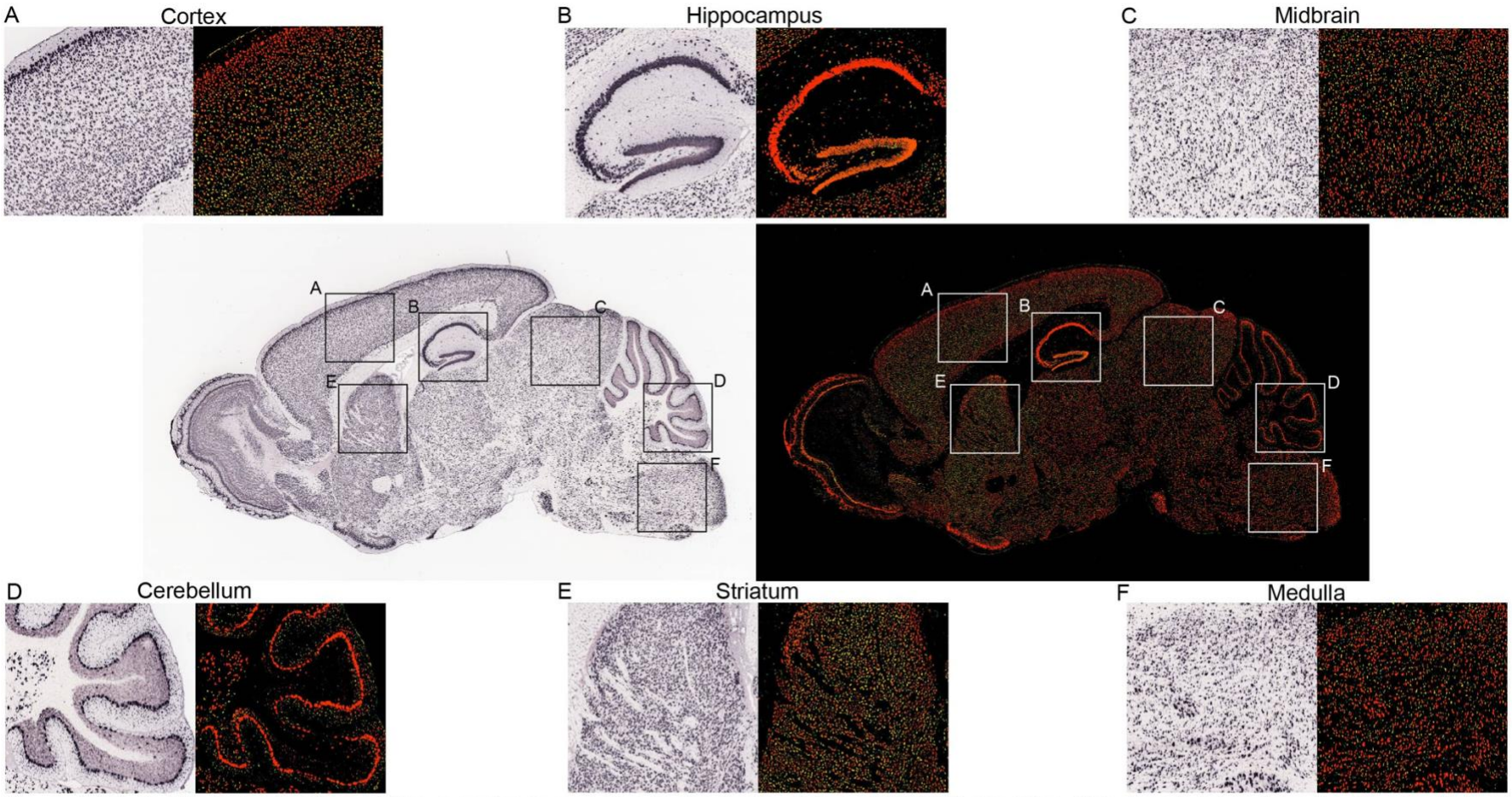

Figure 5.1.1. *In situ* hybridisation of Cre reporter expression in the brain of *Snap25-IRES2-cre* mice. This data is taken from the Allen Institute of Brain Science Transgenic Characterisation database (http://connectivity.brain-map.org/transgenic). Shown here is a representative ISH image of an entire brain section (left centre) and the expression mask of the ISH image (right centre). The expression mask shows areas of detected expression with colour-coding of the expression level: blue (low expression intensity), green (medium intensity) and red (high intensity). A-E are zoomed in images of different brain regions. Section taken from brain of P28 male, image series ID:304699151

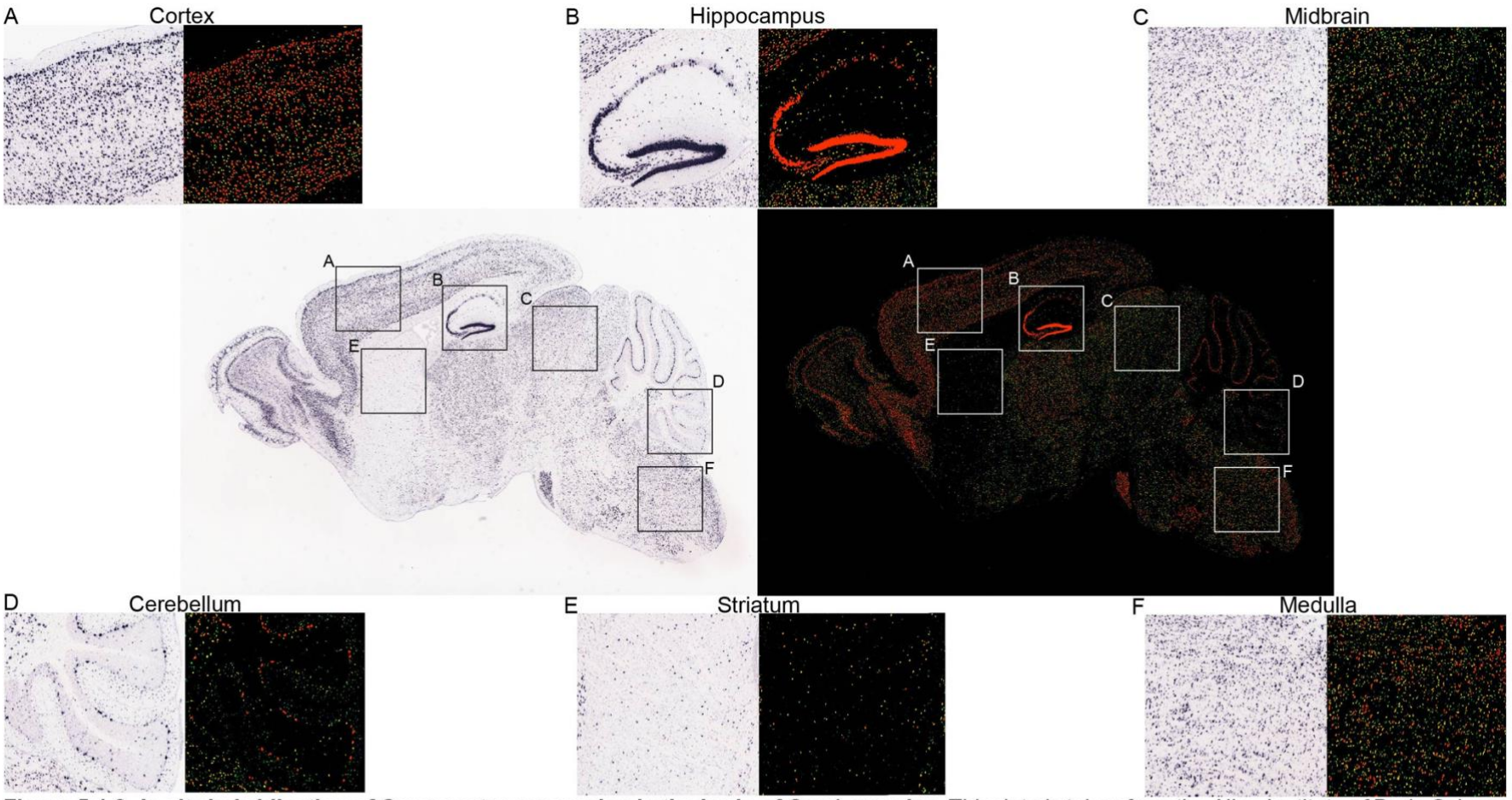

Figure 5.1.2. *In situ* hybridisation of Cre reporter expression in the brain of *Syn1-cre* mice. This data is taken from the Allen Institute of Brain Science Transgenic Characterisation database (http://connectivity.brain-map.org/transgenic). Shown here is a representative ISH image of an entire brain section (left centre) and the expression mask of the ISH image (right centre). The expression mask shows areas of detected expression with colour-coding of the expression level: blue (low expression intensity), green (medium intensity) and red (high intensity). A-F are zoomed in images of different brain regions. Section taken from brain of P28 male, image series ID:100126203

5.2 Experiments to characterise the Cre expression pattern in *Syn1-cre* and *Snap25-IRES2-cre* lines

To explore the specificity of the Cre expression in the *Syn1-cre* and the *Snap25-IRES2-cre* transgenic lines further myself, these lines were crossed to an *Mecp2* reporter mouse line, *Mecp2*^{mCherryStop}, where the C terminus of MeCP2 is tagged with mCherry and a *loxP-floxed* transcriptional *Stop* cassette is upstream of the *Mecp2* coding sequence (Jim Selfridge, unpublished)(Guy *et al*, 2007). Cre-mediated recombination and removal of the transcription *Stop* cassette activates the expression of the MeCP2-mCherry protein which can be detected by flow cytometry, western blot analysis, and confocal microscopy to assess protein expression in different tissues. The *Mecp2*^{mCherryStop} line was crossed previously to a *CMV-cre* line with ubiquitous expression of Cre in order to generate the *Mecp2*^{mCherry} line which has constitutive MeCP2^{mCherry} expression. This line was used as a positive control for MeCP2^{mCherry} expression in experiments in this chapter. Throughout, male mice hemizygous for the X-linked *Mecp2*^{mCherryStop} or *Mecp2*^{mCherry} alleles were used to avoid complicated interpretation of expression patterns due to X-inactivation in females. The fact that I am using an *Mecp2* reporter line to characterise the Cre expression, to determine which line to use to activate the DTR expression from the *Mecp2*$^{FLExDTR(OFF)}$ line, avoids the potential problem of variability of Cre recombination efficiency at different loci. The pattern of recombination of the *Mecp2*$^{FLExDTR(OFF)}$ allele and the *Mecp2*^{Stop} allele should be comparable.

5.2.1 Cre recombinase expression in the Syn1-cre brain is unevenly distributed throughout the brain

Before coming across the Allen Institute's ISH data, I had performed immunofluorescence on brain sections of *Syn1-cre,Mecp2*^{mCherryStop} reporter mice (Figure. 5.2.1). I detected patterns of Cre reporter expression similar to the Allen Institute's ISH data (Figure 5.1.2): particularly sparse expression in the CA1 region of the hippocampus and the cerebellum, and incomplete expression in the cortex. The "patchy" expression of Cre in the *Syn1-cre* brain is suboptimal for this project

objective as it would facilitate incomplete DTR activation and DT-mediated ablation of MeCP2– neurons when combined with the *Mecp2*$^{FLExDTR(OFF)}$ allele.

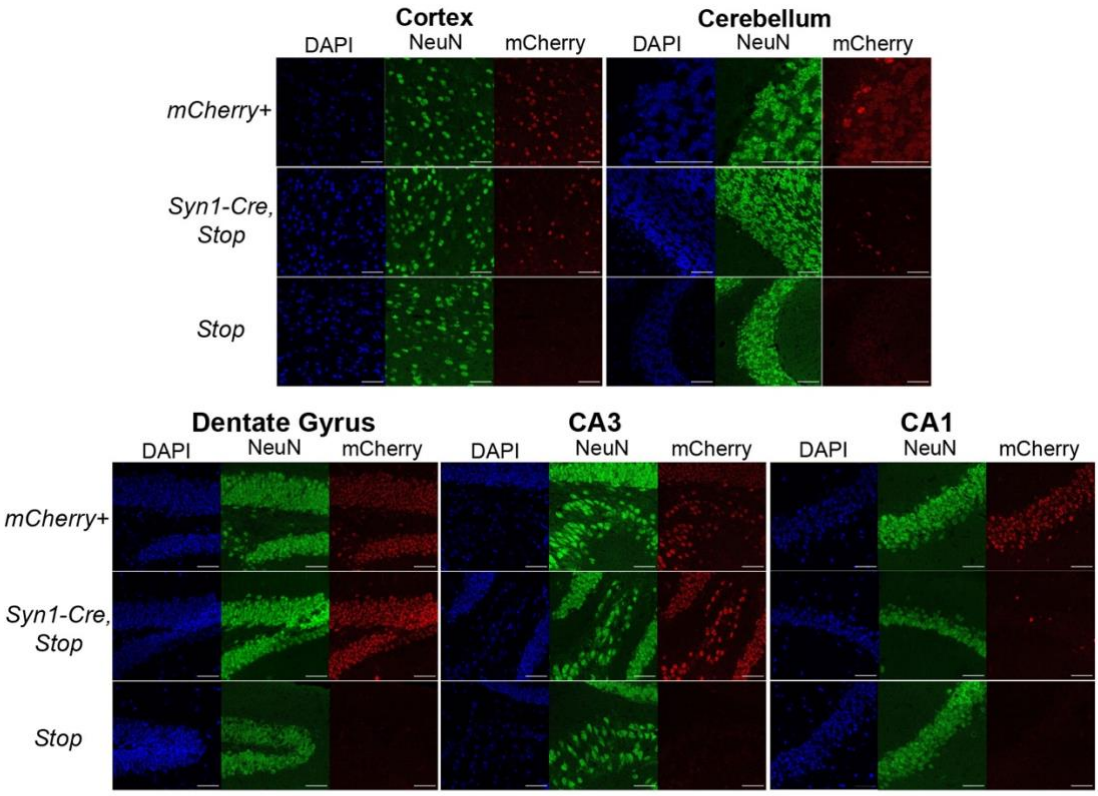

Figure 5.2.1. *Syn1-cre* expression is variable across different brain regions. The Cre-mediated activation of MeCP2^{mCherry} fluorescence was visualised in brain sections of *Syn1-cre,Mecp2*$^{mCherryStop/y}$ *(Syn1-Cre,Stop)* brains. All mice used were male so were hemizygous for the modified *Mecp2* alleles. Brain sections from *Mecp2*$^{mCherry+/y}$ *(mCherry+)* mice which have the *Stop* cassette removed and express MeCP2^{mCherry} constitutively were used as a positive control and *cre*-negative *Mecp2*$^{mCherryStop/y}$ *(Stop)* mice were used as a negative control. Sections were immunolabelled for the neuronal marker NeuN, and stained for DAPI to highlight all cells. Above) Representative images of the cerebellum and cortex are shown. Below) Representative images of different sub-regions within the hippocampus to show that even within a brain region the pattern of expression is variable.

5.2.2 Cre recombinase expression in peripheral tissues

To determine whether Cre recombinase expression is restricted to the brain compared to other tissues, western blot analysis was performed on protein preparations from a panel of tissues from *Syn1-cre,Mecp2*$^{mCherryStop/y}$ and *Snap25-IRES2-cre,Mecp2*$^{mCherryStop/y}$ mice (Figure 5.2.2). The low level of MeCP2^{mCherry} expression in tissues seen in the *Mecp2*$^{mCherryStop/y}$ negative control is due to leaky expression of the *Stopped* allele rather than Cre mediated removal of the *Stop* cassette (Robinson *et al*,

2012; Guy *et al*, 2007). Importantly, in the majority of tissues outside the brain there was no significant difference in MeCP2^{mCherry} expression in *Syn1-cre,Mecp2*$^{mCherryStop/y}$ and *Snap25-IRES2-cre,Mecp2*$^{mCherryStop/y}$ mice compared to *Mecp2*$^{mCherryStop/y}$ control mice, suggesting that there was no Cre-mediated recombination to remove the *Stop* cassette. In the testis, there was a higher level of MeCP2^{mCherry} in the *Syn1-cre, Mecp2*$^{mCherryStop/y}$ tissue (10.3%) compared to in the *Mecp2*$^{mCherryStop/y}$ tissue (0.7%).

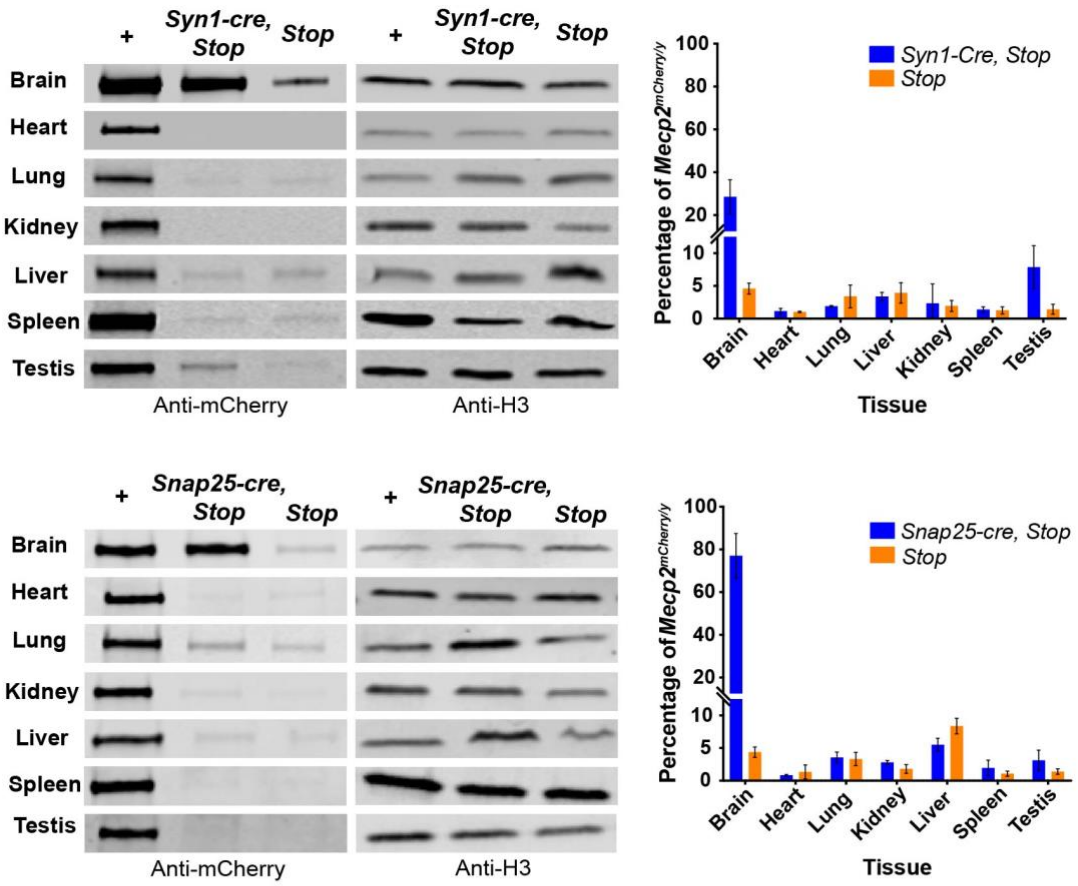

Figure 5.2.2. Cre recombinase expression in *Syn1-cre* and *Snap25-IRES2-cre* transgenic mice is restricted to the brain. Left) Representive images of western blots of MeCP2^{mCherry} expression in a panel of different tissues from: constitutively expressing *Mecp2*$^{mCherry/y}$ (+), *Mecp2*$^{mCherryStop/y}$ (*Stop*) control mice and Syn1-cre,*Mecp2*$^{mCherryStop/y}$ (*Syn1-cre,Stop*) mice or *Snap25-IRES2-cre,Mecp2*$^{mCherryStop/y}$ (*Snap25-cre,Stop*) mice. Right) Graphs showing the MeCP2^{mCherry} protein level in *Stop* and *Syn1-cre,Stop* or *Snap25-cre,Stop* tissues as a pecentage of the level in constitutively expressing *Mecp2*$^{mCherry/y}$ (+), tissues for three biological replicates (3 separate mice). Western blot quantification was perfomed using Image Studio Lite Software (LI-COR biosciences). The MeCP2^{mCherry} signal intensity was normalised to the signal intensity of the H3 loading control for each sample. Three biological replicates per genotype, per tissue were analysed. Plotted here is the mean and standard deviation for the normalised protein level for each genotype as a percentage of the average of the constitutively expressed *Mecp2*$^{mCherry/y}$ (+) samples.

Compared to *Mecp2*$^{mCherry/y}$ mice where MeCP2^{mCherry} is expressed ubiquitously, the level of MeCP2^{mCherry} in the brain is 28.6% for *Syn1-cre,Mecp2*$^{mCherryStop/y}$ mice and 77.0% for *Snap25-IRES2-cre,Mecp2*$^{mCherryStop/y}$ mice (Figure 5.2.2). MeCP2 is highly abundant in neurons relative to glia in the brain; it is around 6-7-fold more highly expressed in neurons compared to glia and in neurons there is approximately $16x10^6$ molecules per neuronal nuclei (Skene *et al*, 2010). Neuronal MeCP2^{mCherry} constitutes the majority of MeCP2^{mCherry} protein in whole brain protein extracts. The relatively low MeCP2^{mCherry} level in the *Syn1-cre,Mecp2*^{mCherryStop} brain agrees with the immunofluorescence analysis shown above (Figure 5.2.1).

5.2.3 Cre recombination frequency throughout the brain

To quantify the total recombination frequency throughout the brain, Southern blot analysis was performed on genomic DNA preparations from whole brain samples for *Mecp2*$^{mCherryStop/y}$, *Mecp2*$^{mCherry/y}$, *Syn1-cre,Mecp2*$^{mCherryStop/y}$ and *Snap25-IRES2-cre,Mecp2*$^{mCherryStop/y}$ mice (Figure 5.2.3). The DNA was digested with EcoRI restriction enzyme and the *Mecp2* locus visualised using a radiolabelled probe which annealed to the 3'UTR to clearly distinguish the larger 8 kb fragment of DNA from the unrecombined locus in *Mecp2*$^{mCherryStop/y}$ brain samples, and the smaller 6 kb fragment produced from the recombined locus in *Mecp2*$^{mCherry/y}$ samples. Quantification of the proportion of unrecombined and recombined fragments showed that the recombination frequency in *Syn1-cre,Mecp2*$^{mCherryStop/y}$ mice is 23.9% and in *Snap25-IRES2-cre,Mecp2*$^{mCherryStop/y}$ mice is 66.8% (Figure 5.2.3). *Nes-cre* which drives expression in both neurons and glia leads to >90% recombination of the *Mecp2*^{Stop} allele in mouse brain (Ross *et al*, 2016). Incomplete expression of *Snap25-IRES2-cre* in the brain suggests that this allele is not expressed in all glial cells.

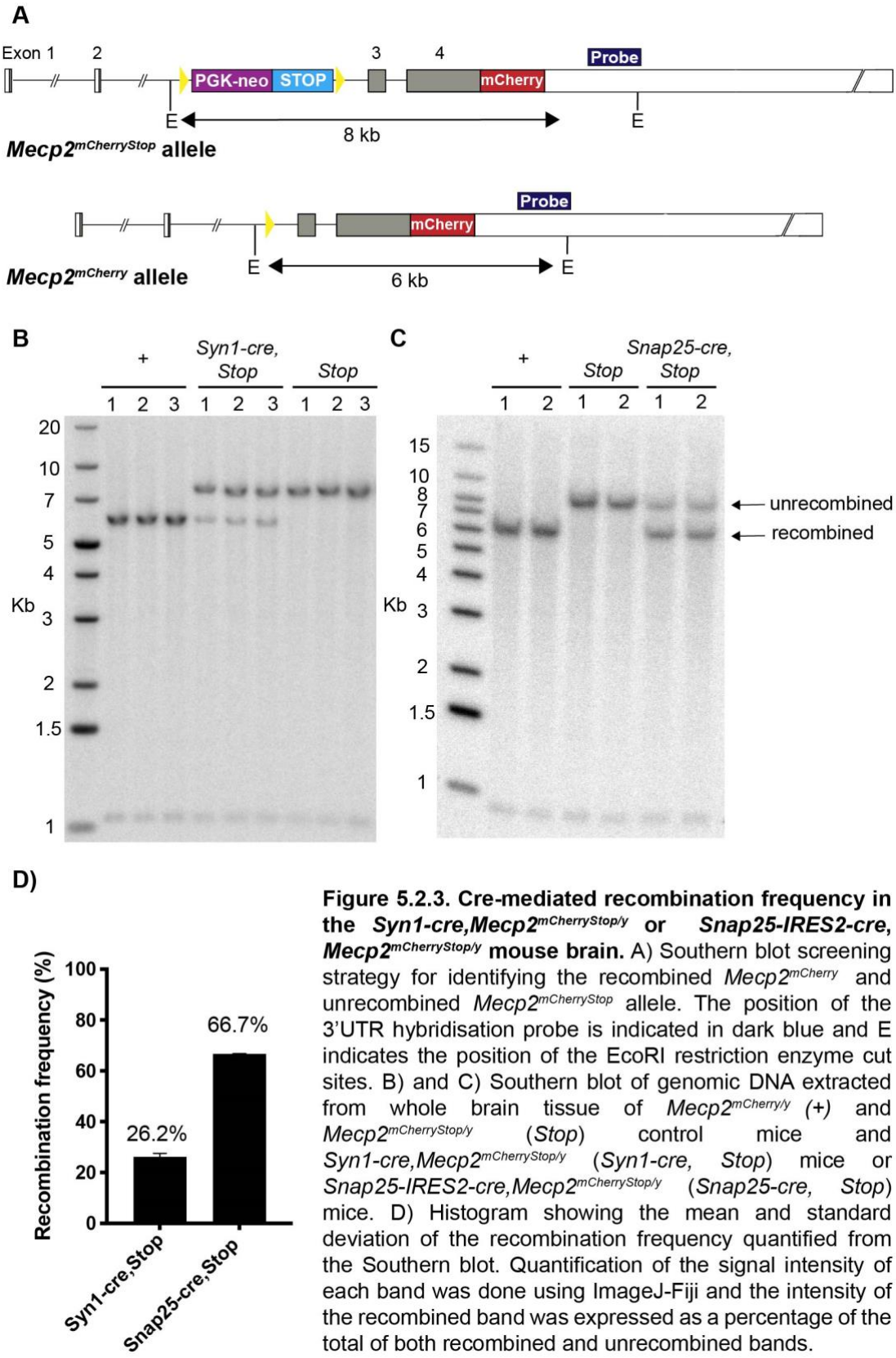

Figure 5.2.3. Cre-mediated recombination frequency in the *Syn1-cre,Mecp2*$^{mCherryStop/y}$ or *Snap25-IRES2-cre, Mecp2*$^{mCherryStop/y}$ mouse brain. A) Southern blot screening strategy for identifying the recombined *Mecp2*^{mCherry} and unrecombined *Mecp2*^{mCherryStop} allele. The position of the 3'UTR hybridisation probe is indicated in dark blue and E indicates the position of the EcoRI restriction enzyme cut sites. B) and C) Southern blot of genomic DNA extracted from whole brain tissue of *Mecp2*$^{mCherry/y}$ *(+)* and *Mecp2*$^{mCherryStop/y}$ (*Stop*) control mice and *Syn1-cre,Mecp2*$^{mCherryStop/y}$ (*Syn1-cre, Stop*) mice or *Snap25-IRES2-cre,Mecp2*$^{mCherryStop/y}$ (*Snap25-cre, Stop*) mice. D) Histogram showing the mean and standard deviation of the recombination frequency quantified from the Southern blot. Quantification of the signal intensity of each band was done using ImageJ-Fiji and the intensity of the recombined band was expressed as a percentage of the total of both recombined and unrecombined bands.

It is tempting to try to relate the recombination frequency in the whole brain to the glia to neuron ratio, to determine whether you would expect more or less cells to express Cre if the expression is restricted to neurons. Modern estimates suggest around 65% of all the cells in the mouse brain are neurons (Herculano-Houzel *et al*, 2006; Herculano-Houzel, 2014; Erö *et al*, 2018)(Blue Brain Cell Atlas: bbp.epfl.ch/nexus/cell-atlas/). If DNA extraction from neuronal and non-neuronal cells was comparably efficient, the Southern blots results suggest that recombination frequency in the *Snap25-IRES2-cre,Mecp2*^{mCherryStop} brain does not substantially exceed the frequency expected if the majority of the neurons were to express Cre recombinase. The recombination frequency in the *Syn1-cre,Mecp2*^{mCherryStop} brain is roughly 1/3 of the frequency expected if all neurons expressed Cre recombinase. This analysis quantitatively shows that Cre is expressed in a much higher proportion of cells in the *Snap25-IRES2-cre* brain compare to the *Syn1-cre* brain. Southern blot analysis on whole brain extracts does not allow the recombination frequency in neurons and non-neuronal cells to be distinguished.

5.2.4 Cre recombination in neurons versus glia

In an attempt to analyse the Cre reporter expression pattern in neurons and glia in the brain, nuclei were extracted from *Mecp2*$^{mCherryStop/y}$, *Mecp2*$^{mCherry/y}$, *Syn1-cre,Mecp2*$^{mCherryStop/y}$ and *Snap25-IRES2-cre,Mecp2*$^{mCherryStop/y}$ mice, stained with fluorescently labelled NeuN and analysed by flow cytometry to determine what proportion of NeuN expressing cells were expressing MeCP2^{mCherry} (Figure 5.2.4). NeuN is a neuron-specific nuclear protein marker expressed in the majority of neurons, whereas glial nuclei are negative for NeuN staining (Mullen *et al*, 1992). Approximately 50,000 single nuclei were analysed per sample and gated into two populations NeuN high and NeuN low based on the level of NeuN fluorescence. Within the NeuN high population assumed to be neurons, in *Mecp2*$^{mCherry/y}$ samples where MeCP2^{mCherry} was ubiquitously expressed, there was a single population of nuclei which are highly expressing mCherry. In the *Mecp2*$^{mCherryStop/y}$ negative control samples where the *Stop* cassette was in place preventing *Mecp2*^{mCherry} expression ubiquitously, there was a single population of nuclei expressing low levels of mCherry. These two populations – one high mCherry and one low mCherry – are also evident in

the NeuN low populations for *Mecp2*$^{mCherry/y}$ and *Mecp2*$^{mCherryStop/y}$ respectively. In the NeuN low population these two subpopulations are shifted down in mCherry expression because endogenous *Mecp2* is expressed at a much lower level in non-neuronal cells in the brain compared to neurons. To determine how these populations change in the *Syn1-cre,Mecp2*$^{mCherryStop/y}$ and *Snap25-IRES2-cre,Mecp2*$^{mCherryStop/y}$ samples, gates were drawn around each of the 4 populations 1) NeuN low; mCherry low (*Stopped* non-neuronal cells), 2) NeuN low; mCherry high (reactivated non-neuronal cells), 3) NeuN high; mCherry low (*Stopped* neurons), 4) NeuN high; mCherry high (reactivated neurons) (Figure 5.2.4). The proportion of NeuN high or low nuclei which fall into either the mCherry high or mCherry low gate where quantified.

Recombination and reactivation of the *Mecp2*^{mCherryStop} allele occurred in 35.1% of NeuN high nuclei (neurons) for *Syn1-cre* and 83.6% for *Snap25-IRES2-cre*, suggesting that the *Snap25-IRES2-cre* is superior in terms of pan-neuronal Cre expression. This assay also suggests that recombination occurred in 23.8% of NeuN low nuclei (non-neuronal cells) in *Syn1-cre;Mecp2*^{mCherryStop} brain and 65.5% of NeuN low nuclei in *Snap25-IRES2-cre;Mecp2*^{mCherryStop} brain. For the *Syn1-cre;Mecp2*^{mCherryStop} nuclei the 4 gated populations clearly overlap with the *Mecp2*$^{mCherry/y}$ positive and *Mecp2*^{mCherryStop} negative control samples (see panels 3 and 5 Figure 5.2.4A). For the high NeuN population of *Snap25-IRES2-cre,Mecp2*^{mCherryStop} nuclei, mCherry high and low populations overlap well with the positive and negative control populations, but this is not the case for the low NeuN populations. The two populations of mCherry expression do not overlap with the control populations as precisely. It is difficult to determine why for this line the plots are reproducibly different, all three biological replicates have similar patterns of distribution of nuclei. This makes it more difficult to draw conclusions for the NeuN-low nuclei in *Snap25-IRES2-cre, Mecp2*^{mCherryStop} samples.

If NeuN expression reliably distiguishes neuronal and non-neuronal nuclei then this analysis shows two things: 1) Cre is expressed in the majority of neurons in the *Snap25-IRES2-cre* brain and is only expressed in 35.1% of neurons in the *Syn1-cre* brain; 2) Cre is expressed in non-neuronal cells in both lines, with the proportion of

Cre+ non-neuronal cells reaching 65.5% in the *Snap25-IRES2-cre* brain. Although the NeuN antibody is thought to be a reliable tool to separate neuronal and non-neuronal cells (Herculano-Houzel & Lent, 2005), there is a possibility that flow cytometry using NeuN staining, miss-identifies a proportion of neurons. Some neuronal subtypes known to be devoid of NeuN immunoreactivity include the cerebellar Purkinje cells, olfactory bulb mitral cells and retinal photoreceptor cells (Mullen *et al*, 1992). In my flow cytometry analysis, the ratio of neuronal to non-neuronal nuclei (Figure 5.2.4 panel 1) is lower than expected based on the cellular composition of the mouse brain (~65% of cells in the mouse brain are neurons (see above 5.2.3)). In my analysis ~30% of the nuclei are NeuN high. The under-representation of NeuN stained nuclei might be explained by either the loss of neuronal nuclei during the nuclei extraction step relative to non-neuronal cells, or incomplete NeuN staining. No nuclear marker which reliably stains all types of glia has been identified. Double staining with a glia and a neuronal marker would give a more conclusive quantification of what proportion of neurons and glia express Cre.

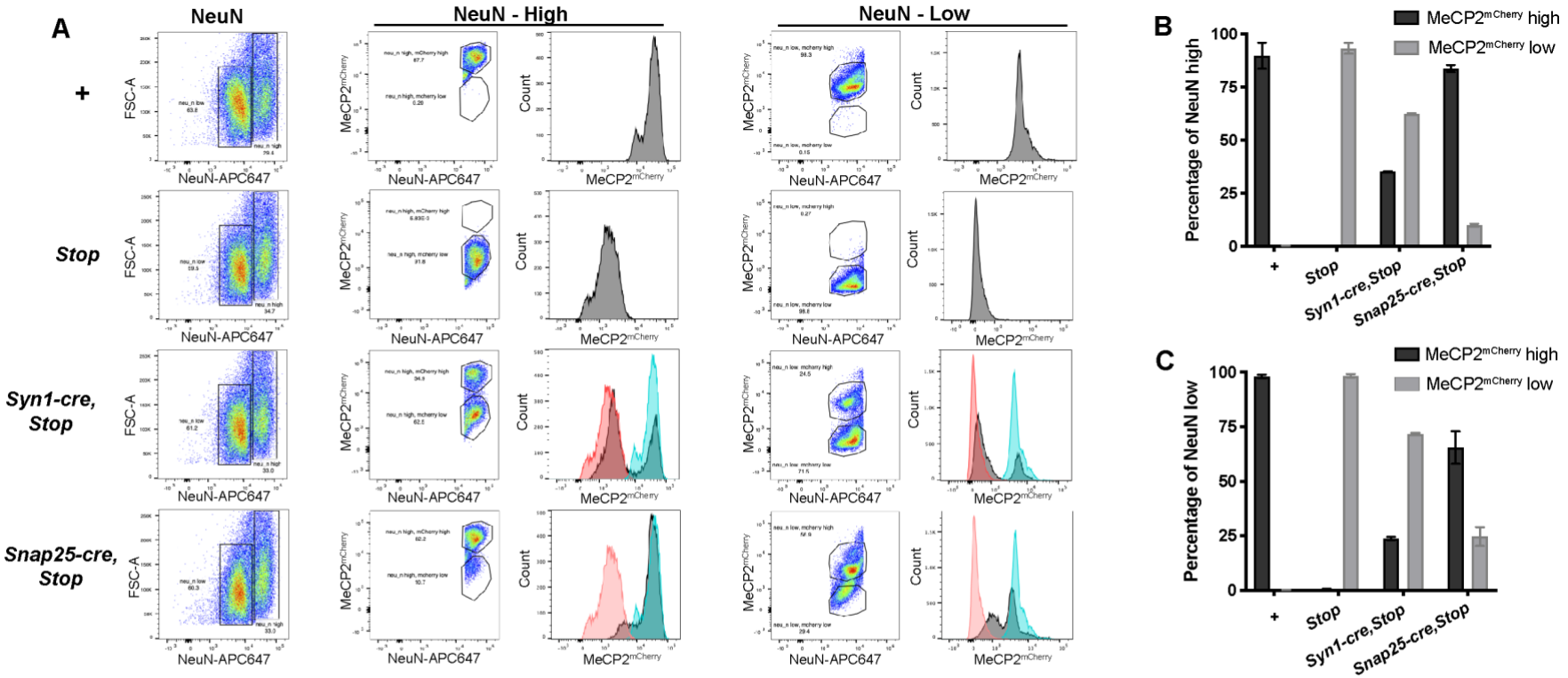

Figure 5.2.4 *Snap25-IRES2-cre* is superior to *Syn1-cre* as a pan-neuronal Cre driver A) Flow cytometry analysis of nuclei extracted from *Mecp2*$^{mCherry/y}$(+), *Mecp2*$^{mCherryStop/y}$(*Stop*), *Syn1-Cre,Mecp2*$^{mCherryStop/y}$(*Syn1-cre,Stop*), *Snap25-IRES2-Cre,Mecp2*$^{mCherryStop/y}$ (*Snap25-cre,Stop*) brains. Representative images for each genotype showing the gating strategy used to identify the proportion of NeuN high neuronal nuclei, and NeuN low non-neuronal nuclei which have activated MeCP2^{mCherry} expression by flow cytometry. Intact, single nuclei (gating strategy shown in the Appendix Figure 8.) were gated and analysed for their NeuN expression (panel 1: y axis: Forward Scatter FCS-A; x axis: NeuN-APC647 fluorescence). The NeuN-high (panel 2 and 3) and NeuN-low (panel 4 and 5) populations were then gated and analysed for MeCP2^{mCherry} expression. Panel 2 and 4: Cell density plots: y axis:mCherry/PE-Texas Red fluorescence; x axis: NeuN-APC647 fluorescence. Panel 3 and 5: Histograms of cell count against mCherry/PE-Texas Red fluorescence. For *Syn1-cre,Stop* and *Snap25-cre,Stop* samples overlays of the + (blue) and *Stop* (red) control samples are shown. B) and C) Bar charts showing the proportion of NeuN-high (B) and NeuN-low (C) nuclei which are within the MeCP2^{mCherry}-high (dark grey) or MeCP2^{mCherry}-low (light grey) gate for three biological replicates of each genotype. Plotted is the mean and standard deviation.

5.3 Discussion

The aim of this chapter was to identify an appropriate transgenic Cre driver line with Cre expression restricted to neurons, to facilitate the neuron-specific activation of the DTR expression from the inducible *Mecp2*$^{FLExDTR(OFF)}$ allele. Described here are experiments to characterise the Cre expression in the *Syn1-cre* and *Snap25-IRES2-cre* transgenic lines.

Firstly, for both the *Syn1-cre* and *Snap25-IRES2-cre* line, in the panel of tissues assayed, Cre expression was largely restricted to the brain. For the *Syn1-cre* line, these findings are consistent with its initial characterisation that reported no significant expression of Cre in these peripheral tissues (Zhu *et al*, 2001). Cre expression in tissues other than the brain has not been previously assessed for the *Snap25-IRES2-cre* line, therefore, this is a novel finding. Ectopic expression of Cre reporter in *Syn1-cre,Mecp2*^{mCherryStop} mice was detected in the testis. Significant Cre expression in the testis has been previously reported for both the *Syn1-cre* driver line and the rat *Syn1* transgenic promoter which drives the transgenic *cre* expression (Rempe *et al*, 2006; Hoesche *et al*, 1993; Luo *et al*, 2020). Careful breeding can negate the potential problem which arises due to germline expression of *cre*. To generate *cre* positive *Mecp2*$^{FLExDTR(OFF)/+}$ heterozygous females, *Mecp2*$^{FLExDTR(OFF)/+}$ females are bred to *cre*+ males to generate progeny required for each experiment. Progeny of this cross i.e. *Mecp2*$^{FLExDTR(OFF)/+}$*,cre* mice are not be bred on to avoid potential recombination in the germline which would give rise to progeny with ubiquitous expression of the DTR. In other transgenic lines, the 4.3 kb rat *Syn1* promoter, was shown to drive ectopic reporter expression in muscle, kidney, uterus and spleen, the level of expression differed for different transgenic lines (Hoesche *et al*, 1993). Findings here suggest that the *Syn1-cre* transgene expression more faithfully recapitulates the endogenous tissue specific expression of Synapsin-1 than these earlier transgenic lines with the same promoter. Encouragingly, in both lines the Cre expression is restricted to the brain, meaning that when combined with the *Mecp2*$^{FLExDTR(OFF)}$ allele, the DTR expression should be localised to the brain, reducing the chance of off-target ablation in peripheral tissues.

The immunofluorescence and flow cytometry analysis confirmed what the Allen Institute for Brain Science *in situ* hybridisation data showed that only a proportion of neurons (~35%) in the *Syn1-cre* line express Cre. *Syn1-cre* transgene expression is unevenly distributed throughout the brain, with some regions having sparse Cre expression. Notably the expression is low in the cerebellum which contains ~60% of all the neurons in the mouse brain (Erö *et al*, 2018; Herculano-Houzel *et al*, 2006)(Blue Brain Cell Atlas: bbp.epfl.ch/ nexus/cell-atlas). In comparison, expression in *Snap25-IRES2-cre* is pan-neuronal, the majority of neurons (83.6%) in the *Snap25-IRES2-cre* line express Cre. Flow cytometry also identified that both lines express Cre in NeuN-negative nuclei (non-neuronal cells). The initial characterisation of the *Syn1-cre* line concluded that there was no Cre expression in astrocytes as no colocalization of Cre reporter immunofluorescence with GFAP the astrocyte marker was detected (Zhu *et al*, 2001). Astrocytes make up only 15% of all glial cells in the brain (Blue Brain Cell Atlas: bbp.epfl.ch/nexus/cell-atlas/). Quantification of the flow cytometry data suggests that almost the same proportion of neurons and non-neuronal cells express Cre in the *Syn1-cre* line (23.8%) and 65.5% of non-neuronal cells express Cre in the *Snap25-IRES2-cre* line.

MeCP2 re-activation experiments where the *Mecp2*^{Stop} allele is conditionally reactivated in a neuronal subtype or brain region has largely shown that MeCP2 is required throughout the brain and the degree of phenotypic reversal of the RTT-like phenotype correlates with the proportion of neurons expressing functional MeCP2 (discussed in Chapter 1 section 1.2.5). If the elimination of the MeCP2-deficient neurons by ablation was to ameliorate the RTT-like phenotype (similarly to the effect of restoring MeCP2 in these neurons) then it is likely that ablating *Syn1-cre* expressing neurons will only partially rescue the RTT-like phenotype whereas the *Snap25-IRES2-cre* line would lead to more widespread removal of the dysfunctional neurons, and a more complete phenotypic rescue. Having said that, a large proportion of the Cre-negative neurons in the *Syn1-cre* brain will be cerebellar neurons shown to be largely devoid of Cre expression. The MeCP2 expression level is significantly lower in the cerebellum than other brain regions (Ross *et al*, 2016), and conditional knock-out (cKO) of *Mecp2* in the cerebellum has relatively mild phenotypic consequences compared to other cKO models (Achilly *et al*, 2021). Consequently, Cre expressing

neurons in the *Syn1-cre* line might contribute to the RTT-like phenotype more than expected based on the percentage of total neurons which express Cre. An interesting experiment to do to compliment this project would be to reintroduce MeCP2 expression in the *Mecp2*^{Stop} line using the *Syn1-cre* and *Snap25-IRES2-cre* to compare the degree of phenotypic rescue in these models. If *Syn1-cre* mediated reactivation was to significantly rescue the phenotypic severity in the *Mecp2*$^{Stop/+}$ heterozygote, using this line for *in vivo* ablation experiments might be advantageous due to the smaller overall number of DTR-susceptible neurons and therefore, extent of induced cell death.

There is the high chance that the outcome of widespread neuronal ablation of 50% neurons (and a proportion of glia) using the pan-neuronal *SNAP25-IRES2-cre* driver to activate the DTR expression, is too much of an insult for the brain to tolerate. Although as mentioned above the higher the proportion of neurons expressing functional MeCP2 the greater the phenotypic rescue, the reintroduction of MeCP2 expression in GABAergic interneurons on the *Mecp2*-null background or heterozygous background using the *Viaat-cre* driver line, rescues many of the RTT-like phenotypes (Ure *et al*, 2016). Conversely, GABAergic *Mecp2* conditional knock-out mice have a severe *Mecp2-null* like phenotype (Chao *et al*, 2010). The phenotype of *Viaat-cre,Mecp2*$^{loxP/+}$ heterozygous females were not addressed in this study. The *Viaat-cre* driver line (also known as *Slc32a1-cre*) was generated by the genomic insertion of a bacterial artificial chromosome (BAC) containing the *cre* transgene expressed from the vesicular inhibitory amino acid transporter (*Viaat*)(also known as *Slc32a1*) promoter (Chao *et al*, 2010). *Viaat* encodes the transporter protein which loads GABA and glycine neurotransmitters into synaptic vesicles (Chaudhry *et al*, 1998; Wojcik *et al*, 2006). The integrated BAC contains the 77.5 kb upstream and 23 kb downstream of the *Viaat* locus to ensure inclusion of all the regulatory elements of *Viaat* promoter (Chao *et al*, 2010).Characterisation of Cre activity in the *Viaat-cre* line using a Cre-dependent fluorescence reporter gene RosaR-eYFP (where eYFP is enhanced yellow fluorescent protein) found there to be 98% colocalization between GABA and YFP (Chao *et al*, 2010). There was no colocalization with glial fibrillary acidic protein (GFAP) the astrocyte marker protein. GABAergic inhibitory neurons account for only ~20% of all neurons in the brain (Erö *et al*,

2018)(bbp.epfl.ch/nexus/cell-atlas). The DTR-mediated ablation of 10% of neurons (half of all inhibitory neurons) using the *Viaat-cre* driver might have a greater chance at being tolerated compared to 50% of all neurons (*Snap25-IRES2-cre* expression neurons) and still have a phenotypic benefit in the heterozygote. The flexibility of this system means that the consequence of ablation of ~50% of a neuronal subtype can be explored in future experiments.

5.3.1 Outstanding questions regarding the Cre expression in Syn1-cre and Snap25-IRES2-cre mice

An important question not assayed here is the developmental trajectory of *cre* expression in each of these lines. In ablation experiments, the onset of Cre expression and subsequent DTR activation will define the earliest developmental time point that neurons will be susceptible to DT. Other groups have addressed this for the *Syn1-cre* line and found that LacZ Cre reporter activation was detectable in the brain, spinal cord and Dorsal Root Ganglion (DRG) from E12.5 onwards (Zhu et al, 2001). Cre activity was distributed in differentiated neurons outside the ventricular regions of the brain and spinal cord. These data are consistent with the pattern of endogenous *Syn1* gene expression (Melloni & DeGennaro, 1994). According to *in situ* hybridisation histochemistry in the rat, the onset of expression of endogenous *Syn1* mRNA coincides with the commitment of neural stem cells to terminal differentiation (Melloni & DeGennaro, 1994). The onset and pattern of *Snap25-IRES2-cre* expression during development has not been reported. Endogenous *Snap25* expression can be detected in E15 rat embryos at low levels (Oyler *et al*, 1991), but earlier time points were not assessed. SNAP-25 is thought to have a role in axon growth, dendritic arborization as well as the formation and function of synapses (Osen-Sand *et al*, 1996, 1993; Grosse *et al*, 1999), implying that it is expressed relatively early in neuronal differentiation. The mRNA abundance increases during postnatal brain development, with the largest increase occurring between birth and postnatal day 5 (Oyler *et al*, 1991). SNAP-25 protein levels were 12-fold higher in the adult compared to the embryonic brain. Brain development is a protracted process with different brain regions developing and maturing at different rates. The onset of Cre expression in both the *Syn1-cre* and

Snap25-IRES2-cre lines will follow the time course of development of each brain region.

Although Cre expression is largely restricted to the brain according to the analysis done here, Cre expression in outstanding peripheral tissues that have not been analysed so far cannot be ruled out. Despite endogenous Synapsin-1 protein expression being largely restricted to the neurons (De Camilli *et al*, 1990), very low levels of expression has been reported in small populations of non-neuronal cells including pancreatic ß cells, osteoblasts, epithelial cells, and astrocytes in culture (reviewed in Cesca *et al*, 2010). SNAP-25 protein has been reported to be expressed in some non-neuronal tissues including endocrine cells such as adrenal medullary chromaffin cells and pancreatic ß cells, which use similar exocytosis machinery to neurons (Roth & Burgoyne, 1994; Jacobsson *et al*, 1994). It will need to be determined whether recombination in the non-neuronal tissues not assayed here for either line is substantial and whether it would have deleterious phenotypic outcomes if the driver where to be used for DT-ablation experiments.

Further work to characterise the extent of expression of *Snap25-IRES2-cre* in glia would be beneficial. Immunostaining brain sections to assess the colocalization of Cre-reporter and different glial cell markers would be the most appropriate way to assess this. An ubiquitously expressed Cre reporter with strong expression in every cell would be better than the $Mecp2^{Stop}$ Cre reporter to analyse Cre reporter expression in glia, as the low expression of *Mecp2* in glia makes it difficult to reliably identify activated and stopped cells.

In conclusion, two pan-neuronal Cre driver lines were characterised to determine which of them would be the most appropriate line to use to activate the DTR expression in neurons when combined with the $Mecp2^{FLExDTR(OFF)}$ allele. The *Snap25-IRES2-cre* driver line was identified to be superior to the *Syn1-cre* line for pan-neuronal expression. Cre is expressed in the majority of neurons in the *Snap25-IRES2-cre* line, whereas, Cre is expressed in a proportion of neurons in the *Syn1-cre* brain with some regions having sparse expression. Although Cre is expressed in some glial cells in both lines (the extent of which needs further investigation) Cre expression is largely restricted to the brain. The higher the proportion of neurons expressing Cre, the greater

the chance of phenotypic rescue (if removal of MeCP2– neurons ameliorates the neurological phenotype). Additionally, the more widespread the DTR expression the greater the likelihood to detect cell ablation following DT administration. For these two reasons the *Snap25-IRES2-cre* transgene was chosen for the preliminary *in vivo* ablation experiment discussed in the following chapter.

Chapter 6 Preliminary *in vivo* neuronal ablation experiments and future work

6.1 Introduction

So far, I have discussed the generation and characterisation of the novel mouse line *Mecp2*$^{FLExDTR(OFF)}$ which facilitates Cre-dependent expression of the Diphtheria Toxin Receptor (DTR) from the endogenous *Mecp2* locus, in place of the *Mecp2* gene, so that the DTR expression is linked to the *Mecp2* knock-out allele. Due to random X-inactivation, in females heterozygous for the *Mecp2*$^{FLExDTR(OFF)/+}$ allele who inherit a *cre* transgene, the DTR will be expressed in cells which: 1) have the *Mecp2*$^{FLExDTR(ON)}$ allele on the active X-chromosome, and 2) express Cre recombinase. The chosen transgenic Cre driver line determines the cell-type specificity of DTR expression and the timing of administration of DT controls the timing of ablation. I have shown that in male hemizygous *Mecp2*$^{\Delta}$*DTR*$^{FLEX/y}$ OFF mice (that do not carry the *cre* transgene), the DTR expression is completely silenced, mice are insensitive to a high dose of DT and as expected due to being *Mecp2* knock-outs they develop RTT-like phenotypes.

Due to the slow nature of mouse experiments and the various hurdles to be overcome whilst tackling this ambitious project including: remaking of the DTR knock-in mouse line to fix the problem with sensitivity to DT in the uninduced state; the slow process of gaining approval to work with Diphtheria Toxin; and of course, the devastating COVID-19 pandemic which halted mouse work for a number of months; only a preliminary *in vivo* ablation experiment using the *Mecp2*$^{FLExDTR(OFF)}$ line was achieved within the PhD timeframe. This chapter discusses the first attempt at neonatal *in vivo* ablation of MeCP2– neurons in heterozygous *Mecp2*$^{FLExDTR(OFF)/+}$*,Snap25-IRES2-cre* mice and suggests further experiments which could follow on from this analysis.

6.2 *In vivo* ablation during neonatal development

The experimental timeline of the first attempt at neuronal ablation during neonatal development is outlined in Figure 6.2.1. The objective was to administer DT to new-born pups, to induce DT-mediated ablation of neurons, then monitor them closely to

see if their neurological function was intact. Following weaning, the pups were genotyped to determine whether the expected genotypes were present. Tissues were collected from a subset of mice to analyse the cellular composition of the brain to determine if substantial ablation had occurred, shown by a higher proportion of MeCP2+ cells (cells expressing the WT *Mecp2* allele from the active X-chromosome) relative to MeCP2– cells (cells expressing the *Mecp2* knock-out, DTR knock-in allele from the active X-chromosome). If significant ablation had occurred, mice would undergo phenotypic scoring to assess their neurological function and whether the RTT-like phenotype was rescued in the $Mecp2^{FLExDTR(OFF)/+}$,*cre*+ mice. Female mice heterozygous for an *Mecp2* knock-out allele start to develop phenotypes from around 3 months onwards (Guy *et al*, 2001; Chen *et al*, 2001), therefore, the cohort of DT treated mice and untreated controls would be scored for activity, gait, hind-limb clasping, breathing, tremor and general condition using the scoring protocol established in the Bird lab (Guy *et al*, 2007), from 3 months up to 1 year old.

DT was administered to offspring of *Snap25-IRES2-cre* x $Mecp2^{\Delta}DTR^{FLEX/+}$ crosses at postnatal day 0-2. We ensured that only female pups were injected to avoid to potential lethality of hemizygous $Mecp2^{\Delta}DTR^{FLEX/y}$,*cre* males (who express the DTR in 100% of neurons). As we are unable to genotype pups before weaning, in an attempt to achieve sufficient numbers of each genotype, 36 female pups from timed mating's of 10 breeding pairs were injected. The expected frequency of $Mecp2^{FLExDTR(OFF)/+}$,*cre* pups is 1/4 of all females, so we aimed for roughly 9 pups of this genotype. A single dose of 30 µg/kg DT via subcutaneous injection was administered to induce ablation of recombined $Mecp2^{FLExDTR(ON)}$ cells which express both Cre and the DTR. This exact dose regime was used in another study to ablate granule cell precursors in the developing cerebellum (Wojcinski *et al*, 2017). For our experiment, subcutaneous P0-2 injections were carried out by Jim Selfridge.

Injected pups were monitored closely for signs of neurological dysfunction by the animal facility technicians. We used pink colouration which indicates normal respiratory and cardiovascular systems, as well as, presence of a milk spot which is a sign of suckling, to indicate intact neurological function. No pups showed any signs of neurological dysfunction following the injection and the majority of pups developed

to >5 weeks old with no health concerns and normal weight gain. Three pups died following injection with no signs of adverse health before death. Only one of these pups had the susceptible genotype: *Mecp2*$^{FLExDTR(OFF)/+}$,*cre*, the other two were WT for *Mecp2*. Genotyping the cohort at weaning revealed all the expected genotypes with no notable differences in the genotype ratios (Figure 6.2.2). Two *Mecp2*$^{FLExDTR(OFF)/+}$,*cre* mice died post-weaning (and genotyping), one from unknown cause, while the other had to be culled because of elongated teeth. At 5 weeks the entire cohort plus un-injected controls were scored using the RTT scoring system (Guy *et al*, 2007). No mice scored positively for a neurological phenotype. Following scoring and weighing, a subset of mice were culled and brains were weighed and harvested along with other tissues. From these weights it seemed as though 2 out of 3 of the DT injected *Mecp2*$^{FLExDTR(OFF)/+}$,*cre* brains were notably smaller than the other genotypes (approximately 18% smaller than the un-injected *Mecp2*$^{FLExDTR(OFF)/+}$,*cre* brains) (Figure 6.2.2). The reduced brain weight did not correlate with reduced body weight. As there was only n=3 of each genotype and only two out of three showed this effect, the significance of this finding was unclear. At week 7, 18 more DT injected mice were weighed and harvested, the difference in brain weights were not as striking when more mice were analysed two weeks later. Brains of *Mecp2*$^{FLExDTR(OFF)/+}$,*cre* mice injected with DT were on average slightly smaller than other genotypes, however, there were no un-injected control mice of the same genotype (*Mecp2*$^{FLExDTR(OFF)/+}$,*cre)* left at this time point to compare to the DT-injected mice, so the slight reduction in brain weight at this stage could be associated with this genotype and be independent of DT treatment. The body weights of the *Mecp2*$^{FLExDTR(OFF)/+}$,*cre* injected mice were not reduced compared to controls. In conclusion, there were no striking differences in survival or phenotype of *Mecp2*$^{FLExDTR(OFF)/+}$,*cre* mice following DT injection compared to injected littermate controls and uninjected *Mecp2*$^{FLExDTR(OFF)/+}$,*cre* mice. At this stage, the phenotypic analysis suggested that either ablation had worked and caused no adverse neurological phenotypes or ablation had not worked or worked inefficiently.

In order to investigate whether ablation of MeCP2– neurons had occurred in these mice, flow cytometry analysis was used to assess the ratio of MeCP2+ versus MeCP2– neurons in 5 week old brains following DT injection at ~P1 (Figure 6.2.3). Nuclei were

extracted from brain tissue of DT-treated and untreated mice, stained for MeCP2 and NeuN and analysed by flow cytometry. If a substantial amount of neuronal ablation of the DTR+, MeCP2– neurons had occurred I would have expected to see a significant increase in the proportion of neuronal nuclei (high NeuN) expressing MeCP2 (MeCP2+) compared to the proportion of MeCP2– neuronal nuclei. Unfortunately, there was not a significant shift toward MeCP2+ nuclei in the *Mecp2*$^{FLExDTR(OFF)/+}$*,cre* DT injected mice compared to the controls (Figure 6.2.3). The ratios of MeCP2– to MeCP2+ neurons were variable for all of the heterozygous brains analysed, it was not 50:50 for all heterozygous brains as one might expect if X-inactivation is random. The MeCP2 and NeuN staining pattern was also variable and needed optimisation (Appendix Figure 10.). The variability of staining suggested that subtle effects of ablation might be difficult to see using this flow cytometry protocol, however, substantial skewing of NeuN high nuclei like a 90:10 ratio of MeCP2+ to MeCP2– nuclei should be clear.

An important variable to consider when attempting to ablate neurons during brain development is how widespread the Cre recombinase activity is in the developing brain prior to DT injection at ~P1. DT will only ablate those neurons which express Cre and have activated the DTR expression before DT injection. If Cre is active in particular brain regions at a later stage in postnatal development, developing neurons in these regions would evade ablation as would activate the DTR expression after DT has been and gone. This would give the impression that DT-ablation had been inefficient at ~P1 but actually neurons yet to express Cre would not have been susceptible to DT (not killable) at ~P1. As discussed in Chapter 5 the activity of Cre in the *Snap25-IRES2-cre* line during development has not been fully characterised. To determine the frequency of recombination at the time of DT injection, I performed Southern blot analysis on the single *Mecp2*$^{FLExDTR(OFF)/+}$*,Snap25-IRES2-cre* pup which died on P4, 2 days after DT injection (Figure 6.2.2). A band produced corresponding to the expected recombined product, showed that there were cells which should express the DTR. At 6 weeks old, the Cre recombination frequency of the Cre reporter allele in whole brain of *Mecp2*^{mCherryStop}*,Snap25-IRES2-cre* mice was ~65% (Chapter 5 section 5.2.3). Due to the proximity of the band corresponding to the WT *Mecp2* allele and the unrecombined *Mecp2*$^{FLExDTR(OFF)}$ allele, I can't reliably quantify the recombination

frequency at P4, however, a rough estimate is ~30%. This shows that at ~P1, Cre-recombination has not occurred in as high a proportion of neurons as in the adult brain. Cre recombination has been shown to occur on both the inactive and active X-chromosome (Chapter 4 Figure 4.5.2), therefore, the recombined proportion of cells quantified by Southern blot includes cells will have the *Mecp2*$^{FLExDTR(ON)}$ allele on the inactive and active X-chromosome. If we assume a 50:50 X-inactivation ratio then only 15% of the recombined cells would have the *Mecp2*$^{FLExDTR(ON)}$ allele (i.e DTR knock-in, *Mecp2* knock-out allele) on the active X-chromosome at ~P1. Southern blot analysis of DNA extracted from a single *Mecp2*$^{FLExDTR(OFF)/+}$*,Snap25-IRES2-cre* pup suggests that at ~P1 roughly 15% of cells in the brain had activated the DTR expression and were potentially sensitive to DT.

A caveat to the conclusions drawn from the Southern blot analysis is that the DNA analysed was extracted from a DT-injected pup who could have lost a proportion of the *Mecp2*$^{FLExDTR(ON)}$ expressing cells due to DT-mediated ablation. Elimination of a significant proportion of the *Mecp2*$^{FLExDTR(ON)}$ expressing cells would lead to a reduction in the signal intensity of the recombined band on the Southern blot. This provides an alternative hypothesis to that suggested above that the lower intensity of the recombined band reflects the lower Cre-recombination frequency in the ~P1 brain compared to the adult. The absence of significant depletion of MeCP2– neurons at 5 weeks post DT injection suggests this significant ablation at ~P1 did not occur. Additionally, DT-induced neuronal death has been suggested to be a delayed process that takes place for 4-7 days (Petrenko *et al*, 2015). This implies that any dying neurons would not have been cleared in the time between DT injection and death for the pup analysed by Southern blot.

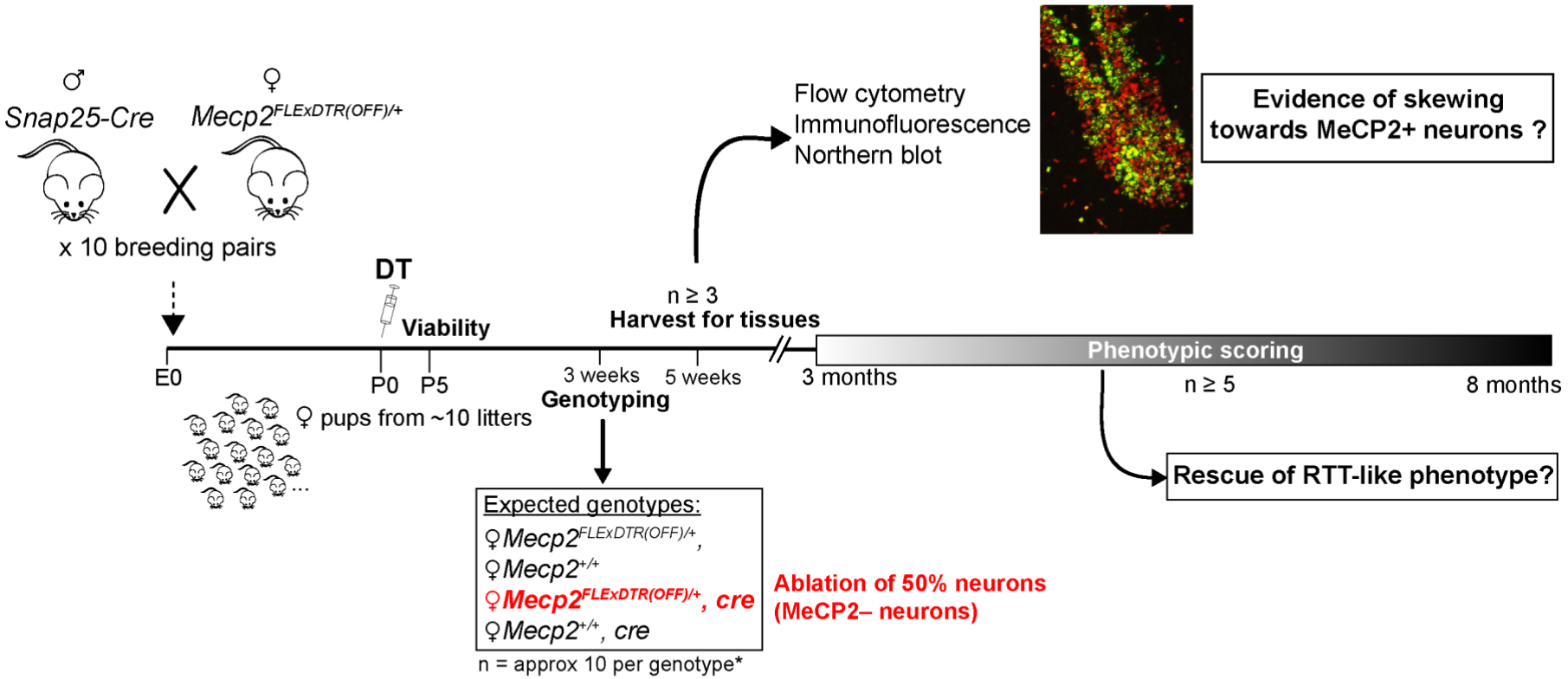

Figure 6.2.1 *In vivo* ablation of MeCP2– neurons of *Mecp2*$^{FLExDTR(OFF)/+}$*,Snap25-IRES2-cre* mice during neonatal development. Schematic representation of the experimental timeline for *in vivo* ablation during early postnatal development. Female pups from 10 litters were injected at P0-2 with a single injection of 30 µg/kg DT via subcutaneous injection. Pups were closely monitored for neurological function and only allowed to develop beyond P5 if no overt signs of ill health were observed. At 3 weeks of age pups were weaned and genotyped from ear biopsies. At 5 weeks n=3 of each genotype were culled and tissues were collected in order to study the cellular composition of the brain. As we didn't detect any evidence of significant cell ablation the experiment was terminated at 7 weeks. If sustantial ablation had occured and we had a sufficient number of each genotype, the experimental cohort would have been continued to be monitored and phenotypic scoring perfomed from 3 months onwards (when *Mecp2*$^{+/-}$ heterozygous females usually start to develop RTT-like phenotypes). This would determine whether removal of MeCP2– neurons from the developing heterozygous brain prevents these mice from developing RTT-like phenotypes.

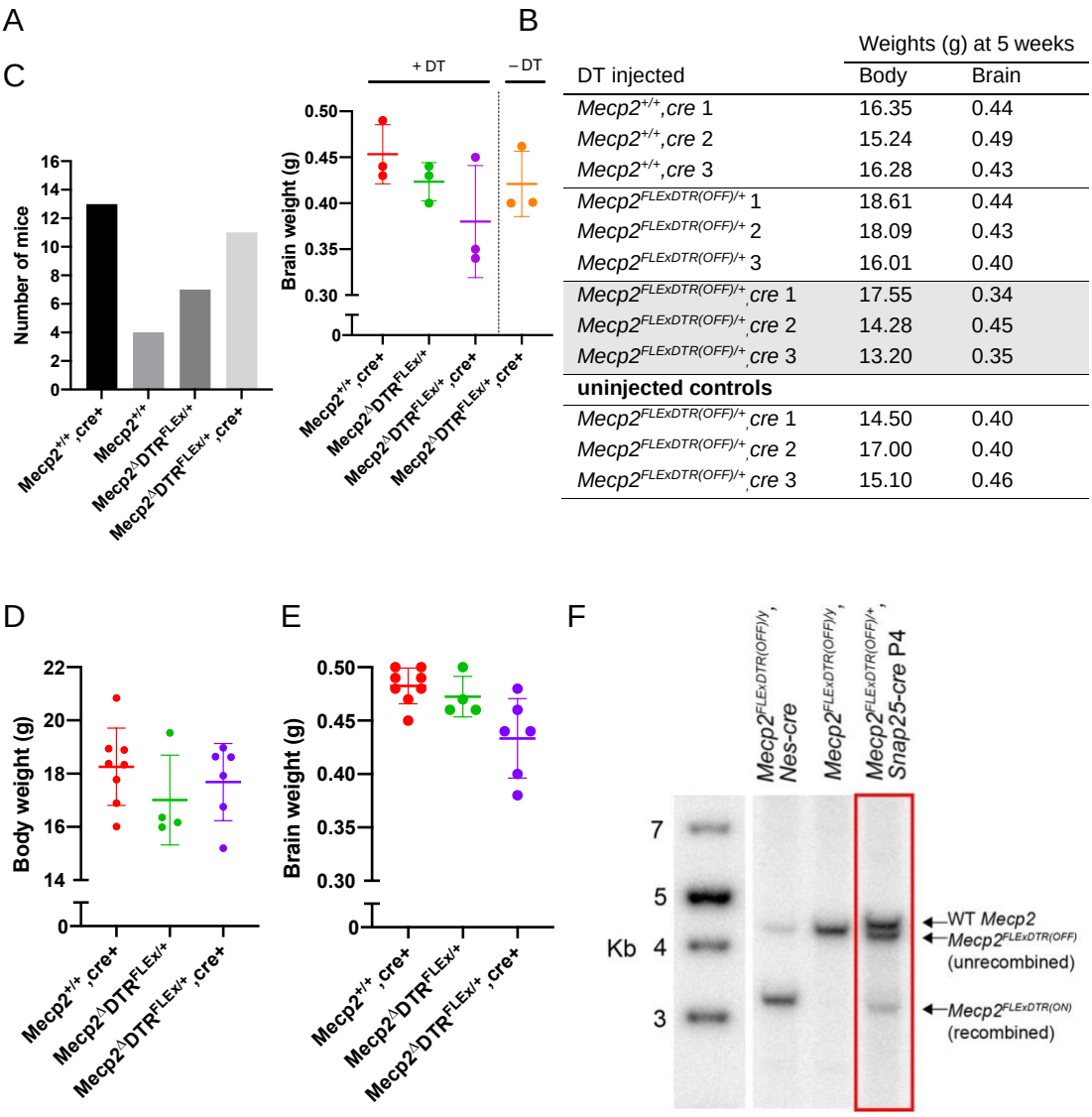

DT injected	Weights (g) at 5 weeks	
	Body	Brain
Mecp2$^{+/+}$,*cre* 1	16.35	0.44
Mecp2$^{+/+}$,*cre* 2	15.24	0.49
Mecp2$^{+/+}$,*cre* 3	16.28	0.43
Mecp2$^{FLExDTR(OFF)/+}$ 1	18.61	0.44
Mecp2$^{FLExDTR(OFF)/+}$ 2	18.09	0.43
Mecp2$^{FLExDTR(OFF)/+}$ 3	16.01	0.40
Mecp2$^{FLExDTR(OFF)/+}$,*cre* 1	17.55	0.34
Mecp2$^{FLExDTR(OFF)/+}$,*cre* 2	14.28	0.45
Mecp2$^{FLExDTR(OFF)/+}$,*cre* 3	13.20	0.35
uninjected controls		
Mecp2$^{FLExDTR(OFF)/+}$,*cre* 1	14.50	0.40
Mecp2$^{FLExDTR(OFF)/+}$,*cre* 2	17.00	0.40
Mecp2$^{FLExDTR(OFF)/+}$,*cre* 3	15.10	0.46

Figure 6.2.2. Genotypes, brain and body weights of mice following DT injection at ~P1. A) Numbers of mice of each genotype at weaning (~P20). B) Brain weights at 5 weeks of age. Each dot represents a mouse. Line: mean; error bars: SD. C) Table showing that the lower brain weights at 5 weeks do not correspond to a lower body weight. D) Brain weights at 7 weeks of age. E) Body weights at 7 weeks of age. B,D,E) Each dot represents a mouse. Line: mean; error bars: SD. F) Southern blot analysis on DNA extracted from the brain of *Mecp2*$^{FLExDTR(OFF)/+}$,*cre* P4 pup found dead following DT injection at P2 (red box). The upper band for this sample corresponds to the WT *Mecp2* allele, the band below that is the unrecombined *Mecp2*$^{FLExDTR(OFF)}$ allele, and the bottom band is recombined *Mecp2*$^{FLExDTR(ON)}$ allele. The lanes to the left correspond to DNA samples analysed for a separate experiment which act as controls for the size of *Mecp2*$^{FLExDTR(OFF)}$ unrecombined (upper) and *Mecp2*$^{FLExDTR(ON)}$ recombined (lower) bands. Lane 1) DNA from male *Mecp2*$^{FLExDTR(OFF)/y}$,*Nes-cre* 6 week old mouse (recombination in ~80% of the brain). Lane 2) DNA from male *Mecp2*$^{FLExDTR(OFF)/y}$ 6 week old mouse (recombination in 0% of the brain).

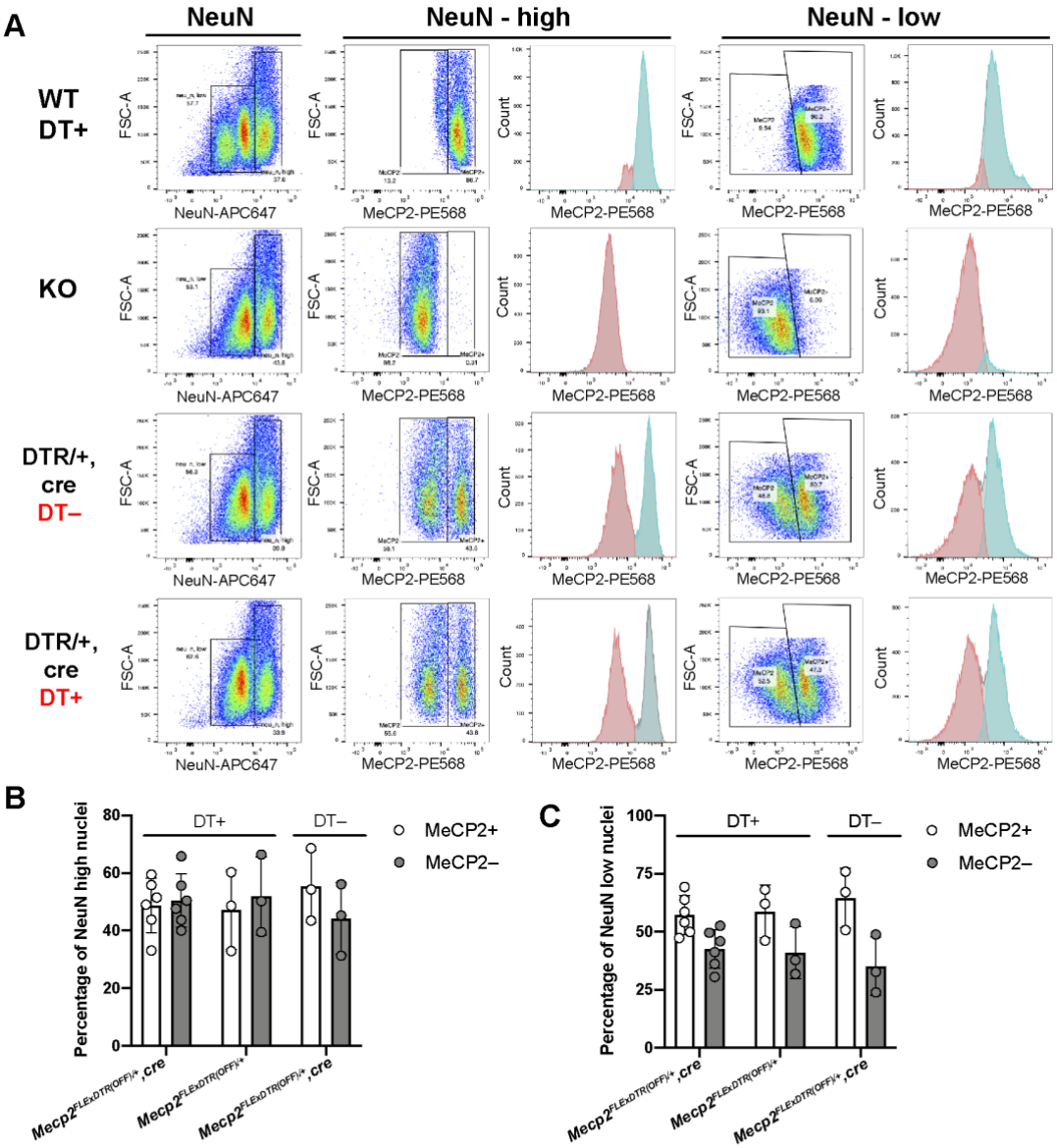

Figure 6.2.3 There was no significant skewing towards MeCP2+ neurons in the *Mecp2*$^{FLExDTR(OFF)/+}$*,Snap25-IRES2-cre* brain at 5-7 weeks following a single DT injection of 30 µg/kg at ~P1. A) Flow cytometry analysis of nuclei extracted from mouse brains stained with fluorescently labelled MeCP2 and NeuN antibodies. Representative plots showing the gating strategy used to identify the proportion of NeuN-high neuronal nuclei, and NeuN-low non-neuronal nuclei which have high or low MeCP2 expression, therefore expressing the WT or knock-out *Mecp2* allele respectively. Genotypes are as follows: WT: *Mecp2*$^{+/+}$ female; KO: *Mecp2*$^{-/y}$ knock-out hemizygous male*; DTR/+,cre*: *Mecp2*$^{FLExDTR(OFF)/+}$*,Snap25-IRES2-cre* heterozygous female. Intact, single nuclei were gated and analysed for their NeuN expression (panel 1: y axis: Forward Scatter FCS-A; x axis: NeuN-APC647 fluorescence). The NeuN-high (panel 2 and 3) and NeuN-low (panel 4 and 5) populations were then gated and analysed for MeCP2-PE568 fluorescence. Panel 2 and 4: Cell density plots: y axis: FCS-A; x axis: MeCP2-PE568. Panel 3 and 5: Histograms of cell count (y-axis) against MeCP2-PE568 (x-axis). The gated MeCP2+ and MeCP2– populations from panel 2 and 4 are overlayed on the histograms: blue: MeCP2+; red: MeCP2–; grey: NeuN-high/NeuN-low. B) and C) Bar charts showing the proportion of NeuN-high (B) and NeuN-low (C) nuclei which are within the MeCP2+ (white) or MeCP2– (grey) gate for each genotype. Each dot represents a single mouse. Bars: mean. Error bars: standard deviation.

6.3 Discussion

The conclusions of the preliminary neonatal *in vivo* neuronal ablation experiment are as follows: at 5 weeks following a single subcutaneous injection of 30 µg/kg of DT at P0-2, *Mecp2*$^{FLExDTR(OFF)/+}$*,cre+* mice showed no signs of overt neurological phenotypes and had no substantial skewing towards MeCP2+ neurons in the brain. It was unclear whether any ablation of MeCP2– neurons had occurred.

One explanation for the lack of significant removal of target cells is that the DT administration did not efficiently induce neuronal ablation. The dose of DT via systemic delivery could have been too low to achieve efficient ablation of enough neurons to see an effect on skewing. We know that this dose has been used previously to efficiently ablate granule progenitor cells in the developing cerebellum (Wojcinski *et al*, 2017). Another study has achieved ~85% ablation of a discrete neuronal subset (AgRP/NPY neurons) in P1 pups following a single subcutaneous injection of 50µg/kg DT (Luquet *et al*, 2005). Another toxin related possibility is that the DT used for injection was inactive. DT is very sensitive to freeze thaw cycles. Stock solutions of DT were aliquoted and care was taken to only thaw the toxin once prior to dilution. Furthermore, other aliquots of the same batch, prepared and stored under the same conditions were shown to induce cell death in culture. Unfortunately, there is no positive control for activity and delivery of DT where there is a clear expected outcome. Optimisation of the DT regime moving forward will be needed to try and achieve significant ablation of neurons during early postnatal brain development.

The second explanation is that Cre recombinase activity was not widespread enough at the time of DT injection to allow substantial neuronal ablation. The Southern blot analysis on DNA extracted from brain tissue from a single *Mecp2*$^{FLExDTR(OFF)/+}$*,Snap25-IRES2-cre* P4 pup showed that there was a large proportion of neurons yet to express Cre recombinase and activate the DTR at P1 and so would have been resistant to DT-ablation. It is difficult to determine whether ablation of the proportion of neurons which had activated the DTR expression would have had a significant effect on the X-inactivation ratio when assessed in the 5 weeks old brain. Especially, if coupled with inefficient DT delivery or action.

6.3.1 Next steps for in vivo ablation experiments in Mecp2$^{FLExDTR(OFF)/+}$,Snap25-IRES2-cre mice

The lower recombination frequency at P1 compared to the adult brain likely reflects the expression pattern of *Snap25* and the developmental trajectory of the mouse brain during postnatal development. As discussed in the previous chapter (section 5.3.1), endogenous SNAP-25 has a role in axonal growth and dendritic arborisation and is upregulated during synaptogenesis (Osen-Sand *et al*, 1996, 1993; Grosse *et al*, 1999; Oyler *et al*, 1991). *Mecp2* (and as extension *Mecp2*$^{FLExDTR(ON)}$) is also upregulated during postnatal-development (Shahbazian *et al*, 2002a; Skene *et al*, 2010). A period of intense synaptogenesis occurs in the first 3 postnatal weeks in rodents, peaking in week 2 (Cizeron *et al*, 2020; Semple *et al*, 2013; Chen *et al*, 2017). There is considerable heterogeneity in the developmental trajectory of different brain regions which mature at different rates. In some regions such as the hippocampus, cerebellum and olfactory bulb neurogenesis is still active until 2-3 weeks after birth. Granule cell precursors (GCP) in the developing cerebellum undergo massive proliferation, peaking at ~P8 in mice (Fujita *et al*, 1966; Fujita, 1967; Sillitoe & Joyner, 2007). The migration and maturation of granule cell neurons is complete by P20. Granule cell neurons are the most numerous neuronal cell type in the brain. Immature neuronal precursors yet to activate *Snap25-IRES2-cre* expression and upregulate *Mecp2*$^{FLExDTR(ON)}$ will evade DT-ablation when administered at ~P1. In addition, any precursor proliferation occurring after DT-injection would give rise to neurons with random X-inactivation, therefore, replacing the lost MeCP2– neurons with MeCP2+ and MeCP2– neurons. The susceptibility of neurons to DT-induced cell death will track the maturation gradients in the brain with differentiating neurons becoming increasingly sensitive to DT as they upregulate both the *Snap25-IRES2-cre* and *Mecp2*$^{FLExDTR(ON)}$ genes.

A good next step would be to analyse brain regions of DT injected *Mecp2*$^{FLExDTR(OFF)/+}$,*Snap25-IRES2-cre* by immunofluorescence to determine whether ablation did occur in earlier born regions, shown by a higher proportion of MeCP2+ cells in these regions. I had a first attempt at this but the antibody staining of the brain sections was not of sufficient quality to quantify MeCP2+ and MeCP2– neurons.

Mosaic expression was detectable in areas of the hippocampus and cortex. Another method to assess ablation in different brain regions would be to perform flow cytometry on dissected brain regions to see if the skewing is more significant when looking at isolated regions. For example earlier matured cortex versus later matured cerebellum.

In future ablation experiments using *Mecp2*$^{FLExDTR(OFF)/+}$*,Snap25-IRES2-cre* mice, more DT injections throughout the first week of postnatal development might be needed to achieve efficient ablation of MeCP2– neurons. If the susceptibility of neurons to DT was to occur in a gradient throughout the developing brain, this could facilitate a way of removing neurons more gradually as they reach a certain level of maturity by administering DT at staggered times during early postnatal development. Going forward with this project, characterising the developmental trajectory of Cre recombination during neonatal development would be useful, but experimentally non-trivial. This could be achieved by analysing the pattern of *Mecp2*^{mCherryStop} Cre-reporter expression, activated by *Snap25-IRES2-cre* (see Chapter 5 for details), in brain sections at different time points during early postnatal development.

6.3.2 Improving the assay for ablation of MeCP2– neurons

To improve the ability to distinguish MeCP2–, DTR+ cells and MeCP2+, DTR– cells in the heterozygous brain, endogenous expression of fluorescent reporter proteins would be ideal, to remove the variability associated with antibody-labelling. When originally designing this MeCP2– cell ablation system I wanted to have a fluorescent protein to report the expression of the DTR. In the first line generated, the *Mecp2*^{StopDTR} line, I inserted a P2A self-cleaving peptide and the enhanced GFP (EGFP) protein coding sequence (with an NLS) following the DTR, to mediate bicistronic expression of nuclear EGFP with the transmembrane DTR protein (See Chapter 3 for details). Visualising neurons in the brain is made easier with a reporter protein localised to the nucleus. Disappointingly the EGFP was not detectable in recombined cells making it useless as a reporter protein, therefore, in the subsequent *Mecp2*$^{FLExDTR(OFF)}$ line, the reporter protein was not included. Instead the proposed method to identify DTR+ cells was to identify MeCP2– cells in the heterozygous brain as the DTR is expressed from

the KO allele. In future experiments we could combine the *Mecp2*$^{FLExDTR(OFF)}$ allele with a line where WT MeCP2 is tagged with a fluorescent protein (GFP or mCherry). Cells expressing the WT MeCP2 from the active X will be GFP or mCherry positive and the cells expressing the DTR from the *Mecp2* KO allele will be GFP or mCherry negative. Flow cytometry analysing endogenous fluorescence would give more reliable data on whether there is a higher proportion of MeCP2+ neurons following DT-mediated ablation as it would not rely on antibody staining. Likewise, endogenous fluorescence of MeCP2-GFP/mCherry can be analysed in brain sections to determine the mosaic distribution of neurons.

6.3.3 Proof-of-principle in vivo ablation in peripheral tissues

Unfortunately, I am yet to show evidence of *in vivo* cell ablation using the inducible *Mecp2*$^{FLExDTR(OFF)}$ mouse line. To get an idea of whether *in vivo* ablation can be achieved using this system, rather than ploughing ahead to try to address the phenotypic outcome of DT treatment, we could focus on testing the system by assaying for markers of apoptosis in brain sections in the days following DT injection. The functionality of the system could be tested by inducing ablation in a peripheral tissue, where DT delivery is efficient and tissue damage is straightforward to assess. This was done in methods papers describing the generation and characterisation of novel DT-mediated ablation systems (Saito *et al*, 2001; Buch *et al*, 2005). Saito and colleagues (2001), chose to model their system in hepatocytes, because hepatocyte damage can be easily monitored *in vivo* by histological analysis of liver sections and measurement of aspartate aminotransferase (AST) and alanine aminotransferase (ALT) activities in serum. Buch and colleagues, (2005), ablated T and B lymphocytes by crossing to different lymphocyte-specific Cre driver lines and used flow cytometry to analyse the T to B lymphocyte ratio to assess the efficiency of ablation. Oligodendrocytes, the myelinating glial cells in the brain were also targeted to show efficient ablation of cells in the central nervous system following DT administration (Buch *et al*, 2005). Substantial apoptotic cell death was visualised by TUNEL staining brain sections 3 days following DT administration. Histological analysis of DT-treated mouse brains also revealed severe destruction of myelinated structures throughout the CNS.

As a proof-of-principle experiment to test my ablation system, a Cre driver could be used which targets the DTR expression to a tissue where visualisation of cell death is more straightforward. This would take advantage of the ubiquitous expression of *Mecp2*. The *Albumin-cre* driver line is available in our animal facility and could be used to achieve activation of *Mecp2*$^{FLExDTR(ON)}$ expression specifically in the liver. Efficient delivery of DT to the liver would be achieved easily by IP injection of adult mice. Mice would be sacrificed soon after DT administration to assay for apoptosis markers. Tissue damage can also be assessed by assaying serum AST and ALT levels and also visually by histology of tissue sections as mentioned above (Saito *et al*, 2001). I can assess the proportion of hepatocytes expressing the WT *Mecp2* allele versus the DTR allele. The low expression of MeCP2 in the liver might make it harder to distinguish MeCP2+ and MeCP2– cells. The reduction in DTR expressing cells assayed by *in situ* hybridisation of DTR mRNA or DTR protein in tissue sections, or even by northern blot of RNA extracts from liver tissue can be done. Doses used for cell ablation in the liver will likely not be able to be directly extrapolated to neuronal ablation in the CNS, as DT delivery to the brain is likely less efficient. The DTR expression in neurons is much higher than in the liver and the efficiency of *in vivo* cell ablation has been shown to correlate with the level of the DTR expression (Saito *et al*, 2001).

In conclusion, moving forward with MeCP2– neuron ablation experiments in *Mecp2*$^{FLExDTR(OFF)/+}$*,Snap25-IRES2-cre* mice, the DT injection regime will need to be optimised to achieve efficient ablation of target cells during early postnatal development. It is imperative that we determine whether significant ablation of target neurons occurs following DT-injection before addressing the phenotypic outcome of ablation in the mice. Combining the *Mecp2*$^{FLExDTR(OFF)}$ allele with an X-linked *Mecp2* fluorescent reporter gene would allow more reliable and sensitive quantification of the ratio of MeCP2– to MeCP2+ neurons following DT treatment. The flexibility of the system allows us to perform ablation experiments in peripheral tissues which could be a straightforward way to address whether sensitivity to DT is mediated by Cre recombination *in vivo* in *Mecp2*$^{FLExDTR(OFF)}$ mice.

Chapter 7 Challenges and limitations of the DTR/DT-ablation system and alternative approaches to study the loss-of-function of MeCP2

7.1 Introduction

The cell ablation system chosen to mediate selective ablation of MeCP2-deficient neurons during development in the heterozygous Rett Syndrome (RTT) mouse model was the Toxin-Receptor Cell Knock-out (TRECK) system (Saito *et al*, 2001). To recap, target cells in mice are made susceptible to Diphtheria Toxin (DT) by the cell-type specific expression of the human Diphtheria Toxin Receptor (DTR). Mice are naturally resistant to DT, so are uniquely suited to this ablation tool. DTR expressing cells are selectively ablated upon DT administration to mice via intraperitoneal injection or other delivery routes. Once taken up by DTR expressing cells, DT induces apoptosis by inhibiting protein synthesis.

"As compared to techniques for studying *in vivo* gene functionality, the tools for studying cell functionalities are disparate and technically complex" (Liu *et al*, 2019). There have been many methods developed for targeted ablation of populations of cells, each method has distinct features and limitations. No one method can be universally applied to all cell types in the context of tissue compartments *in vivo*. When starting out on this ambitious project, the DTR/DT-ablation system was an attractive technique to use for inducible, selective ablation of neurons in mice, mainly due to its extensive use in ablating post-mitotic neurons in the CNS, the seemly straightforward way to genetically engineer target cells to be susceptible to cell death and the flexibility of timing of ablation. It soon became clear that the very high toxicity of DT creates challenges for both the experimental procedure and outcomes. The safety aspects of handling and administering the toxin add obstacles which complicate otherwise simple cell culture and mouse experiments. I put together two lengthy risk assessments for using DT in cell culture and administering it to mice (see Appendix Documents 1 and 2). The high toxicity of DT means that even very low levels of off-target DTR expression can lead to toxic effects following DT administration. Generating a leak-proof DTR knock-in allele took up the majority of my time during the PhD. In the first

ESC and mouse line generated (*Mecp2*^{StopDTR}) a transcriptional *Stop* upstream of the DTR coding sequence did not sufficiently suppress the expression of the DTR in Cre-negative cells. Leaky DTR expression led to adverse effects in *Mecp2*^{StopDTR} mice lacking the *cre* transgene. The allele was re-designed and a new ESC and mouse line were generated, namely the *Mecp2*$^{FLExDTR(OFF)}$ line. This time Cre recombination inverted the DTR coding sequence into the sense orientation to activate expression. This method successfully overcame the leaky expression and mediated selective expression of the DTR in Cre+ cells only. With hindsight more attention should have been made at the outset of the project to remove any potential for leaky DTR expression i.e. the FLEx approach should have been adopted from start. *Mecp2*$^{FLExDTR(OFF)}$ mice (with no *cre* transgene) were shown to be resistant to high doses of toxin and *Mecp2*$^{FLExDTR(ON)}$ (activated by Cre recombination) cells in culture were killed following DT-treatment. The *Mecp2*$^{FLExDTR(OFF)}$ line should facilitate the selective ablation of Cre expressing MeCP2– neurons in the heterozygous mouse model, experiments we hope to explore in the future (discussed in Chapter 6).

In this final chapter, I discuss the potential challenges and limitations associated with the DTR/DT-ablation system which may or may not affect future applications of the *Mecp2*$^{FLExDTR(OFF)}$ model. I also suggest alternative approaches to study the consequence of loss-of-function of MeCP2-deficient neurons in the heterozygous mouse model of RTT.

7.2 DTR-mediated neuronal ablation challenges and limitations

7.2.1 Dose-dependent killing using the DTR/DT-ablation system

A limitation of the DTR/DT-ablation technique is thought to be the narrow pharmacological window caused by the extreme toxicity of DT (Liu *et al*, 2019), prohibiting dose-dependent studies. Although WT mice were originally described to be resistant to very high doses of DT (50-100µg/kg (lethal dose in humans 0.1µg/kg))(Saito *et al*, 2001; Cha *et al*, 2003), there have been reports of significant off-target effects and mortality in DT treated mice administered multiple high doses

of toxin, independent of the DTR (Christiaansen *et al*, 2014; Goldwich *et al*, 2012; Luquet *et al*, 2005). Off-target effects of the DT-ablation when using high doses of toxin would muddy the interpretation of the phenotypic outcome of DT treatment. In contrast to these reports, efficient ablation of the target cell population has been frequently reported in DTR/DT-ablation models using lower doses without toxic off-target effects. Furthermore, some models have permitted clear dose-dependent efficiency of on-target ablation, an application which could be desirable moving forward (Buch *et al*, 2005; Chen *et al*, 2005). Targeted low dose stereotaxic injections into the striatum were shown to mediate unilateral ablation of DTR+ neurons when injected into only one striatum, despite bilateral expression of the DTR (Durieux *et al*, 2009). Bilateral injections were shown to lead to complete bilateral ablation of both striata. This study illustrated that controlled ablation of a discrete subset of DTR expressing cells can be achieved following targeted microinjection of a low dose of DT.

The effective dose of DT will differ for each transgenic line and will be dependent on the sensitivity of the target cells and the delivery route of DT. The efficiency of on-target ablation has been shown to correlate with the DTR expression level (Saito *et al*, 2001). In our system, doses administered systemically will need to be higher to achieve sufficient levels of DT in the CNS to achieve neuronal ablation whilst avoiding toxicity in peripheral tissues. The very high expression level of *Mecp2* (and by extension the *Mecp2*$^{FLExDTR(ON)}$ allele) will potentially increase the sensitivity of target neurons to DT which should in turn reduce the effective dose required for efficient ablation. In future *in vivo* ablation experiments, care needs to be taken when choosing a dose regime and appropriate treated control mice should always be included.

7.2.2 Cell ablation during embryogenesis

Originally the aim was to carry out *in vivo* ablation experiments throughout development, however, an underappreciated potential limitation of the DTR-mediated ablation system is the inability to efficiently ablate cells during prenatal development, due to inefficient DT penetration of the placental barrier. There are a few studies which claim to deliver DT to the developing embryo. One achieved targeted cell ablation in

the embryo but used unprecedently high doses of DT administered IP to the mother (Corbeaux *et al*, 2010). Another, delivered DT directly to the embryos by microinjection (Landsman *et al*, 2011).

Activation of the cell-type specific expression of the DT fragment A (DT-A) which contains the catalytic domain only, has been commonly used to remove populations of cells during embryogenesis. One interesting recent study used DT-A-ablation to facilitate neural blastocyst complementation (NBC), which can be used to study the development and function of specific forebrain regions (Chang *et al*, 2018). This involved Cre-activated expression of DT-A in host-derived dorsal telencephalic progenitors, to give rise to a fetus which developed without a forebrain. Injection of donor ESCs into these host transgenic blastocysts expressing DT-A, enabled NBC where donor-derived progenitors populated the vacant forebrain niche in the host embryo. Replacing the DTR within the FLEx switch in the *Mecp2*$^{FLExDTR(OFF)}$ allele with the DT-A, would allow Cre-dependent ablation of the desired cell type during embryogenesis upon the onset of Cre expression. One of the main reasons for using the DTR expression followed by DT administration was to have more control over the timing of ablation and to allow us to ablate neurons later in development. A tamoxifen inducible Cre-ERT fusion transgene could be used to make the DT-A expression temporally inducible, although the lack of a commercially available pan-neuronal Cre-ERT driver limits the use of Cre-dependent DT-A expression to some neuronal subtypes. If future experiments reveal that widespread ablation in neonates is too late in neurodevelopment to be tolerated, we might hypothesise that ablation of neuronal precursors during prenatal development would allow greater plasticity and recovery of brain development. For these experiments another ablation system would likely need to be engineered.

7.2.3 Potential toxic bystander effects of widespread neuronal ablation

A possible outcome of widespread neuronal ablation is toxic effects of cell death on surrounding cells which could mask the potential of the brain for compensatory plasticity or regeneration. Although DT-induced neuronal death is associated with minimal signs of necrotic damage, inflammation and broken blood-brain-barrier

(Petrenko *et al*, 2015; Arruda-Carvalho *et al*, 2011), DT toxicity relies on a strong inhibition of protein synthesis, which has no clinical equivalent. Characterisation of neurons following DT-mediated ablation suggests that cell death occurs through a caspase-independent atypical cell apoptosis process occurring over prolonged period of 4-7 days (Petrenko *et al*, 2015). Alternative cell ablation methods which directly manipulate the intrinsic apoptosis pathway could induce "suicide" of the target cells with few bystander effects. Caspases, a family of cysteine proteases are synthesised as inactive monomeric zymogens (pro-caspases) and execute apoptosis following dimerization (reviewed in Earnshaw *et al*, 1999). Taking advantage of this, "artificial death switches" were constructed: synthetic dimerization systems where pro-caspases are fused to FK506-binding protein (FKBP12) a chemically induced dimerization (CID)-binding site (MacCorkle *et al*, 1998; Steller, 1998; Fan *et al*, 1999). Addition of the lipid-permeable ligands FK506, Rapamycin and their derivatives causes pro-caspase dimerization, activation and induces apoptosis. The complication of using FK506 and Rapamycin *in vivo* is that they can interact with endogenously expressed FKBPs interfering with their pathological functions. These ligands have immunosuppressive and nephrotoxic properties (Finn, 1999; Kolos *et al*, 2018). To negate this problem the second-generation dimerizer, AP20187 (ARIAD Pharmaceuticals) derived from FK1012 (a semi-synthetic dimer of FK506), was engineered to bind to a mutated FKBP12 dimerization domain but not the endogenously expressed WT FKBP12 and thus was pharmacologically inert (Clackson *et al*, 1998). Transgenic mice with localised expression of mutant FKBP12-pro-caspase fusion constructs have been used *in vivo* to ablate a range of cell types (Mallet *et al*, 2002; Pajvani *et al*, 2005; Wang *et al*, 2008; Fujioka *et al*, 2011). A transgenic mouse model which expressed an inducible, dimerize-able Caspase-3 (the key activator of apoptosis) specifically in hepatocytes, achieved dose dependent hepatocyte ablation following injection of a chemical inducer of dimerization (CID) (Mallet *et al*, 2002). Up to 85% ablation of hepatocytes allowed viability and promoted liver regeneration. In contrast, substantial mortality as a result of DTR-mediated hepatocyte destruction has been reported (Saito *et al*, 2001). The dimerize-able Caspase-3 ablation system is an attractive alternative tool for inducible widespread

neuronal elimination with reduced damage to surrounding cells, which could be important for promoting compensatory plasticity.

7.3 Neuronal inactivation as an alternative strategy to study the loss-of-function of MeCP2– neurons

An alternative strategy to *in vivo* elimination is the selective inhibition of cell activities (Liu *et al*, 2019). Selective inhibition of MeCP2– neurons in the CNS would allow the investigation of whether silencing the aberrantly functioning mutant neurons would alleviate their burden on the MeCP2+ neurons around them and improve neurological function.

Neurodevelopment proceeds through an excessive overproduction of neurons and connections followed by considerable refinement through programmed cell death of neurons and synaptic pruning (see section 1.6.1). Abundant evidence supports that neural activity plays an important role in neurodevelopment: spontaneous neuronal activity is critical for early neuronal circuit assembly, and experience-dependent activity is required for the formation and stability of synapses to refine mature circuits (Pan & Monje, 2020; Hua & Smith, 2004). Seminal work of Hubel and Wiesel highlighted the importance of experience-dependent neuronal activity in the neurodevelopment of the visual system. Monocular deprivation (suturing one eye shut) during postnatal development in kittens and monkeys led to an increase in neuronal representation of the normal eye (Wiesel, 1982). This shift in ocular dominance was prevented when neuronal activity in the visual cortex was blocked using the neurotoxin Tetrodotoxin (Reiter *et al*, 1986). Interestingly, the mosaic expression of X-linked genes has been used to explore activity-dependent competition in the organization and maintenance in the olfactory system where neurons are continually replenished throughout life (Zhao & Reed, 2001). The X-linked gene OCNC1 is essential for odorant-evoked activity in olfactory neurons. In female mice heterozygous for the OCNCI knock-out allele, OCNC1-deficient neurons were slowly depleted and out-competed by WT-expressing neurons, which was reversed by odorant deprivation. This study and others exploring the effects of activity blockage in the development of motor, memory and sensory circuits have shown that activity-dependent competition

between inactive and neighbouring active neurons drives the depletion of axons from inactive neurons (Balice-Gordon & Lichtman, 1994; Burrone *et al*, 2002; Yasuda *et al*, 2011; Buffelli *et al*, 2003; Hua *et al*, 2005; Yu *et al*, 2004). Global activity blockage did not have the same effect showing that competition is required. If the MeCP2– neurons were to be selectively silenced instead of eliminated entirely during the protracted period of refinement during neurodevelopment, those silenced connections might be increasingly likely to be eliminated, and be outcompeted by MeCP2+ neural connections.

A commonly used technique to inactivate discrete populations of neurons is the targeted expression of the light chain of tetanus neurotoxin (TeNT) that cleaves synaptobrevin/VAMP2, a core synaptic vesicle protein required for exocytosis and inhibits synaptic transmission (Schiavo *et al*, 1992; Link *et al*, 1992). Doxycycline-dependent control of TeNT light chain expression has been used to mediate inducible blockade of synaptic transmission (Yamamoto *et al*, 2003). The use of TeNT is limited by the difficulty in achieving both spatially restricted and temporally inducible expression. A widely adopted chemogenetic technology used to inducibly silence or activate a genetically defined subset of neurons involves DREADDs ("Designer Receptors Exclusively Activated by Designer Drugs)(Armbruster *et al*, 2007). DREADDS are modified muscarinic G-protein coupled receptors (GPCRs) which can be activated by pharmacologically inert drug-like small molecules. GPCRs are the largest class of neuronal signal-transducing molecules which can excite, inhibit, or otherwise modulate neuronal firing depending on the specific downstream signalling cascade to which they are coupled (Allen & Roth, 2011). The DREADD platform was initially developed through directed evolution of muscarinic GPCRs in yeast, which facilitated the creation of a family of modified receptors with nanomolecular potency for activation by Clozapine-N-oxide (CNO), a relative insensitivity to acetylcholine (the native ligand) and no detectible constitutive activity (Armbruster *et al*, 2007). CNO rapidly penetrates the blood-brain barrier and has favourable pharmokinetics in mice (Bender *et al*, 1994), and humans (Jann *et al*, 1994) and can be administered systemically or noninvasively (e.g. in food or drinking water)(Sternson & Roth, 2014).

The most commonly used inhibitory-DREADD (hM4Di) is a mutated M4 receptor which is coupled to a Gi-protein-signalling cascade which when activated silences neurons (Armbruster *et al*, 2007). Activation of the hM4Di receptor inhibits neuronal activity by two mechanisms: 1) activation of G-protein inwardly rectifying potassium channels (GIRKs) thereby causing hyperpolarization (Armbruster *et al*, 2007) and 2) inhibition of presynaptic release of neurotransmitters (Stachniak *et al*, 2014). Viral approaches have been used to achieve cell type-specific DREADD expression (reviewed in Urban & Roth, 2015). Many of which use Flip-Excision (FLEx) switches to achieve DREADD expression in Cre expressing neurons. The other approach to achieve cell-type specific DREADD expression is transgenic expression using cell-type specific promoters. The DREADD technology is rapidly evolving with new variants and chemical actuators being readily engineered to overcome limitations of the system (Sternson & Roth, 2014; Whissell *et al*, 2016; Urban & Roth, 2015; Roth, 2016).

DREADD technology would be a good alternative approach to the DTR-mediated ablation to study the effects of loss-of-function of the MeCP2– neurons in the mosaic heterozygous brain. To achieve selective inhibition of MeCP2– neurons in the female heterozygote, the hM4Di inhibitory-DREADD would be expressed in place of *Mecp2* in a Cre-dependent manner in exactly the same way the DTR is expressed in the $Mecp2^{FLExDTR(OFF)}$ allele (to generate $Mecp2^{\Delta}hM4Di^{FLEx}$ mice). Recombinase-mediated cassette exchange (RMCE) in ESCs or zygotes could be used to swap the DTR cassette with the hM4Di cassette as discussed further in section 4.6.2. CNO administration to $Mecp2^{\Delta}hM4Di^{FLEx/+}$*,cre* mice would lead to selective, inducible silencing of MeCP2–, Cre+ cells.

Unlike the proof-of-principle DTR system, DREADDs have the potential to be clinically translated (reviewed in English & Roth, 2015). In rodent models, control of neuronal activity using DREADDs have demonstrated the ability to ameliorate disease phenotypes in Parkinson disease (Dell'Anno *et al*, 2014), Down Syndrome (Fortress *et al*, 2015), epilepsy (Kätzel *et al*, 2014; Krook-Magnuson & Soltesz, 2015) and autism (Peñagarikano *et al*, 2015). DREADDs have successfully manipulated neural activity in the non-human primate brain (Nagai *et al*, 2016; Eldridge *et al*, 2015). One

recent study investigated the functional role of nucleus acumbens (NAc) Neuropeptide Y (NPY) neurons in anxiety-like behaviour by assessing the impact of selectively activating these neurons using the hM3Dq DREADD and selectively ablating them using the DTR-ablation system (Yamada *et al*, 2020). Ablation of NAc NPY neurons significantly increased anxiety-like behaviour and activation significantly reduced the anxiety-like behaviour. Eliminating MeCP2– neurons using the DTR-ablation system and silencing them using inactivation-DREADDs would investigate the consequence of loss-of-function of the MeCP2– neurons in the mosaic brain, tackling the question from two different angles. The selective inactivation of MeCP2– neurons addresses how the brain responds to having inactivated neurons interspersed with active ones. The DTR-ablation approach tests the brains response to the absolute removal of the neurons which raises additional questions about cell clearance and potential toxic bystander effects.

7.4 Concluding remarks

This thesis describes the development of a novel system for the selective *in vivo* ablation of MeCP2-deficient neurons in the heterozygous mouse model of RTT syndrome. The main biological questions this system was developed to address are: 1) Is large-scale neuronal cell death based on X-inactivation choice compatible with brain development at any stage? 2) Does the removal of MeCP2– neurons from the mosaic heterozygous mouse brain ameliorate the RTT-like neurological phenotypes? These questions are yet to be addressed, but a tool has been developed here which shows promise in its ability to address these bold questions in the future.

The *Mecp2*$^{FLExDTR(OFF)}$ mouse model has so far been shown to facilitate leak-proof Cre-dependent DTR expression from the X-linked *Mecp2* knock-out allele. DT administration to *Mecp2*$^{FLExDTR(OFF)/+}$*,cre+* mice should allow efficient, selective ablation of Cre+ MeCP2-deficient cells at different stages in postnatal development. There is considerable flexibility of the ablation system developed here. The target cell-type susceptible to DT is defined by the cell-type specific Cre driver line and the developmental timing of ablation is controlled by the DT-injection regime. DT-mediated ablation can be further restricted to a neuronal subtype if widespread

neuronal ablation is too much of an insult for the brain to tolerate. Furthermore, ablation experiments using this line are not restricted to neurons, this system can be used to explore the effects of elimination of cells based on their X-inactivation choice in any cell-type, tissue or organ (Cre driver permitting), and any stage of life. As discussed in this final chapter there are associated challenges and potential limitations of the DTR/DT-ablation system which might affect future neuronal ablation experiments, namely inefficient ablation during prenatal development, potential toxic effects of widespread cell death on surrounding cells and limited dose-dependent ablation efficiency. As all current cell-ablation tools have their distinct limitations, the DTR/DT method described here may provide a "first look" at whether this ambitious line of research leads to interesting biological findings. Emerging alternative neuronal-ablation or inhibition tools could build on this work in the future.

Chapter 8 References

Abdala APL, Dutschmann M, Bissonnette JM & Paton JFR (2010) Correction of respiratory disorders in a mouse model of Rett syndrome. *Proc. Natl. Acad. Sci. U. S. A.* **107:** 18208–18213

Achilly NP, He L, Kim OA, Ohmae S, Wojaczynski GJ, Lin T, Sillitoe R V., Medina JF & Zoghbi HY (2021) Deleting Mecp2 from the entire cerebellum rather than its neuronal subtypes causes a delay in motor learning in mice. *Elife* **10:** e64833

Ahern TH, Krug S, Carr A V, Murray EK, Fitzpatrick E, Bengston L, McCutcheon J, Vries GJ De & Forger NG (2013) Cell Death Atlas of the Postnatal Mouse Ventral Forebrain and Hypothalamus: Effects of Age and Sex Todd. *J. Comp. Neurol.* **521:** 2551–2569

Akbarian S, Chen RZ, Gribnau J, Rasmussen TP, Fong H, Jaenisch R & Jones EG (2001) Expression pattern of the Rett syndrome gene MeCP2 in primate prefrontal cortex. *Neurobiol. Dis.* **8:** 784–91

Allen JA & Roth BL (2011) Strategies to discover unexpected targets for drugs active at G protein-coupled receptors. *Annu. Rev. Pharmacol. Toxicol.* **51:** 117–144

Amir RE, Van den Veyver I. B, Wan M, Tran CQ, Francke U & Zoghbi HY (1999) Rett syndrome is caused by mutations in X-linked MECP2, encoding methyl-CpG-binding protein 2. *Nat. Genet.* **23:** 185–188

Amir RE, Van Den Veyver IB, Schultz R, Malicki DM, Tran CQ, Dahle EJ, Philippi A, Timar L, Percy AK, Motil KJ, Lichtarge O, Smith EOB, Glaze DG & Zoghbi HY (2000) Influence of mutation type and X chromosome inactivation on Rett syndrome phenotypes. *Ann. Neurol.* **47:** 670–679

Amos-Landgraf JM, Cottle A, Plenge RM, Friez M, Schwartz CE, Longshore J & Willard HF (2006) X Chromosome-Inactivation Patterns of 1,005 Phenotypically Unaffected Females. *Am. J. Hum. Genet.* **79:** 493–499

Araki K, Araki M, Miyazaki JI & Vassalli P (1995) Site-specific recombination of a transgene in fertilized eggs by transient expression of Cre recombinase. *Proc. Natl. Acad. Sci. U. S. A.* **92:** 160–164

Araki K, Araki M & Yamamura K ichi (2002) Site-directed integration of the cre gene mediated by Cre recombinase using a combination of mutant lox sites. *Nucleic Acids Res.* **30:** e103

Archer H, Evans J, Leonard H, Colvin L, Ravine D, Christodoulou J, Williamson S, Charman T, Bailey MES, Sampson J, De Klerk N & Clarke A (2007) Correlation between clinical severity in patients with Rett syndrome with a p.R168X or p.T158M MECP2 mutation, and the direction and degree of skewing of X-chromosome inactivation. *J. Med. Genet.* **44:** 148–152

Ariani F, Hayek G, Rondinella D, Artuso R, Mencarelli MA, Spanhol-Rosseto A, Pollazzon M, Buoni S, Spiga O, Ricciardi S, Meloni I, Longo I, Mari F, Broccoli V, Zappella M & Renieri A (2008) FOXG1 Is Responsible for the Congenital Variant of Rett Syndrome. *Am. J. Hum. Genet.* **83:** 89–93

Armbruster BN, Li X, Pausch MH, Herlitze S & Roth BL (2007) Evolving the lock to fit the key to create a family of G protein-coupled receptors potently activated by an inert ligand. *Proc. Natl. Acad. Sci. U. S. A.* **104:** 5163–5168

Armstrong D, Dunn JK, Antalffy B & Trivedi R (1995) Selective Dendritic Alteration in the Cortex of Rett Syndrome. *J. Neuropathol. Exp. Neurol.* **54:** 195–201

Armstrong DD (2001) Rett syndrome neuropathology review 2000. *Brain Dev.* **23:** 72–76

Armstrong DD (2005) Neuropathology of Rett syndrome. *J. Child Neurol.* **20:** 747–753

Armstrong DD, Dunn JK, Schultz RJ, Herbert DA, Glaze DG & Motil KJ (1999) Organ growth in Rett syndrome: A postmortem examination analysis. *Pediatr. Neurol.* **20:** 125–129

Armstrong J, Póo P, Pineda M, Aibar E, Geán E, Català V & Monrós E (2001) Classic Rett Syndrome in a Boy as a Result of Somatic Mosaicism for a MECP2 Mutation. *Ann. Neurol.* **50:** 692

Arruda-Carvalho M, Sakaguchi M, Akers KG, Josselyn SA & Frankland PW (2011) Posttraining Ablation of Adult-Generated Neurons Degrades Previously Acquired Memories. *J. Neurosci.* **31:** 15113–15127

Arruda-carvalho XM, Akers XKG, Guskjolen A, Sakaguchi M, Josselyn SA & Frankland PW (2014) Posttraining Ablation of Adult-Generated Olfactory Granule Cells Degrades Odor – Reward Memories. **34:** 15793–15803

Asaka Y, Jugloff DGM, Zhang L, Eubanks JH & Maki R (2006) Hippocampal synaptic plasticity is impaired in the Mecp2 -null mouse model of Rett syndrome. *Neurobiol. Dis.* **21:** 217–227

Atasoy D, Aponte Y, Su HH & Sternson SM (2008) A FLEX Switch Targets Channelrhodopsin-2 to Multiple Cell Types for Imaging and Long-Range Circuit Mapping. *J. Neurosci.* **28:** 7025–7030

Auger A, Park M, Nitschke F, Minassian LM, Beilhartz GL, Minassian BA & Melnyk RA (2015) Efficient Delivery of Structurally Diverse Protein Cargo into Mammalian Cells by a Bacterial Toxin. *Mol. Pharm.* **12:** 2962–2971

Azim E, Jiang J, Alstermark B & Jessell TM (2014) Skilled reaching relies on a V2a propriospinal internal copy circuit. *Nature* **508:** 357–363

Azofeifa J, Voit T, Hübner C & Cremer M (1995) X-chromosome methylation in

manifesting and healthy carriers of dystrophinopathies: concordance of activation ratios among first degree female relatives and skewed inactivation as cause of the affected phenotypes Springer-Verlag

Baker SA, Chen L, Wilkins AD, Yu P, Lichtarge O & Zoghbi HY (2013) A newly characterized AT-hook domain in MeCP2 determines clinical course of Rett syndrome and related disorders. *Cell* **152:** 984–996

Balice-Gordon RJ & Lichtman JW (1994) Long-term synapse loss induced by focal blockade of postsynaptlc receptors. *Nature* **372:** 519–524

Ballas N, Lioy DT, Grunseich C & Mandel G (2009) Non-cell autonomous influence of MeCP2-deficient glia on neuronal dendritic morphology. *Nat. Neurosci.* **12:** 311–317

Bao X, Downs J, Wong K, Williams S & Leonard H (2013) Using a large international sample to investigate epilepsy in Rett syndrome. *Dev. Med. Child Neurol.* **55:** 553–558

Bassi MT, Ramesar RS, Caciotti B, Winship IM, De Grandi A, Riboni M, Townes PL, Beighton P, Ballabio A & Borsani G (1999) X-linked Late-Onset Sensorineural Deafness Caused by a Deletion Involving OA1 and Novel Gene Containing WD-40 repeats. *Am. J. Hum. Genet.* **64:** 1604–1616

Bauman ML, Kemper TL & Arin DM (1995) Pervasive neuroanatomic abnormalities of the brain in three cases of rett's syndrome. *Neurology* **45:** 1581–1586

Baumann N & Pham-Dinh D (2001) Biology of oligodendrocyte and myelin in the mammalian central nervous system. *Physiol. Rev.* **81:** 871–927

Bebbington a, Percy a, Christodoulou J, Ravine D, Ho G, Jacoby P, Anderson a, Pineda M, Ben Zeev B, Bahi-Buisson N, Smeets E & Leonard H (2010) Updating the profile of C-terminal MECP2 deletions in Rett syndrome. *J. Med. Genet.* **47:** 242–8

Bebbington A, Anderson A, Ravine D, Fyfe S, Pineda M, De Klerk N, Ben-Zeev B, Yatawara N, Percy A, Kaufmann WE & Leonard H (2008) Investigating genotype-phenotype relationships in Rett syndrome using an international data set. *Neurology* **70:** 868–875

Bebbington A, Downs J, Percy A, Pineda M, Zeev B Ben, Bahi-Buisson N & Leonard H (2012) The phenotype associated with a large deletion on MECP2. *Eur. J. Hum. Genet.* **20:** 921–927

Behringer RR, Mathews LS, Palmiter RD & Brinster RL (1988) Dwarf mice produced by genetic ablation of growth-hormone expressing cells. *Genes Dev.* **2:** 453–461

Belichenko NP, Belichenko P V. & Mobley WC (2009a) Evidence for both neuronal cell autonomous and nonautonomous effects of methyl-CpG-binding protein 2 in the cerebral cortex of female mice with Mecp2 mutation. *Neurobiol. Dis.* **34:** 71–

Belichenko P V., Oldfors A, Hagberg B & Dahlström A (1994) Rett syndrome: 3-D confocal microscopy of cortical pyramidal dendrites and afferents. *Neuroreport* **5:** 1509–1513

Belichenko P V., Wright EE, Belichenko NP, Masliah E, Li HH, Mobley WC & Francke U (2009b) Widespread Changes in Dendritic and Axonal Morphology in Mecp2-Mutant Mouse Models of Rett Syndrome: Evidence for Disruption of Neuronal Networks. *J. Comp. Neurol.* **514:** 240–258

Bender D, Holschbach M & Stöcklin G (1994) Synthesis of n.c.a. carbon-11 labelled clozapine and its major metabolite clozapine-N-oxide and comparison of their biodistribution in mice. *Nucl. Med. Biol.* **21:** 921–925

Bhaskara S, Chyla BJ, Amann JM, Knutson SK, Cortez D, Sun Z-W & Hiebert SW (2008) Deletion of Histone Deacetylase 3 reveals critical roles in S-phase progression and DNA damage control. *Mol. Cell* **30:** 61–72

Bhatnagar S, Zhu X, Ou J, Lin L, Chamberlain L, Zhu LJ, Wajapeyee N & Green MR (2014) Genetic and pharmacological reactivation of the mammalian inactive X chromosome. *Proc. Natl. Acad. Sci. U. S. A.* **111:** 12591–12598

Bienvenu T, Carrié A, De Roux N, Vinet M-C, Jonveaux P, Couvert P, Villard L, Arzimanoglou A, Beldjord C, Fontes M, Tardieu M & Chelly J (2000) MECP2 mutations account for most cases of typical forms of Rett syndrome. *Hum. Mol. Genet.* **9:** 1377–1384

Blaschke AJ, Staley K & Chun J (1996) Widespread programmed cell death in proliferative and postmitotic regions of the fetal cerebral cortex. *Development* **122:** 1165–1174

Blaschke AJ, Weiner JA & Chun J (1998) Programmed cell death is a universal feature of embryonic and postnatal neuroproliferative regions throughout the central nervous system. *J. Comp. Neurol.* **396:** 39–50

Blue ME, Boskey AL, Doty SB, Fedarko NS, Hossain MA & Shapiro JR (2015) Osteoblast function and bone histomorphometry in a murine model of Rett syndrome. *Bone* **76:** 23–30

De Bona C, Zappella M, Hayek G, Meloni I, Vitelli F, Bruttini M, Cusano R, Loffredo P, Longo I & Renieri A (2000) Preserved speech variant is allelic of classic Rett syndrome. *Eur. J. Hum. Genet.* **8:** 325–330

Borrelli E, Heyman R, Hsi M & Evans RM (1988) Targeting of an inducible toxic phenotype in animal cells. *Proc. Natl. Acad. Sci. USA* **85:** 7572–7576

Bové J, Prou D, Perier C & Przedborski S (2005) Toxin-induced models of Parkinson's disease. *NeuroRx* **2:** 484–494

Boxer LD, Renthal W, Greben AW, Whitwam T, Silberfeld A, Stroud H, Li E, Yang MG, Kinde B, Griffith EC, Bonev B & Greenberg ME (2020) MeCP2 Represses the Rate of Transcriptional Initiation of Highly Methylated Long Genes. *Mol. Cell* **77:** 294-309.e9

Branda CS & Dymecki SM (2004) Talking about a revolution: The Impact on Site-Specific Recombinases on Genetic Analyses in Mice. *Dev. Cell* **6:** 7–28

Braunschweig D, Simcox T, Samaco RC & LaSalle JM (2004) X-chromosome inactivation ratios affect wild-type MeCP2 expression within mosaic Rett syndrome and Mecp2-/+ mouse brain. *Hum. Mol. Genet.* **13:** 1275–1286

Breitman ML, Clapoff S, Rossant J, Tsui L-C, Glode M, Maxwell IH & Bernstein A (1987) Genetic Ablation: Targeted Expression of a Toxin Gene Causes Microphthalmia in Transgenic mice. *Science (80-.).* **238:** 1563–1565

Breitman ML, Rombola H, Maxwell IH, Klintworth GK & Bernstein A (1990) Genetic Ablation in Transgenic Mice with an Attenuated Diphtheria Toxin A Gene. *Mol. Cell. Biol.* **10:** 474–9

Brockschnieder D, Pechmann Y, Sonnenberg-Riethmacher E & Riethmacher D (2006) An Improved Mouse Line for Cre-Induced Cell Ablation Due to Diphtheria Toxin A, Expressed From the Rosa26 Locus. *Genesis* **44:** 322–327

Brown CJ & Robinson WP (2000) The causes and consequences of random and non-random X chromosome inactivation in humans. *Clin. Genet.* **58:** 353–363

Brown K, Selfridge J, Lagger S, Connelly J, De Sousa D, Kerr A, Webb S, Guy J, Merusi C, Koerner M V. & Bird A (2016) The molecular basis of variable phenotypic severity among common missense mutations causing Rett syndrome. *Hum. Mol. Genet.* **25:** 558–570

Buch T, Heppner FL, Tertilt C, Heinen TJ a J, Kremer M, Wunderlich FT, Jung S & Waisman A (2005) A Cre-inducible diphtheria toxin receptor mediates cell lineage ablation after toxin administration. *Nat. Methods* **2:** 419–426

Buchovecky CM, Turley SD, Brown HM, Kyle SM, McDonald JG, Liu B, Pieper AA, Huang W, Katz DM, Russell DW, Shendure J & Justice MJ (2013) A suppressor screen in Mecp2 mutant mice implicates cholesterol metabolism in Rett syndrome. *Nat. Genet.* **45:** 1013–1020

Budden SS, Dorsey HC & Steiner RD (2005) Clinical profile of a male with Rett syndrome. *Brain Dev.* **27:** S69–S71

Buerger A, Rozhitskaya O, Sherwood MC, Dorfman AL, Bisping E, Abel ED, Pu WT, Izumo S & Jay PY (2006) Dilated Cardiomyopathy Resulting From High-Level Myocardial Expression of Cre-Recombinase. *J. Card. Fail.* **12:** 392–398

Buffelli M, Burgess RW, Feng G, Lobe CG, Lichtman JW & Sanes JR (2003) Genetic evidence that relative synaptic efficacy biases the outcome of synaptic

competition. *Nature* **424:** 430–434

Bult CJ, Blake JA, Smith CL, Kadin JA, Richardson JE & Group the MGD (2019) Mouse Genome Database (MGD) 2019. *Nucleic Acids Res.* **47:** D801–D806

Burrone J, O'Byrne M & Murthy VN (2002) Multiple forms of synaptic plasticity triggered by selective suppression of activity in individual neurons. *Nature* **420:** 414–418

Busque L, Mio R, Mattioli J, Brais E, Biais N, Lalonde Y, Maragh M & Gilliland DG (1996) Nonrandom X-inactivation patterns in normal females: Lyonization ratios vary with age. *Blood* **88:** 59–65

Buss RR, Sun W & Oppenheim RW (2006) Adaptive roles of programmed cell death during nervous system development. *Annu. Rev. Neurosci.* **29:** 1–35

Calabrese JM, Sun W, Song L, Mugford JW, Williams L, Yee D, Starmer J, Mieczkowski P, Crawford GE & Magnuson T (2012) Site-specific silencing of regulatory elements as a mechanism of x inactivation. *Cell* **151:** 951–963

Calfa G, Li W, Rutherford JM & Pozzo-Miller L (2015) Excitation/inhibition imbalance and impaired synaptic inhibition in hippocampal area CA3 of Mecp2 knockout mice. *Hippocampus* **25:** 159–168

De Camilli P, Benfenati F, Valtorta F & Greengard P (1990) The synapsins. *Annu. Rev. Cell Biol.* **6:** 433–460

Camus P, Abbadi N, Perrier MC, Chéry M & Gilgenkrantz S (1996) X chromosome inactivation in 30 girls with Rett syndrome: Analysis using the probe. *Hum. Genet.* **97:** 247–250

Carney RM, Wolpert CM, Ravan SA, Shahbazian M, Ashley-Koch A, Cuccaro ML, Vance JM & Pericak-Vance MA (2003) Identification of MeCP2 mutations in a Series of Females with Autistic Disorder. *Pediatr. Neurol.* **28:** 205–211

Carrel L & Willard HF (2005) X-inactivation profile reveals extensive variability in X-linked gene expression in females. *Nature* **434:** 400–404

Carrette LLG, Blum R, Ma W, Kelleher RJ & Lee JT (2018) Tsix–Mecp2 female mouse model for Rett syndrome reveals that low-level MECP2 expression extends life and improves neuromotor function. *Proc. Natl. Acad. Sci. U. S. A.* **115:** 8185–8190

Carrette LLG, Wang C, Wei C, Press W, Ma W, Kelleher III RJ & Lee JT (2017) A mixed modality approach towards Xi reactivation for Rett syndrome and other X-linked disorders. *PNAS* **115:** E668–E675

Carrière C, Seeley ES, Goetze T, Longnecker DS & Korc M (2007) The Nestin progenitor lineage is the compartment of origin for pancreatic intraepithelial neoplasia. *PNAS* **104:** 4437–4442

Cecconi F, Alvarez-Bolado G, Meyer BI, Roth KA & Gruss P (1998) Apaf1 (CED-4 homolog) regulates programmed cell death in mammalian development. *Cell* **94:** 727–737

Cesca F, Baldelli P, Valtorta F & Benfenati F (2010) The synapsins: Key actors of synapse function and plasticity. *Prog. Neurobiol.* **91:** 313–348

Cha J, Chang MY, Richardson JA & Eidels L (2003) Transgenic mice expressing the diphtheria toxin receptor are sensitive to the toxin. *Mol. Microbiol.* **49:** 235–240

Chahrour M, Jung SY, Shaw C, Zhou X, Wong STC, Qin J & Zoghbi HY (2008) MeCP2, a Key Contributor to Neurological Disease, Activates and Represses Transcription. *Science (80-.).* **320:** 1224–1229

Chang AN, Liang Z, Dai H-Q, Chapdelaine-Williams AM, Andrews N, Bronson RT, Schwer B & Alt FW (2018) Neural blastocyst complementation enables mouse forebrain organogenesis. *Nature* **563:** 126–130

Chao H-T, Chen H, Samaco RC, Xue M, Chahrour M, Yoo J, Neul JL, Gong S, Lu H-C, Heintz N, Ekker M, Rubenstein JLR, Noebels JL, Rosenmund C & Zoghbi HY (2010) Dysfunction in GABA signalling mediates autism-like stereotypies and Rett syndrome phenotypes. *Nature* **468:** 263–269

Chao H-T, Zoghbi HY & Rosenmund C (2007) MeCP2 Controls Excitatory Synaptic Strength by Regulating Glutamatergic Synapse Number. *Neuron* **56:** 58–65

Chapleau CA, Calfa GD, Lane MC, Albertson AJ, Larimore JL, Kudo S, Armstrong DL, Percy AK & Pozzo-Miller L (2009) Dendritic spine pathologies in hippocampal pyramidal neurons from Rett syndrome brain and after expression of Rett-associated MECP2 mutations. *Neurobiol. Dis.* **35:** 219–233

Chaudhry FA, Reimer RJ, Bellocchio EE, Danbolt NC, Osen KK, Edwards RH & Storm-Mathisen J (1998) The vesicular GABA transporter, VGAT, localizes to synaptic vesicles in sets of glycinergic as well as GABAergic neurons. *J. Neurosci.* **18:** 9733–9750

Chen H, Kohno K & Gong Q (2005) Conditional ablation of mature olfactory sensory neurons mediated by diphtheria toxin receptor. *J. Neurocytol.* **34:** 37–47

Chen RZ, Akbarian S, Tudor M & Jaenisch R (2001) Deficiency of methyl-CpG binding protein-2 in CNS neurons results in a Rett-like phenotype in mice. *Nat. Genet.* **27:** 327–331

Chen VS, Morrison JP, Southwell MF, Foley JF, Bolon B & Elmore SA (2017) Histology Atlas of the Developing Prenatal and Postnatal Mouse Central Nervous System, with Emphasis on Prenatal Days E7.5 to E18.5. *Toxicol. Pathol.* **45:** 705–744

Cheng L, Duan B, Huang T, Zhang Y, Chen Y, Britz O, Garcia-Campmany L, Ren X, Vong L, Lowell BB, Goulding M, Wang Y & Ma Q (2017) Identification of

spinal circuits involved in touch-evoked dynamic mechanical pain. *Nat Neurosci.* **20:** 804–814

Cheval H, Guy J, Merusi C, De Sousa D, Selfridge J & Bird A (2012) Postnatal inactivation reveals enhanced requirement for MeCP2 at distinct age windows. *Hum. Mol. Genet.* **21:** 3806–3814

Cholewa-waclaw J, Shah R, Webb S, Chhatbar K, Ramsahoye B, Pusch O, Yu M, Waclaw B & Bird A (2019) Quantitative modelling predicts the impact of DNA methylation on RNA polymerase II traffic. *PNAS* **116:** 14995–15000

Christiaansen AF, Boggiatto PM & Varga SM (2014) Limitations of Foxp3+ Treg depletion following viral infection in DEREG mice. *J. Immunol. Methods* **406:** 58–65

Christodoulou J, Grimm A, Maher T & Bennetts B (2003) RettBASE: The IRSA MECP2 variation database-a new mutation database in evolution. *Hum. Mutat.* **21:** 466–472

Cizeron M, Qiu Z, Koniaris B, Gokhale R, Komiyama NH, Fransén E & Grant SGN (2020) A brainwide atlas of synapses across the mouse life span. *Science (80-.).* **369:** 270–275

Clackson T, Yang W, Rozamus LW, Hatada M, Amara JF, Rollins CT, Stevenson LF, Magari SR, Wood SA, Courage NL, Lu X, Cerasoli F, Gilman M & Holt DA (1998) Redesigning an FKBP-ligand interface to generate chemical dimerizers with novel specificity. *Proc. Natl. Acad. Sci. U. S. A.* **95:** 10437–10442

Clark AJ, Iwobi M, Cui W, Crompton M, Harold G, Hobbs S, Kamalati T, Knox R, Neil C, Yull F & Gusterson B (1997) Selective cell ablation in transgenic mice expressing E . coli nitroreductase. *Gene Ther.* **4:** 101–110

Clayton-Smith J, Watson P, Ramsden S & Black GCM (2000) Somatic mutation in MECP2 as a non-fatal neurodevelopmental disorder in males. *Lancet* **356:** 830–832

Cohen D, Lazar G, Couvert P, Desportes V, Lippe D, Mazet P & Héron D (2002) MECP2 Mutation in a Boy with Language DIsorder and Schizophrenia. *Am J Psychiatry* **159:** 148–149

Cohen DRS, Matarazzo V, Palmer AM, Tu Y, Jeon OH, Pevsner J & Ronnett G V. (2003) Expression of MeCP2 in olfactory receptor neurons is developmentally regulated and occurs before synaptogenesis. *Mol. Cell. Neurosci.* **22:** 417–429

Collier RJ (1975) Diphtheria toxin: mode of action and structure. *Bacteriol. Rev.* **39:** 54–85

Collier RJ & Kandel J (1971) Structure and activity of diphtheria toxin. *J. Biol. Chem.* **246:** 1496–1503

Collins AL, Levenson JM, Vilaythong AP, Richman R, Armstrong DL, Noebels JL, Sweatt JD & Zoghbi HY (2004) Mild overexpression of MeCP2 causes a progressive neurological disorder in mice. *Hum. Mol. Genet.* **13:** 2679–2689

Conti V, Gandaglia A, Galli F, Tirone M, Bellini E, Campana L, Kilstrup-Nielsen C, Rovere-Querini P, Brunelli S & Landsberger N (2015) MeCP2 Affects Skeletal Muscle Growth and Morphology through Non Cell-Autonomous Mechanisms. *PLoS One* **10:** e0130183

Coovert DD, Le TT, McAndrew PE, Strasswimmer J, Crawford TO, Mendell JR, Coulson SE, Androphy EJ, Prior TW & Burghes AHM (1997) The survival motor neuron protein in spinal muscular atrophy. *Hum. Mol. Genet.* **6:** 1205–1214

Corbeaux T, Hess I, Swann JB, Kanzler B, Haas-assenbaum A & Boehm T (2010) Thymopoiesis in mice depends on a Foxn1 -positive thymic epithelial cell lineage. *PNAS* **107:** 16613–16618

Cowan MW, Fawcett JW, O'Leary DDM & Stanfield BB (1984) Regressive events in neurogenesis. *Science (80-.).* **225:** 1258–1265

Cowan WM (2001) Viktor Hamburger and Rita Levi-Montalcini : The Path to the Discovery of the Nerve Growth Factor. *Annu. Rev. Neurosci.* **24:** 551–600

Coy JF, Sedlacek Z, Bächner D, Delius H & Poustka A (1999) A complex pattern of evolutionary conservation and alternative polyadenylation within the long 3 ' -untranslated region of the methyl-CpG-binding protein 2 gene (MeCP2) suggests a regulatory role in gene expression. *Hum. Mol. Genet.* **8:** 1253–1262

Cuddapah VA, Pillai RB, Shekar K V, Lane JB, Motil, Kathleen J, Skinner SA, Tarquinio DC, Glaze DG, Mcgwin G, Kaufmann WE, Percy AK, Neul JL & Olsen ML (2014) Methyl-CpG-binding protein 2 (MECP2) mutation type associated with disease severity in Rett Syndrome. *J. Med. Genet.* **51:** 152–158

D'Cruz JA, Wu C, Zahid T, El-Hayek Y, Zhang L & Eubanks JH (2010) Alterations of cortical and hippocampal EEG activity in MeCP2-deficient mice. *Neurobiol. Dis.* **38:** 8–16

D'Esposito M, Quaderi NA, Ciccodicola A, Bruni P, Esposito T, D'Urso M & Brown SD. (1996) Isolation, physical mapping, and Northern analysis of the X-linked human gene encoding methyl CpG-binding protein, MECP2. *Mamm. Genome* **7:** 533–535

Dani VS, Chang Q, Maffei A, Turrigiano GG, Jaenisch R & Nelson SB (2005) Reduced cortical activity due to a shift in the balance between excitation and inhibition in a mouse model of Rett syndrome. *Proc. Natl. Acad. Sci. U. S. A.* **102:** 12560–12565

Dayer AG, Bottani A, Bouchardy I, Fluss J, Antonarakis SE, Haenggeli CA & Morris MA (2007) MECP2 mutant allele in a boy with Rett syndrome and his unaffected heterozygous mother. *Brain Dev.* **29:** 47–50

Degano AL, Pasterkamp RJ & Ronnett G V. (2009) MeCP2 deficiency disrupts axonal guidance, fasciculation, and targeting by altering Semaphorin 3F function. *Mol. Cell. Neurosci.* **42:** 243–254

Delacour A, Nepote V, Trumpp A & Herrera PL (2004) Nestin expression in pancreatic exocrine cell lineages. *Mech. Dev.* **121:** 3–14

Dell'Anno MT, Caiazzo M, Leo D, Dvoretskova E, Medrihan L, Colasante G, Giannelli S, Theka I, Russo G, Mus L, Pezzoli G, Gainetdinov RR, Benfenati F, Taverna S, Dityatev A & Broccoli V (2014) Remote control of induced dopaminergic neurons in Parkinson ' s disease. *J. Clin. Invest.* **124:** 3215–3229

Derecki NC, Cronk JC, Lu Z, Xu E, Abbott SBG, Guyenet PG & Kipnis J (2012) Wild-type microglia arrest pathology in a mouse model of Rett syndrome. *Nature* **484:** 105–109

Dickinson M., Flenniken A., Ji X, Teboul L, Wong MD, White JK, Meehan TF, Weninger WJ, Westerberg H, Adissu H, Baker CN & Bower L (2016) High-throughput Discovery of Novel Developmental Phenotypes. *Natue* **537:** 508–514

Donnelly MLL, Hughes LE, Luke G, Mendoza H, Ten Dam E, Gani D & Ryan MD (2001a) The 'cleavage' activities of foot-and-mouth disease virus 2A site-directed mutants and naturally occurring '2A-like' sequences. *J. Gen. Virol.* **82:** 1027–1041

Donnelly MLL, Luke G, Mehrotra A, Li X, Hughes LE, Gani D & Ryan MD (2001b) Analysis of the aphthovirus 2A/2B polyprotein 'cleavage' mechanism indicates not a proteolytic reaction, but a novel translational effect: A putative ribosomal 'skip'. *J. Gen. Virol.* **82:** 1013–1025

Downs J, Torode I, Wong K, Ellaway C, Elliott EJ, Christodoulou J, Jacoby P, Thomson MR, Izatt MT, Askin GN, McPhee BI, Bridge C, Cundy P & Leonard H (2016) The natural history of scoliosis in females with rett syndrome. *Spine (Phila. Pa. 1976).* **41:** 856–863

Downs J, Wong K, Ravikumara M, Ellaway C, Elliott EJ, Christodoulou J, Jacoby P & Leonard H (2014) Experience of gastrostomy using a quality care framework: The example of rett syndrome. *Med. (United States)* **93:** e328

Dragatsis I & Zeitlin S (2001) A method for the generation of conditional gene repair mutations in mice. *Nucleic Acids Res.* **29:** e10

Drazin R, Kandel J & Collier RJ (1971) Structure and activity of diphtheria toxin. *J. Biol. Chem.* **246:** 1504–1510

Du F, Nguyen MVC, Karten A, Felice CA, Mandel G & Ballas N (2016) Acute and crucial requirement for MeCP2 function upon transition from early to late adult stages of brain maturation. *Hum. Mol. Genet.* **25:** 1690–1702

Duffield JS, Forbes SJ, Constandinou CM, Clay S, Partolina M, Vuthoori S, Wu S,

Lang R & Iredale JP (2005) Selective depletion of macrophages reveals distinct , opposing roles during liver injury and repair. *J. Clin. Invest.* **115:** 56–65

Durand S, Patrizi A, Quast KB, Hachigian L, Pavlyuk R, Saxena A, Carninci P, Hensch TK & Fagiolini M (2012) NMDA Receptor Regulation Prevents Regression of Visual Cortical Function in the Absence of Mecp2. *Neuron* **76:** 1078–1090

Durieux PF, Bearzatto B, Guiducci S, Buch T, Waisman A, Zoli M, Schiffmann SN & de Kerchove d'Exaerde A (2009) D2R striatopallidal neurons inhibit both locomotor and drug reward processes. *Nat. Neurosci.* **12:** 393–395

van Dyck L & Morrow EM (2017) Genetic control of postnatal human brain growth. *Curr Opin Neurol* **30:** 114–124

Earnshaw WC, Martins LM & Kaufmann SH (1999) Mammalian Caspases: Structure, Activation, Substrates, and Functions During Apoptosis. *Annu. Rev. Biochem* **68:** 383–424

Eldridge MAG, Lerchner W, Saunders RC, Kaneko H, Krausz KW, Gonzalez FJ, Ji B, Higuchi M, Minamimoto T & Richmond BJ (2015) Chemogenetic disconnection of monkey orbitofrontal and rhinal cortex reversibly disrupts reward value. *Nat. Neurosci.* **19:** 37–39

Ellaway C, Peat J, Leonard H & Christodoulou J (2001) Sleep dysfunction in Rett syndrome: Lack of age related decrease in sleep duration. *Brain Dev.* **23:** 101–103

English JG & Roth BL (2015) Chemogenetics-a transformational and translational platform. *JAMA Neurol.* **72:** 1361–1366

Erö C, Gewaltig MO, Keller D & Markram H (2018) A cell atlas for the mouse brain. *Front. Neuroinform.* **12:**

Van Esch H (2011) MECP2 duplication syndrome. *Mol. Syndromol.* **2:** 128–136

Van Esch H, Bauters M, Ignatius J, Jansen M, Raynaud M, Hollanders K, Lugtenberg D, Bienvenu T, Jensen LR, Ge J, Moraine C, Marynen P, Fryns J & Froyen G (2005) Duplication of the MECP2 Region Is a Frequent Cause of Severe Mental Retardation and Progressive Neurological Symptoms in Males. *Am. J. Hum. Genet.* **77:** 442–453

Fan L, Freeman K, Khan T, Pham E & Spencer D (1999) Improved artificial death switches based on caspases and FADD. *Hum. Gene Ther.* **10:** 2273–2285

Fehr S, Bebbington A, Ellaway C, Rowe P, Leonard H & Downs J (2011) Altered attainment of developmental milestones influences the age of diagnosis of Rett syndrome. *J. Child Neurol.* **26:** 980–987

Fehr S, Wilson M, Downs J, Williams S, Murgia A, Sartori S, Vecchi M, Ho G, Polli

R, Psoni S, Bao X, De Klerk N, Leonard H & Christodoulou J (2013) The CDKL5 disorder is an independent clinical entity associated with early-onset encephalopathy. *Eur. J. Hum. Genet.* **21:** 266–273

De Felice C, Guazzi G, Rossi M, Ciccoli L, Signorini C, Leoncini S, Tonni G, Latini G, Valacchi G & Hayek J (2010) Unrecognized Lung Disease in Classic Rett Syndrome. *Chest* **138:** 386–392

De Felipe P, Hughes LE, Ryan MD & Brown JD (2003) Co-translational, intraribosomal cleavage of polypeptides by the foot-and-mouth disease virus 2A peptide. *J. Biol. Chem.* **278:** 11441–11448

de Felipe P, Luke GA, Hughes LE, Gani D, Halpin C & Ryan MD (2006) E unum pluribus: multiple proteins from a self-processing polyprotein. *Trends Biotechnol.* **24:** 68–75

Feng YQ, Seibler J, Alami R, Eisen A, Westerman KA, Leboulch P, Fiering S & Bouhassira EE (1999) Site-specific chromosomal integration in mammalian cells: Highly efficient CRE recombinase-mediated cassette exchange. *J. Mol. Biol.* **292:** 779–785

Fey MF, Liechti-Gallati S, Von Rohr A, Borisch B, Theilkas L, Schneider V, Oestreicher M, Nagel S, Ziemiecki A & Tobler A (1994) Clonality and X-inactivation patterns in hematopoietic cell populations detected by the highly informative M27β DNA probe. *Blood* **83:** 931–938

Fink AJP, Croce KR, Huang ZJ, Abbott LF, Jessell TM & Azim E (2014) Presynaptic inhibition of spinal sensory feedback ensures smooth movement. *Nature* **508:** 43–48

Finkel RS, McDermott MP, Kaufmann P, Darras BT, Chung WK, Sproule DM, Kang PB, Foley AR, Yang ML, Martens WB, Oskoui M, Glanzman AM, Flickinger J, Montes J, Dunaway S, O'Hagen J, Quigley J, Riley S, Benton M, Ryan PA, et al (2014) Observational study of spinal muscular atrophy type I and implications for clinical trials. *Neurology* **83:** 810 LP – 817

Finn WF (1999) FK506 nephrotoxicity. *Ren. Fail.* **21:** 319–329

Forni PE, Scuoppo C, Imayoshi I, Taulli R, Dastrù W, Sala V, Betz UAK, Muzzi P, Martinuzzi D, Vercelli AE, Kageyama R & Ponzetto C (2006) High levels of Cre expression in neuronal progenitors cause defects in brain development leading to microencephaly and hydrocephaly. *J. Neurosci.* **26:** 9593–9602

Fortress AM, Hamlett ED, Vazey EM, Aston-Jones G, Cass WA, Boger HA & Granholm ACE (2015) Designer receptors enhance memory in a mouse model of down syndrome. *J. Neurosci.* **35:** 1343–1353

Fujioka M, Tokano H, Fujioka KS, Okano H & Edge ASB (2011) Generating mouse models of degenerative diseases using Cre/lox-mediated in vivo mosaic cell ablation. *J. Clin. Invest.* **121:** 2462–2469

Fujita S (1967) Quantitative analysis of cell proliferation and differentiation in the cortex of the postnatal mouse cerebellum. *J. Cell Biol.* **32:** 277–287

Fujita S, Shimada M & Nakamura T (1966) H3-Thymidine autoradiographic studies on the cell proliferation and differentiation in the external and the internal granular layers of the mouse cerebellum. *J. Comp. Neurol.* **128:** 191–207

Fukuda T, Itoh M, Ichikawa T, Washiyama K & Goto YI (2005) Delayed maturation of neuronal architecture and synaptogenesis in cerebral cortex of Mecp2-deficient mice. *J. Neuropathol. Exp. Neurol.* **64:** 537–544

Furman BL (2015) Streptozotocin-Induced Diabetic Models in Mice and Rats. *Curr. Protoc. Pharmacol.* **70:** 5.47.1-5.47.20

Fyffe SL, Neul JL, Samaco RC, Chao HT, Ben-Shachar S, Moretti P, McGill BE, Goulding EH, Sullivan E, Tecott LH & Zoghbi HY (2008) Deletion of Mecp2 in Sim1-Expressing Neurons Reveals a Critical Role for MeCP2 in Feeding Behavior, Aggression, and the Response to Stress. *Neuron* **59:** 947–958

Gabel HW, Kinde B, Stroud H, Gilbert CS, Harmin DA, Kastan NR, Hemberg M, Ebert DH & Greenberg ME (2015) Disruption of DNA-methylation-dependent long gene repression in Rett syndrome. *Nature* **522:** 89–93

Gadalla KKE, Bailey MES & Cobb SR (2011) MeCP2 and Rett syndrome: Reversibility and potential avenues for therapy. *Biochem. J.* **439:** 1–14

Gadalla KKE, Bailey MES, Spike RC, Ross PD, Woodard KT, Kalburgi SN, Bachaboina L, Deng J V, West AE, Samulski RJ, Gray SJ & Cobb SR (2013) Improved Survival and Reduced Phenotypic Severity Following AAV9 / MECP2 Gene Transfer to Neonatal and Juvenile Male Mecp2 Knockout Mice. **21:** 18–30

Gadalla KKE, Ross PD, Hector RD, Bahey NG, Bailey MES & Cobb SR (2015) Gene therapy for Rett syndrome: Prospects and challenges. *Future Neurol.* **10:** 467–483

Gadalla KKE, Vudhironarit T, Hector RD, Sinnett S, Bahey NG, Bailey MES, Gray SJ & Cobb SR (2017) Development of a Novel AAV Gene Therapy Cassette with Improved Safety Features and Efficacy in a Mouse Model of Rett Syndrome. *Mol. Ther. - Methods Clin. Dev.* **5:** 180–190

Gale RE, Fielding AK, Harrison CN & Linch DC (1997) Acquired skewing of X-chromosome inactivation patterns in myeloid cells of the elderly suggests stochastic clonal loss with age. *Br. J. Haematol.* **98:** 512–519

Gandaglia A, Brivio E, Carli S, Palmieri M, Bedogni F, Stefanelli G, Bergo A, Leva B, Cattaneo C, Pizzamiglio L, Cicerone M, Bianchi V, Kilstrup-nielsen C, Annessa ID, Marino D Di, Adamo PD, Antonucci F, Frasca A & Landsberger N (2019) A Novel Mecp2 Y120D Knock-in Model Displays Similar Behavioral Traits But Distinct Molecular Features Compared to the Mecp2 -Null Mouse Implying Precision Medicine for the Treatment of Rett Syndrome. *Mol.*

Neurobiol. **56:** 4838–4854

Garg SK, Lioy DT, Cheval H, McGann JC, Bissonnette JM, Murtha MJ, Foust KD, Kaspar BK, Bird A & Mandel G (2013) Systemic delivery of MeCP2 rescues behavioral and cellular deficits in female mouse models of Rett syndrome. *J. Neurosci.* **33:** 13612–20

Gavrieli Y, Sherman Y & Ben-Sasson SA (1992) Identification of Programmed Cell Death In Situ via Specific Labeling of Nuclear DNA Fragmentation. *J. Cell Biol.* **119:** 493–501

Gemelli T, Berton O, Nelson ED, Perrotti LI, Jaenisch R & Monteggia LM (2006) Postnatal loss of methyl-CpG binding protein 2 in the forebrain is sufficient to mediate behavioral aspects of Rett syndrome in mice. *Biol. Psychiatry* **59:** 468–476

Gibson JH, Williamson SL, Arbuckle S & Christodoulou J (2005) X chromosome inactivation patterns in brain in Rett syndrome: Implications for the disease phenotype. *Brain Dev.* **27:** 266–270

Gill DM & Dinius LL (1971) Observations on the structure of diphtheria toxin. *J. Biol. Chem.* **246:** 1485–1491

Glaze DG (2005) Neurophysiology of Rett syndrome. *J Child Neurol* **20:** 740–746

Glaze DG, Percy AK, Skinner S, Motil KJ, Neul JL, Barrish JO, Lane JB, Geerts SP, Annese RF, Graham LJ, Mcnair L & Lee H-S (2010) Epilepsy and the natural history of Rett syndrome. *Neurology* **74:** 909–912

Goda Y & Davis GW (2003) Mechanisms of Synapse Assembly and Disassembly. *Neuron* **40:** 243–264

Goffin D, Allen M, Zhang L, Amorim M, Wang ITJ, Reyes ARS, Mercado-Berton A, Ong C, Cohen S, Hu L, Blendy JA, Carlson GC, Siegel SJ, Greenberg ME & Zhou Z (2012) Rett syndrome mutation MeCP2 T158A disrupts DNA binding, protein stability and ERP responses. *Nat. Neurosci.* **15:** 274–283

Goffin D & Zhou Z (2012) The neural circuit basis of Rett Syndrome. *Front Biol* **7:** 428–435

Goldwich A, Steinkasserer A, Gessner A & Amann K (2012) Impairment of podocyte function by diphtheria toxin-a new reversible proteinuria model in mice. *Lab. Investig.* **92:** 1674–1685

Gopaul DN, Guo F & Van Duyne GD (1998) Structure of the Holliday junction intermediate in Cre-loxP site-specific recombination

Gropp E, Shanabrough M, Borok E, Xu AW, Janoschek R, Buch T, Plum L, Balthasar N, Hampel B, Waisman A, Barsh GS, Horvath TL & Brüning JC (2005) Agouti-related peptide-expressing neurons are mandatory for feeding. *Nat. Neurosci.* **8:**

1289–1291

Grosse G, Grosse J, Tapp R, Kuchinke J, Gorsleben M, Fetter I, Höhne-Zell B, Gratzl M & Bergmann M (1999) SNAP-25 requirement for dendritic growth of hippocampal neurons. *J. Neurosci. Res.* **56:** 539–546

Gu H, Marth JD, Orban PC, Mossmann H & Rajewsky K (1994) Deletion of a DNA Polymerase B Gene Segment in T Cells Using Cell Type-Specific Gene Targeting. *Science (80-.).* **265:** 103–106

Guo C, Li Y, Gow CH, Wong M, Zha J, Yan C, Liu H, Wang Y, Burris TP & Zhang J (2015) The Optimal Corepressor Function of Nuclear Receptor Corepressor (NCoR) for Peroxisome Proliferator-activated Receptor γ Requires G Protein Pathway Suppressor 2. *J. Biol. Chem.* **290:** 3666–3679

Guo F, Gopaul DN & Van Duyne GD (1997) Structure of Cre recombinase complexed with DNA in a site-specific recombination synapse. *Nature* **389:** 40–46

Guo JU, Su Y, Shin JH, Shin J, Li H, Xie B, Zhong C, Hu S, Le T, Fan G, Zhu H, Chang Q, Ming G & Song H (2014) Distribution, recognition and regulation of non-CpG methylation in the adult mammalian brain. *Nat. Neurosci.* **17:** 215–222

Guy J, Alexander-Howden B, FitzPatrick L, DeSousa D, Koerner M V., Selfridge J & Bird A (2018) A mutation-led search for novel functional domains in MeCP2. *Hum. Mol. Genet.* **27:** 2531–2545

Guy J, Gan J, Selfridge J, Cobb S & Bird A (2007) Reversal of Neurological Defects in a Mouse Model of Rett Syndrome. *Science (80-.).* **315:** 1143–1147

Guy J, Hendrich B, Holmes M, Martin JE & Bird A (2001) A mouse Mecp2-null mutation causes neurological symptoms that mimic Rett syndrome. *Nat. Genet.* **27:** 322–326

Hagberg B (1985) Rett's Syndrome: Prevalence and Impact on Progressive Severe Mental Retardation in Girls. *Acta Paediatr.* **74:** 405–408

Hagberg B, Aicardi J, Dias K & Ramos O (1983) A Progressive Syndrome of Autism, Dementia, Ataxia, and Loss of Purposeful Hand Use in Girls: Rett's Syndrome: Report of 35 cases. *Ann. Neurol.* **14:** 471–479

Hagberg B, Goutières F, Hanefeld F, Rett A & Wilson J (1985) Rett syndrome: Criteria for inclusion and exclusion. *Brain Dev.* **7:** 372–373

Hagberg B, Hanefeld F, Percy A & Skjeldal O (2002) An update on clinically applicable diagnostic criteria in Rett syndrome: Comments to Rett syndrome clinical criteria consensus panel satellite to European Paediatric Neurology Society Meeting Baden Baden, Germany, 11 September 2001. *Eur. J. Paediatr. Neurol.* **6:** 293–297

Hagberg B, Witt-Engerström I, Opitz JM & Reynolds JF (1986) Rett Syndrome: A

suggested staging system for describing impairment profile with increasing age towards adolescence. *Am. J. Med. Genet.* **25:** 47–59

Hagberg BA & Skjeldal OH (1994) Rett variants: A suggested model for inclusion criteria. *Pediatr. Neurol.* **11:** 5–11

Hagberg G, Stenbom Y & Witt Engerström I (2000) Head growth in Rett syndrome. *Acta Paediatr.* **89:** 198–202

Hakem R, Hakem A, Duncan GS, Henderson JT, Woo M, Soengas MS, Elia A, De La Pompa JL, Kagi D, Khoo W, Potter J, Yoshida R, Kaufman SA, Lowe SW, Penninger JM & Mak TW (1998) Differential requirement for Caspase 9 in apoptotic pathways in vivo. *Cell* **94:** 339–352

Hanefeld F (1985) The Clinical Pattern of the Rett Syndrome. *Brain Dev.* **7:** 320–325

Harris JA, Hirokawa KE, Sorensen SA, Gu H, Mills M, Ng LL, Bohn P, Mortrud M, Ouellette B, Kidney J, Smith KA, Dang C, Sunkin S, Bernard A, Oh SW, Madisen L & Zeng H (2014) Anatomical characterization of Cre driver mice for neural circuit mapping and manipulation. *Front. Neural Circuits* **8:** 76

Hatori M, Le H, Vollmers C, Keding SR, Tanaka N, Schmedt C, Jegla T & Panda S (2008) Inducible ablation of melanopsin-expressing retinal ganglion cells reveals their central role in non-image forming visual responses. *PLoS One* **3:**

Hayashi S & McMahon AP (2002) Efficient recombination in diverse tissues by a tamoxifen-inducible form of Cre: A tool for temporally regulated gene activation/inactivation in the mouse. *Dev. Biol.* **244:** 305–318

Heckman LD, Chahrour MH & Zoghbi HY (2014) Rett-causing mutations reveal two domains critical for MeCP2 function and for toxicity in MECP2 duplication syndrome mice. *Elife* **3:** 1–17

Herculano-Houzel S (2014) The glia/neuron ratio: How it varies uniformly across brain structures and species and what that means for brain physiology and evolution. *Glia* **62:** 1377–1391

Herculano-Houzel S & Lent R (2005) Isotropic fractionator: A simple, rapid method for the quantification of total cell and neuron numbers in the brain. *J. Neurosci.* **25:** 2518–2521

Herculano-Houzel S, Mota B & Lent R (2006) Cellular scaling rules for rodent brains. *Proc. Natl. Acad. Sci. U. S. A.* **103:** 12138–12143

Higashi AY, Ikawa T, Muramatsu M, Economides AN, Niwa A, Okuda T, Murphy AJ, Rojas J, Heike T, Nakahata T, Kawamoto H, Kita T & Yanagita M (2009) Direct Hematological Toxicity and Illegitimate Chromosomal Recombination Caused by the Systemic Activation of CreERT2. *J. Immunol.* **182:** 5633–5640

Hoesche C, Sauerwald A, Veh RW, Krippl B & Kilimann MW (1993) The 5′-flanking

region of the rat synapsin I gene directs neuron-specific and developmentally regulated reporter gene expression in transgenic mice. *J. Biol. Chem.* **268:** 26494–26502

Hoess R, Wierzbicki A & Abremski K (1985) Formation of small circular DNA molecules via an in vitro site-specific recombination system. *Gene* **40:** 325–329

Hoess RH, Wierzbicki A & Abremski K (1986) The role of the loxP spacer region in PI site-specific recombination. *Nucleic Acids Res.* **14:** 2287–2300

Hoess RH, Ziese M & Sternberg N (1982) P1 site-specific recombination: Nucleotide sequence of the recombining sites. *Proc. Natl. Acad. Sci. USA* **79:** 3398–3402

Hoffbuhr K, Devaney ; J M, Lafleur ; B, Sirianni ; N, Scacheri ; C, Giron ; J, Schuette ; J, Innis ; J, Marino ; M, Philippart ; M, Narayanan ; V, Umansky ; R, Kronn ; D, Hoffman ; E P & Naidu S (2001) MeCP2 mutations in children with and without the phenotype of Rett syndrome. *Neurology* **56:** 1486–1495

Honjo T, Nishizuka Y & Hayaishi O (1968) Diphtheria toxin-dependent adenosine diphosphate ribosylation of aminoacyl transferase II and inhibition of protein synthesis. *J. Biol. Chem.* **243:** 3553–3555

Hooper M, Hardy K, Handyside A, Hunter S & Monk M (1987) HPRT-deficient (Lesch-Nyhan) mouse embryos derived from germline colonization by cultured cells. *Nature* **326:** 292–295

Hosford BE, Liska JP & Danzer SC (2016) Ablation of newly generated hippocampal granule cells has disease-modifying effects in epilepsy. *J. Neurosci.* **36:** 11013–11023

Hosford BE, Rowley S, Liska JP & Danzer SC (2017) Ablation of peri-insult generated granule cells after epilepsy onset halts disease progression. *Sci. Rep.* **7:** 1–11

Hsiao YH, Hung HC, Chen SH & Gean PW (2014) Social interaction rescues memory deficit in an animal model of Alzheimer's disease by increasing BDNF-Dependent Hippocampal Neurogenesis. *J. Neurosci.* **34:** 16207–16219

Hu W, Ferris SP, Tweten RK, Wu G, Radaeva S, Gao B, Bronson RT, Halperin JA & Qin X (2008) Rapid conditional targeted ablation of cells expressing human CD59 in transgenic mice by intermedilysin. *Nat. Med.* **14:** 98–103

Hua JY, Smear MC, Baier H & Smith SJ (2005) Regulation of axon growth in vivo by activity-based competition. *Nature* **434:** 1022–1025

Hua JY & Smith SJ (2004) Neural activity and the dynamics of central nervous system development. *Nat. Neurosci.* **7:** 327–332

Huang S & Moody SA (1992) Does lineage determine the dopamine phenotype in the tadpole hypothalamus?: A quantitative analysis. *J. Neurosci.* **12:** 1351–1362

Isles AR, Dan M, Milsom C, Skynner MJ, Cui W, Clark J, Keverne EB & Allen ND (2001) Conditional ablation of neurones in transgenic mice. *J. Neurobiol.* **47:** 183–193

Iwasaki K, Komiya H, Kakizaki M, Miyoshi C, Abe M, Sakimura K, Funato H & Yanagisawa M (2018) Ablation of central serotonergic neurons decreased REM sleep and attenuated arousal response. *Front. Neurosci.* **12:** 1–13

Jacobsson G, Bean AJ, Scheller RH, Juntti-Berggren L, Deeney JT, Berggren PO & Meister B (1994) Identification of synaptic proteins and their isoform mRNAs in compartments of pancreatic endocrine cells. *Proc. Natl. Acad. Sci. U. S. A.* **91:** 12487–12491

Jang SK, Kräusslich HG, Nicklin MJ, Duke GM, Palmenberg AC & Wimmer E (1988) A segment of the 5' nontranslated region of encephalomyocarditis virus RNA directs internal entry of ribosomes during in vitro translation. *J. Virol.* **62:** 2636–2643

Jann MW, Lam YW & Chang WH (1994) Rapid formation of clozapine in guinea-pigs and man following clozapine-N-oxide administration. *Arch. Int. Pharmacodyn. Ther.* **328:** 243—250

Jellinger K, Armstrong D, Zoghbi HY & Percy AK (1988) Neuropathology of Rett syndrome. *Acta Neuropathol.* **76:** 142–158

Jepsen K, Hermanson O, Onami TM, Gleiberman AS, Lunyak V, McEvilly RJ, Kurokawa R, Kumar V, Liu F, Seto E, Hedrick SM, Mandel G, Glass CK, Rose DW & Rosenfeld MG (2000) Combinatorial Roles of the Nuclear Receptor Corepressor in Transcription and Development. *Cell* **102:** 753–763

Jepsen K, Solum D, Zhou T, McEvilly RJ, Kim HJ, Glass CK, Hermanson O & Rosenfeld MG (2007) SMRT-mediated repression of an H3K27 demethylase in progression from neural stem cell to neuron. *Nature* **450:** 415–419

Jin C, Kang H, Yoo T, Ryu JR, Yoo YE, Ma R, Zhang Y, Kang HR, Kim Y, Seong H, Bang G, Park S, Kwon SK, Sun W, Kim H, Kim JY, Kim E & Han K (2021) The Neomycin Resistance Cassette in the Targeted Allele of Shank3B Knock-Out Mice Has Potential Off-Target Effects to Produce an Unusual Shank3 Isoform. *Front. Mol. Neurosci.* **13:** 1–12

Johnson BS, Zhao Y, Fasolino M, Lamonica JM, Kim YJ, Georgakilas G, Wood KH, Bu D, Cui Y, Goffin D, Vahedi G, Kim TH & Zhou Z (2017) Biotin tagging of MeCP2 in mice reveals contextual insights into the Rett syndrome transcriptome. *Nat. Med.* **23:** 1203–1214

Julu PO, Kerr AM, Apartopoulos F, Al-Rawas S, Engerström IW, Engerström L, Jamal GA & Hansen S (2001) Characterisation of breathing and associated central autonomic dysfunction in the Rett disorder. *Arch. Dis. Child.* **85:** 29–37

Jung BP, Jugloff DGM, Zhang G, Logan R, Brown S & Eubanks JH (2003) The

Expression of Methyl CpG Binding Factor MeCP2 Correlates with Cellular Differentiation in the Developing Rat Brain and in Cultured Cells. *J. Neurobiol.* **55:** 86–96

Jung S, Unutmaz D, Wong P, Sano G-I, Los K De, Sparwasser T, Wu S, Vuthoori S, Ko K, Zavala F, Pamer, Eric G, Littman DR & Lang RA (2002) In Vivo Depletion of CD11c+ Dendritic Cells Abogates Priming of CD8+ T Cells by Exogenous Cell-Associated Antigens. *Immunity* **17:** 211–220

Kachinsky AM, Dominov JA & Miller JB (1994) Myogenesis and the intermediate filament protein, nestin. *Dev. Biol.* **165:** 216–228

Kachinsky AM, Dominov JA & Miller JB (1995) Intermediate filaments in cardiac myogenesis: Nestin in the developing mouse heart. *J. Histochem. Cytochem.* **43:** 843–847

Kamal B, Russell D, Payne A, Constante D, Tanner KE, Isaksson H, Mathavan N & Cobb SR (2015) Biomechanical properties of bone in a mouse model of Rett syndrome. *Bone* **71:** 106–114

Kankirawatana P, Leonard H, Ellaway C, Scurlock J, Mansour A, Makris CM, Dure IV LS, Friez M, Lane J, Kiraly-Borri C, Fabian V, Davis M, Jackson J, Christodoulou J, Kaufmann WE, Ravine D & Percy AK (2006) Early progressive encephalopathy in boys and MECP2 mutations. *Neurology* **67:** 164–166

Kantor DB & Kolodkin AL (2003) Curbing the Excesses of Youth. *Neuron* **38:** 849–852

Katz DM, Bird A, Coenraads M, Gray SJ, Menon DU, Philpot BD & Tarquinio DC (2016) Rett Syndrome : Crossing the Threshold to Clinical Translation. *Trends Neurosci.* **39:** 100–113

Kätzel D, Nicholson E, Schorge S, Walker MC & Kullmann DM (2014) Chemical-genetic attenuation of focal neocortical seizures. *Nat. Commun.* **5:**

Kerr AM, Montague J & Stephenson JB (1987) The Hands, and the Mind, Pre- and Post Regression in Rett Syndrome. *Brain Dev.* **9:** 487–490

Kerr AM, Nomura Y, Armstrong D, Anvret M, Belichenko P V., Budden S, Cass H, Christodoulou J, Clarke A, Ellaway C, D'Esposito M, Francke U, Hulten M, Julu P, Leonard H, Naidu S, Schanen C, Webb T, Engerstrom IW, Yamashita Y, et al (2001) Guidelines for reporting clinical features in cases with MECP2 mutations. *Brain Dev.* **23:** 208–211

Kerr AM & Stephenson JBP (1985) Rett's syndrome in the west of Scotland. *Br. Med. J.* **291:** 579–582

Kerr B, Alvarez-Saavedra M, Sáez MA, Saona A & Young JI (2008) Defective body-weight regulation , motor control and abnormal social interactions in Mecp2 hypomorphic mice. *Hum. Mol. Genet.* **17:** 1707–1717

Kim JH, Lee SR, Li LH, Park HJ, Park JH, Lee KY, Kim MK, Shin BA & Choi SY (2011) High Cleavage Efficiency of a 2A Peptide Derived from Porcine Teschovirus-1 in Human Cell Lines, Zebrafish and Mice. *PLoS One* **6:** e18556

Kim Y, Yang GR, Pradhan K, Venkataraju KU, Bota M, García del Molino LC, Fitzgerald G, Ram K, He M, Levine JM, Mitra P, Huang ZJ, Wang XJ & Osten P (2017) Brain-wide Maps Reveal Stereotyped Cell-Type-Based Cortical Architecture and Subcortical Sexual Dimorphism. *Cell* **171:** 456-469.e22

Kinde B, Wu DY, Greenberg ME & Gabel HW (2016) DNA methylation in the gene body influences MeCP2-mediated gene repression. *PNAS* **113:** 15114–15119

Kishi N & Macklis JD (2004) MECP2 is progressively expressed in post-migratory neurons and is involved in neuronal maturation rather than cell fate decisions. *Mol. Cell. Neurosci.* **27:** 306–321

Kishi N & Macklis JD (2010) MeCP2 functions largely cell-autonomously, but also non-cell-autonomously, in neuronal maturation and dendritic arborization of cortical pyramidal neurons. *Exp. Neurol.* **222:** 51–58

Kitamura D, Roes J, Kuhn R & Rajewsky K (1991) A B cell-deficient mouse by targeted disruption of the membrane exon of the immunoglobulin μ-chain gene. *Nature* **350:** 423–426

Klauck SM, Lindsay S, Beyer KS, Splitt M, Burn J & Poustka A (2002) A mutation Hot Spot for Nonspecific X-Linked Mental Retardation in the MECP2 Gene Causes the PPM-X syndrome. *Am. J. Hum. Genet.* **70:** 1034–1037

Kline DD, Ogier M, Kunze DL & Katz DM (2010) Exogenous brain-derived neurotrophic factor rescues synaptic dysfunction in Mecp2-null mice. *J. Neurosci.* **30:** 5303–5310

Knudsen GPS, Neilson TCS, Pedersen J, Kerr A, Schwartz M, Hulten M, Bailey MES & Ørstavik KH (2006) Increased skewing of X chromosome inactivation in Rett syndrome patients and their mothers. *Eur. J. Hum. Genet.* **14:** 1189–1194

Koerner M V., Fitzpatrick L, Selfridge J, Guy J, De Sousa D, Tillotson R, Kerr A, Sun Z, Lazar MA, Lyst MJ & Bird A (2018) Toxicity of overexpressed MeCP2 is independent of HDAC3 activity. *Genes Dev.* **32:** 1514–1524

Kolb AF (2001) Selection-marker-free modification of the murine β-casein gene using a lox2722 Site. *Anal. Biochem.* **290:** 260–271

Kolos JM, Voll AM, Bauder M & Hausch F (2018) FKBP Ligands-Where We Are and Where to Go? *Front. Pharmacol.* **9:** 1425

Kortüm F, Das S, Flindt M, Morris-Rosendahl D, Stefanova I, Goldstein A, Horn D, Klopocki E, Kluger G, Martin P, Rauch A, Roumer A, Saitta S, Walsh LE, Wieczorek D, Uyanik G, Kutsche K & Dobyns WB (2011) The core FOXG1 syndrome phenotype consists of postnatal microcephaly, severe mental

retardation, absent language, dyskinesia, and corpus callosum hypogenesis. *J Med Genet* **48:** 396–406

Kriaucionis S & Bird A (2004) The major form of MeCP2 has a novel N-terminus generated by alternative splicing. *Nucleic Acids Res.* **32:** 1818–1823

Kron M, Howell CJ, Adams IT, Ransbottom M, Christian D, Ogier M & Katz DM (2012) Brain activity mapping in Mecp2 mutant mice reveals functional deficits in forebrain circuits, including key nodes in the default mode network, that are reversed with ketamine treatment. *Neurobiol. Dis.* **32:** 13860–13872

Krook-Magnuson E & Soltesz I (2015) Beyond the hammer and the scalpel: selective circuit control for the epilepsies. *Nat. Neurosci.* **18:** 331–338

Kruusvee V, Lyst MJ, Taylor C, Tarnauskaite Ž, Bird AP & Cook AG (2017) Structure of the MeCP2 – TBLR1 complex reveals a molecular basis for Rett syndrome and related disorders. *PNAS***:** E3243-3250

Kuida K, Haydar TF, Kuan C-Y, Gu Y, Taya C, Karasuyama H, Su MS-S, Rakic P & Flavell RA (1998) Reduced Apoptosis and Cytochrome c-Mediated Caspase Activation in Mice Lacking Caspase 9. *Cell* **94:** 325–337

Kuida K, Zheng TS, Na S, Kuan C-Y, Yang D, Karasuyama H, Rakic P & Flavell RA (1996) Decreased apoptosis in the brain and premature lethality in CPP32-deficient mice. *Nature* **384:** 368–372

Kyle SM, Saha PK, Brown HM, Chan LC & Justice MJ (2016) MeCP2 co-ordinates liver lipid metabolism with the NCoR1/HDAC3 corepressor complex. *Hum. Mol. Genet.* **25:** 3029–3041

Lagger S, Connelly JC, Schweikert G, Webb S, Selfridge J, Ramsahoye BH, Yu M, He C, Sanguinetti G, Sowers LC, Walkinshaw MD & Bird A (2017) MeCP2 recognizes cytosine methylated tri-nucleotide and di-nucleotide sequences to tune transcription in the mammalian brain. *PLoS Genet.* **13:** 1–26

Lakso M, Sauer B, Mosinger B, Lee EJ, Manning RW, Yu SH, Mulder KL & Westphal H (1992) Targeted oncogene activation by site-specific recombination in transgenic mice. *Proc. Natl. Acad. Sci. U. S. A.* **89:** 6232–6236

Lam C, Yeung W, Ko C, Poon PM., Chan K, Lo IFM, Chan LYS, Hui J, Wong V, Pang C, Lo YMD & Fok T (2000) Spectrum of mutations in the MECP2 gene in patients with infantile autism and Rett syndrome. *J Med Genet* **37:** e41

Lamonica JM, Veasey S, Zhou Z, Lamonica JM, Kwon DY, Goffin D, Fenik P, Johnson BS, Cui Y, Guo H, Veasey S & Zhou Z (2017) Elevating expression of MeCP2 T158M rescues DNA binding and Rett syndrome – like phenotypes. *J. Clin. Invest.* **127:** 1889–1904

Landsman L, Nijagal A, Whitchurch TJ, VanderLaan RL, Zimmer WE, MacKenzie TC & Hebrok M (2011) Pancreatic mesenchyme regulates epithelial

organogenesis throughout development. *PLoS Biol.* **9:** e1001143

Lawson-yuen A, Liu D, Han L, Jiang ZI, Tsai GE, Basu C, Picker J, Feng J & Coyle JT (2007) Ube3a mRNA and protein expression are not decreased in Mecp2R168X mutant mice. *Brain Res.* **14:** 1–6

Lee G & Saito I (1998) Role of nucleotide sequences of loxP spacer region in Cre-mediated recombination. *Gene* **216:** 55–65

Lee J-Y, Ristow M, Lin X, White MF, Magnuson MA & Hennighausen L (2006) RIP-Cre Revisited, Evidence for Impairments of Pancreatic-Cell Function. *J. Biol. Chem.* **281:** 2649–2653

Lee JYL, Leonard H, Piek JP & Downs J (2013) Early development and regression in Rett syndrome. *Clin. Genet.* **84:** 572–576

Lem J, Applebury ML, Falk JD, Flannery JG & Simon MI (1991) Tissue-Specific and Developmental Regulation of Rod Opsin Chimeric Genes in Transgenic Mice. *Neuron* **6:** 201–210

Lendahl U, Zimmerman LB & McKay RDG (1990) CNS stem cells express a new class of intermediate filament protein. *Cell* **60:** 585–595

Leonard H & Bower C (1998) Is the girl with Rett syndrome normal at birth? *Dev. Med. Child Neurol.* **40:** 115–121

Leonard H, Cobb S & Downs J (2016) Clinical and biological progress over 50 years in Rett syndrome. *Nat. Rev. Neurol.* **13:** 37–51

Leonard H, Silberstein J, Falk R, Houwink-Manville I, Ellaway C, Raffaele LS, Engerström IW & Schanen C (2001) Occurrence of Rett syndrome in boys. *J. Child Neurol.* **16:** 333–338

Lessing D, Dial TO, Wei C, Payer B, Carrette LLG, Kesner B, Szanto A, Jadhav A, Maloney DJ, Simeonov A, Theriault J, Hasaka T, Bedalov A, Bartolomei MS & Lee JT (2016) A high-throughput small molecule screen identifies synergism between DNA methylation and Aurora kinase pathways for X reactivation. *Proc. Natl. Acad. Sci. U. S. A.* **113:** 14366–14371

Lewis JD, Meehan RR, Henzel WJ, Maurer-Fogy I, Jeppesen P, Klein F & Bird A (1992) Purification, sequence, and cellular localization of a novel chromosomal protein that binds to Methylated DNA. *Cell* **69:** 905–914

Li L, Suzuki T, Mori N & Greengard P (1993) Identification of a functional silencer element involved in neuron-specific expression of the synapsin I gene. *Proc. Natl. Acad. Sci. U. S. A.* **90:** 1460–1464

Lichtman JW & Colman H (2000) Synapse elimination and indelible memory. *Neuron* **25:** 269–278

Link E, Edelmann L, Chou JH, Binz T, Yamasaki S, Eisel U, Baumert M, Südhof TC, Niemann H & Jahn R (1992) Tetanus toxin action: Inhibition of neurotransmitter release linked to synaptobrevin proteolysis. *Biochem. Biophys. Res. Commun.* **189:** 1017–1023

Lioy DT, Garg SK, Monaghan CE, Raber J, Foust KD, Kasper BK, Hirrlinger PG, Kirchhoff F, Bissonnette JM, Ballas N & Mandel G (2011) A role for glia in the progression of Rett syndrome. *Nature* **475:** 497–500

Lister R, Mukamel EA, Nery JR, Urich M, Puddifoot CA, Johnson ND, Lucero J, Huang Y, Dwork AJ, Schultz MD, Yu M, Tonti-Filippini J, Heyn H, Hu S, Wu JC, Rao A, Esteller M, He C, Haghighi FG, Sejnowski TJ, et al (2013) Global epigenomic reconfiguration during mammalian brain development. *Science (80-.).* **341:** 1237905

Liu F, Dai S, Feng D, Peng X, Qin Z, Kearns AC, Huang W, Chen Y, Ergün S, Wang H, Rappaport J, Bryda EC, Chandrasekhar A, Aktas B, Hu H, Chang SL, Gao B & Qin X (2019) Versatile cell ablation tools and their applications to study loss of cell functions. *Cell. Mol. Life Sci.* **76:** 4725–4743

Liu X, Ma L, Liu H, Gan J, Xu Y, Zhang T, Mu P, Wu J, Shi Y, Zhang Y, Gong L & He M (2020) Cell-type-specific gene inactivation and in situ restoration via recombinase-based flipping of targeted genomic region. *J. Neurosci.* **40:** 7169–7186

Logie C & Stewart AF (1995) Ligand-regulated site-specific recombination. *Proc. Nail. Acad. Sci. USA* **92:** 5940–5944

Loonstra A, Vooijs M, Beverloo HB, Allak B Al, Van Drunen E, Kanaar R, Berns A & Jonkers J (2001) Growth inhibition and DNA damage induced by Cre recombinase in mammalian cells. *Proc. Natl. Acad. Sci. U. S. A.* **98:** 9209–9214

Lowell BB, S-Susulic V, Hamann A, Lawitts JA, Himms-Hagen J, Boyer BB, Kozak LP & Flier JS (1993) Development of obesity in transgenic mice after genetic ablation of brown adipose tissue. *Nature* **366:** 740–742

Luche H, Weber O, Rao TN, Blum C & Fehling HJ (2007) Faithful activation of an extra-bright red fluorescent protein in ‘knock-in’ Cre-reporter mice ideally suited for lineage tracing studies. *Eur. J. Immunol.* **37:** 43–53

Luikenhuis S, Giacometti E, Beard CF & Jaenisch R (2004) Expression of MeCP2 in postmitotic neurons rescues Rett syndrome in mice. *Proc. Natl. Acad. Sci. U. S. A.* **101:** 6033–8

Luo L, Ambrozkiewicz MC, Benseler F, Chen C, Dumontier E, Falkner S, Furlanis E, Gomez AM, Hoshina N, Huang WH, Hutchison MA, Itoh-Maruoka Y, Lavery LA, Li W, Maruo T, Motohashi J, Pai ELL, Pelkey KA, Pereira A, Philips T, et al (2020) Optimizing Nervous System-Specific Gene Targeting with Cre Driver Lines: Prevalence of Germline Recombination and Influencing Factors. *Neuron*

106: 37-65.

Luquet S, Perez FA, Hnasko TS & Palmiter RD (2005) NPY/AgRP neurons are essentials for feeding in adult mice but can be ablated in neonates. *Science (80-.).* **310:** 683–685

Lyon MF (1961) Gene Action in the X-chromosom (Mus musculus L.). *Nature* **190:** 372–373

Lyst MJ, Ekiert R, Ebert DH, Merusi C, Nowak J, Guy J, Kastan NR, Robinson ND, Lima F De, Rappsilber J, Greenberg ME & Bird A (2013) Rett syndrome mutations abolish the interaction of MeCP2 with the NCoR / SMRT co-repressor. *Nat. Neurosci.* **16:** 1–14

Lyst MJ, Ekiert R, Guy J, Selfridge J, Koerner M V., Merusi C, De Sousa D & Bird A (2018) Affinity for DNA Contributes to NLS Independent Nuclear Localization of MeCP2. *Cell Rep.* **24:** 2213–2220

MacCorkle RA, Freeman KW & Spencer DM (1998) Synthetic activation of caspases: Artificial death switches. *Proc. Natl. Acad. Sci. U. S. A.* **95:** 3655–3660

Mallet VO, Mitchell C, Guidotti J-E, Jaffray P, Fabre M, Spencer D, Arnoult D, Kahn A & Gilgenkrantz H (2002) Conditional cell ablation by tight control of caspase-3 dimerization in transgenic mice. *Nat. Biotechnol.* **20:** 1234–1239

Martínez de Paz A, Khajavi L, Martin H, Gimeno RC, Dieck ST, Cheema MS, Mut JVS, Moksa MM, Carles A & Brodie NI (2019) MeCP2 - E1 isoform is a dynamically expressed , weakly DNA - bound protein with different protein and DNA interactions compared to MeCP2 - E2. *Epigenetics Chromatin* **12:** 1–16

Masuyama T, Matsuo M, Jing JJ, Tabara Y, Kitsuki K, Yamagata H, Kan Y, Miki T, Ishii K & Kondo I (2005) Classic Rett syndrome in a boy with R133C mutation of MECP2. *Brain Dev.* **27:** 439–442

Matagne V, Ehinger Y, Saidi L, Borges-Correia A, Barkats M, Bartoli M, Villard L & Roux JC (2017) A codon-optimized Mecp2 transgene corrects breathing deficits and improves survival in a mouse model of Rett syndrome. *Neurobiol. Dis.* **99:** 1–11

Matarazzo V, Cohen D, Palmer AM, Simpson PJ, Khokhar B, Pan SJ & Ronnett G V. (2004) The transcriptional repressor Mecp2 regulates terminal neuronal differentiation. *Mol. Cell. Neurosci.* **27:** 44–58

McCauley MD, Wang T, Mike E, Herrera J, Beavers DL, Huang T, Ward CS, Skinner S, Percy AK, Glaze DG, Wehrens XHT & Neul JL (2011) Pathogenesis of Lethal Cardiac Arrythmias in Mecp2 Mutant Mice: Implication for Therapy in Rett Syndrome. *Sci. Transl. Med.* **3:** 113ra125

McGraw CM, Samaco RC & Zoghbi HY (2011) Adult neural function requires MeCP2. *Science (80-.).* **333:** 186

Medrihan L, Tantalaki E, Aramuni G, Sargsyan V, Dudanova I, Missler M & Zhang W (2008) Early defects of GABAergic synapses in the brain stem of a MeCP2 mouse model of Rett syndrome. *J. Neurophysiol.* **99:** 112–121

Meier ID, Bernreuther C, Tilling T, Neidhardt J, Wong YW, Schulze C, Streichert T & Schachner M (2010) Short DNA sequences inserted for gene targeting can accidentally interfere with off-target gene expression. *FASEB J.* **24:** 1714–1724

Meins M, Lehmann J, Gerresheim F, Herchenbach J, Hagedorn M, Hameister K & Epplen JT (2005) Submicroscopic duplication in Xq28 causes increased expression of the MECP2 gene in a boy with severe mental retardation and features of Rett syndrome. *J. Med. Genet.* **42:** 1–6

Mekada E, Okada Y & Uchida T (1988) Identification of Diphtheria Toxin Receptor and a Nonproteinous Diphtheria Toxin-binding Molecule in Vero Cell Membrane. *J. Cell Biol.* **107:** 511–519

Mekada E, Senoh H, Iwamoto R, Okada Y & Uchida T (1991) Purification of Diphtheria Toxin Receptor from Vero Cells*. *J. Biol. Chem.* **266:** 20457–20462

Melloni RH & DeGennaro LJ (1994) Temporal onset of synapsin I gene expression coincides with neuronal differentiation during the development of the nervous system. *J. Comp. Neurol.* **342:** 449–462

Mendell JR, Al-Zaidy S, Shell R, Arnold WD, Rodino-Klapac LR, Prior TW, Lowes L, Alfano L, Berry K, Church K, Kissel JT, Nagendran S, L'Italien J, Sproule DM, Wells C, Cardenas JA, Heitzer MD, Kaspar A, Corcoran S, Braun L, et al (2017) Single-Dose Gene-Replacement Therapy for Spinal Muscular Atrophy. *N. Engl. J. Med.* **377:** 1713–1722

Méndez-Ferrer S, Michurina T V., Ferraro F, Mazloom AR, MacArthur BD, Lira SA, Scadden DT, Ma'ayan A, Enikolopov GN & Frenette PS (2010) Mesenchymal and haematopoietic stem cells form a unique bone marrow niche. *Nature* **466:** 829–834

Meng X, Wang W, Lu H, He LJ, Chen W, Chao ES, Fiorotto ML, Tang B, Herrera JA, Seymour ML, Neul JL, Pereira FA, Tang J, Xue M & Zoghbi HY (2016) Manipulations of MeCP2 in glutamatergic neurons highlight their contributions to rett and other neurological disorders. *Elife* **5:** 1–21

Merritt JK, Collins BE, Erickson KR, Dong H & Neul JL (2020) Pharmacological read-through of R294X Mecp2 in a novel mouse model of Rett syndrome. *Hum. Mol. Genet.* **29:** 2461–2470

Middlebrook JL & Dorland RB (1977) Response of cultured mammalian cells to the exotoxins of Pseudomonas aeruginosa and Corynebacterium diphtheriae: differential cytotoxicity. *Can. J. Microbiol.* **23:** 183–189

Migeon BR, Dunn MA, Thomas G, Schmeckpeper BJ & Naidu4' S (1995) Studies of X Inactivation and Isodisomy in Twins Provide Further Evidence That the X

Chromosome Is Not Involved in Rett Syndrome. *Am. J. Hum. Genet.* **56:** 647–653

Minkovsky A, Sahakyan A, Bonora G, Damoiseaux R, Dimitrova E, Rubbi L, Pellegrini M, Radu CG & Plath K (2015) A high-throughput screen of inactive X chromosome reactivation identifies the enhancement of DNA demethylation by 5-aza-2′-dC upon inhibition of ribonucleotide reductase. *Epigenetics and Chromatin* **8:** 1–17

Minks J, Robinson WP & Brown CJ (2008) A skewed view of X chromosome inactivation. *J. Clin. Invest.* **118:** 20–23

Minocha S, Sung TL, Villeneuve D, Lammers F & Herr W (2016) Compensatory embryonic response to allele-specific inactivation of the murine X-linked gene Hcfc1. *Dev. Biol.* **412:** 1–17

Mitamura T, Higashiyama S, Taniguchi N, Klagsbrun M & Mekada E (1995) Diphtheria toxin binds to the epidermal growth factor (EGF)-like domain of human heparin-binding EGF-like growth factor/diphtheria toxin receptor and inhibits specifically its mitogenic activity. *J. Biol. Chem.* **270:** 1015–1019

Mnatzakanian GN, Lohi H, Munteanu I, Alfred SE, Yamada T, MacLeod PJM, Jones JR, Scherer SW, Schanen NC, Friez MJ, Vincent JB & Minassian BA (2004) A previously unidentified MECP2 open reading frame defines a new protein isoform relevant to Rett syndrome. *Nat. Genet.* **36:** 339–341

Mo A, Mukamel EA, Davis FP, Luo C, Henry GL, Picard S, Urich MA, Nery JR, Sejnowski TJ, Lister R, Eddy SR, Ecker JR & Nathans J (2015) Epigenomic Signatures of Neuronal Diversity in the Mammalian Brain. *Neuron* **86:** 1369–1384

Monk M & Harper MI (1979) Sequential X chromosome inactivation couples with cellular differentiation in early mouse embryos. *Nature* **281:** 311–313

Monrós E, Armstrong J, Aibar E, Poo P, Canós I & Pineda M (2001) Rett syndrome in Spain: mutation analysis and clinical correlations. *Brain Dev.* **23:** 251–253

Moog U, Smeets EEJ, Van Roozendaal KEP, Schoenmakers S, Herbergs J, Schoonbrood-Lenssen AMJ & Schrander-Stumpel CTRM (2003) Neurodevelopmental disorders in males related to the gene causing Rett syndrome in females (MECP2). *Eur. J. Paediatr. Neurol.* **7:** 5–12

Mosley M, Shah C, Morse KA, Miloro SA, Holmes MM, Ahern TH & Forger NG (2017) Patterns of cell death in the perinatal mouse forebrain. *J Comp Neurol* **525:** 47–64

Mullaney BC, Johnston M V. & Blue ME (2004) Developmental expression of methyl-CpG binding protein 2 is dynamically regulated in the rodent brain. *Neuroscience* **123:** 939–949

Mullen RJ, Buck CR & Smith AM (1992) NeuN, a neuronal specific nuclear protein in vertebrates. *Development* **116:** 201–211

Murphy JR (2011) Mechanism of diphtheria toxin catalytic domain delivery to the eukaryotic cell cytosol and the cellular factors that directly participate in the process. *Toxins (Basel).* **3:** 294–308

Nagai Y, Kikuchi E, Lerchner W, Inoue KI, Ji B, Eldridge MAG, Kaneko H, Kimura Y, Oh-Nishi A, Hori Y, Kato Y, Hirabayashi T, Fujimoto A, Kumata K, Zhang MR, Aoki I, Suhara T, Higuchi M, Takada M, Richmond BJ, et al (2016) PET imaging-guided chemogenetic silencing reveals a critical role of primate rostromedial caudate in reward evaluation. *Nat. Commun.* **7:** 1–8

Naglich JG, Metherall JE, Russell DW & Eidels L (1992) Expression cloning of a diphtheria toxin receptor: Identity with a heparin-binding EGF-like growth factor precursor. *Cell* **69:** 1051–1061

Naiche L. & Papaioannou VE (2007) Cre Activity Causes Widespread Apoptosis and Lethal Anemia During Embryonic Development. *Genesis* **45:** 768–775

Naidu S, Kitt CA, Wong DF, Price DL, Troncoso JC & Moser HW (1988) Research on Rett syndrome: Strategy and preliminary results. *J. Child Neurol.* **3:** S78–S86

Naidu S, Murphy M, Moser HW, Rett A, Opitz JM & Reynolds JF (1986) Rett syndrome - natural history in 70 cases. *Am. J. Med. Genet.* **25:** 61–72

Nan X, Campoy FJ & Bird A (1997) MeCP2 Is a Transcriptional Repressor with Abundant Binding Sites in Genomic Chromatin. *Cell* **88:** 471–481

Nan X, Meehan RR & Bird A (1993) Dissection of the methyl-CpG binding domain from the chromosomal protein MeCP2. *Nucleic Acids Res.* **21:** 4886–4892

Nan X, Ng H, Johnson CA, Laherty CD, Turner BM, Eisenman RN & Bird A (1998) Transcriptional repression by the methyl-CpG-binding protein MeCP2 involves a histone deacetylase complex. *Nature* **393:** 386–389

Nelson ED, Kavalali ET & Monteggia LM (2006) MeCP2-Dependent Transcriptional Repression Regulates Excitatory Neurotransmission. *Curr. Biol.* **16:** 710–716

Neul JL (2012) The relationship of Rett syndrome and MECP2 disorders to autism. *Dialogues Clin. Neurosci.* **14:** 253–262

Neul JL, Fang P, Barrish J, Lane J, Caeg EB, Smith EO, Zoghbi H, Percy A & Glaze DG (2008) Specific Mutations in Methyl-CpG-Binding Protein 2 Confer Different Severity in Rett Syndrome. *Neurology* **70:** 1313–1321

Neul JL, Kaufmann WE, Glaze DG, Christodoulou J, Clarke AJ, Bahi-Buisson N, Leonard H, Bailey MES, Schanen NC, Zappella M, Renieri A, Huppke P & Percy AK (2010) Rett syndrome: Revised diagnostic criteria and nomenclature. *Ann. Neurol.* **68:** 944–950

Nguyen MVC, Du F, Felice CA, Shan X, Nigam A, Mandel G, Robinson JK & Ballas N (2012) MeCP2 Is Critical for Maintaining Mature Neuronal Networks and Global Brain Anatomy during Late Stages of Postnatal Brain Development and in the Mature Adult Brain. *J. Neurosci.* **32:** 10021–10034

Nguyen MVC, Felice CA, Du F, Covey M V, Robinson JK, Mandel G & Ballas N (2013) Oligodendrocyte Lineage Cells Contribute Unique Features to Rett Syndrome Neuropathology. *Neurobiol. Dis.* **33:** 18764–18774

Nissenkorn A, Levy-Drummer RS, Bondi O, Renieri A, Villard L, Mari F, Mencarelli MA, Lo Rizzo C, Meloni I, Pineda M, Armstrong J, Clarke A, Bahi-Buisson N, Mejaski BV, Djuric M, Craiu D, Djukic A, Pini G, Bisgaard AM, Melegh B, et al (2015) Epilepsy in Rett syndrome - Lessons from the Rett networked database. *Epilepsia* **56:** 569–576

O'Connor R., Zayzafoon M, Farach-Carson MC & Schanen NC (2009) Mecp2 Deficiency Decreases Bone Formation and Reduces Bone Volume in a Rodent Model of Rett Syndrome. *Bone* **45:** 346–356

Oberoi J, Fairall L, Watson PJ, Yang JC, Czimmerer Z, Kampmann T, Goult BT, Greenwood JA, Gooch JT, Kallenberger BC, Nagy L, Neuhaus D & Schwabe JWR (2011) Structural basis for the assembly of the SMRT/NCoR core transcriptional repression machinery. *Nat. Struct. Mol. Biol.* **18:** 177–185

Ohhata T & Wutz A (2013) Reactivation of the inactive X chromosome in development and reprogramming. *Cell. Mol. Life Sci.* **70:** 2443–2461

Olson EN, Arnold HH, Rigby PWJ & Wold BJ (1996) Know your neighbors: Three phenotypes in null mutants of the myogenic bHLH gene MRF4. *Cell* **85:** 1–4

Oppenheim RW (1985) Naturally occurring cell death during neural development. *Trends Neurosci.* **8:** 487–493

Oppenheim RW (1989) The neurotrophic theory and naturally occurring motoneuron death. *Trends Neurosci.* **12:** 252–255

Oppenheim RW (1991) Cell death during development of the nervous system. *Ann. Rev. Neurosci.* **14:** 453–501

Oppenheim RW (2001) Viktor Hamburger (1900-2001). Journey of a neuroembryologist to the end of the millennium and beyond. *Neuron* **31:** 179–190

Orban PC, Chui D & Marth JD (1992) Tissue-and site-specific DNA recombination in transgenic mice. *Proc. Natl. Acad. Sci.* **89:** 6861–6865

Osen-Sand A, Catsicas M, Staple JK, Jones KA, Ayala G, Knowles J, Grenningloh G & Catsicas S (1993) Inhibition of axonal growth by SNAP-25 antisense oligonucleotides in vitro and in vivo. *Nature* **364:** 445–448

Osen-Sand A, Staple JK, Naldi E, Schiavo G, Rossetto O, Petitpierre S, Malgaroli A, Montecucco C & Catsicas S (1996) Common and distinct fusion proteins in axonal growth and transmitter release. *J. Comp. Neurol.* **367:** 222–234

Oyler GA, Polli JW, Wilson MC & Billingsley ML (1991) Developmental expression of the 25-kDa synaptosomal-associated protein (SNAP-25) in rat brain. *Proc. Natl. Acad. Sci. U. S. A.* **88:** 5247–5251

Pajvani UB, Trujillo ME, Combs TP, Iyengar P, Jelicks L, Roth KA, Kitsis RN & Scherer PE (2005) Fat apoptosis through targeted activation of caspase 8: A new mouse model of inducible and reversible lipoatrophy. *Nat. Med.* **11:** 797–803

Palmer A, Qayumi J & Ronnett G (2008) MeCP2 mutation causes distinguishable phases of acute and chronic defects in synaptogenesis and maintenance, respectively. *Mol. Cell. Neurosci.* **37:** 794–807

Palmiter R (2001) Interrogation by Toxin. *Nat. Biotechnol.* **19:** 731–732

Palmiter RD, Behringer RR, Quaife CJ, Maxwell F, Maxwell IH & Brinster RL (1987) Cell Lineage Ablation in Transgenic Mice by Cell-Specific Expression of a Toxin Gene. *Cell* **50:** 435–443

Pan Y & Monje M (2020) Activity shapes neural circuit form and function: A historical perspective. *J. Neurosci.* **40:** 944–954

Panighini A, Duranti E, Santini F, Maffei M, Pizzorusso T, Funel N, Taddei S, Bernardini N, Ippolito C, Virdis A & Costa M (2013) Vascular Dysfunction in a Mouse Model of Rett Syndrome and Effects of Curcumin Treatment. *PLoS One* **8:** e64863

Pappenheimer AM (1977) Diphtheria Toxin. *Ann. Rev. Biochem.* **46:** 69–94

Pappenheimer JA. M, Harper AA., Michael M & Brockes JP. (1982) Diphtheria Toxin and Related Proteins : Effect of Route of Injection on Toxicity and the Determination of Cytotoxicity for Various Cultured Cells. *J. Infect. Dis.* **145:** 94–102

Pasque V & Plath K (2015) X Chromosome Reactivation in Reprogramming and in Development. *Curr Opin Cell Biol* **37:** 75–83

Pegoraro E, Schimke RN, Arahata K, Hayashi Y, Stern H, Marks H, Glasberg MR, Carroll JE, Taber JW, Wessel HB, Bauserman SC, Marks WA, Toriello H V, Higgins J V, Appleton S, Schwartz L, Garcia CA & Hoffman EP (1994) Detection of New Paternal Dystrophin Gene Mutations in Isolated Cases of Dystrophinopathy in Females. *Am. J. Hum. Genet* **54:** 989–1003

Pelka GJ, Watson CM, Christodoulou J & Tam PPL (2005) Distinct expression profiles of Mecp2 transcripts with different lengths of 3'UTR in the brain and visceral organs during mouse development. *Genomics* **85:** 441–452

Pelletier J & Sonenberg N (1988) Internal initiation of translation of eukaryotic mRNA directed by a sequence derived from poliovirus RNA. *Nature* **334:** 320–325

Peñagarikano O, Lázaro MT, Lu XH, Gordon A, Dong H, Lam HA, Peles E, Maidment NT, Murphy NP, Yang XW, Golshani P & Geschwind DH (2015) Exogenous and evoked oxytocin restores social behavior in the Cntnap2 mouse model of autism. *Sci. Transl. Med.* **7:** 271ra8 1–11

Percy AK, Lee H, Neul JL, Lane JB, Skinner SA, Geerts SP, Graham J, McNair L, Motil KJ, Barrish JO & Glaze DG (2010a) Profiling Scoiosis in Rett Sydnrome. *Pediatr. Res.* **67:** 435–439

Percy AK, Neul JL, Glaze DG, Motil KJ, Skinner SA, Khwaja O, Lee HS, Lane JB, Barrish JO, Annese F, McNair L, Graham J & Barnes K (2010b) Rett syndrome diagnostic criteria: Lessons from the Natural History Study. *Ann. Neurol.* **68:** 951–955

Petrenko V, Mihhailova J, Salmon P & Kiss JZ (2015) Apoptotic neurons induce proliferative responses of progenitor cells in the postnatal neocortex. *Exp. Neurol.* **273:** 126–137

Pham CTN, Macivor DM, Hug BA, Heusel JW & Ley TJ (1996) Long-range disruption of gene expression by a selectable marker cassette. *Proc. Natl. Acad. Sci. U. S. A.* **93:** 13090–13095

Pitcher MR, Herrera JA, Buffington SA, Kochukov MY, Merritt JK, Fisher AR, Schanen NC, Costa-Mattioli M & Neul JL (2015) Rett syndrome like phenotypes in the R255X Mecp2 mutant mouse are rescued by MECP2 transgene. *Hum. Mol. Genet.* **24:** 2662–2672

Plenge RM, Hendrich BD, Schwartz C, Arena JF, Naumova A, Sapienza C, Winter RM & Willard HF (1997) A promoter mutation in the XIST gene in two unrelated families with skewed X-chromosome inactivation. *Nature* **17:** 353–356

Plenge RM, Stevenson RA, Lubs HA, Schwartz CE & Willard HF (2002) Skewed X-Chromosome Inactivation Is a Common Feature of X-Linked Mental Retardation Disorders. *Am. J. Hum. Genet* **71:** 168–173

Plummer NW, Ungewitter EK, Smith KG, Yao HHC & Jensen P (2017) A new mouse line for cell ablation by diphtheria toxin subunit A controlled by a Cre-dependent FLEx switch. *Genesis* **55:** 1–8

Pozzo-Miller L, Pati S & Percy AK (2015) Rett Syndrome: Reaching for Clinical Trials. *Neurotherapeutics* **12:** 631–640

Przanowski P, Wasko U, Zheng Z, Yu J, Sherman R, Zhu LJ, McConnell MJ, Tushir-Singh J, Green MR & Bhatnagar S (2018) Pharmacological reactivation of inactive X-linked Mecp2 in cerebral cortical neurons of living mice. *Proc. Natl. Acad. Sci. U. S. A.* **115:** 7991–7996

Puck JM, Nussbaum RL, Conley ME & Stokes J (1987) Carrier Detection in X-linked Severe Combined Immunodeficiency Based on Patterns of X Chromosome Inactivation. *J. Clin. Invest***:** 1395–1400

Rajewsky K, Gu H, Kühn R, Betz UAK, Müller W, Roes J & Schwenk F (1996) Perspectives Series: Molecular Medicine in Genetically Engineered Animals. *J. Clin. Invest.* **98:** 600–603

Ramirez-Solis R, Zheng H, Whiting J, Krumlauf R & Bradley A (1993) Hoxb-4 (Hox-2.6) Mutant Mice Show Homeotic Transformation of a Cervical Vertebra and Defects in the Closure of the Sternal Rudiments. *Cell* **73:** 279–294

Ranichandran V, Chawla A & Roche PA (1996) Identification of a novel syntaxin- and synaptobrevin/ VAMP-binding protein, SNAP-23, expressed in non-neuronal tissues. *J. Biol. Chem.* **271:** 13300–13303

Rees HA & Liu DR (2018) Base editing: precision chemistry on the genome and transcriptome of living cells. *Nat. Rev. Genet.* **19:** 770–788

Reichwald K, Thiesen J, Wiehe T, Weitzel J, Strätling WH, Kioschis P, Poustka A, Rosenthal A & Platzer M (2000) Comparative sequence analysis of the MECP2 -locus in human and mouse reveals new transcribed regions. *Mamm. Genome* **11:** 182–190

Reiter H., Waitzman D. & Stryker M. (1986) Cortical activity blockade prevents ocular dominance plasticity in the kitten visual cortex. *Exp. Brain Res.* **65:** 182–188

Rempe D, Vangeison G, Hamilton J, Li Y, Jepson M & Federoff HJ (2006) Synapsin I Cre transgene expression in male mice produces germline recombination in progeny. *Genesis* **44:** 44–49

Renieri A, Mari F, Mencarelli MA, Scala E, Ariani F, Longo I, Meloni I, Cevenini G, Pini G, Hayek G & Zappella M (2009) Diagnostic criteria for the Zappella variant of Rett syndrome (the preserved speech variant). *Brain Dev.* **31:** 208–216

Renthal W, Boxer LD, Hrvatin S, Li E, Silberfeld A, Nagy MA, Griffith EC, Vierbuchen T & Greenberg ME (2018) Characterization of human mosaic Rett syndrome brain tissue by single-nucleus RNA sequencing. *Nat. Neurosci.* **21:** 1670–1679

Rett A (1966) [On a unusual brain atrophy syndrome in hyperammonemia in childhood]. *Wien. Med. Wochenschr.* **116:** 723—726

Révy D, Jaouen F, Salin P, Melon C, Chabbert D, Tafi E, Concetta L, Langa F, Amalric M, Kerkerian-Le Goff L, Marie H & Beurrier C (2014) Cellular and Behavioral Outcomes of Dorsal Striatonigral Neuron Ablation: New Insights into Striatal Functions. *Neuropsychopharmacology* **39:** 2662–2672

Rizo J & Südhof TC (2002) Snares and munc18 in synaptic vesicle fusion. *Nat. Rev. Neurosci.* **3:** 641–653

Robinson L, Guy J, McKay L, Brockett E, Spike RC, Selfridge J, De Sousa D, Merusi C, Riedel G, Bird A & Cobb SR (2012) Morphological and functional reversal of phenotypes in a mouse model of Rett syndrome. *Brain* **135:** 2699–2710

Rolando S (1985) Rett syndrome: Report of eight cases. *Brain Dev.* **7:** 290–296

Ross PD, Guy J, Selfridge J, Kamal B, Bahey N, Tanner KE, Gillingwater TH, Jones RA, Loughrey CM, McCarroll CS, Bailey MES, Bird A & Cobb S (2016) Exclusive expression of MeCP2 in the nervous system distinguishes between brain and peripheral Rett syndrome-like phenotypes. *Hum. Mol. Genet.* **0:** 1–16

Ross SR, Graves RA & Spiegelman BM (1993) Targeted expression of a toxin gene to adipose tissue : transgemc mice resistant to obesity. *Genes Dev.* **7:** 1318–1324

Roth BL (2016) DREADDs for Neuroscientists. *Neuron* **89:** 683–694

Roth D & Burgoyne RD (1994) SNAP-25 is present in a SNARE complex in adrenal chromaffin cells. *FEBS Lett.* **351:** 207–210

Ryan MD, Donnelly M, Lewis A, Mehrotra AP, Wilkie J & Gani D (1999) A Model for Nonstoichiometric, Cotranslational Protein Scission in Eukaryotic Ribosomes. *Bioorg. Chem.* **27:** 55–79

Ryan MD, King AMQ & Thomas GP (1991) Cleavage of foot-and-mouth disease virus polyprotein is mediated by residues located within a 19 amino acid sequence. *J. Gen. Virol.* **72:** 2727–2732

Saito M, Iwawaki T, Taya C, Yonekawa H, Noda M, Inui Y, Mekada E, Kimata Y, Tsuru A & Kohno K (2001) Diphtheria toxin receptor-mediated conditional and targeted cell ablation in transgenic mice. *Nat. Biotechnol.* **19:** 746–750

Samaco RC, Fryer JD, Ren J, Fyffe S, Chao H, Sun Y, Greer JJ, Zoghbi HY & Neul JL (2008) A partial loss of function allele of Methyl-CpG-binding protein 2 predicts a human neurodevelopmental syndrome. *Hum. Mol. Genet.* **17:** 1718–1727

Samaco RC, Mandel-Brehm C, Chao HT, Ward CS, Fyffe-Maricich SL, Ren J, Hyland K, Thaller C, Maricich SM, Humphreys P, Greer JJ, Percy A, Glaze DG, Zoghbi HY & Neul JL (2009) Loss of MeCP2 in aminergic neurons causes cell-autonomous defects in neurotransmitter synthesis and specific behavioral abnormalities. *Proc. Natl. Acad. Sci. U. S. A.* **106:** 21966–21971

Sauer B (1987) Functional Expression of the cre-lox Site-Specific Recombination System in the Yeast Saccharomyces cerevisiae. *Mol. Cell. Biol.* **7:** 2087–2096

Sauer B (1996) Multiplex Cre/lox recombination permits selective site-specific DNA targeting to both a natural and an engineered site in the yeast genome

Sauer B (1998) Inducible Gene Targeting in Mice Using the Cre/lox System. *Methods* **14:** 381–392

Sauer B & Henderson N (1988) Site-specific DNA recombination in mammalian cells by the Cre recombinase of bacteriophage P1. *Proc. Nail. Acad. Sci. USA* **85:** 5166–5170

Scacheri PC, Crabtree JS, Novotny EA, Garrett-Beal L, Chen A, Edgemon KA, Marx SJ, Spiegel AM, Chandrasekharappa SC & Collins FS (2001) Bidirectional transcriptional activity of PGK-neomycin and unexpected embryonic lethality in heterozygote chimeric knockout mice. *Genesis* **30:** 259–263

Sceniak MP, Lang M, Enomoto AC, James Howell C, Hermes DJ & Katz DM (2016) Mechanisms of Functional Hypoconnectivity in the Medial Prefrontal Cortex of Mecp2 Null Mice. *Cereb. Cortex* **26:** 1938–1956

Schanen C & Francke U (1998) A Severely affected male born into Rett Syndrome kindrer supports X-linked inheritance and allws extension of the exclusion map. *Am J Hum Genet* **63:** 267–269

Schanen C, Houwink EJF, Dorrani N, Lane J, Everett R, Feng A, Cantor RM & Percy A (2004) Phenotypic manifestations ofMECP2 mutations in classical and atypical rett syndrome. *Am. J. Med. Genet.* **126A:** 129–140

Schanen NC, Dahle EJR, Capozzoli F, Holm VA, Zoghbi HY & Francke U (1997) A New Rett Syndrome Family Consistent with X-Linked Inheritance Expands the X Chromosome Exclusion Map. *Am. J. Hum. Genet.* **61:** 634–641

Schiavo G, Benfenatit F, Poulain B, Rossetto O, Laureto PP De, Dasguptall BR, Montecucco C & Biomembrane CCNR (1992) Tetanus and botulinum-B neurotoxins block neurotransmitter release by proteolytic cleavage of synaptobrevin. *Nature* **359:** 832–835

Schmidt EE, Taylor DS, Prigge JR, Barnett S & Capecchi MR (2000) Illegitimate Cre-dependent chromosome rearrangements in transgenic mouse spermatids. *Proc. Natl. Acad. Sci. U. S. A.* **97:** 13702–13707

Schnütgen F, De-Zolt S, Van Sloun P, Hollatz M, Floss T, Hansen J, Altschmied J, Seisenberger C, Ghyselinck NB, Ruiz P, Chambon P, Wurst W & Von Melchner H (2005) Genomewide production of multipurpose alleles for the functional analysis of the mouse genome. *Proc. Natl. Acad. Sci. U. S. A.* **102:** 7221–7226

Schnütgen F, Doerflinger N, Calléja C, Wendling O, Chambon P & Ghyselinck NB (2003) A directional strategy for monitoring Cre-mediated recombination at the cellular level in the mouse. *Nat. Biotechnol.* **21:** 562–565

Schober A (2004) Classic toxin-induced animal models of Parkinson's disease: 6-OHDA and MPTP. *Cell Tissue Res.* **318:** 215–224

Schoch S, Cibelli G & Thiel G (1996) Neuron-specific Gene Expression of Synapsin 1. *J. or Biol. Chem.* **271:** 3317–3323

Schüle B, Armstrong DD, Vogel H, Oviedo A & Francke U (2008) Severe congenital

encephalopathy caused by MECP2 null mutations in males: Central hypoxia and reduced neuronal dendritic structure. *Clin. Genet.* **74:** 116–126

Schultz R, Glaze D, Motil K, Hebert D & Percy A (1998) Hand and foot growth failure in Rett syndrome. *J. Child Neurol.* **13:** 71–74

Schultz RJ, Glaze DG, Motil KJ, Armstrong DD, Del Junco DJ, Hubbard CR & Percy AK (1993) The Pattern of Growth Failure in Rett Syndrome. *Am. J. Dis. Child.* **147:** 633–637

Schwartzman JS, Bernardino A, Nishimura A, Gomes RR & Zatz M (2001) Rett syndrome in a boy with a 47,XXY karyotype confirmed by a rare mutation in the MECP2 gene. *Neuropediatrics* **32:** 162–164

Sejersen T & Lendahl U (1993) Transient expression of the intermediate filament nestin during skeletal muscle development. *J. Cell Sci.* **106:** 1291–1300

Semple BD, Blomgre K, Gimlin K, Ferriero DM & Noble-Haeusslein J (2013) Brain development in rodents and humans: Identifying benchmarks of maturation and vulnerability to injury across species. *Prog Neurobiol* **106**–**107:** 1–16

Serbedzija GN, Chen JN & Fishman MC (1998) Regulation in the heart field of zebrafish. *Development* **125:** 1095–1101

Shahbazian MD, Antalffy B, Armstrong DL & Zoghbi HY (2002a) Insight into Rett syndrome: MeCP2 levels display tissue- and cell-specific differences and correlate with neuronal maturation. *Hum. Mol. Genet.* **11:** 115–124

Shahbazian MD, Sun Y & Zoghbi HY (2002b) Balanced X chromosome inactivation patterns in the Rett syndrome brain. *Am. J. Med. Genet.* **111:** 164–168

Shahbazian MD, Young JI, Yuva-Paylor LA, Spencer CM, Antalffy BA, Noebels JL, Armstrong DL, Paylor R & Zoghbi HY (2002c) Mice with truncated MeCP2 recapitulate many Rett syndrome features and display hyperacetylation of histone H3. *Neuron* **35:** 243–254

Siegel RW, Jain R & Bradbury A (2001) Using an in vivo phagemid system to identify non-compatible *loxP* sequences. *FEBS Lett.* **505:** 467–473

Sillitoe R V. & Joyner AL (2007) Morphology, molecular codes, and circuitry produce the three-dimensional complexity of the cerebellum. *Annu. Rev. Cell Dev. Biol.* **23:** 549–577

Sinnamon JR, Kim SY, Corson GM, Song Z, Nakai H, Adelman JP & Mandel G (2017) Site-directed RNA repair of endogenous Mecp2 RNA in neurons. *Proc. Natl. Acad. Sci.***:** 201715320

Sinnamon JR, Kim SY, Fisk JR, Song Z, Nakai H, Jeng S, Mcweeney SK & Mandel G (2020) In Vivo Repair of a Protein Underlying a Neurological Disorder by Programmable RNA Editing. *Cell Rep.* **32:** 107878

Sinnett SE, Hector RD, Gadalla KKE, Heindel C, Chen D, Zaric V, Bailey MES, Cobb SR & Gray SJ (2017) Improved MECP2 Gene Therapy Extends the Survival of MeCP2-Null Mice without Apparent Toxicity after Intracisternal Delivery. *Mol. Ther. - Methods Clin. Dev.* **5:** 106–115

Sirianni N, Naidu S, Pereira J, Pillotto RF & Hoffman EP (1998) Rett syndrome: Confirmation of X-linked dominant inheritance, and localization of the gene to Xq28. *Am. J. Hum. Genet.* **63:** 1552–1557

Skarnes WC, Auerbach BA & Joyner AL (1992) A gene trap approach in mouse embryonic stem cells: the lacZ reporter is activated by splicing, reflects endogenous gene expression, and is mutagenic in mice. *Genes Dev.* **6:** 903–918

Skene PJ, Illingworth RS, Webb S, Kerr ARW, James KD, Turner DJ, Andrews R & Bird AP (2010) Neuronal MeCP2 Is Expressed at Near Histone-Octamer Levels and Globally Alters the Chromatin State. *Mol. Cell* **37:** 457–468

Smrt RD, Eaves-Egenes J, Barkho BZ, Santistevan NJ, Zhao C, Aimone JB, Gage FH & Zhao X (2007) Mecp2 deficiency leads to delayed maturation and altered gene expression in hippocampal neurons. *Neurobiol. Dis.* **27:** 77–89

Sohal VS, Zhang F, Yizhar O & Deisseroth K (2009) Parvalbumin neurons and gamma rhythms enhance cortical circuit performance. *Nature* **459:** 698–702

Song C, Feodorova Y, Guy J, Peichl L, Jost KL, Kimura H, Cardoso MC, Bird A, Leonhardt H, Joffe B & Solovei I (2014) DNA methylation reader MECP2 : cell type- and differentiation stage-specific protein distribution. *Epigenetics and Chromatin* **7:** 1–16

Sonntag S, Dedek K, Dorgau B, Schultz K, Schmidt KF, Cimiotti K, Weiler R, Löwel S, Willecke K & Janssen-Bienhold U (2012) Ablation of retinal horizontal cells from adult mice leads to rod degeneration and remodeling in the outer retina. *J. Neurosci.* **32:** 10713–10724

Spruijt CG, Gnerlich F, Smits AH, Pfaffeneder T, Jansen PWTC, Bauer C, Münzel M, Wagner M, Müller M, Khan F, Eberl HC, Mensinga A, Brinkman AB, Lephikov K, Müller U, Walter J, Boelens R, Van Ingen H, Leonhardt H, Carell T, et al (2013) Dynamic Readers for 5-(Hydroxy)methylcytosine and its Axidized Derivatives. *Cell* **152:** 1146–1159

Sripathy S, Leko V, Adrianse RL, Loe T, Foss EJ, Dalrymple E, Lao U, Gatbonton-Schwager T, Carter KT, Payer B, Paddison PJ, Grady WM, Lee JT, Bartolomei MS & Bedalov A (2017) Screen for reactivation of MeCP2 on the inactive X chromosome identifies the BMP/TGF-β superfamily as a regulator of XIST expression. *Proc. Natl. Acad. Sci.***:** 201621356

Stachniak TJ, Ghosh A & Sternson SM (2014) Chemogenetic Synaptic Silencing of Neural Circuits Localizes a Hypothalamus→Midbrain Pathway for Feeding Behavior. *Neuron* **82:** 797–808

Steller H (1998) Artificial death switches: Induction of apoptosis by chemically induced caspase multimerization. *Proc. Natl. Acad. Sci. U. S. A.* **95:** 5421–5422

Sternberg N & Hamilton D (1981) Bacteriophage P1 Site-specific Recombination. I. Recombination Between loxP Sites. *J. Mol. Biol.* **150:** 467–486

Sternson SM & Roth BL (2014) Chemogenetic tools to interrogate brain functions. *Annu. Rev. Neurosci.* **37:** 387–407

Stiles J & Jernigan TL (2010) The Basics of Brain Development. *Neuropsychol. Rev.* **20:** 327–348

Sun YJ & Baumer A (1999) Nonrandom X inactivation and selection of fragile X full mutation in fetal fibroblasts. *Am. J. Med. Genet.* **86:** 162–164

Suter B, Treadwell-Deering D, Zoghbi HY, Glaze DG & Neul JL (2014) MECP2 Mutations in people without Rett Syndrome. *J. Autism Dev. Disord. Autism Dev Disord.* **44:** 703–711

Szymczak AL & Vignali DAA (2005) Development of 2A peptide-based strategies in the design of multicistronic vectors. *Expert Opin. Biol. Ther.* **5:** 627–638

Tan S-S, Williams EA & Tam PPL (1993) X-chromosome inactivation occurs at different times in different tissues of the post-implantation mouse embryo. **3:** 170–174

Taneja P, Ogier M, Brooks-Harris G, Schmid DA, Katz DM & Nelson SB (2009) Pathophysiology of Locus Ceruleus Neurons in a Mouse Model of Rett syndrome. *J. Neurosci.* **29:** 12187–12195

Tarquinio DC, Hou W, Neul JL, Kaufmann WE, Glaze DG, Motil KJ, Skinner SA, Lee H-S & Percy AK (2015) The Changing Face of Survival in Rett Syndrome and MECP2-Related disorders . *Pediatr Neurol* **53:** 402–411

Tarquinio DC, Motil KJ, Hou W, Lee HS, Glaze DG, Skinner SA, Neul JL, Annese F, McNair L, Barrish JO, Geerts SP, Lane JB & Percy AK (2012) Growth failure and outcome in Rett syndrome: Specific growth references. *Neurology* **79:** 1653–1661

The Rett Syndrome Diagnostic Criteria Work Group (1988) Diagnostic criteria for rett syndrome. *Ann. Neurol.* **23:** 425–428

Thiel G, Lietz M & Cramer M (1998) Biological activity and modular structure of RE-1-silencing transcription factor (REST), a repressor of neuronal genes. *J. Biol. Chem.* **273:** 26891–26899

Thomaidou D, Mione MC, Cavanagh JFR & Parnavelas JG (1997) Apoptosis and its relation to the cell cycle in the developing cerebral cortex. *J. Neurosci.* **17:** 1075–1085

Thorel F, Népote V, Avril I, Kohno K, Desgraz R, Chera S & Herrera PL (2010) Conversion of Adult Pancreatic α-cells to β-cells After Extreme β-cell Loss. *Nature* **464:** 1149–1154

Thyagarajan B, Guimarães MJ, Groth AC & Calos MP (2000) Mammalian genomes contain active recombinase recognition sites. *Gene* **244:** 47–54

Tillotson R & Bird A (2020) The Molecular Basis of MeCP2 Function in the Brain. *J. Mol. Biol.* **432:** 1602–1623

Tillotson R, Selfridge J, Koerner M V., Gadalla KKE, Guy J, De Sousa D, Hector RD, Cobb SR & Bird A (2017) Radically truncated MeCP2 rescues Rett syndrome-like neurological defects. *Nature* **550:** 398–401

Topçu M, Akyerli C, Sayi A, Törüner GA, Koçoglu SR, Cimbis M & Özçelik T (2002) Somatic mosaicism for a MECP2 mutation associated with classic Rett syndrome in a boy. *Eur. J. Hum. Genet.* **10:** 77–81

Trappe R, Laccone F, Cobilanschi J, Meins M, Huppke P, Hanefeld F & Engel W (2001) MECP2 Mutations in Sporadic Cases of Rett Syndrome Are Almost Exclusively of Paternal Origin. *Am. J. Hum. Genet.* **68:** 1093–1101

Tremblay MÈ, Stevens B, Sierra A, Wake H, Bessis A & Nimmerjahn A (2011) The Role of Microglia in the Healthy Brain. *J. Neurosci.* **31:** 16064–16069

Tronche F, Kellendonk C, Kretz O, Gass P, Anlag K, Orban PC, Bock R, Klein R & Schütz G (1999) Disruption of the glucocorticoid receptor gene in the nervous system results in reduced anxiety. *Nature* **23:** 99–103

Tudor M, Akbarian S, Chen RZ & Jaenisch R (2002) Transcriptional profiling of a mouse model for Rett syndrome reveals subtle transcriptional changes in the brain. *PNAS* **99:** 15536–15541

Uhlén M, Fagerberg L, Hallström BM, Lindskog C, Oksvold P, Mardinoglu A, Sivertsson Å, Kampf C, Sjöstedt E, Asplund A, Olsson IM, Edlund K, Lundberg E, Navani S, Szigyarto CAK, Odeberg J, Djureinovic D, Takanen JO, Hober S, Alm T, et al (2015) Tissue-based map of the human proteome. *Science (80-.).* **347:** 394–347

Urban DJ & Roth BL (2015) DREADDs (designer receptors exclusively activated by designer drugs): Chemogenetic tools with therapeutic utility. *Annu. Rev. Pharmacol. Toxicol.* **55:** 399–417

Urbanowicz A, Downs J, Girdler S, Ciccone N & Leonard H (2015) Aspects of speech-language abilities are influenced by MECP2 mutation type in girls with Rett syndrome. *Am. J. Med. Genet. Part A* **167:** 354–362

Ure K, Lu H, Wang W, Ito-Ishida A, Wu Z, He LJ, Sztainberg Y, Chen W, Tang J & Zoghbi HY (2016) Restoration of Mecp2 expression in GABAergic neurons is sufficient to rescue multiple disease features in a mouse model of Rett syndrome.

Elife **5:** 1–21

Varley KE, Gertz J, Bowling KM, Parker SL, Reddy TE, Pauli-Behn F, Cross MK, Williams BA, Stamatoyannopoulos JA, Crawford GE, Absher DM, Wold BJ & Myers RM (2013) Dynamic DNA methylation across diverse human cell lines and tissues. *Genome Res.* **23:** 555–567

Vashi N & Justice MJ (2019) Treating Rett syndrome: from mouse models to human therapies. *Mamm. Genome* **30:** 90–110

Vawter MP, Schulmann A, Alhassen L, Alhassen W, Hamzeh AR, Sakr J, Pauluk L, Yoshimura R, Wang X, Dai Q, Sanathara N, Civelli O & Alachkar A (2020) Melanin Concentrating Hormone Signaling Deficits in Schizophrenia: Association With Memory and Social Impairments and Abnormal Sensorimotor Gating. *Int. J. Neuropsychopharmacol.* **23:** 53–65

Villard L (2007) MECP2 mutations in males. *J. Med. Genet.* **44:** 417–423

Villard L, Kpebe ; A, Cardoso ; C, Chelly ; J, Tardieu ; M & Fontes M (2000) Two affected boys in a Rett syndrome family Clinical and molecular findings. *Neurol.* **55:** 1188–1193

Vorsanova SG, Yurov YB, Ulas VY, Demidova IA, Sharonin VO, Kolotii AD, Gorbatchevskaia NL, Beresheva AK & Soloviev I V. (2001) Cytogenetic and molecular-cytogenetic studies of Rett syndrome (RTT): A retrospective analysis of a Russian cohort of RTT patients (the investigation of 57 girls and three boys). *Brain Dev.* **23:** S196–S201

Vukovic J, Borlikova GG, Ruitenberg MJ, Robinson GJ, Sullivan RKP, Walker TL & Bartlett PF (2013) Immature doublecortin-positive hippocampal neurons are important for learning but not for remembering. *J. Neurosci.* **33:** 6603–6613

Wan M, Lee SSJ, Zhang X, Houwink-Manville I, Song HR, Amir RE, Budden S, Naidu SB, Pereira JLP, Lo IFM, Zoghbi HY, Schanen NC & Francke U (1999) Rett syndrome and beyond: Recurrent spontaneous and familial MECP2 mutations at CpG hotspots. *Am. J. Hum. Genet.* **65:** 1520–1529

Wang D, Tai PWL & Gao G (2019) Adeno-associated virus vector as a platform for gene therapy delivery. *Nat. Rev. Drug Discov.* **18:** 358–378

Wang D, Zhang F & Gao G (2020) CRISPR-Based Therapeutic Genome Editing: Strategies and In Vivo Delivery by AAV Vectors. *Cell* **181:** 136–150

Wang DD & Bordey A (2008) The astrocyte odyssey. *Prog. Neurobiol.* **86:** 342–367

Wang G, Witkin JW, Hao G, Bankaitis VA, Scherer PE & Baldini G (1997) Syndet is a novel SNAP-25 related protein expressed in many tissues. *J. Cell Sci.* **110:** 505–513

Wang J, Wegener JE, Huang T, Sripathy S, De Jesus-Cortes H, Xu P, Tran S, Knobbe

W, Leko V, Britt J & Starwalt R (2015) Wild-type microglia do not reverse pathology in mouse models Rett syndrome. *Nature* **521:** E1–E4

Wang Z V., Mu J, Schraw TD, Gautron L, Elmquist JK, Zhang BB, Brownlee M & Scherer PE (2008) PANIC-ATTAC: A mouse model for inducible and reversible β-cell ablation. *Diabetes* **57:** 2137–2148

Ward CS, Arvide EM, Huang TW, Yoo J, Noebels JL & Neul JL (2011) MeCP2 is critical within HoxB1-derived tissues of mice for normal lifespan. *J. Neurosci.* **31:** 10359–10370

Watson P, Black G, Ramsden S, Barrow M, Super M, Kerr B & Clayton-Smith J (2001) Angelman syndrome phenotype associated with mutations in MECP2, a gene encoding a methyl CpG binding protein. *J. Med. Genet.* **38:** 224–228

Weaving LS, Williamson SL, Bennetts B, Davis M, Ellaway CJ, Leonard H, Thong M-K, Delatycki M, Thompson EM, Laing N & Christodoulou J (2003) Effects of MECP2 mutation type, location and X-inactivation in modulating Rett syndrome phenotype. *Am. J. Med. Genet.* **118A:** 103–114

Weese-Mayer DE, Lieske SP, Boothby CM, Kenny AS, Bennett HL, Silvestri JM & Ramirez JM (2006) Autonomic nervous system dysregulation: Breathing and heart rate perturbation during wakefulness in young girls with rett syndrome. *Pediatr. Res.* **60:** 443–449

Weng SM, McLeod F, Bailey MES & Cobb SR (2011) Synaptic plasticity deficits in an experimental model of rett syndrome: Long-term potentiation saturation and its pharmacological reversal. *Neuroscience* **180:** 314–321

West DB, Engelhard EK, Adkisson M, Nava AJ, Kirov J V., Cipollone A, Willis B, Rapp J, de Jong PJ & Lloyd KC (2016) Transcriptome Analysis of Targeted Mouse Mutations Reveals the Topography of Local Changes in Gene Expression. *PLoS Genet.* **12:** 1–19

Whissell PD, Tohyama S & Martin LJ (2016) The use of DREADDs to deconstruct behavior. *Front. Genet.* **7:** 1–15

Wiesel TN (1982) The postnatal development of the visual cortex and the influence of environment - Nobel Lecture, 8 December 1981. *Nature* **299:** 583–591

Wojcik SM, Katsurabayashi S, Guillemin I, Friauf E, Rosenmund C, Brose N & Rhee JS (2006) A Shared Vesicular Carrier Allows Synaptic Corelease of GABA and Glycine. *Neuron* **50:** 575–587

Wojcinski A, Lawton AK, Bayin NS, Lao Z, Stephen DN & Joyner AL (2017) Cerebellar granule cell replenishment postinjury by adaptive reprogramming of Nestin+ progenitors. *Nat. Neurosci.* **20:** 1361–1370

Wong K, Leonard H, Jacoby P, Ellaway C & Downs J (2015) The trajectories of sleep disturbances in Rett syndrome. *J. Sleep Res.* **24:** 223–233

Wood L & Shepherd GMG (2010) Synaptic circuit abnormalities of motor-frontal layer 2/3 pyramidal neurons in a mutant mouse model of Rett syndrome. *Neurobiol. Dis.* **38:** 281–287

Xu M, Song P, Huang W, He R, He Y, Zhou X, Gu Y, Pan S & Hu Y (2018) Disruption of AT-hook 1 domain in MeCP2 protein caused behavioral abnormality in mice. *Biochim. Biophys. Acta - Mol. Basis Dis.* **1864:** 347–358

Yamada S, Islam MS, van Kooten N, Bovee S, Oh YM, Tsujimura A, Watanabe Y & Tanaka M (2020) Neuropeptide Y neurons in the nucleus accumbens modulate anxiety-like behavior. *Exp. Neurol.* **327:** 113216

Yamaizumi M, Mekada E, Uchida T & Okada Y (1978) One molecule of diphtheria toxin fragment a introduced into a cell can kill the cell. *Cell* **15:** 245–250

Yamamoto M, Wada N, Kitabatake Y, Watanabe D, Anzai M, Yokoyama M, Teranishi Y & Nakanishi S (2003) Reversible suppression of glutamatergic neurotransmission of cerebellar granule cells in vivo by genetically manipulated expression of tetanus neurotoxin light chain. *J. Neurosci.* **23:** 6759–6767

Yang F, Babak T, Shendure J & Disteche CM (2010) Global survey of escape from X inactivation by RNA-sequencing in mouse. *Genome Res.* **20:** 614–622

Yasuda M, Johnson-Venkatesh EM, Zhang H, Parent JM, Sutton MA & Umemori H (2011) Multiple Forms of Activity-Dependent Competition Refine Hippocampal Circuits In Vivo. *Neuron* **70:** 1128–1142

Yoshida H, Kong YY, Yoshida R, Elia AJ, Hakem A, Hakem R, Penninger JM & Mak TW (1998) Apaf1 is required for mitochondrial pathways of apoptosis and brain development. *Cell* **94:** 739–750

Young D, Nagarajan L, de Klerk N, Jacoby P, Ellaway C & Leonard H (2007) Sleep problems in Rett syndrome. *Brain Dev.* **29:** 609–616

Young DJ, Bebbington A, Anderson A, Ravine D, Ellaway C, Kulkarni A, De Klerk N, Kaufmann WE & Leonard H (2008) The diagnosis of autism in a female: could it be Rett syndrome? *Eur J Pediatr* **167:** 661–669

Young JI & Zoghbi HY (2004) X-Chromosome Inactivation Patterns Are Unbalanced and Affect the Phenotypic Outcome in a Mouse Model of Rett Syndrome. *Am. J. Hum. Genet.* **74:** 511–520

Yu CR, Power J, Barnea G, Donnell SO, Brown HE V, Osborne J, Axel R & Gogos JA (2004) Spontaneous Neural Activity Is Required for the Establishment and Maintenance of the Olfactory Sensory Map. **42:** 553–566

Zaghlula M, Glaze DG, Enns GM, Potocki L, Schwabe AL & Suter B (2018) Current clinical evidence does not support a link between TBL1XR1 and Rett syndrome: Description of one patient with Rett features and a novel mutation in TBL1XR1, and a review of TBL1XR1 phenotypes. *Am. J. Med. Genet.* **176:** 1683–1687

Zappella M (1992) The Rett Girls with Preserved Speech. *Brain Dev.* **14:** 98–101

Zappella M, Meloni I, Longo I, Canitano R, Hayek G, Rosaia L, Mari F & Renieri A (2003) Study of MECP2 gene in Rett Syndrome Variants and Autistic Girls. *Am. J. Med. Genet.* **119B:** 102–107

Zappella M, Meloni I, Longo I, Hayek G & Renieri A (2001) Preserved speech variants of the Rett syndrome: Molecular and clinical analysis. *Am. J. Med. Genet.* **104:** 14–22

Zhang L, He J, Jugloff DGM & Eubanks JH (2008) The MeCP2-null Mouse Hippocampus Displays Altered Basal Inhibitory Rhythms and Is Prone to Hyperexcitability. *Hippocampus* **18:** 294–309

Zhao H & Reed RR (2001) X Inactivation of the OCNC1 Channel Gene Reveals a Role for Activity-Dependent Competition in the Olfactory System. *Cell* **104:** 651–660

Zhou Z, Hong EJ, Cohen S, Zhao W, Ho HH, Schmidt L, Chen WG, Lin Y, Savner E, Griffith EC, Hu L, Steen JAJ, Weitz CJ & Greenberg ME (2006) Brain-Specific Phosphorylation of MeCP2 Regulates Activity- Dependent Bdnf Transcription, Dendritic Growth, and Spine Maturation. *Neuron* **52:** 255–269

Zhu Y, Romero MI, Ghosh P, Ye Z, Charnay P, Rushing EJ, Marth JD & Parada LF (2001) Ablation of NF1 function in neurons induces abnormal development of cerebral cortex and reactive gliosis in the brain. *Genes Dev.* **15:** 859–876

Zimmerman L, Lendahl U, Cunningham M, Mckay R, Parr B, Gavin B, Mann J, Vassileva C & Mcmahon A (1994) Independent Regulatory Elements in the Nestin Gene Direct Transgene Expression to Neural Stem Cells ￼or Muscle Precursors. *Neuron* **12:** 11–24

Zoghbi H (1988) Genetic Aspects of Rett Syndrome. *J. Child Neurol.* **3:** S76–S78

Zoghbi HY, Percy AK, Schultz RJ & Fill C (1990) Patterns of X chromosome inactivation in the rett syndrome. *Brain Dev.* **12:** 131–135

Chapter 9 Appendix

Name	Sequence (5'-3')
***Mecp2*^{StopDTR} targeting vector**	
LoxP sites	ATAACTTCGTATAGCATACATTATACGAAGTTAT
En-2 Splice acceptor (SA)	GATCCCCTAGTTTGTGATAGGCCTTTTAGCTACATCTGCCAATCCATCTCATTTTCACACA CACACACCACTTTCCTTCTGGTCAGTGGGCACATGCCCAGCCTCAAGTTTATATCACCACC CCCAATGCCCAACACTTGTATGGCCTTGGGCGGGTCATCCCCCCCCCCCCCACCCCCAGTAT CTGCAACCTCAAGCTTGGGTGCGTGGGTTGTGGATAAGTAGCTAGACTCCAGCAACCAGTA ACCTCTGCCCTTTCTCCTCCATGACAACCAGGTCCCAGGTCCCGAAAACCAAAGAAGAAGA ACCCTAACAAAGAGGACAAGCGGCCTCGCACAGCCTTCACTGCTGAGCAGCTCCAGAGGCT CAAGGCTGAGTTTCAGACCAACAGGTACCTGACAGAGCAGCGGCGCCAGAGTCTGGCACAG GAGCTC
SV40 polyA	TTGTTTATTGCAGCTTATAATGGTTACAAATAAAGCAATAGCATCACAAATTTCACAAATA AAGCATTTTTTTCACTGCATTCTAGTTGTGGTTTGTCCAAACTCATCAATGTATCTTATCA TGTCTGGATC
bGH polyA	CGACTGTGCCTTCTAGTTGCCAGCCATCTGTTGTTTGCCCCTCCCCCGTGCCTTCCTTGAC CCTGGAAGGTGCCACTCCCACTGTCCTTTCCTAATAAAATGAGGAAATTGCATCGCATTGT CTGAGTAGGTGTCATTCTATTCTGGGGGGTGGGGTGGGGCAGGACAGCAAGGGGGAGGATT GGGAAGAGAATAGCAGGCATG
NeoStop cassette	Taken from targeting vector used in (Guy *et al*, 2007) HpaI restriction enzyme site in the *Stop* cassette was mutated
HB-EGF (DTR) *minus start and stop codons	AAGCTGCTGCCGTCGGTGGTGCTGAAGCTCTTTCTGGCTGCAGTTCTCTCGGCACTGGTGA CTGGCGAGAGCCTGGAGCGGCTTCGGAGAGGGCTAGCTGCTGGAACCAGCAACCCGGACCC TCCCACTGTATCCACGGACCAGCTGCTACCCCTAGGAGGCGGCCGGGACCGGAAAGTCCGT GACTTGCAAGAGGCAGATCTGGACCTTTTGAGAGTCACTTTATCCTCCAAGCCACAAGCAC TGGCCACACCAAACAAGGAGGAGCACGGGAAAAGAAAGAAGAAAGGCAAGGGGCTAGGGAA GAAGAGGGACCCATGTCTTCGGAAATACAAGGACTTCTGCATCCATGGAGAATGCAAATAT GTGAAGGAGCTCCGGGCTCCCTCCTGCATCTGCCACCCGGGTTACCATGGAGAGAGGTGTC ATGGGCTGAGCCTCCCAGTGGAAAATCGCTTATATACCTATGACCACACAACCATCCTGGC CGTGGTGGCTGTGGTGCTGTCATCTGTCTGTCTGCTGGTCATCGTGGGGCTTCTCATGTTT AGGTACCATAGGAGAGGAGGTTATGATGTGGAAAATGAAGAGAAAGTGAAGTTGGGCATGA CTAATTCCCAC
P2A	GGAAGCGGAGCTACTAACTTCAGCCTGCTGAAGCAGGCTGGAGACGTGGAGGAGAACCCTG GACCT
SV40 NLS	CCCAAGAAGAAGAGGAAGGTG
EGFP *minus stop codon	ATGGTGAGCAAGGGCGAGGAGCTGTTCACCGGGGTGGTGCCCATCCTGGTCGAGCTGGACG GCGACGTAAACGGCCACAAGTTCAGCGTGTCCGGCGAGGGCGAGGGCGATGCCACCTACGG CAAGCTGACCCTGAAGTTCATCTGCACCACCGGCAAGCTGCCCGTGCCCTGGCCCACCCTC GTGACCACCCTGACCTACGGCGTGCAGTGCTTCAGCCGCTACCCCGACCACATGAAGCAGC ACGACTTCTTCAAGTCCGCCATGCCCGAAGGCTACGTCCAGGAGCGCACCATCTTCTTCAA GGACGACGGCAACTACAAGACCCGCGCCGAGGTGAAGTTCGAGGGCGACACCCTGGTGAAC CGCATCGAGCTGAAGGGCATCGACTTCAAGGAGGACGGCAACATCCTGGGGCACAAGCTGG AGTACAACTACAACAGCCACAACGTCTATATCATGGCCGACAAGCAGAAGAACGGCATCAA GGTGAACTTCAAGATCCGCCACAACATCGAGGACGGCAGCGTGCAGCTCGCCGACCACTAC CAGCAGAACACCCCCATCGGCGACGGCCCCGTGCTGCTGCCCGACAACCACTACCTGAGCA CCCAGTCCGCCCTGAGCAAAGACCCCAACGAGAAGCGCGATCACATGGTCCTGCTGGAGTT CGTGACCGCCGCCGGGATCACTCTCGGCATGGACGAGCTGTACAAGTAA
CRISPR plasmid	
gRNA	CACCGTTAGCTGACTTTACATAGAG
Cas9 plasmid	PX330-U6-Chimeric_BB-CBh-hSpCas9 (Addgene ID: 42230)
cDNA expression vectors	
Mecp2 Exon 1 Gibson assembly fragment	TACCGCGGGCCCGGGATCCAAAAACCCGTCCGGAAAATGGCCGCCGCTGCCGCCACCGCCG CCGCCGCCGCCGCGCCGAGCGGAGGAGGAGGAGGAGGCGAGGAGGAGAGACTGGAGGAAAA G
DTR-P2A-GFP Gibson assembly fragment	AGGAGAGACTGGAGGAAAAGAAGCTGCTGCCGTCGGTGGTGCTGAAGCTCTTTCTGGCTGC AGTTCTCTCGGCACTGGTGACTGGCGAGAGCCTGGAGCGGCTTCGGAGAGGGCTAGCTGCT GGAACCAGCAACCCGGACCCTCCCACTGTATCCACGGACCAGCTGCTACCCCTAGGAGGCG GCCGGGACCGGAAAGTCCGTGACTTGCAAGAGGCAGATCTGGACCTTTTGAGAGTCACTTT ATCCTCCAAGCCACAAGCACTGGCCACACCAAACAAGGAGGAGCACGGGAAAAGAAAGAAG AAAGGCAAGGGGCTAGGGAAGAAGAGGGACCCATGTCTTCGGAAATACAAGGACTTCTGCA TCCATGGAGAATGCAAATATGTGAAGGAGCTCCGGGCTCCCTCCTGCATCTGCCACCCGGG TTACCATGGAGAGAGGTGTCATGGGCTGAGCCTCCCAGTGGAAAATCGCTTATATACCTAT GACCACACAACCATCCTGGCCGTGGTGGCTGTGGTGCTGTCATCTGTCTGTCTGCTGGTCA TCGTGGGGCTTCTCATGTTTAGGTACCATAGGAGAGGAGGTTATGATGTGGAAAATGAAGA GAAAGTGAAGTTGGGCATGACTAATTCCCACGGAAGCGGAGCTACTAACTTCAGCCTGCTG AAGCAGGCTGGAGACGTGGAGGAGAACCCTGGACCTCCCAAGAAGAAGAGGAAGGTGATGG TGAGCAAGGGCGAGGAGCTGTTCACCGGGGTGGTGCCCATCCTGGTCGAGCTGGACGGCGA

	CGTAAACGGCCACAAGTTCAGCGTGTCCGGCGAGGGCGAGGGCGATGCCACCTACGGCAAG CTGACCCTGAAGTTCATCTGCACCACCGGCAAGCTGCCCGTGCCCTGGCCCACCCTCGTGA CCACCCTGACCTACGGCGTGCAGTGCTTCAGCCGCTACCCCGACCACATGAAGCAGCACGA CTTCTTCAAGTCCGCCATGCCCGAAGGCTACGTCCAGGAGCGCACCATCTTCTTCAAGGAC GACGGCAACTACAAGACCCGCGCCGAGGTGAAGTTCGAGGGCGACACCCTGGTGAACCGCA TCGAGCTGAAGGGCATCGACTTCAAGGAGGACGGCAACATCCTGGGGCACAAGCTGGAGTA CAACTACAACAGCCACAACGTCTATATCATGGCCGACAAGCAGAAGAACGGCATCAAGGTG AACTTCAAGATCCGCCACAACATCGAGGACGGCAGCGTGCAGCTCGCCGACCACTACCAGC AGAACACCCCCATCGGCGACGGCCCCGTGCTGCTGCCCGACAACCACTACCTGAGCACCCA GTCCGCCCTGAGCAAAGACCCCAACGAGAAGCGCGATCACATGGTCCTGCTGGAGTTCGTG ACCGCCGCCGGGATCACTCTCGGCATGGACGAGCTGTACAAGTAAGCGACTCTAGATCATA ATCA
DTR cDNA AgeI – NotI fragment	GGATCCACCGGTCGCCACCATGAAGCTGCTGCCGTCGGTGGTGCTGAAGCTCTTTCTGGCT GCAGTTCTCTCGGCACTGGTGACTGGCGAGAGCCTGGAGCGGCTTCGGAGAGGGCTAGCTG CTGGAACCAGCAACCCGGACCCTCCCACTGTATCCACGGACCAGCTGCTACCCCTAGGAGG CGGCCGGGACCGGAAAGTCCGTGACTTGCAAGAGGCAGATCTGGACCTTTTGAGAGTCACT TTATCCTCCAAGCCACAAGCACTGGCCACACCAAACAAGGAGGAGCACGGGAAAAGAAAGA AGAAAGGCAAGGGGCTAGGGAAGAAGAGGGACCCATGTCTTCGGAAATACAAGGACTTCTG CATCCATGGAGAATGCAAATATGTGAAGGAGCTCCGGGCTCCCTCCTGCATCTGCCACCCG GGTTACCATGGAGAGAGGTGTCATGGGCTGAGCCTCCCAGTGGAAAATCGCTTATATACCT ATGACCACACAACCATCCTGGCCGTGGTGGCTGTGGTGCTGTCATCTGTCTGTCTGCTGGT CATCGTGGGGCTTCTCATGTTTAGGTACCATAGGAGAGGAGGTTATGATGTGGAAAATGAA GAGAAAGTGAAGTTGGGCATGACTAATTCCCACTGAAGCGGCCGCGACTCT
DTR Gibson assembly fragment pDTR-IRES-GFP plasmid	CAAGCTTGGTACCGAGCTCGGATCCACCGGTCGCCACCATGAAGCTGCTGCCGTCGGTGGT GCTGAAGCTCTTTCTGGCTGCAGTTCTCTCGGCACTGGTGACTGGCGAGAGCCTGGAGCGG CTTCGGAGAGGGCTAGCTGCTGGAACCAGCAACCCGGACCCTCCCACTGTATCCACGGACC AGCTGCTACCCCTAGGAGGCGGCCGGGACCGGAAAGTCCGTGACTTGCAAGAGGCAGATCT GGACCTTTTGAGAGTCACTTTATCCTCCAAGCCACAAGCACTGGCCACACCAAACAAGGAG GAGCACGGGAAAAGAAAGAAGAAAGGCAAGGGGCTAGGGAAGAAGAGGGACCCATGTCTTC GGAAATACAAGGACTTCTGCATCCATGGAGAATGCAAATATGTGAAGGAGCTCCGGGCTCC CTCCTGCATCTGCCACCCGGGTTACCATGGAGAGAGGTGTCATGGGCTGAGCCTCCCAGTG GAAAATCGCTTATATACCTATGACCACACAACCATCCTGGCCGTGGTGGCTGTGGTGCTGT CATCTGTCTGTCTGCTGGTCATCGTGGGGCTTCTCATGTTTAGGTACCATAGGAGAGGAGG TTATGATGTGGAAAATGAAGAGAAAGTGAAGTTGGGCATGACTAATTCCCACTGAAGCGGC GGTTAACGAATTCCGCCCCT
***Mecp2*$^{FLExDTR(OFF)}$ targeting vector**	
FRT sites	GAAGTTCCTATTCTCTAGAAAGTATAGGAACTTC
Lox2272 sites	ATAACTTCGTATAAAGTATCCTATACGAAGTTAT
LoxP sites	ATAACTTCGTATAATGTATGCTATACGAAGTTAT
5' lox sites + intervening DNA	ATAACTTCGTATAAAGTATCCTATACGAAGTTATATCAAAATAGGAAGACCAATGCTTCAC CATCGACCCGAATTGCCAAGCATCACCATCGACCCATAACTTCGTATAATGTATGCTATAC GAAGTTAT Taken from Addgene plasmid #28304 pAAV-FLEX-GFP
3' lox sites + intervening DNA	ATAACTTCGTATAGGATACTTTATACGAAGTTATCATTGGGATTCTTCCTATTTTGATCCA AGCATCACCATCGACCCTCTAGTCCAGATCTCACCATCGACCCATAACTTCGTATAGCATA CATTATACGAAGTTAT Taken from Addgene plasmid #28304 pAAV-FLEX-GFP

Appendix Table 1. Sequence components on *Mecp2*^{StopDTR} and *Mecp2*$^{FLExDTR(OFF)}$ targeting vectors.

ATGAAGCTGCTGCCGTCGGTGGTGCTGAAGCTCTTTCTGGCTGCAGTTCTCTCGGCACTGGTGACTGG
CGAGAGCCTGGAGCGGCTTCGGAGAGGGCTAGCTGCTGGAACCAGCAACCCGGACCCTCCCACTGTAT
CCACGGACCAGCTGCTACCCCTAGGAGGCGGCCGGGACCGGAAAGTCCGTGACTTGCAAGAGGCAGAT
CTGGACCTTTTGAGAGTCACTTTATCCTCCAAGCCACAAGCACTGGCCACACCAAACAAGGAGGAGCA
CGGGAAAAGAAAGAAGAAAGGCAAGGGGCTAGGGAAGAAGAGGGACCCATGTCTTCGGAAATACAAGG
ACTTCTGCATCCATGGAGAATGCAAATATGTGAAGGAGCTCCGGGCTCCCTCCTGCATCTGCCACCCG
GGTTACCATGGAGAGAGGTGTCATGGGCTGAGCCTCCCAGTGGAAAATCGCTTATATACCTATGACCA
CACAACCATCCTGGCCGTGGTGGCTGTGGTGCTGTCATCTGTCTGTCTGCTGGTCATCGTGGGGCTTC
TCATGTTTAGGTACCATAGGAGAGGAGGTTATGATGTGGAAAATGAAGAGAAAGTGAAGTTGGGCATG
ACTAATTCCCACTGA

Appendix Figure 1. Human Heparin-binding EGF-like growth factor (HBEGF) DTR coding sequence. Sequence ID NCBI: NM_001945.2. Ensembl: ENST00000230990.6

MKLLPSVVLKLFLAAVLSALVTGESLERLRRGLAAGTSNPDPPTVSTDQLLPLGGGRDRKVRDLQEAD
LDLLRVTLSSKPQALATPNKEEHGKRKKKGKGLGKKRDPCLRKYKDFCIHGECKYVKELRAPSCICHP
GYHGERCHGLSLPVENRLYTYDHTTILAVVAVVLSSVCLLVIVGLLMFRYHRRGGYDVENEEKVKLGM
TNSH

Appendix Figure 2. Human Heparin-binding EGF-like growth factor (HBEGF)(the DTR) protein sequence. 208 amino acids. Sequence ID: NCBI: NP_001936.1; ENSP00000230990.6

ATGGCCGCCGCTGCCGCCACCGCCGCCGCCGCCGCCGCGCCGAGCGGAGGAGGAGGAGGAGGCGAGGA
GGAGAGACTGGAGGAAAAGAAGCTGCTGCCGTCGGTGGTGCTGAAGCTCTTTCTGGCTGCAGTTCTCT
CGGCACTGGTGACTGGCGAGAGCCTGGAGCGGCTTCGGAGAGGGCTAGCTGCTGGAACCAGCAACCCG
GACCCTCCCACTGTATCCACGGACCAGCTGCTACCCCTAGGAGGCGGCCGGGACCGGAAAGTCCGTGA
CTTGCAAGAGGCAGATCTGGACCTTTTGAGAGTCACTTTATCCTCCAAGCCACAAGCACTGGCCACAC
CAAACAAGGAGGAGCACGGGAAAAGAAAGAAGAAAGGCAAGGGGCTAGGGAAGAAGAGGGACCCATGT
CTTCGGAAATACAAGGACTTCTGCATCCATGGAGAATGCAAATATGTGAAGGAGCTCCGGGCTCCCTC
CTGCATCTGCCACCCGGGTTACCATGGAGAGAGGTGTCATGGGCTGAGCCTCCCAGTGGAAAATCGCT
TATATACCTATGACCACACAACCATCCTGGCCGTGGTGGCTGTGGTGCTGTCATCTGTCTGTCTGCTG
GTCATCGTGGGGCTTCTCATGTTTAGGTACCATAGGAGAGGAGGTTATGATGTGGAAAATGAAGAGAA
AGTGAAGTTGGGCATGACTAATTCCCACGGAAGCGGAGCTACTAACTTCAGCCTGCTGAAGCAGGCTG
GAGACGTGGAGGAGAACCCTGGACCTCCCAAGAAGAAGAGGAAGGTGATGGTGAGCAAGGGCGAGGAG
CTGTTCACCGGGGTGGTGCCCATCCTGGTCGAGCTGGACGGCGACGTAAACGGCCACAAGTTCAGCGT
GTCCGGCGAGGGCGAGGGCGATGCCACCTACGGCAAGCTGACCCTGAAGTTCATCTGCACCACCGGCA
AGCTGCCCGTGCCCTGGCCCACCCTCGTGACCACCCTGACCTACGGCGTGCAGTGCTTCAGCCGCTAC
CCCGACCACATGAAGCAGCACGACTTCTTCAAGTCCGCCATGCCCGAAGGCTACGTCCAGGAGCGCAC
CATCTTCTTCAAGGACGACGGCAACTACAAGACCCGCGCCGAGGTGAAGTTCGAGGGCGACACCCTGG
TGAACCGCATCGAGCTGAAGGGCATCGACTTCAAGGAGGACGGCAACATCCTGGGGCACAAGCTGGAG
TACAACTACAACAGCCACAACGTCTATATCATGGCCGACAAGCAGAAGAACGGCATCAAGGTGAACTT
CAAGATCCGCCACAACATCGAGGACGGCAGCGTGCAGCTCGCCGACCACTACCAGCAGAACACCCCCA
TCGGCGACGGCCCCGTGCTGCTGCCCGACAACCACTACCTGAGCACCCAGTCCGCCCTGAGCAAAGAC
CCCAACGAGAAGCGCGATCACATGGTCCTGCTGGAGTTCGTGACCGCCGCCGGGATCACTCTCGGCAT
GGACGAGCTGTACAAGTAA

Appendix Figure 3. *Mecp2*^{DTR} e1 isoform coding sequence. Coding sequence corresponding to the e1 isoform of mRNA expressed from the recombined *Mecp2*^{StopDTR} locus. Grey= *Mecp2* exon 1; purple = coding sequence of 1st 3 amino acids of exon 3 of *Mecp2*; red = DTR (– met and stop codon); black = P2A; yellow = SV40 NLS; green = EGFP (+*Mecp2* STOP codon)

MAAAAATAAAAAAPSGGGGGGEEERLEEKKLLPSVVLKLFLAAVLSALVTGESLERLRRGLAAGTSNP
DPPTVSTDQLLPLGGGRDRKVRDLQEADLDLLRVTLSSKPQALATPNKEEHGKRKKKGKGLGKKRDPC
LRKYKDFCIHGECKYVKELRAPSCICHPGYHGERCHGLSLPVENRLYTYDHTTILAVVAVVLSSVCLL
VIVGLLMFRYHRRGGYDVENEEKVKLGMTNSHGSGATNFSLLKQAGDVEENPG

Appendix Figure 4. *Mecp2*^{DTR} protein sequence following P2A self-cleavage. 257 amino acids. Grey: N-terminus of MeCP2e1; red: DTR (minus M); black: P2A.

ATGGCCGCCGCTGCCGCCACCGCCGCCGCCGCCGCCGCGCCGAGCGGAGGAGGAGGAGGAGGCGAGGA
GGAGAGACTGGAGGAAAAGAAGCTGCTGCCGTCGGTGGTGCTGAAGCTCTTTCTGGCTGCAGTTCTCT
CGGCACTGGTGACTGGCGAGAGCCTGGAGCGGCTTCGGAGAGGGCTAGCTGCTGGAACCAGCAACCCG
GACCCTCCCACTGTATCCACGGACCAGCTGCTACCCCTAGGAGGCGGCCGGGACCGGAAAGTCCGTGA
CTTGCAAGAGGCAGATCTGGACCTTTTGAGAGTCACTTTATCCTCCAAGCCACAAGCACTGGCCACAC
CAAACAAGGAGGAGCACGGGAAAAGAAAGAAGAAAGGCAAGGGGCTAGGGAAGAAGAGGGACCCATGT
CTTCGGAAATACAAGGACTTCTGCATCCATGGAGAATGCAAATATGTGAAGGAGCTCCGGGCTCCCTC
CTGCATCTGCCACCCGGGTTACCATGGAGAGAGGTGTCATGGGCTGAGCCTCCCAGTGGAAAATCGCT
TATATACCTATGACCACACAACCATCCTGGCCGTGGTGGCTGTGGTGCTGTCATCTGTCTGTCTGCTG
GTCATCGTGGGGCTTCTCATGTTTAGGTACCATAGGAGAGGAGGTTATGATGTGGAAAATGAAGAGAA
AGTGAAGTTGGGCATGACTAATTCCCACTGA

Appendix Figure 5. *Mecp2*$^{FLExDTR(ON)}$ e1 isoform coding sequence. DNA coding sequence corresponding to the e1 isoform of mRNA expressed from the recombined *Mecp2*$^{FLExDTR(ON)}$ locus. Grey: MeCP2 exon 1; Red: DTR (– met codon, +*Mecp2* STOP codon); Purple: coding sequence of 1st 3 amino acids of exon 3.

MAAAAATAAAAAAPSGGGGGGEEERLEEKKLLPSVVLKLFLAAVLSALVTGESLERLRRGLAAGTSNP
DPPTVSTDQLLPLGGGRDRKVRDLQEADLDLLRVTLSSKPQALATPNKEEHGKRKKKGKGLGKKRDPC
LRKYKDFCIHGECKYVKELRAPSCICHPGYHGERCHGLSLPVENRLYTYDHTTILAVVAVVLSSVCLL
VIVGLLMFRYHRRGGYDVENEEKVKLGMTNSH

Appendix Figure 6. *Mecp2*$^{FLExDTR(ON)}$ protein sequence. 236 amino acids. Grey: N-terminus of MeCP2e1; red: DTR (minus M).

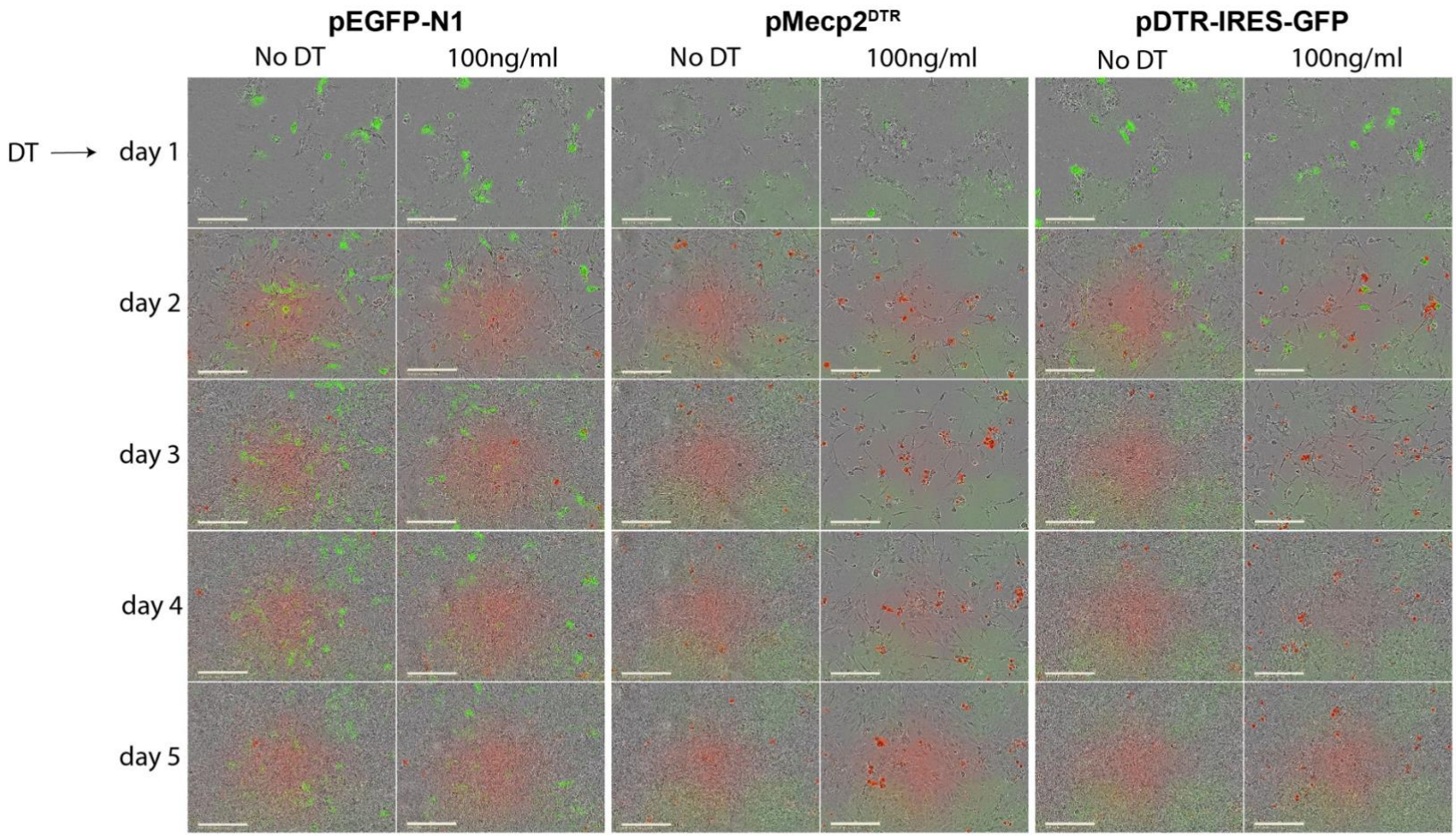

Appendix Figure 7. Incucyte images of NIH3T3 cells transfected with DTR expressing plasmid and treated with DT. NIH3T3 cells transfected with pEGFP-N1, pMecp2^{DTR}, and pDTR-IRES-GFP expression vectors were FACS sorted for EGFP expression on day 0. 24 hours later 100ng/ml DT and Incucyte Cytotox Red dye were added to the medium and cells were imaged by the Incucyte. Shown here is phase and fluorescence images taken every 24 hours following DT treatment for treated and untreated cells. Scale bar = 200 µm.

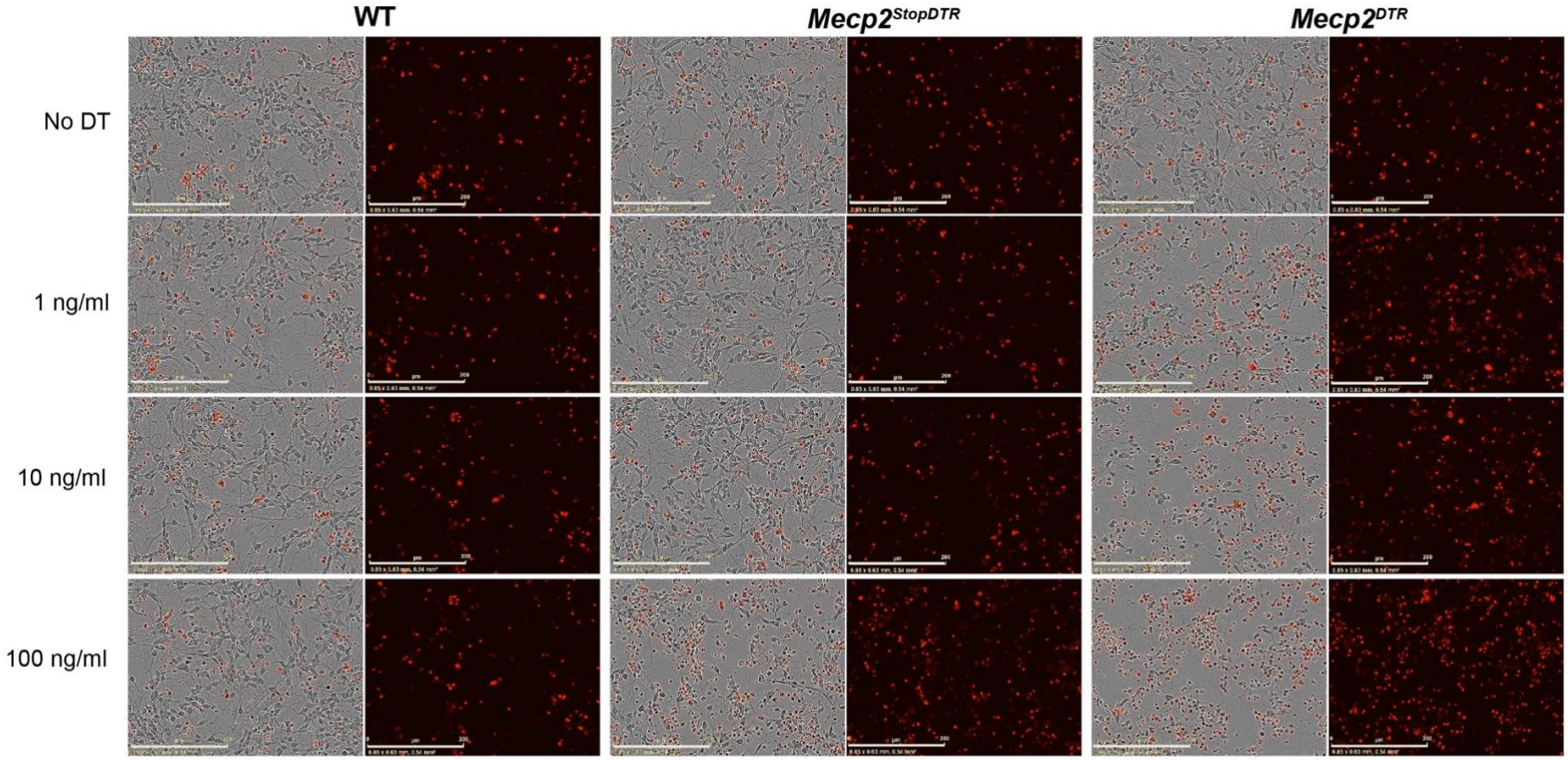

Appendix Figure 8. Incucyte images of *Mecp2*^{StopDTR} and *Mecp2*^{DTR} ESC-derived neurons treated with different doses of DT. Shown here are representative phase and fluorescent images of DT and Incucyte Cytotox Red Dye treated cells 30 hours following DT treatment. Scale bar = 200 μM.

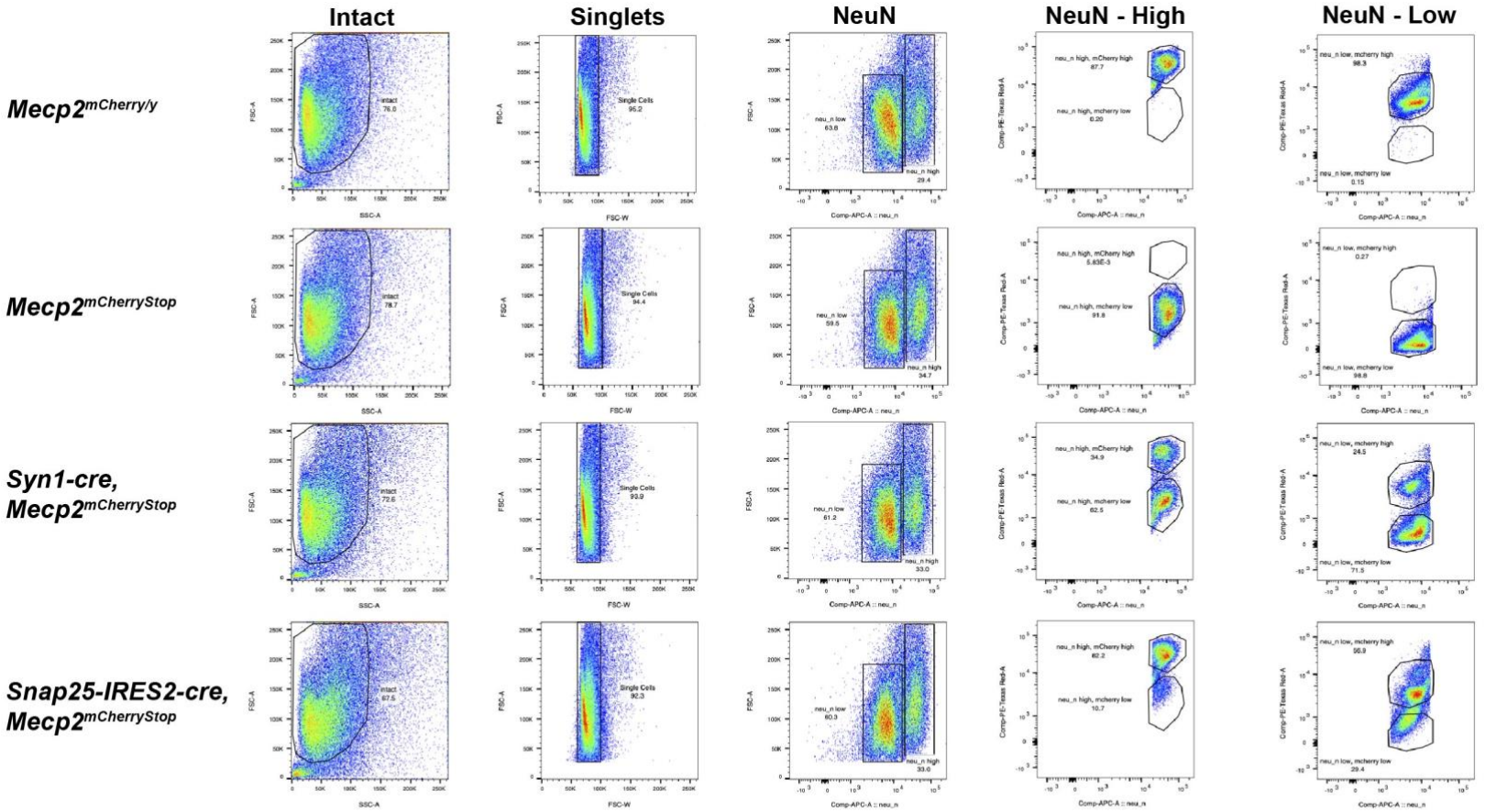

Appendix Figure 9. Flow cytometry gating method used to quantify the proportion of NeuN expressing neurons which have activted the Cre reporter expression. Flow cytometry analysis of nuclei extracted from *Mecp2*^{mCherry}, *Mecp2*^{mCherryStop}, *Syn1-Cre,Mecp2*^{mCherryStop}, *Snap25-IRES2-Cre,Mecp2*^{mCherryStop} brains. Representative images for each genotype showing the gating strategy used to identify the proportion of NeuN high neuronal nuclei which have activated mCherry expression by flow cytometry. From left to right; intact (panel 1), singlet (panel 2) nuclei were gated and analysed for their NeuN expression (panel 3). The NeuN-high (panel 4) and NeuN-low (panel 5) populations were then gated and analysed for mCherry fluorescence.

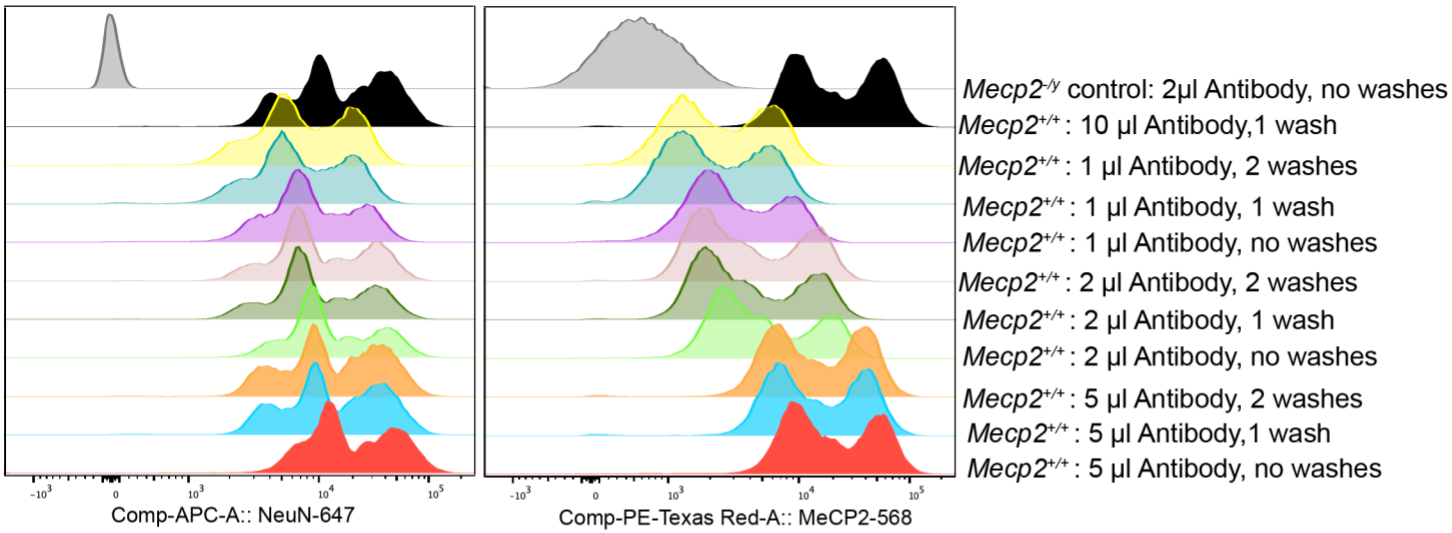

Appendix Figure 10. Optimisation of the MeCP2 and NeuN antibody nucei staining protochol for flow cytometry. Nuclei were extracted from brains from 3 female mice, WT for MeCP2. Nuclei from male *Mecp2*$^{-/y}$ knock-out mice were used as a negative MeCP2 epitope control. Nuclei were extracted as described in Chapter 2 section 2.9.4. Antibodies were labelled using APEX™ Alexa Fluor™ Antibody labelling Kit 647/568 kits and eluted in a final volume of 50µl. Nuclei were stained following the protocol outlined in Chapter 2 section 2.9.5 with added wash steps following the antibody incubations. Samples with no washes were analysed by flow cytometry directly after antibody incubations. For washes: nuclei were centrifuged 600xg for 5 mins at 4°C following antibody incubation, resuspended in 1 ml PBTB, centrifuged again, 1X wash samples were resuspended in 250µl PBTB for flow cytometry, 2X wash samples were washed again in 1 ml PBTB, centrifuged and then resuspended in 250µl PBTB and analysed by flow cytometry. For MeCP2 staining there are two peaks: lowly expressing glia and highly expressing neurons. For NeuN staining there are two peaks: low NeuN non-neuronal nuclei and high NeuN neuronal nuclei. For MeCP2-568 staining: the intensity of signal clearly goes down with antibody concentration. There is not a substantial difference between plots for 10µl and 5µl antibody, suggesting that at 5µl the anitibody has become saturated. Washes do not make a big difference to the staining profiles for both antibodies. For NeuN-647 staining: the profiles for all the different staining conditions are largely overlapping, suggesting that the antibody is saturated at the lowest concentration.

Appendix Document 1. Risk Assessment for administration of Diphtheria Toxin to cell cultures for cell viability assays.

BA Risk Assessment Form: Biological Agents and Materials

A BA risk assessment is required for any work involving the possession, use or exposure to biological agents and related materials. In addition, please note that the possession or use of any hazard group 3 biological agents or the hazard group 2 biological agents *Bordetella pertussis*, *Corynebacterium diphtheriae* and *Neisseria meningitidis* requires written permission from your School Biological Safety Committee and HSE. Please complete this form and register any hazard group 2 and 3 biological agents using Retain. The School Biological Safety Adviser provides advice to Principal Investigators on biological agent risk assessment, HSE notification and licences. You should read the guidance provided on BA risk assessment and biological safety on the Biosafety Unit website. Please complete those boxes that apply to your work.

Section 1 Basic Details

Title of project	Administration of Diphtheria Toxin to cell cultures for cell viability assays.
Local reference number	AB_KP_DT1
HSE reference number	
Principal investigator	Adrian Bird
School / Institute	School of Biological Sciences
Date of assessment	
Location of work (Buildings and room numbers or fieldwork)	4.1 (fume hood), 2.24 (incucyte), 6.6b (Cat 2 lab)

Section 2 Project

This section should describe the project which should be reasonably detailed but not exhaustive.

2.1: Description of project and activities

Cellular ablation studies will be performed using Diphtheria Toxin (DT). Cultures of genetically modified mouse embryonic stem cells and mouse NIH3T3 cells which express the Diphtheria Toxin Receptor (DTR), will be cultured in medium containing DT. The viability of cells will be assessed by visualising the amount of cell death in the Incucyte (an incubator fitted with a microscope). Cell cultures containing DT will not be further processed after the analysis of viability and will be disposed of appropriately.

Section 3 Risk Assessment

This section should describe any potential risks to humans and or the environment. It should include a clear and explicit justification of any statements made about the risks with a logical explanation and any relevant evidence or references. The level of risk is estimated using the matrix given at the end of this form and then stating the risk as either Effectively zero, Low, Low / Medium, Medium or High.

3.1: Biological agents or materials

Microorganisms (Group 1)	
Human pathogens (Group 2)	
Human pathogens (Group 3)	
Specified animal pathogens (Group 2)	

Specified animal pathogens (Group 3)	
Plant pathogens or pests	
Toxins	Diphtheria Toxin
Carcinogens	
Allergens	
Human tissues, cells or materials	
Human cell cultures	
Animal tissues, cells or materials	
Animal cell cultures	JuO9 Mouse embryonic stem cells and mouse NIH3T3 fibroblast cells
Plant tissues, cells or materials	
Plant cell cultures	
Humans	
Animals	
Plants	
Soils	
Environmental samples or materials	
Waste	
Other biological materials	

3.2: Type of work

Select all that apply	Laboratory / ~~Fieldwork~~ / ~~Other~~

3.3: Human, animal or plant diseases or conditions or environment damage associated with the biological agents

DT can be extremely toxic at very low levels. The lethal dose of DT for humans is 0.1μg of toxin per kg of body weight. All contact should be avoided. Do not breathe dust, fume or vapours of DT powder or solutions.

Hazard statement(s): H300 Fatal if swallowed.
Precautionary statement(s): P264 Wash hands thoroughly after handling P301 + P310 IF SWALLOWED: Immediately call a POISON CENTER or doctor/ physician.
Hazard symbol(s): Toxic
R-phrase(s): R28 Very toxic if swallowed.
S-phrase(s): S36/S37/39 Wear suitable protective clothing, gloves and eye/face protection. S45 In case of accident or if you feel unwell, seek medical advice immediately (show the label where possible) S28 After contact with skin, wash immediately with plenty of soap and water.

Potential health effects:
Inhalation - May be harmful if inhaled. May cause respiratory tract irritation.
Ingestion - May be fatal if swallowed.
Skin - May be harmful if absorbed through skin. May cause skin irritation.
Eyes - May cause eye irritation.
Signs and Symptoms of Exposure - Fever, Headache.

3.4: Potential routes of exposure to humans, animals or plants or release to environment

Select all that apply	Inhalation / Ingestion / Injection / Absorption / ~~Other~~

Inhalation, Ingestion, Injection, Absorption

3.5: Use of biological agents or materials

Select all that apply	Small scale / ~~Medium scale~~ / ~~Large scale~~ / ~~Fieldwork~~ / ~~Animals~~ / ~~Plants~~ / ~~Other~~

Small scale

3.6: Frequency of use	
Select one	Daily / ~~Weekly~~ / ~~Monthly~~ / ~~Other~~
Daily	
3.7: Maximum amount or concentration used	
Select one	~~Negligible~~ / Low / ~~Medium~~ / ~~High~~
1mg of lyophilized DT power is the maximum amount of toxin handled at any time during the experiment. As the lethal dose of DT is 0.1μg/kg this amount greatly exceeds the lethal dose of DT for an average person. Therefore, once reconstituted DT at a concentration of 1mg/ml is to be aliquoted into volumes of 100μl and 10μl to prevent the handling of large volumes of concentrated toxin after reconstitution.	
3.8: Levels of infectious aerosols	
Select one	Negligible / ~~Low~~ / ~~Medium~~ / ~~High~~
None	
3.9: Potential for exposure to biological agents or materials	
Select one	~~Negligible~~ / Low / ~~Medium~~ / ~~High~~
Spillage of DT powder, reconstituted DT or DT containing cell culture medium or accidental injection.	
3.10: Who might be at risk	
Select all that apply	Research Staff / Other Staff / Students / ~~Visitors~~ / ~~Public~~ / ~~Young people~~ ~~(<18yrs)~~ / ~~New and expectant mothers~~ / ~~Other~~
Research Staff, Other Staff, Students	
3.11: Overall assessment of risk to human health (Prior to use of controls)	
Level of risk (Select one)	~~Effectively zero~~ / ~~Low~~ / ~~*Medium/Low*~~ / ~~Medium~~ / High
3.12: Overall assessment of risk to environment (Prior to use of controls)	
Level of risk (Select one)	Effectively zero / ~~Low~~ / ~~Medium/Low~~ / ~~Medium~~ / ~~High~~

Section 4 Control Measures to Eliminate or Reduce Risks of Exposure or Release	
This section should describe the types of controls which will be required to carry out the work safely. You must follow the hierarchy of risk control by choosing the most effective control measures needed to safely carry out your work and not just the easiest controls. Please do not include detailed standard operating procedures which should be specified in separate documents.	
4.1: Containment laboratories or facilities	
Select all that apply	Laboratory / ~~Animal facility~~ / ~~Plant facility~~ / ~~Other~~
Laboratory	
4.2: Containment level	
Select one	~~Containment level 1~~ / Containment level 2 / ~~Containment level 3~~
Containment level 2 An incubator with built in microscope in containment level 1 (S2.24) will be used to visualise cells. Cell culture dishes/flasks containing DT will be prepared in a containment level 2 lab and transported in a sealed container to the containment level 1 incubator in room. The DT contaminated medium will remain in this locked incubator throughout the time it's in containment level 1, therefore access will be restricted.	
4.3: Microbiological safety cabinets (MSC) and isolators	
Select all that apply	~~Class I~~ / Class II / ~~Class III~~ / ~~Isolator~~ / Other
DT in lyophilised powder is to be handled in a fume hood. Reconstituted DT and DT containing cell culture medium should be handled in a Class II MSC or fume hood.	
4.4: Sharps controls	

A needle and syringe will be used to reconstitute the DT powder by injecting water/PBS through lid of purchased vial of DT. The needle will not come in contact with the DT powder. A cytotoxic waste sharps bin will be placed in the fume hood where reconstitution will be done. The needle will be disposed of immediately after use. Sharps used for reconstitution will be disposed of in sharps bin via normal incineration route.

4.5: Special controls

The amount of lyophilized DT powder purchased at any one time is 1mg.

DT stock solution should be aliquoted into volumes of 100µl or less of 1mg/ml DT.

Cell culture medium containing DT at concentrations of 0.01 – 500 ng/µl should be handled in a volume less than 50 ml.

Cell culture medium containing DT will be inactivated before being taken for autoclave (see sections 4.10 and 4.11).

All containers in contact with DT will be disposed of appropriately and never recycled.

Waste materials contaminated with DT should be kept as low as possible and put straight into a new autoclave bag, sealed and taken straight for autoclave.

4.6: Personal protective equipment (PPE)

Select all that apply	Lab coat / ~~Lab gown~~ / ~~Surgical scrubs~~ / ~~Disposable clothing~~ / ~~Apron~~ / ~~Safety spectacles~~ / ~~Goggles~~ / ~~Face shield~~ / Gloves / ~~Headwear~~ / ~~Footwear~~ / ~~Other~~

Lab coat with long sleeves.

Double gloving with thin nitrile gloves.

Eye/face protection: Safety goggles and face mask (3M:9310) should be worn when handling DT.

4.7: Respiratory protective equipment (RPE)

Select all that apply	~~Filter mask~~ / ~~Half face respirator~~ / ~~Full face respirator~~ / ~~Powered respirator~~ / ~~Breathing apparatus~~ / ~~Other~~

None

4.8: Storage controls

Lyophilised DT powder is to be stored at 4°C in a locked container. Reconstituted DT (1mg/ml) should be aliquoted into labelled vials that are tightly closed and stored at -20°C inside a labelled, leak-spill-proof secondary container inside a locked container. Cell culture flasks/dishes are disposable, leak-spill-proof, plastic containers. The smallest volume of cell culture container possible for the intended experiment will be used to reduce to volume of DT containing medium handled. Culture flasks containing DT medium should be put on a secondary tray and be clearly labelled with the name of the toxin and biohazard labels. A sign will be put on the incubator door stating “Toxin in use”.

4.9: Transport controls

Transport DT within the building in secondary, sealed, labelled, non-breakable containers.

4.10: Inactivation controls

Select all that apply	Disinfection / Autoclave / ~~Fumigation~~ / ~~Incineration~~ / ~~Other~~

Disinfection

Please give details of disinfectant(s), method and validation including concentration of disinfectant and contact time (eg supplier’s instructions or local validation).

DT can be inactivated by being treated with 1M NaOH or 1% NaOCl (10% bleach) for 30 minutes contact time or by heat inactivation via autoclave.

Autoclaving

Please give details of autoclave method and validation.

All contaminated materials will be inactivated by autoclaving (100% kill) at 134°C for 5 minutes prior to disposal of plastic waste. Autoclaves will be validated by annual (at least) thermocouple mapping and each run will be monitored by continuous chart or digital recording of the temperature / time profile and chemical indicators (eg Browne TST indicator test strips). No contaminated materials will be recycled after autoclaving.

Other
(Please give details of method and validation).

4.11: Waste disposal routes

Reconstituted powder DT (1mg/ml) will never be disposed of in volumes greater than 100µl at a time and therefore all waste falls below the >/= 20% threshold for categorisation as special waste. Diphtheria Toxin is a high molecular weight proteinaceous toxin of biological origin and can be inactivated either by treatment with a 1 M solution of NaOH, 1% NaOCl (or 10% bleach) or by heat inactivation by autoclave (1,2,3,4). Diphtheria Toxin will not be disposed of as a powder but will be dissolved in water prior to toxin inactivation by normal autoclave disposal route (2). Liquid, sharps and containers will be disposed of as clinical waste for disposal via normal autoclave route.

Cell culture medium containing DT, due to the large volume, will be collected in plastic disposable containers, inactivated with of 1M NaOH or 1% NaOCl (or 10% bleach) for 30 minutes before being autoclaved.

In-case of spill follow spill guide-lines and dispose of both solid and liquid toxin by inactivating it in a solution of 1M NaOH or 1% NaOCl (or 10% bleach) and wipe down possibly contaminated surfaces with 1 M NaOH or 1% NaOCl (or 10% bleach) (1). Followed by cleaning the surface with water to remove NaOH and NaOCl.

After all procedures all potentially contaminated surfaces should be wiped down with 1 M NaOH or 1% NaOCl (or 10% bleach) to inactivate any DT that may have inadvertently spilled (1). Followed by cleaning the surface with water to remove NaOH and NaOCl.

Note that bleach solutions should be prepared fresh daily.

References:

(1) Wharram B. L., et al., (2005). Podocyte Depletion Causes Glomerulosclerosis: Diphtheria Toxin-Induced Podocyte Depletion in Rats Expressing Human Diptheria Toxin Receptor Transgene. J Am Soc Nephrol 16: 2941 – 2952
(2) University of Virginia Biosafety Manual and Standard Operating Procedures For Biosafety Level 2 Agents. University of Virginia Office of Environmental Health and Safety, May, 2007.
(3) Biosafety in Microbiological and Biomedical Laboratories, 4th Edition, Centre for Disease Control and Prevention – National Institutes for Health, USDHHS, May, 1999
(4) University of Washington Environmental Health and Safety: Toxins of Biological Origin Safe Work Practices. Research and Occupational Safety, December, 2013

4.12: Immunisations (if applicable)

All laboratory members that will be working with DT should have an up-to-date tetanus-diphtheria toxoid (Td) or equivalent immunization.

4.13: Instructions, training and supervision

Inexperienced staff and students will be supervised by an experienced member of staff until deemed competent in the handling procedures. If in doubt about handling DT, users must consult an experienced member of the lab.

4.14: HSE notification (if applicable)

4.15: Specified Animal Pathogen Order (SAPO) licence (if applicable)

4.16: Plant Health Order (PHO) licence (if applicable)
4.17: Import, export or other licence (if applicable)

Section 5 Emergency Procedures

This section should describe any emergency procedures used to deal with accidental exposure, release or spillages.

5.1: Emergency procedures

SWALLOWED

- DT may be fatal if swallowed. TRANSFER EXPOSED INDIVIDUAL TO A&E WITHOUT DELAY BY AMBULANCE (Phone 999). A copy of the material safety data sheet should be provided to the medical doctor.
- Do NOT induce vomiting unless directed to do so by medical personnel. Never give anything by mouth to an unconscious person.

EYE exposure

- Immediately hold eyelids apart and flush the eye continuously with running water.
- Ensure complete irrigation of the eye by keeping the eyelids apart and away from the eye and moving the eyelids by occasionally lifting the upper and lower lids.
- Continue flushing until advised to stop by the Poisons information Centre or a doctor, or at least 15 minutes.
- TRANSPORT TO A&E or DOCTOR WITHOUT DELAY.
- Removal of contact lenses after an eye injury should only be undertaken by a skilled personnel.

SKIN exposure

- Immediately remove all contaminated clothing, including footwear.
- Flush skin and hair with running water (and soap if available).
- Seek medical attention in event of irritation.
-

INHALED

- If fumes or combustion products are inhaled remove from contaminated area.
- Lay patient down. Keep warm and rested.
- Prostheses such as false teeth, which may block airway, should be removed, where possible, prior to initiating first aid procedures.
- Apply artificial respiration if not breathing, preferably with a demand valve resuscitator, bag-valve mask device, or pocket mask as trained. Perform CPR if necessary.
- TRANSPORT TO HOSPITAL or DOCTOR WITHOUT DELAY.

Spillages Procedure

Liquid spills:

Wear a lab coat, safety glasses/goggles, and two pairs of disposable nitrile gloves to avoid contact with eyes, skin and clothing. Cover spill with absorbent paper towels and apply 1M NaOH or 1% NaOCl (or 10% bleach), allowing 30-min contact time to deactivate DT before disposing of towelling in clinical waste for disposal by autoclave. Ventilate area and wash contaminated area thoroughly with more 1M NaOH or 1% NaOCl (or 10% bleach) allowing 30 min contact time, then rinse with water and dispose of waste in clinical waste for disposal by autoclave.

Powder spills inside of [*fume hood/ MSC]*:

Wear a lab coat and two pairs of nitrile gloves. Gently cover powder spill with dampened absorbent paper towels to avoid raising dust. Apply 1M NaOH or 1% NaOCl (or 10% bleach) and allow 30-min contact time to deactivate DT before disposing of towelling in clinical waste for disposal by autoclave. Wash contaminated area thoroughly with more 1M NaOH or 1% NaOCl (or 10% bleach) allowing 30 min contact time, then rinse with water and dispose of waste in clinical waste for disposal by autoclave.

Powder spills outside of a *[fume hood/ MSC]*: Remove all personnel from the room and restrict access. Wear chemical safety glasses/goggles, face shield, overshoes, overalls and nitrile gloves. Follow procedures above to clean up spill.

5.2: Emergency contacts

Name	Position	Telephone
Katie Paton	PhD	
John Connelly	Post-Doc	

Section 6 Emergency Planning

This section should describe any emergency plan used to deal with serious accidental release. An emergency plan is only required for high risk work.

6.1: In case of serious accidental release is an emergency plan required to protect humans or environment	~~Yes~~ / No

NO

Risk Estimation Matrix

Consequence of hazard	**Likelihood of hazard**			
	High	**Medium**	**Low**	**Negligible**
Severe	High	High	Medium	Effectively zero
Modest	High	Medium	Medium / Low	Effectively zero
Minor	Medium / Low	Low	Low	Effectively zero
Negligible	Effectively zero	Effectively zero	Effectively zero	Effectively zero

Appendix Document 2. Risk Assessment for administration of Diphtheria Toxin to cell cultures for cell viability assays.

BA Risk Assessment Form: Biological Agents and Materials

A BA risk assessment is required for any work involving the possession, use or exposure to biological agents and related materials. In addition, please note that the possession or use of any hazard group 3 biological agents or the hazard group 2 biological agents *Bordetella pertussis*, *Corynebacterium diphtheriae* and *Neisseria meningitidis* requires written permission from your School Biological Safety Committee and HSE. Please complete this form and register any hazard group 2 and 3 biological agents using Retain. The School Biological Safety Adviser provides advice to Principal Investigators on biological agent risk assessment, HSE notification and licences. You should read the guidance provided on BA risk assessment and biological safety on the Biosafety Unit website. Please complete those boxes that apply to your work.

Section 1 Basic Details

Title of project	Administration of Diphtheria Toxin to mice for *in vivo* cell ablation studies.
Local reference number	BA 1618
HSE reference number	
Principal investigator	Adrian Bird
School / Institute	School of Biological Sciences
Date of assessment	September 2018
Location of work (Buildings and room numbers or fieldwork)	Roslin institute BRF

Section 2 Project

This section should describe the project which should be reasonably detailed but not exhaustive.

2.1: Description of project and activities

Mice are insensitive to Diphtheria Toxin (DT), a cytotoxic molecule which once inside cells inhibits protein synthesis and causes apoptosis. Expression of the human Diphtheria Toxin Receptor (DTR) in a cell type specific manner in mice allows you to selectively ablate those cells by administering DT to the mice. *In vivo* neuronal ablation studies will be performed by injecting genetically modified mice which express the DTR specifically in a subset of neurons with DT (RA for genetically modified mice ICMB04_287). Ablation studies will be performed at different stages during development starting during embryogenesis. In this case pregnant mothers who do not express the DTR and are insensitive to the toxin will be administered the toxin via intraperitoneal (IP) injection so that neurons in the developing brain of her progeny are ablated. Ablation studies will also be done later in development by administering DT via IP to postnatal mice. Brain tissues from DT treated mice will be harvested and the cellular viability will be assessed by analysing the cellular make-up of the Brain tissue. Off-target cellular ablation will be assessed by analysing the cellular make-up of other mouse tissues.

Section 3 Risk Assessment

This section should describe any potential risks to humans and or the environment. It should include a clear and explicit justification of any statements made about the risks with a logical explanation and any relevant evidence or references. The level of risk is estimated using the matrix given at the end of this form and then stating the risk as either Effectively zero, Low, Low / Medium, Medium or High.

3.1: Biological agents or materials

Microorganisms (Group 1)	
Human pathogens (Group 2)	
Human pathogens (Group 3)	
Specified animal pathogens (Group 2)	
Specified animal pathogens (Group 3)	
Plant pathogens or pests	
Toxins	Diphtheria Toxin
Carcinogens	
Allergens	
Human tissues, cells or materials	
Human cell cultures	
Animal tissues, cells or materials	Mouse tissues; Various including - Brain, liver, kidney, heart, spleen, lung
Animal cell cultures	
Plant tissues, cells or materials	
Plant cell cultures	
Humans	
Animals	GM Mice (Risk assessment ICMB04_287)
Plants	
Soils	
Environmental samples or materials	
Waste	
Other biological materials	

3.2: Type of work

Select all that apply	Laboratory / ~~Fieldwork~~ / ~~Other~~

3.3: Human, animal or plant diseases or conditions or environment damage associated with the biological agents

Diphtheria Toxin

DT can be extremely toxic at very low levels. The lethal dose of DT for humans is 0.1μg of toxin per kg of body weight. All contact should be avoided. Do not breathe fumes or vapours of DT solutions.

Hazard statement(s): H300 Fatal if swallowed.

Precautionary statement(s): P264 Wash hands thoroughly after handling P301 + P310 IF SWALLOWED: Immediately call a POISON CENTER or doctor/ physician.

Hazard symbol(s): Toxic

Potential health effects:

Inhalation - May be harmful if inhaled. May cause respiratory tract irritation.

Ingestion - May be fatal if swallowed.

Skin - May be harmful if absorbed through skin. May cause skin irritation.

Eyes - May cause eye irritation.

Signs and Symptoms of Exposure - Fever, Headache.

Laboratory Animal Allergens (LAA) Laboratory animal allergens (LAA) are an allergic hypersensitivity response which may develop as a result of exposure to animal allergens. The main sources are urine, fur, hair, dander, saliva, droppings and serum. Typical symptoms include rhinitis, conjunctivitis and skin rashes. The condition may not only affect a person's health but their ability to continue working within an animal laboratory environment.	
3.4: Potential routes of exposure to humans, animals or plants or release to environment	
Select all that apply	Inhalation / Ingestion / Injection / Absorption / ~~Other~~
Ingestion, Injection, Absorption, Inhalation	
3.5: Use of biological agents or materials	
Select all that apply	Small scale / ~~Medium scale~~ / ~~Large scale~~ / ~~Fieldwork~~ / ~~Animals / Plants~~ / ~~Other~~
Small scale	
3.6: Frequency of use	
Select one	Daily / ~~Weekly~~ / ~~Monthly~~ / ~~Other~~
Daily	
3.7: Maximum amount or concentration used	
Select one	~~Negligible~~ / Low / ~~Medium~~ / ~~High~~
The maximum concentration of DT handled at any one time will be 5μg/ml and the volume will not exceed 1ml. In any one study a maximum of 10 animals would be injected with up to a maximum concentration of 50μg/kg toxin in a volume less than 20ml/kg. For example the maximum amount a 20g mouse will be injected with is 1μg in a maximum volume of 400μl.	
3.8: Levels of infectious aerosols	
Select one	Negligible / ~~Low~~ / ~~Medium~~ / ~~High~~
N/A	
3.9: Potential for exposure to biological agents or materials	
Select one	~~Negligible~~ / Low / ~~Medium~~ / ~~High~~
Main potential routes of exposure of DT are through spillage of reconstituted DT or accidental injection. Diphtheria Toxin activity is not found in the urine or faeces of rodents receiving doses of less than 50 μg/kg (1), therefore animals treated with DT, bedding, cages etc.. in contact with DT treated animals will not be a risk to the handler. Due to this fact the risk associated with tissues taken from a DT treated animal should be negligible, however, these tissues will be treated as contaminated and harvested in a Class II microbiological safety cabinet (MSC) and any materials in contact with tissue will be inactivated and disposed of in an appropriate manner (section 4.10, 4.11).	
3.10: Who might be at risk	
Select all that apply	Research Staff / Other Staff / Students / ~~Visitors~~ / ~~Public~~ / ~~Young people~~ ~~(<18yrs)~~ / ~~New and expectant mothers~~ / ~~Other~~
Research Staff, Other Staff, Students	
3.11: Overall assessment of risk to human health (Prior to use of controls)	
Level of risk (Select one)	~~Effectively zero~~ / ~~Low~~ / ~~*Medium/Low*~~ / ~~Medium~~ / High
3.12: Overall assessment of risk to environment (Prior to use of controls)	
Level of risk (Select one)	Effectively zero / ~~Low~~ / ~~Medium/Low~~ / ~~Medium~~ / ~~High~~

Section 4 Control Measures to Eliminate or Reduce Risks of Exposure or Release

This section should describe the types of controls which will be required to carry out the work safely. You must follow the hierarchy of risk control by choosing the most effective control measures needed to safely carry out your work and not just the easiest controls. Please do not include detailed standard operating procedures which should be specified in separate documents.

4.1: Containment laboratories or facilities

Select all that apply	~~Laboratory~~ / Animal facility / ~~Plant facility~~ / ~~Other~~

Animal Facility

4.2: Containment level

Select one	~~Containment level 1~~ / Containment level 2 / ~~Containment level 3~~

Roslin BRF - containment level 2 facility

4.3: Microbiological safety cabinets (MSC) and isolators

Select all that apply	~~Class I~~ / Class II / ~~Class III~~ / ~~Isolator~~ / ~~Other~~

All work with DT including mouse injections and harvesting of tissue from DT treated animals is to be carried out in Class II MSC.

Individually ventilated caging (IVC) for the mice is used in the Roslin-BRF which contains the air in contact with the mice and creates a barrier between the handler and the animal. This reduces the potential contact with LAA. All work with mice outside an IVC during the proposed experiments here including DT injections and harvesting tissues will be done in a MSC and therefore the barrier will be maintained.

4.4: Sharps controls

A needle and syringe will be used to inject diluted DT into mice. When injecting solution, no re-sheathing of needles will take place, and aerosols will not be created while loading the syringe or expelling unwanted air.

Animals will be restrained manually using authorized and appropriate methods by trained and competent individuals (see section 4.13) and extreme care will be taken to avoid bites and needle stick injury.

Taking the following points into consideration, manual restraint of mice (by hand) for DT administration via IP injection without the use of puncture resistant gloves is the most appropriate method to use.

No mechanical restraints for mice exist suitable for use in IP injections.

The use of puncture resistant gloves will impact the dexterity of the individual and would lead to improper restraint of the animal, meaning they are likely to be more mobile, and thereby increase the risk of needle sticks. Puncture resistant gloves are not disposable and will also increase the risk of contamination with DT.

Only immunised staff will be permitted to administer the toxin

The maximum concentration and volume of toxin in a syringe at any one time will not exceed the lethal dose for humans.

4.5: Special controls

DT stock solution will be diluted to appropriate concentrations elsewhere at Kings buildings campus before being transported to the animal facility in an appropriate manner (section 4.9). Vials of DT will be contained within a secondary, sealable plastic container when outside a MSC. Volumes of diluted toxin will be kept to a minimum volume and excess diluted DT will be inactivated with 1M NaOH or 1% NaOCl (10% bleach) for 30 minutes before being taken for autoclave (see sections 4.10 and 4.11). Waste materials contaminated with DT should be kept as low as possible and put straight into a new autoclave bag, sealed and taken straight for autoclave. Surfaces worked on with DT and

apparatus such as pipettes will be cleaned following work with 1M NaOH or 1% NaOCl (10% bleach) followed by H_20 or 70% Ethanol.

4.6: Personal protective equipment (PPE)

Select all that apply	Lab coat / Lab gown / ~~Surgical scrubs~~ / ~~Disposable clothing~~ / ~~Apron~~ / ~~Safety spectacles~~ / Goggles / Face shield / Gloves / ~~Headwear~~ / ~~Footwear~~ / ~~Other~~

Disposable lab coat or gown with long sleeves and elasticated cuffs must be worn at all times and autoclaved and disposed of with DT contaminated waste after use.

Double gloving with nitrile gloves and gloves should be pulled over cuffs of the lab coat. Gloves must meet the EN374 standards.

The toxin will be contained inside the secondary container until it is inside a MSC. Once inside the MSC and only then will the secondary container be opened and vials of the toxin taken out. Risk of exposure to the toxin outside the MSC should not be possible. Eye/face protection is only needed if directly handling the vials of toxin outside the MSC, however this will be avoided.

Gloves will be worn when handling the mice to prevent exposure of hands to LAAs.

4.7: Respiratory protective equipment (RPE)

Select all that apply	Filter mask / ~~Half face respirator~~ / ~~Full face respirator~~ / ~~Powered respirator~~ / ~~Breathing apparatus~~ / ~~Other~~

Frequent users of the Roslin-BRF animal facility require to have routine Occupational Health skin and lung function tests whilst working in the animal facility with the first test taking place prior to having an induction into the facility. Occupational health may also advise individuals on specific RPE requirements. Short term visitors who do not receive occupational health surveillance require to wear RPE (P3 half face masks) during their visit to the animal facility.

4.8: Storage controls

Stock reconstituted DT (1mg/ml) will be stored in Kings buildings and aliquots of diluted DT for injections will be taken to Roslin, used and left over solution will be inactivated and disposed of appropriately (see sections 4.10 and 4.11). DT solution will not be stored in Roslin.

4.9: Transport controls

Transported in private vehicle (covered by insurance). Packaged in 1ml plastic vials at 5ug/ml with leak proof lids, held securely in place with tape. Outer package consists of a Nalgene® screw cap, rigid plastic container (500mL) and is lined with absorbent pad such as way that under normal conditions of transport the inner packages cannot break, be punctured or leak their contents. The outer package will contain sufficient absorbent material to absorb the entire contents of the inner packaging. Outer package will be labelled as "UN 3172 Toxins Extracted From Living Sources, Liquid N.O.S, Excepted Quantity". A copy of the safety data sheet (SDS) will be secured to the container and the associated hazard symbols will be clearly marked to inform any persons who might come across the container in the case of a car accident such as the emergency services that the contents are highly toxic.

The outer package will be autoclavable and reserved for the sole purpose of transporting the toxin. After each visit to the animal facility the box will be decontaminated by either autoclaving or 1M NaOH or 1% NaOCl (10% bleach) treatment at Kings Building's.

Frozen tissues will be transported on dry ice within a Dewar/container within a further two layers of containment; the tissues will be in screw cap nunclon cryovials which will be put into a secure secondary plastic container. Both the Dewar and secondary plastic container

will be reserved for this sole purpose and decontaminated between uses by either autoclaving or 1M NaOH or 1% NaOCl (10% bleach) treatment.

4.10: Inactivation controls

Select all that apply	Disinfection / Autoclave / ~~Fumigation~~ / ~~Incineration~~ / ~~Other~~

Disinfection

Please give details of disinfectant(s), method and validation including concentration of disinfectant and contact time (eg supplier's instructions or local validation).

DT can be inactivated by being treated with 1M NaOH or 1% NaOCl (10% bleach) for 30 minutes contact time or by heat inactivation via autoclave.

Autoclaving

Please give details of autoclave method and validation.

All contaminated materials will be inactivated by autoclaving (100% kill) at 136°C for 1 hour minutes prior to disposal of plastic waste. Autoclaves will be validated by annual (at least) thermocouple mapping and each run will be monitored using chemical indicators (eg Browne TST indicator test strips). No contaminated materials will be recycled after autoclaving.

Contaminated animal carcasses will be inactivated by autoclaving at 136°C for a hold time of 1 hour prior to disposal.

4.11: Waste disposal routes

Diphtheria Toxin is a high molecular weight proteinaceous toxin of biological origin and can be inactivated either by treatment with a 1 M solution of NaOH, 1% NaOCl (or 10% bleach) or by heat inactivation by autoclave (1,2,3,4). Diphtheria Toxin will not be disposed of as a powder but will be dissolved in water prior to toxin inactivation by normal autoclave disposal route (2). Liquid, sharps and containers will be disposed of as clinical waste for disposal via normal autoclave route.
In-case of spill follow spill guide-lines and dispose of both solid and liquid toxin by inactivating it in a solution of 1M NaOH or 1% NaOCl (10% bleach) and wipe down possibly contaminated surfaces with 1 M NaOH or 1% NaOCl (10% bleach) (1). Followed by cleaning the surface with water to remove NaOH and NaOCl.

DT contaminated sharps will be inactivated by autoclaving before being disposed of according to standard practice for sharps (see 4.10). Dispose of any other contaminated materials as clinical waste for disposal via autoclave route or treat first with 1M NaOH or 1% NaOCl (10% bleach) (see 4.10).

Carcasses of mice treated with DT will be autoclaved at 136°C for a hold time of 1 hour prior to disposal as animal by products in the yellow clinical waste bins.

After all procedures all potentially contaminated surfaces should be wiped down with 1 M NaOH or 1% NaOCl (or 10% bleach) to inactivate any DT that may have inadvertently spilled (1). Followed by cleaning the surface with water to remove NaOH and NaOCl.

Note that bleach solutions should be prepared fresh daily and can be disposed of to drain by flushing with copious amounts of H_20.

References:

Wharram B. L., et al., (2005). Podocyte Depletion Causes Glomerulosclerosis: Diphtheria Toxin-Induced Podocyte Depletion in Rats Expressing Human Diphtheria Toxin Receptor Transgene. J Am Soc Nephrol 16: 2941 – 2952

University of Virginia Biosafety Manual and Standard Operating Procedures For Biosafety Level 2 Agents. University of Virginia Office of Environmental Health and Safety, May, 2007.

Biosafety in Microbiological and Biomedical Laboratories, 4th Edition, Centre for Disease Control and Prevention – National Institutes for Health, USDHHS, May, 1999

University of Washington Environmental Health and Safety: Toxins of Biological Origin Safe Work Practices. Research and Occupational Safety, December, 2013

4.12: Immunisations (if applicable)

l. A log should be kept for all members of staff and students who have up to date immunizations and therefore can work with the toxin.

Currently in the UK, babies and children are immunized against Diphtheria at;

8, 12 and 16 weeks - 6-in-1 vaccine (3 separate doses)

3 years 4 months – 4-in-1 pre-school booster

14 years – 3-in-1 teenage booster

For full immunization a booster is required every 10 years following childhood vaccinations.

4.13: Instructions, training and supervision

Any person who is involved with any aspect of these experiments will be made familiar with the risk assessment before experiments are underway. Only suitably trained staff or students who have up to date immunisations against Diphtheria Toxin (DT) will handle DT, perform the DT injections into mice or harvest tissues from DT treated mice (see section 4.12).

Training for Intraperitoneal injection into mice is carried out by a designated trainer within the animal facility recognized by the Named Training Competency Officer (NTCO) for Bioresearch and Veterinary Services (BVS). This training is carried out within the guidelines of the Standard Operating Procedure (SOP) for administering an I.P injection into Mice. Once deemed competent to perform the technique without supervision this is logged in the traniee's Personal Licence Holder Training Record which is held centrally by the BVS.

DT treated mice or bedding, cages etc.. in contact with DT treated animals will not be a risk to staff or students handling them (see section 3.9). Staff involved with disposal of the DT contaminated waste and DT treated carcasses will be instructed on the correct method for doing so and be familiar with the risk assessment.

4.14: HSE notification (if applicable)

4.15: Specified Animal Pathogen Order (SAPO) licence (if applicable)

4.16: Plant Health Order (PHO) licence (if applicable)

4.17: Import, export or other licence (if applicable)

Section 5 Emergency Procedures

This section should describe any emergency procedures used to deal with accidental exposure, release or spillages.

5.1: Emergency procedures

Emergency contacts:

Ambulance phone - 999

National Poison Information Service phone - 111.

SWALLOWED

DT may be fatal if swallowed. TRANSFER EXPOSED INDIVIDUAL TO A&E WITHOUT DELAY BY AMBULANCE (Phone 999). A copy of the safety data sheet (SDS) should be provided to the medical doctor.
Do NOT induce vomiting unless directed to do so by medical personnel. Never give anything by mouth to an unconscious person.

EYE exposure
Immediately hold eyelids apart and flush the eye continuously with running water.
Ensure complete irrigation of the eye by keeping the eyelids apart and away from the eye and moving the eyelids by occasionally lifting the upper and lower lids.
Continue flushing until advised to stop by the Poisons information Centre or a doctor, or at least 15 minutes.
TRANSPORT TO A&E or DOCTOR WITHOUT DELAY. A copy of the safety data sheet (SDS) should be provided to the medical doctor.
Removal of contact lenses after an eye injury should only be undertaken by a skilled personnel.

SKIN exposure
Immediately remove all contaminated clothing, including footwear.
Flush skin and hair with running water (and soap if available).
Seek medical attention in event of irritation.

INHALED
If fumes or combustion products are inhaled remove from contaminated area.
Lay patient down. Keep warm and rested.
Prostheses such as false teeth, which may block airway, should be removed, where possible, prior to initiating first aid procedures.
Apply artificial respiration if not breathing, preferably with a demand valve resuscitator, bag-valve mask device, or pocket mask as trained. Perform CPR if necessary.
TRANSPORT TO A&E or DOCTOR WITHOUT DELAY. A copy of the safety data sheet (SDS) should be provided to the medical doctor.

NEEDLESTICK
If an accidental skin prick occurs, encourage bleeding from wound, wash with copious amounts of water. TRANSPORT TO A&E or DOCTOR WITHOUT DELAY. A copy of the safety data sheet (SDS) should be provided to the medical doctor.
If accidental i.v or i.m injection occurs TRANSPORT TO A&E immediately. A copy of the safety data sheet (SDS) should be provided to the medical doctor.

Spillages Procedure

Liquid spills:
Clear the area and communicate to others that a spillage of Diphtheria Toxin has occurred and warn them not to enter the area. Wear a lab coat, safety glasses/goggles, a disposable P3 mask and two pairs of disposable nitrile gloves to avoid contact with eyes, skin, clothing and inhalation. Cover spill with absorbent paper towels and apply 1M NaOH or 1% NaOCl (or 10% bleach), allowing 30-min contact time to deactivate DT before disposing of towelling in clinical waste for disposal by autoclave. Ventilate area and wash contaminated area thoroughly with more 1M NaOH or 1% NaOCl (or 10% bleach) allowing 30 min contact time, then rinse with water and dispose of waste in clinical waste for disposal by autoclave.

5.2: Emergency contacts

Name	Position	Telephone
Katie Paton	PhD	
Jim Selfridge	Post-Doc	
Prof Adrian Bird	PI	

Section 6 Emergency Planning	
This section should describe any emergency plan used to deal with serious accidental release. An emergency plan is only required for high risk work.	
6.1: In case of serious accidental release is an emergency plan required to protect humans or environment	~~Yes~~ / No
NO	

Risk Estimation Matrix				
Consequence of hazard	**Likelihood of hazard**			
	High	**Medium**	**Low**	**Negligible**
Severe	High	High	Medium	Effectively zero
Modest	High	Medium	Medium / Low	Effectively zero
Minor	Medium / Low	Low	Low	Effectively zero
Negligible	Effectively zero	Effectively zero	Effectively zero	Effectively zero